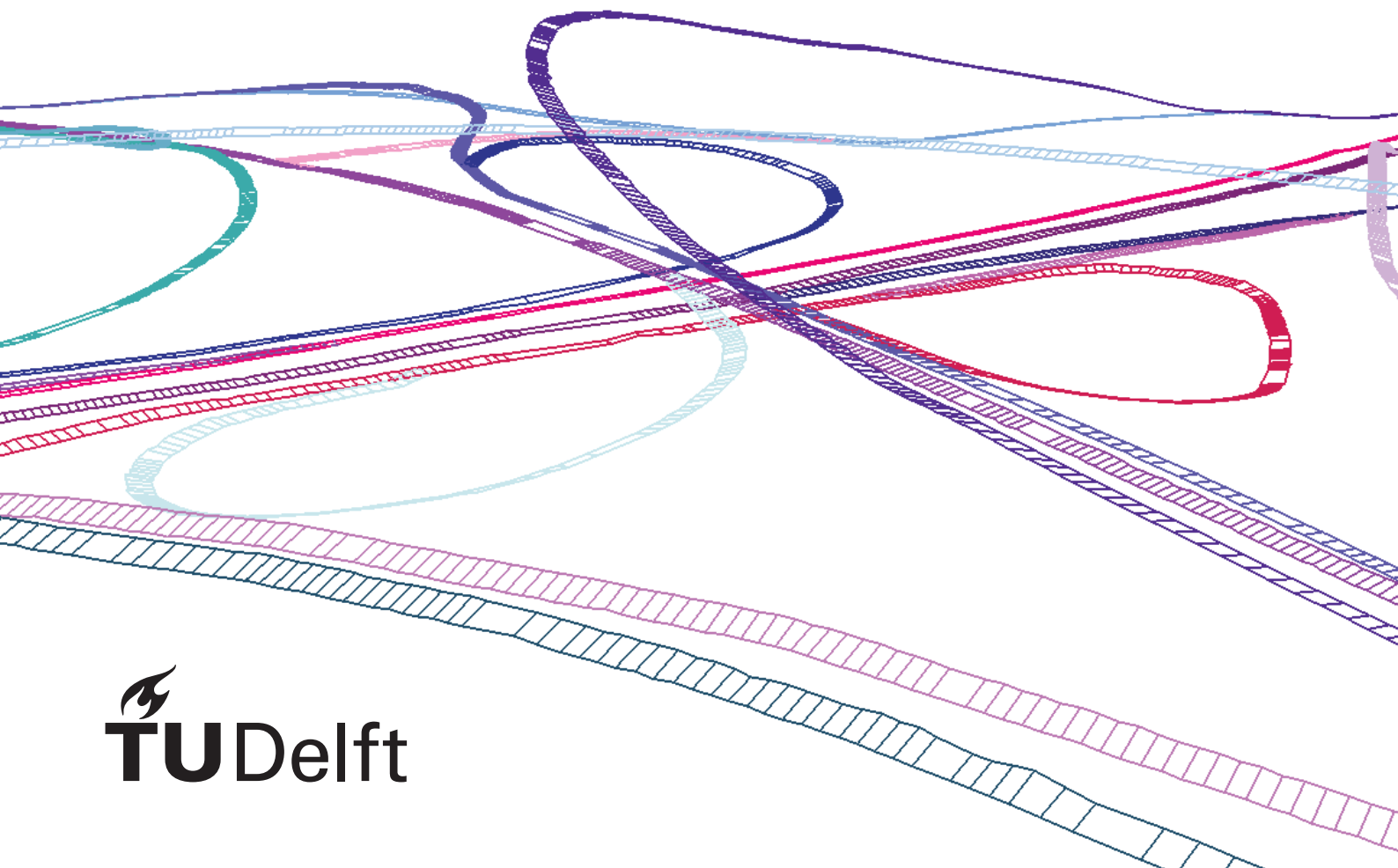


MSc thesis in Geomatics

# Constructing a digital 3D road network for The Netherlands

Kristof Kenesei  
2021





**MSc thesis in Geomatics**

**Constructing a digital 3D road network for The  
Netherlands**

Kristof Kenesei

February 2020

A thesis submitted to the Delft University of Technology in partial  
fulfillment of the requirements for the degree of Master of Science in  
Geomatics

Kristof Kenesei: *Constructing a digital 3D road network for The Netherlands* (2020)  
© This work is licensed under a Creative Commons Attribution 4.0 International License. To view a copy of this license, visit <http://creativecommons.org/licenses/by/4.0/>.

The work in this thesis was carried out in the:



3D Geoinformation  
Department of Urbanism  
Faculty of the Built Environment & Architecture  
Delft University of Technology

Supervisors: Ravi Peters  
Jantien Stoter  
Co-reader: Stelios Vitalis

# Abstract

This research concerned the design and implementation of a system to perform the 3D conversion of a nationwide road network using airborne Lidar data and land-based road elevation measurements, preserving its topology and quantifying output elevation accuracy. While the system was designed with generality in mind, specific Dutch open data datasets were used as input which were also used in a commercial project with the same goals. In addition to designing a scientifically sound equivalent of the commercial implementation, this research also explored purely academic goals, such as selecting road surface laser reflections accurately and using them for 2.5D road surface modelling purposes. Our system was based on decomposing the 3D conversion task into individually solvable 2.5D sub-problems to enable the use of efficient terrain modelling methods, and to prove that scaling via multiprocessing would be possible, which is relevant because of the nationwide scale. At the 10-30 points per  $\text{m}^2$  sampling density we worked with, the road surfaces are oversampled. We found that because our elevation estimates are based on road reflections only, and because road surfaces are smooth and relatively flat, the output quality and accuracy depends only on the specific technique used to extract the elevations from the Lidar data. Using our methods, the output elevation accuracy represents a 30% increase relative to the Lidar input data, amounting to 10.6 cm at 95% certainty with our specific datasets. This assumed to be violated only where local density drops below 3 points per  $\text{m}^2$ , which occurs where roads are occluded by opaque objects unless the land-based road surface measurements can help dropping below this threshold. Elsewhere, more than 98% of the road network conforms with the minimum point density. The 2.5D-based decomposition was found to be an effective means of simplifying the problem and terrain modelling methods were successfully used in the procedure. More than 90% of the traffic-occupied road surfaces are included in the resulting surface models, and about 70% of the total paved surfaces. The output elevations could be extracted directly from them. Our 3D conversion quality and accuracy represents an improvement relative to the commercial results, mostly due to the better prioritising of the input elevation sources, in addition to our solution's capacity to handle complex small to medium-scale occlusion better, including complex relationships between roads such as multi-level motorway junctions.



# Contents

<b>1</b>	<b>Introduction</b>	<b>1</b>
1.1	Motivation . . . . .	1
1.2	The NDW commission . . . . .	2
1.3	Field and relevance . . . . .	3
1.4	Research questions . . . . .	3
<b>2</b>	<b>Related work</b>	<b>7</b>
2.1	Road identification in point clouds . . . . .	7
2.1.1	Research using point clouds only . . . . .	7
2.1.2	Research using input point clouds and approximate road locations . . . . .	9
2.2	Lidar accuracy and sampling density . . . . .	12
2.2.1	Accuracy description of Lidar sensing . . . . .	13
2.2.2	Accuracy description of Lidar-derived DTMs . . . . .	14
2.3	Input assessment . . . . .	16
2.3.1	Nationaal Wegenbestand – NWB . . . . .	17
2.3.2	Actueel Hoogtebestand Nederland – AHN . . . . .	19
2.3.3	Digitaal Topografisch Bestand – DTB . . . . .	21
2.4	Methods of existing implementations . . . . .	24
2.4.1	NDW prototype . . . . .	24
2.4.2	RHDHV’s commercial implementation . . . . .	25
<b>3</b>	<b>Methodology and methods</b>	<b>29</b>
3.1	Methodological framework . . . . .	29
3.1.1	Preparation . . . . .	29
3.1.2	Preliminary analysis, proposal writing . . . . .	29
3.1.3	Analysis . . . . .	30
3.1.4	Finalisation . . . . .	30
3.2	Overview of methods . . . . .	30
3.2.1	Proposed processing pipeline . . . . .	32
3.2.2	Dependency of methods on specific datasets . . . . .	35
3.2.3	A note on DTB’s role . . . . .	36
3.2.4	Accuracy assessment of processing steps . . . . .	36
3.3	Detailed methods . . . . .	39
3.3.1	Splitting NWB into NBRS . . . . .	39
3.3.2	Elevation estimation . . . . .	41
3.3.3	Lidar segmentation . . . . .	43
3.3.4	Edge approximation . . . . .	46
3.3.5	Active contour optimisation . . . . .	49
3.3.6	TIN construction . . . . .	51
3.3.7	TIN-based interpolation and vertex snapping . . . . .	55
3.4	Accuracy assessment . . . . .	57
3.4.1	Detecting regions with poor sampling . . . . .	57
3.4.2	Effect of interpolation of accuracy . . . . .	59
3.4.3	Evaluating TIN surface completeness . . . . .	60
3.5	Comparison with commercial results . . . . .	60
3.6	Programming framework . . . . .	60

## Contents

<b>4 Results</b>	<b>63</b>
4.1 Manual pre-processing . . . . .	63
4.1.1 Producing the testing datasets . . . . .	63
4.1.2 Description of testing datasets . . . . .	64
4.2 Results of processing steps . . . . .	66
4.2.1 Splitting NWB into NBRs . . . . .	67
4.2.2 Elevation estimation . . . . .	69
4.2.3 Lidar segmentation . . . . .	74
4.2.4 Edge approximation . . . . .	78
4.2.5 Active contour optimisation . . . . .	82
4.2.6 TIN construction . . . . .	86
4.2.7 Interpolation in TIN and snapping . . . . .	94
4.3 Accuracy assessment . . . . .	97
4.3.1 Empirical accuracy assessment . . . . .	97
4.3.2 Formal accuracy assessment . . . . .	99
4.3.3 Ratio of accurate vertices . . . . .	101
4.3.4 TIN completeness . . . . .	102
4.3.5 Tabulated values . . . . .	103
4.4 Comparison with commercial implementation . . . . .	105
4.4.1 Representative example comparisons . . . . .	105
4.4.2 Tabulated RMSE values . . . . .	109
<b>5 Conclusions</b>	<b>111</b>
5.1 Usefulness and generality of datasets . . . . .	111
5.1.1 General remarks about AHN3 and DTB . . . . .	112
5.1.2 On the impact of input quality . . . . .	112
5.2 Effectiveness of processing steps . . . . .	113
5.2.1 Decomposing the 3D problem into 2.5D sub-problems . . . . .	113
5.2.2 Surface modelling effectiveness . . . . .	113
5.2.3 NWB 3D-conversion effectiveness . . . . .	114
5.3 Accuracy-related conclusions . . . . .	115
5.4 Accuracy assessment conclusions . . . . .	115
5.5 Conclusions of comparison with commercial results . . . . .	116
5.6 Summary conclusions . . . . .	117
5.7 Future work . . . . .	118
5.7.1 Eliminating active contour optimisation . . . . .	118
5.7.2 Improving TIN construction effectiveness . . . . .	119
5.7.3 Performance and scaling . . . . .	119
5.7.4 Conditionally accepting preliminary elevations as final . . . . .	120
5.7.5 Using the support dataset more intelligently . . . . .	121
<b>6 Reproducibility self-assessment</b>	<b>123</b>
6.1 Self-reflection . . . . .	123

# List of Figures

2.1	Illustration of the results of phase coded disk (PCD) convolution from Clode et al. [2007]. . . . .	9
2.2	Illustration of the contour optimisation procedure used in Boyko and Funkhouser [2011]. . . . .	10
2.3	Examples of 3D-converted multi-level road vector geometry from Oude Elberink and Vosselman [2006]. . . . .	11
2.4	Illustration of the effects of terrain slope on vertical accuracy from Hodgson and Bresnahan [2004]. . . . .	13
2.5	An example render of Nationaal Wegenbestand (NWB), colour-coded to indicate the owner. . . . .	17
2.6	Render comparing Actueel Hoogtebestand Nederland 3 (AHN3) with the relevant 2D NWB centrelines. . . . .	19
2.7	Example render of AHN3 at Knooppunt Deil, SW of Geldermalsen, showing ground points and bridges. . . . .	20
2.8	Example render of AHN3 at Knooppunt Deil, SW of Geldermalsen, showing ground points and motorway signs. . . . .	21
2.9	Renders of Digitaal Topografisch Bestand (DTB) <i>verflijnen</i> overlain with NWB centrelines, illustrating "compatibility issues" and individual DTB issues. . . . .	22
2.10	Renders of DTB all line features (above) and <i>verflijnen</i> only (below) overlain with AHN3 in 3D. . . . .	24
2.11	Illustrations of Royal HaskoningDHV (RHDHV)'s procedures to convert NWB to a 3D dataset. . . . .	26
3.1	Flowchart-style illustration of the top-level methodology of my dissertation research. . . . .	31
3.2	Illustration of the top-level steps and output of my processing pipeline. . . . .	32
3.3	Flowchart-style illustration of the non-branching road segment(s) (NBRS) generation step of the pipeline. . . . .	40
3.4	Flowchart-style illustration of the elevation estimation step of the pipeline. . . . .	42
3.5	Flowchart-style illustration of the Lidar segmentation step of the pipeline. . . . .	44
3.6	Flowchart-style illustration of the edge approximation step of the pipeline. . . . .	47
3.7	Flowchart-style illustration of the active contour optimisation step of the pipeline. . . . .	49
3.8	Flowchart-style overview of the triangular irregular network (TIN) construction step of the pipeline. . . . .	52
3.9	Flowchart-style illustration of the details of TIN initialisation and construction. . . . .	54
3.10	Flowchart-style illustration of the elevation interpolation step of the pipeline. . . . .	56
4.1	Visualisations illustrating the results of manual pre-processing. . . . .	64
4.2	Visualisations illustrating the results of NBRS generation. . . . .	68
4.3	Visualisations illustrating the preliminary elevation estimation results. . . . .	70
4.4	Visualisations illustrating the vertex densification feature. . . . .	70
4.5	Visualisations comparing preliminary 3D conversion results with the AHN3 point cloud. . . . .	72
4.6	Visualisations illustrating the results of Lidar segmentation. . . . .	74
4.7	Visualisations illustrating the disagreement between AHN3 and DTB. . . . .	76
4.8	Visualisation illustrating the handling of gaps in AHN3 coverage during Lidar segmentation. . . . .	78
4.9	Visualisations illustrating the results of preliminary edge approximation. . . . .	79
4.10	Visualisations illustrating challenging edge approximation scenarios. . . . .	81
4.11	Visualisations illustrating various degrees of active contour optimisation success. . . . .	83
4.12	Visualisations comparing optimised edges to the underlying attractor maps. . . . .	85
4.13	Visualisations illustrating the results of TIN initialisation and extension. . . . .	87
4.14	Visualisations providing an overview of constructed TINS and illustrating TIN artefacts. . . . .	90
4.15	Visualisations comparing final 3D conversion results to preliminary conversion, sub-clouds, and preliminary edges. . . . .	93

## List of Figures

4.16 Visualisations comparing final 3D conversion results to the underlying <a href="#">TIN</a> models. . . . .	96
4.17 Charts demonstrating the outcome of the empirical accuracy assessment process. . . . .	98
4.18 Charts illustrating the formal accuracy assessment results on two <i>wegvakken</i> . . . . .	99
4.19 Visualisations showing the subclouds, <a href="#">TINs</a> and 3D-NWB centrelines in the area concerned by Figure 4.18. . . . .	100
4.20 2D Visualisations comparing Basisregistratie Grootchalige Topografie ( <a href="#">BGT</a> ) road edges with the <a href="#">TINs</a> , with <a href="#">NWB</a> centrelines and with Luchtfoto 2020 satellite imagery. . . . .	102
4.21 Charts comparing the academic and commercial results using two <i>wegvakken</i> from <i>Knooppunt Deil</i> . . . . .	105
4.22 Charts comparing the academic and commercial results using two <i>wegvakken</i> from dataset <i>Gorinchem</i> . . . . .	107
4.23 Charts comparing the academic and commercial results using two <i>wegvakken</i> from dataset <i>Knooppunt Ridderkerk</i> . . . . .	108
6.1 Reproducibility criteria to be assessed. . . . .	123

# List of Tables

4.1	Inventory of testing datasets . . . . .	66
4.2	Tabulated 3D-NWB accuracy and completeness results per testing dataset. . . . .	104
4.3	Tabulated academic and commercial 3D-NWB similarity quantification results. . . . .	109



# Acronyms

DTM	digital terrain model .....	7
GIS	geographical information system .....	3
GNSS	global navigation satellite system .....	1
INS	inertial navigation system .....	12
IMU	inertial measurement unit .....	13
GUI	graphical user interface .....	109
DT	Delaunay triangulation .....	91
CDT	constrained Delaunay triangulation .....	11
TIN	triangular irregular network .....	ix
NDW	Nationaal Dataportal Wegverkeer .....	2
RWS	Rijkswaterstaat .....	xiii
RHDHV	Royal HaskoningDHV .....	ix
MLE	maximum likelihood estimation .....	3
RMSE	root mean squared error .....	3
ALS	airborne laser scanning .....	7
MLS	mobile laser scanning .....	8
NWB	Nationaal Wegenbestand .....	ix
AHN	Actueel Hoogtebestand Nederland .....	11
AHN2	Actueel Hoogtebestand Nederland 2 .....	12
AHN3	Actueel Hoogtebestand Nederland 3 .....	ix
AHN3	Actueel Hoogtebestand Nederland 3 .....	ix
DTB	Digitaal Topografisch Bestand .....	ix
BGT	Basisregistratie Grootschalige Topografie .....	x
RANSAC	random sample consensus .....	8
PCD	phase coded disk .....	ix
IDW	inverse distance weighting .....	14
NBRS	non-branching road segment(s) .....	ix
JTE ID	<i>junctie</i> (intersection) ID number .....	41
R-roads	Rijkswegen (motorways) .....	17
P-roads	Provinciewegen (provincial roads) .....	17
G-roads	Gemeentewegen (municipal roads) .....	17
W-roads	Rijkswaterstaat ( <a href="#">RWS</a> )-managed roads .....	17



# 1 Introduction

## 1.1 Motivation

Constructing and maintaining an up-to-date graph-like road network on the national level has a range of firmly established uses. Owing to its structure, it can be used efficiently for modelling and simulation purposes, such as traffic flow simulations, passenger transport modelling, construction and upgrade impact modelling (to pinpoint optimal locations and types of investment), and traffic noise load modelling (Bell and Lida [1997]; Zhu and Li [2007]; Zhang [2011]; Durán Fernández and Santos [2014]; Peng et al. [2020]). It can also be used for navigation; a graph-like road network representation is at the heart of most road navigation services (Yue et al. [2008]). Combined with other data sets, we can mention an even wider range of use cases: complemented by ecological statistics and models, it can offer insight into the impact of the presence of roads, and planned road construction on the flora and fauna in their vicinity.

Or to mention a different type of example, an accredited model representing the road network in a digital format may be used as a shared working space when aggregating geospatial data relating to road infrastructure from various sources. It makes it possible for geographical road locations, topographical relationships, and arbitrary semantic information to reside in the same network-type data model, making analysis techniques more straightforward, enforcing consistency and saving effort for data providers who would otherwise all need to maintain their own road model (Ekpenyong et al. [2007]). This example is closely related to the ambitions the provider of the Dutch digital road network, which is the primary subject of this research, has with their road network model.

One may remark that a two-dimensional representation with *approximate* geographical locations may suffice for many of the purposes I listed as examples above, topology being the main concern in network analysis. For instance, global navigation satellite system ([GNSS](#)) navigation software often use snapping methods to ensure that the navigating vehicle always traverses the road graph – ensuring that even for imperfect positioning results navigation remains continuous (Fouque and Bonnifait [2008]; Chen and Hsu [2020]). Traffic flow simulations are primarily concerned with traffic loads, road properties, and how roads are subdivided by intersections among other aspects. *Mostly*, they are not concerned with the exact geographical locations of roads – as long as the topology is relatively accurate, any geographical permutation of the network will yield largely invariant results (Thomson and Richardson [1995]).

However, some applications are concerned with the road network in the context of its surroundings, which makes the accuracy of its georeferencing a relevant topic. Noise modelling is such an application, because modelling the propagation of road noise concerns deriving the noise load affecting various objects in the vicinity of the the roads. Furthermore, the propagation of the noise itself requires taking into account objects that may suppress or amplify the noise, such as buildings, noise barriers and terrain (Ishiyama et al. [1991]; Bennett [1997]; Guarnaccia and Quartieri [2012]). A realistic noise propagation model takes into account the height of the road, as well as the vertical extent of surrounding objects. However, typical digital representations of national road networks tend to only describe lateral road positions, a factor that may limit their use in such noise propagation applications. For instance, consider two buildings at the side of a road, a tall one *behind* a shorter one. A 2D semantic road model would tell us that the entirety of the taller building receives a decreased noise load, because the shorter one – positioned between the taller building and the road – suppresses it. In reality, this observation is invalid because the part of the taller building which is visible from the road above the shorter building receives the full noise load. To be able to represent such 3D relationships in our model correctly, we need both buildings and roads to be fully three-dimensional.

## 1 Introduction

2D-projected digital road models with mediocre accuracy have attracted great scientific and commercial attention since the advent of digital cartography and satellite navigation (Taylor et al. [2001]; Fouque and Bonnifait [2008]; Yue et al. [2008]; Chen and Hsu [2020]). However, accurate 3D representations are still atypical, owing to factors such as increased cost of generation and maintenance, increased complexity of visualisation and analysis, and a lack of significant use cases (Zhu and Li [2007]; Wang et al. [2014]). As a result, 2D road models are common in terms of both public and private geospatial providers, whereas accurate 3D road models are rare in comparison.

When a use case arises and an accurate 3D model is needed, providers generally face two choices: to produce a new model, or to enrich an existing 2D model with elevation data. The decision generally depends on the quality of the available 2D data set relative to the requirements for the 3D model, as well as that of the dataset(s) available as sources of elevation data, with which the 2D model can be enriched, among other factors (Zhu and Li [2007, 2008]; Wang et al. [2014]). In terms of the source of elevation data, the rule of thumb in the geospatial field is that data acquisition is far more expensive than re-using existing datasets, especially openly available ones. As a result, many providers first attempt to find a way to convert their datasets into 3D using existing data in such a cost-effective manner.

### 1.2 The NDW commission

In certain projects the accuracy requirement and restrictions on the modelling procedure may be prescribed legally. Such is the case for the client of the present dissertation research, the Nationaal Dataportal Wegverkeer ([NDW](#)) (National Road Traffic Data Portal), part of [RWS](#) (Directorate-General for Public Works and Water Management), a Dutch government organisation who are in the process of enriching their pre-existing open data 2D road model, called [NWB](#) (National Road Database), with 3D data, to attain compliance with the new version of the Dutch noise legislation or *geluidwetgeving*, coming into effect on the 1<sup>st</sup> of January 2022. The new version of the legislation prescribes, among other things, a horizontal *and* vertical accuracy of 20 centimetres for the road model underlying the noise simulations. Due to cost considerations and reasons related to [NDW](#)'s data acquisition pipeline, the pre-existing 2D version of [NWB](#) will be converted into a 3D dataset (dubbed 3D-NWB) primarily using open data geospatial datasets. They have produced a prototype implementation themselves, and subsequently contracted the consultant firm [RHDHV](#) to create a commercial implementation based on their experience with the prototype. The development of this tool was concluded in December 2020, with a preliminary version of the results already publicly available on their website in addition to the traditional 2D version.

Thus for [NDW](#), the next year will be about assessing the quality of their new product and improving it as they see necessary. In particular, they wish to assess how it fares in terms of the requirements set by the law. This dissertation research attempts to contribute to this assessment by presenting an original system design and implementation that favours scientific correctness, and in which output accuracy can be qualitatively and quantitatively examined. By comparing the results of this academic implementation to that of the commercial one, it becomes possible to indirectly evaluate the commercial results' general quality and accuracy in an indirect manner. My work also explores various related geomatics topics in the process, which I specifically refer to as the academic aims of this project, in the present report.

My research was carried out in consultation with the above commercial parties. In fact, the stages leading up to the submission of my dissertation proposal involved continuous consultation with personnel both at [NDW](#) and [RHDHV](#) while the commercial implementation was still being developed, to ensure that my research fits well with [NDW](#)'s plans and the commercial implementation - in addition to answering various questions inspired purely by academic interest. In simple terms, the initial idea for this project was to complete [NDW](#)'s commission - same as the commercial project - but by designing a system that builds primarily on geomatics tools and the results of which can be analysed in terms of empirical or formal mathematical accuracy.

## 1.3 Field and relevance

For reasons that will later become clear (see Section 2.3), I primarily focused on a Lidar point cloud and a 3D topographical line dataset as elevation sources. In both of these datasets, it is clearly evidenced that roads are occasionally in complex three-dimensional relationships with one another and with their environment. For instance, they cross above and below other roads and are also frequently occluded by other objects such as vegetation and buildings. Already in the planning phase of the project the question had arisen, how such real-world geometries should be dealt with in the conversion process - evidently they will require special treatment relative to well-exposed road surfaces. The answer to this question is closely linked with which field of geoscience my project is positioned in.

The likely candidates in the context of digital road network modelling are geographical information system ([GIS](#)) and geomatics. It is thus worth discussing briefly how each typically treats 3D objects. One of the reasons why 2D road models are popular is that their geometry and network properties can be analysed using a multitude of well-proven [GIS](#) methods and software kits. However, in [GIS](#) models, even if elevation measurements exist, they are generally only present as an *elevation attribute* (i.e. a semantic data field, like street names), because [GIS](#) geometrical models do not typically support true 3D operations. This is conceptually identical to projecting the geometries onto the horizontal plane. Geometric models that treat the vertical dimension explicitly are more common in geomatics; namely 2.5D and 3D models. While using 2.5D models restricts the types of physical entities that can be modelled, it also greatly simplifies certain types of analysis conceptually and computationally. This makes it ideal for working on similar scales to [GIS](#); on the national scale for instance, as in this research.

While 2.5D modelling initially appears to be a good candidate for this project, we may observe that it is by definition unsuitable for handling the 3D relationships that roads have with each other and with their environment. However, much like how the concept of divide-and-conquer works in computer science, it is also possible decompose three-dimensional, geometrical problems into smaller sub-problems until they become natively compatible with 2.5D methods which are simpler to solve individually than the 3D problem as a whole. This research is positioned in the field of geomatics because my system design is specifically intended to explore how 2.5D methods can be applied in a way that enables the *piecewise* modelling of a national road network. The divide-and-conquer concept will be applied to decompose the road network into segments that can be individually, locally regarded as *terrain* (i.e. a mathematical surface) and hence be modelled in 2.5D.

Geomatics is comprised of a wide range of disciplines, several of which are relevant to the present research. As it focuses on 2.5D methods to a great extent, it overlaps with the geomatics field of *digital terrain modelling* in terms of how it generates and stores the digital representation of road surfaces, and as a consequence, the manner in which it will derive elevations from them: using *spatial interpolation*. As the overview of the methods in Section 3.2 reveals, it also strongly overlaps with the geomatics discipline of *feature extraction* (and to a lesser extent, *photogrammetry*), because of the intermediate steps used by the pipeline to derive the 2.5D road surface models from our input datasets.

This is in line with my goal to study how a combination of mainly geomatics-based tools and methods can be used to accomplish the tasks required by [NDW](#), and to also assess their accuracy and suitability when used in this way. However, I also use [GIS](#) methods "under the hood" in all parts of the project - for instance, 2D geometry intersection tests, orientation tests and spatial queries are pervasive in the implementation, and are thus often mentioned in the detailed description of the processing steps found in Section 3.3. Furthermore, my research often touches on mathematics and statistics, for instance I use polynomial fitting and maximum likelihood estimation (maximum likelihood estimation ([MLE](#))) throughout the implementation (as examples of the former) and metrics such as standard deviation and root mean squared error ([RMSE](#)) (as examples of the latter).

## 1.4 Research questions

My main research question is "*How can we achieve a 3D conversion of the [NWB](#) dataset using Dutch open geospatial data and a primarily 2.5D-based surface modelling methodology, while guaranteeing optimal and quan-*

## 1 Introduction

tifiable accuracy and completeness?". It was distilled from the main areas of interest that we settled on during the preparatory stages of the project, while planning the project with my academic mentors, as well as [NDW](#) and [RHDHV](#). The question is comprised of two halves, which I initially intended to devote equal amounts of attention to - the question of devising a system design and implementing it, and that of assessing its effectiveness and the accuracy and completeness of the output it generates (as well as comparing it with the commercial results).

During the realisation of the project, I eventually settled on focusing more time and effort on the system design and integration, both because it required more time than initially anticipated, and because the quality and accuracy assessment of the results (and their comparison with the commercial results) was more straightforward than expected, leaving more time to work on the implementation. Furthermore, I found that many of the accuracy-related questions depend strongly on the exact specifications of the system design and its implementation, meaning that not all the work necessary to answer those questions was clearly separated into a dedicated accuracy assessment process - much of it needed to be considered and evaluated during the development process.

The two halves of the main research question were created by collecting my sub-questions into these two categories; pipeline design and implementation, and accuracy assessment. Below I present some of these sub-questions, to characterise in somewhat more detail, what specifically my attention was directed towards in this research project.

1. Sub-questions related to *performing* the elevation-enrichment of [NWB](#) using Dutch open geospatial data and predominantly via 2.5D geomatics methods
  - a) What are the exact methods of the commercial implementation and what do we suspect its theoretical shortcomings to be?
  - b) Does the literature suggest any methods that are particularly suitable to this research? If so, can we make use of them in our own methods?
  - c) How can the academic methods best make use of the combined information content of the datasets that the commercial implementation uses?
  - d) How should the road network be subdivided into parts that each represent a 2.5D problem? Can they be processed individually to facilitate easy parallel processing?
  - e) As we are using Lidar data, can we produce an accurate and complete [TIN](#) surface model for each 2.5D "unit"? Can we interpolate elevations for [NWB](#) through this model?
  - f) How do we "stitch" the results of the individual 2.5D procedures back together into a 3D road network with the correct topology?
  - g) Can the implementation be made robust enough to handle all (or *most*) challenging road layouts correctly, such as complex motorway junctions?
  - h) How can we make the implementation perform well in areas where input elevation data is scarce or missing over longer distances, such as in tunnels?
  - i) Can the computational complexity of the program be kept low enough to be suitable for processing all the relevant roads?
  - j) While solving [NDW](#)'s specific problem, can we also ensure that our solution generalises well to other problems of a similar type?
  - k) Can the pipeline and the implementation be clearly separated into "modules" to facilitate easy partial reuse?
2. Sub-questions related to the *assessment* of the overall quality, completeness and accuracy of the output and its similarity to the commercial results
  - a) In related work, what methods are typically used to measure empirical and theoretical output accuracy?

- b) According to related work, what typically defines output accuracy? Do local factors also play a role, or is it reasonable to estimate it for the procedure globally?
- c) What is the accuracy of our input elevation data sources? Can we structure the pipeline in a way that their input accuracy can be propagated to the output in a straightforward manner?
- d) To facilitate the above, can we derive our output directly from input data points, despite the large number of processing steps that are potentially necessary?
- e) What is the effect of uncertainty in the lateral positions of [NWB](#) centrelines on the effectiveness of our methods, and on the output accuracy?
- f) The road surface model [TINS](#) are also important products of the pipeline. How can we assess the overall quality and completeness of these?
- g) Can we indicate it in the output, which input elevation source each output elevation estimate was derived from, and to use this capability to derive the output accuracy from the appropriate input dataset's accuracy?
- h) How are temporal inconsistencies between the datasets manifested in the output? Can these be detected by the processing steps?
- i) In case we can estimate accuracy on the local scale, what physical features or sensing issues do drops in accuracy correspond to? If this corresponds to problems with the input, what properties of the input should be improved?
- j) How good is the agreement between the commercial and the academic results? What physical features or sensing issues do disagreement between the results correspond to?
- k) Under what conditions does the academic solution perform better or worse than the commercial one, and what does this tell us about the two underlying sets of methods?



## 2 Related work

I found and studied a large number of research papers as part of the literature review stage of this project. When I started the review, I already had a good starting point on what specifically to research, because I had known that my focus would be restricted to three specific, openly available Dutch geospatial datasets, and because I had already settled on a range of specifics regarding the goals and requirements of the project. The three datasets were picked early on in the planning process for reasons related to our wish to mainly use the same datasets as the commercial solution does.

As it is the most up-to-date detailed elevation source, and thus suitable for performing detailed surface modelling in addition to the 3D conversion of lines, my primary candidate became the national airborne laser scanning ([ALS](#)) point cloud of The Netherlands. The name of the latest release of this product is abbreviated [AHN3](#). As a result of this choice, there are two main areas that I focused on as part of my literature review: road feature reconstruction from Lidar point clouds, and the theoretical and empirical propagation of Lidar accuracy into derived models. The literature review concerning these two areas is presented below in two independent parts.

The other two datasets are [NWB](#) itself, and a 3D line dataset called [DTB](#) which has coverage in many areas where [AHN3](#) does not. Detailed information about the choices regarding the datasets, as well as an analysis about their detailed properties, can be found in in Section [2.3](#).

### 2.1 Road identification in point clouds

My main domain of interest was feature extraction from Lidar data, because tasks of this type characterised the bulk of the planned processing pipeline. Our intention was to not only query a digital terrain model ([DTM](#)) for elevations around the [NWB](#) road centrelines - an example of a simple way in which one could perform a *rudimentary* 3D conversion - but to create spatial models of road edges and surfaces, and only then proceed to extracting elevations for the centrelines. This requires one to identify, or at least approximate the geometries of these features by choosing the point cloud points that best describe them and applying various operations to them.

We may thus regard point cloud feature extraction as the top-level geomatics topic concerned by this research, with most other operations, such as 2.5D surface modelling and mathematical tools, as residing a level lower in the hierarchy. We are using them for the purpose of identifying and modelling discrete physical features found in the point cloud (and the support dataset, which will be discussed later in this chapter).

#### 2.1.1 Research using point clouds only

##### Approaches based on photogrammetry

In terms of point cloud feature extraction techniques relevant to roads specifically, I studied a range of papers detailing a wide spectrum of methods. One strategy, most prominently represented by [Hu \[2003\]](#); [Hu et al. \[2004\]](#); [Zhu and Mordohai \[2009\]](#); [Zhu and Hyppä \[2014\]](#); [Lin et al. \[2015\]](#), is based on the idea of transitioning to a photogrammetric analysis at some point in the process, generally quite early on. First, a set of pre-processing techniques to better characterise potential road points in the source Lidar data are applied, generally by performing some form of filtering (e.g. setting intensity thresholds applicable to Lidar returns from bitumen), or by extracting ground planes using various techniques and

## 2 Related work

selecting points that lie close to them. Then, images are rendered from the point cloud from various angles, often using colour-coding based on point properties, and applying photogrammetric methods to identify roads. Sometimes, high-definition aerial or satellite imagery is incorporated in the photogrammetric workflows. The success rates of such strategies are mediocre, and they rely strongly on manual parametrisation. In particular, they are unsuitable for large study areas with inhomogeneous types and distributions of roads, as also concluded by the excellent review of this type of relevant work in the literature review section of the paper [Yang et al. \[2013\]](#).

### Approaches based on curb detection

A further popular set of strategies rely on road curb detection. [Vosselman and Liang \[2009\]](#), [Zhang \[2010\]](#), and [Yang et al. \[2013\]](#) are examples of such research. [Vosselman and Liang \[2009\]](#) presents a method in which a [DTM](#) is generated, points close to its surface are selected from the point cloud and small, curb-like jumps in elevation are algorithmically detected using thresholds. The curb points are selected, and a feature extraction method (random sample consensus ([RANSAC](#)) in this case) is used to construct 3D lines from them. Gaps in the lines are closed procedurally, and B-splines are fitted to optimise the shapes of the road edges. In [Zhang \[2010\]](#), road cross-sections are constructed and inspected in 1D, and points are "classified" based on whether they are likely to represent road surfaces, curbs, or off-road surfaces. To do this, they process mobile laser scanning ([MLS](#)) data on-the-fly (during acquisition) via a supervised classifier, and use the Hough transform to model the road surface. The curbs are found where the points first deviate from the model.

In [Yang et al. \[2013\]](#) a similar approach is presented in which cross-sections are identified by looking at [MLS](#) scan properties (time of acquisition, specifically), and then non-road points are filtered out in 1D based on the absolute elevation of the road (known from constant elevation of the sensor above it) and curbs of a specific type are identified in the 1D series of ground points - all via a single moving-window operation that uses applicable thresholds.

While the results of the curb detection-based methods are more flexible, more accurate and more complete in general than the photogrammetric methods, they are not well suited for my project out-of-the box. These approaches work best with [MLS](#) data, where the data is either natively produced in the form of road cross-sections (the scan lines of a car-mounted front facing sensor), or can be easily extracted from the point cloud in such a form. Furthermore, in [MLS](#) sensing the road elevation is generally known, by considering the sensor's constant position relative to the vehicle's [GNSS](#) sensor - this is not the case in [ALS](#). Lastly, while the above method may work well in places where curbs are well-defined, this is not a reasonable assumption to make for an [ALS](#) dataset with nationwide coverage, such as our particular input.

The work [Vosselman and Liang \[2009\]](#) is not entirely bound by the above limitations. It demonstrates that a relatively simple approach can be used to detect curbs without the need for the point cloud to be comprised natively of cross-sections, and for accurate road elevations to already exist. However, the fact that it also uses curb detection with fixed thresholds undermines my confidence in it. Working with a national dataset and focusing on large roads (including motorways, one of our main targets for 3D conversion) means that the assumption that well-defined, relatively uniform road curbs will exist and be reliably detectable everywhere is not a sensible assumption.

### Other, purely Lidar-based approaches

There are many other papers that deal with this task without relying on external vector data. For instance, [Clode et al. \[2004\]](#) and [Clode et al. \[2007\]](#) present a set of methods in which first a [DTM](#) is generated, then points close to the [DTM](#) are selected and are further filtered based on intensity and sampling density thresholds applicable to reflections from flat bitumen surfaces. The results are converted to a raster mask which is then refined via morphological operations. It is then used to produce the output: a point cloud in which road points are marked semantically (i.e. they are classified as such). In the 2007 paper, they extended the procedure by convolving the results with a [PCD](#), which can create a 2D map of the predicted road parameters wherever it moves through road points. Like the morphological

operations above, the PCD-convolution is in fact a photogrammetric method, because it also acts on a raster generated from the classified point cloud prior to its application. Nevertheless, the method is still more relevant to us than the rest of the photogrammetry-based research mentioned here. An example visualisation of its output is shown in Figure 2.1, the vector magnitude in any given pixel quantifies the support that exists there for the presence of a road centreline - it is effectively a centreline detector. They describe it as an alternative to using the Hough-transform for finding road centrelines, which, according to their research, is not reliable enough in this context. This spatial map can then be used to generate a vector dataset describing the geometry of the roads.

The research [Gross and Thoennesen \[2006\]](#) shows that point neighbourhood information can be used to generate covariance matrices of individual points, which can in turn be used directly to indicate if the point belongs to a linear feature. They also describe how lines can be assembled from the selected points efficiently. Although their methods have very well documented mathematical foundations which could be reproduced in any programming language, their applicability in my research, especially in the context of small or even non-existent curbs, is uncertain.

Other methods relying purely on the Lidar points themselves exist, but like [Zhang \[2010\]](#), they are typically intended for real-time MLS applications - such as the fully convolutional neural network-based solution in [Caltagirone et al. \[2017\]](#). The literature review in [Yang et al. \[2013\]](#) offers an excellent overview of such additional methods, but they will not be described here any further, as I found them not to be relevant to this project.

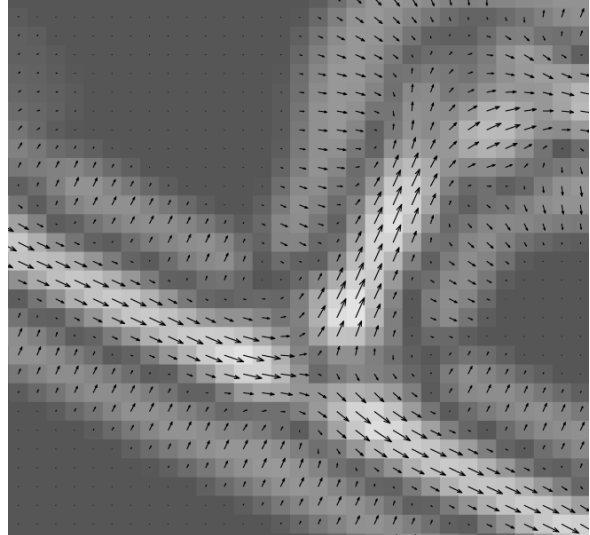


**Figure 2.1:** Illustration of the results of PCD convolution from [Clode et al. \[2007\]](#).

### 2.1.2 Research using input point clouds and approximate road locations

This section contains brief descriptions of research that used similar input data to mine *in addition to* Lidar data; mainly vector datasets estimating road centreline positions. These relevant papers describe work that used analogous input data to achieve similar goals to mine - as a result, they contain the methods that are the most relevant to my own research.

#### Relatively simple approaches

The work [Hatger and Brenner \[2003\]](#) presents two approaches based on region-growing. The first one is based on growing planes in the entire study area from Lidar points. Finding this to be too complex computationally, they propose another approach of treating Lidar scan lines individually, partitioning each into parametrised line segments via linear regression and then inspecting the succession of scan lines and identifying neighbouring segments that are roughly parallel. The resulting groups of (roughly parallel) 3D lines are then treated as cross-sections of planar regions, and an additional region growing step is performed to find any points that might have been left out in the previous steps. The results of this can then either be prepared as a full, 3D planar partition of the study area onto which road polylines can simply be projected, or they can be further refined first by eliminating small, meaningless planes via a RANSAC-based workflow.

The work [Cai and Rasdorf \[2008\]](#) shows that enriching road centrelines with elevations can be achieved using even more simplistic methods. Their first method is based on finding points on opposite sides

## 2 Related work

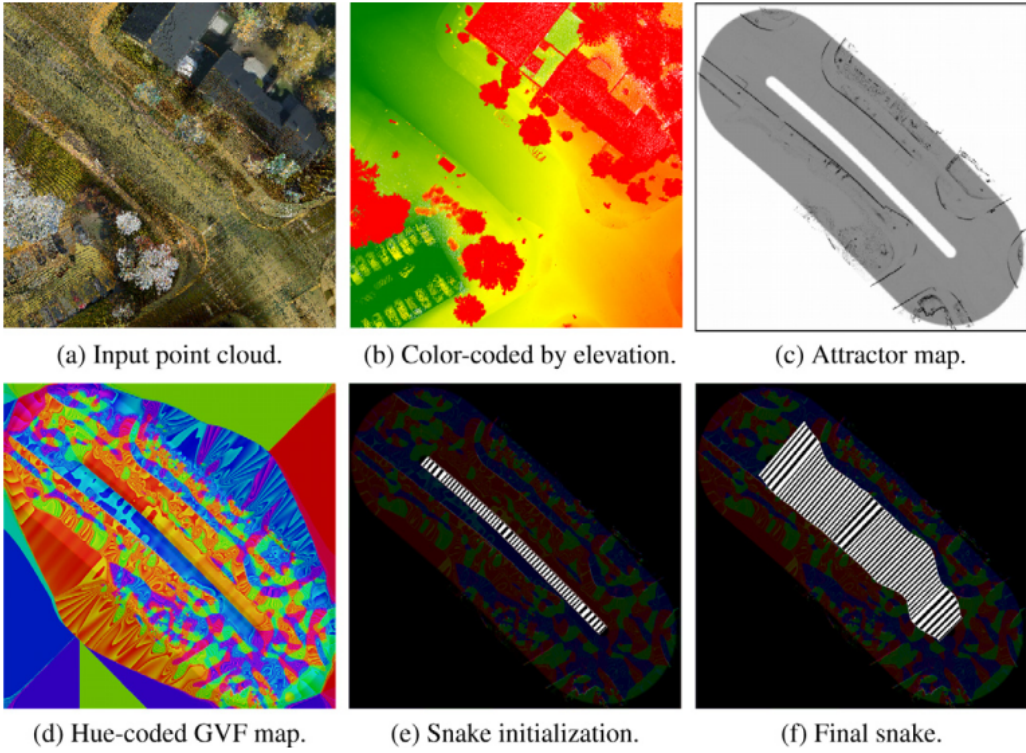


**Figure 2.2:** Illustration of the contour optimisation procedure used in Boyko and Funkhouser [2011].

of roads (in 2D) at similar distances from them, and in suitable locations to form approximate cross-sections. The centrelines are intersected with the cross-sections and are given elevations at the points of intersection. The elevations are computed by interpolating linearly inside the cross-sections, using the elevations of the two points that define each of them. Their second method is even simpler; for each road vertex (or some sampling along its length), they locate the closest Lidar point and associate its elevation with it. The simplicity of these methods is reminiscent of the [NDW](#) prototype and the commercial solution developed for [RHDHV](#) (described in Section 2.4), and highlights that a rough approximation for the road elevations can, in practice, be made either directly from the point cloud or from a derived [DTM](#) in a straightforward manner. However, far more sophisticated methods have been developed by other authors.

### Complex approaches based on active contour optimisation

One landmark paper, Boyko and Funkhouser [2011], describes a method in which a set of 2D input LineStrings are used to identify and label road points in an [ALS](#) point cloud. The input lines contain road intersection nodes and patches, from which centrelines are derived. They first associate the input lines with elevations by fitting spline curves through Lidar points close to the centrelines in 2D. Suitable Lidar points are selected by minimising an error function that includes terms related to the distance from the location of interpolation, and to elevation variance. The resulting network is guaranteed to be continuous and smooth because the densified input polylines are used as spline control points. Since the entire system of splines is connected, this is also guaranteed to minimise the effects of local issues, such as occlusion.

The point cloud is then partitioned on disk, based on fitting support planes along the 3D-converted lines and fetching points that are close to them, solving performance-related issues of working with too many Lidar points at once, and further minimising the effects of 2.5D violations related to overlapping features. They then construct scalar maps for each resulting segment that penalises points away from road edges (both inwards and outwards). These maps, called attractor maps, are composed from

rasters penalising locations that are outside the range in which edges are expected to be found (relative to the centrelines), and rasters produced by a curb detection metric related to the normal vectors of the point cloud points. Lastly, they apply an active contour optimisation technique (specifically, ribbon snakes) that yields the road edges in 3D, and then labels points between the two edges as road points. An illustration is shown in Figure 2.2, taken from their paper. In the attractor map, darker colours represent stronger attraction, resulting in the active contour converging to them in the optimisation procedure. The GVF map is a vector map that contributes to favourable active contour convergence and is not described any further here (please refer to the original paper). The initial contour is based on the road centreline (from external vector data).

The results of Göpfert et al. [2011] demonstrate that active contour optimisation can be used to estimate road outlines without the need for the involved pre-processing steps of Boyko and Funkhouser [2011]. They convert the input point cloud directly into a DTM, and then into attractor maps. They use the same general type of active contour optimisation, and generate output centrelines and road edges with comparable quality to that of the outputs of Boyko and Funkhouser [2011]. It is worth mentioning that the type of active contour optimisation used by these two papers also optimises the road centrelines in conjunction with the road edges, which is particularly important in places where the 2D georeferencing of the original centrelines is poor.

### Relevant work with Dutch data

The work Oude Elberink and Vosselman [2006] is relevant not only because of the methods it applies, but also the specific datasets. They enrich the best-known Dutch open data national topographical vector dataset (the present-day equivalent of which is BGT) with elevations, and as their source of elevations, they use Actueel Hoogtebestand Nederland (AHN) data (the first edition of AHN, the third edition of which I used in my own research).

They do not exclusively consider roads; all polygonal vector objects are extruded to 3D. Like in Hatger and Brenner [2003], a region growing approach is proposed as the foundation of the elevation extraction workflow. They use the Hough transform to find seed points whose neighbourhood suggests a planar structure, fit planes and then grow them by checking the point-to-plane distance of new points, labelling points with the identifier of the plane they belong to. The vector data is then overlain on these regions and for each polygon, the plane is selected which is represented by the greatest number of labelled points in its interior. These points are re-fitted a plane, and each such plane is used to extrude the corresponding overlaid vector geometry simply by projecting the polygon onto its surface. To improve upon the results of this simple extrusion, they suggest the application of algorithmic topological corrections. Furthermore, to model the interior of the extruded polygons in more detail, they recommend the construction of a constrained Delaunay triangulation (CDT) for each, first by inserting its edges as constraints, and then by inserting the Lidar points that its surface is based on. The CDT can be refined procedurally to ensure smoothness. The main limitations of their methods are that the extracted elevations (from the region growing approach) are not reliably accurate, and that it cannot handle overlapping objects, such as roads in motorway junctions. 3D visualisations of the results of this approach and typical artefacts are shown in 2.3. The specific artefacts shown

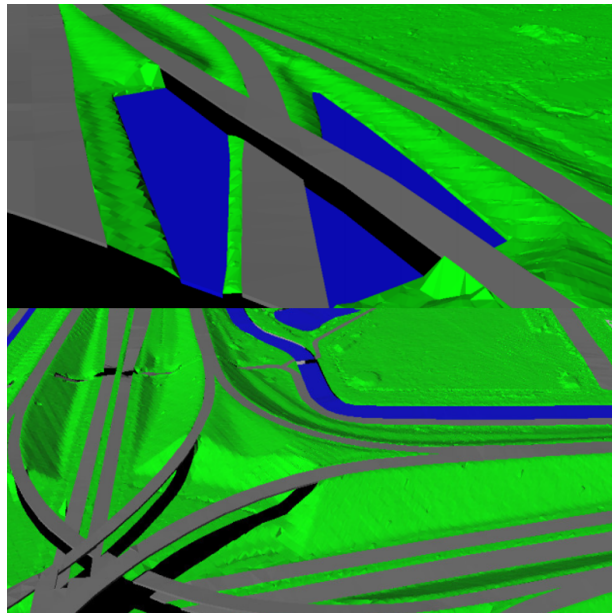


**Figure 2.3:** Examples of 3D-converted multi-level road vector geometry from Oude Elberink and Vosselman [2006].

## 2 Related work

in the figure demonstrate that in multi-level road layouts, only the topmost road is fully converted to 3D.

Their method was later extended in [Oude Elberink and Vosselman \[2009\]](#) to work well in complex multi-level road settings by using point cloud segmentation in a manner resembling what I already described in the context of [Boyko and Funkhouser \[2011\]](#), which we may regard in general as decomposing the 3D problem into 2.5D sub-problems, also a main aim of my own research. In his doctoral thesis [Oude Elberink \[2010\]](#) he combined this method with the overall procedure in [Oude Elberink and Vosselman \[2006\]](#) to form one integral whole. Furthermore he extended it with a road extraction quality and accuracy assessment procedure, which was later perfected and also published separately in [Oude Elberink and Vosselman \[2012\]](#).

Their quality and accuracy assessment methodology is comprised of two separate procedures and the comparison of their results: a theoretical (error propagation-based) evaluation, and an empirical one against reference data. Their error propagation-based evaluation takes into account metrics such as [GNSS](#) and inertial navigation system ([INS](#)) noise in the Lidar survey (suggesting that they had access to low-level information about the dataset), plane fit quality and observed Lidar noise. It also considers interpolation/extrapolation uncertainty, relevant in places where not enough relevant Lidar points could be located and thus such gap-filling measures were used. They found that these theoretical errors were generally below 20 cm, with noticeable increases only occurring where Lidar coverage was extremely sparse or non-existent, leading to the necessity of using interpolation or extrapolation.

Interestingly, their reference data was [DTB](#) for the empirical evaluation of accuracy, which is also the support dataset I used in my research (see Section 2.3.3). In general, their comparison with [DTB](#) showed good agreement with their road surface extraction results, except for the same places where the theoretical approach also suggested large errors, and in particular in places where this was also combined with intense vertical road curvature locally, which [DTB](#) managed to capture, but not their results. In places with good Laser coverage, the agreement was much better, often near-perfect. Although not explicitly mentioned, it appears that they still used the earliest version of [AHN](#) (not [Actueel Hoogtebestand Nederland 2 \(AHN2\)](#)) in this research, which may explain how it is possible that they encountered low point densities even in well-exposed road segments. [AHN2](#) and [AHN3](#) no longer have this problem, as mentioned in 2.3.2 and in many other subsequent parts of this report.

### On using a support dataset in addition to Lidar data

In Section 2.3 in this chapter, I discuss that this research is also concerned with another source of elevations, which I often refer to as the "support dataset" in this report because [AHN3](#) is given priority to in the analysis, wherever it exists. It is a 3D line dataset, not an [ALS](#) or [MLS](#) point cloud. The one area *not* explicitly covered in any of the papers I examined is the use of such external 3D vector data as a further constraint when extracting road elevations and/or geometries from point clouds.

In relevant work, occlusion is generally accepted to represent gaps in coverage, and elevations are simply interpolated or extrapolated inside them if possible - or if not, they are not considered any further. In the case of my research, [NDW](#) is interested in producing a 3D conversion of [NWB](#) with the highest possible *completeness*. Exploring how information from the two datasets can be combined is also interesting academically, thus my work will examine how [DTB](#) can be used to patch in gaps in [AHN3](#) coverage. While doing so, I will be building solely on my own ideas, as I could not find work that is directly relevant to this topic.

## 2.2 Lidar accuracy and sampling density

Relevant aspects of Lidar-related accuracy assessment can be divided into two main sub-topics: interpreting the reported global and/or local accuracy and areal sampling density of the Lidar surveys themselves, and assessing the accuracy of terrain models that one may derive from Lidar point clouds, and the elevations that can be interpolated from them. Although some of the relevant work I studied

overlaps with both of these areas, I separated the discussion below into two sections based on them. As Lidar sensing accuracy and sampling density underlies that of the derived models, I discuss it first below.

## 2.2.1 Accuracy description of Lidar sensing

### Global and local influences on accuracy

Many papers describe that the accuracy of Lidar-derived DTMs depends primarily on the accuracy of the sensing method itself. The notable paper [Hodgson and Bresnahan \[2004\]](#) describes the most fundamental sensing errors of Lidar measurements to be introduced by GNSS errors, INS errors, inertial measurement unit (IMU) errors, errors introduced by the waveform analysis algorithm and lastly, a general error factor that depends on the flying height. Combined, these are the primary factors that contribute to the *measurement* accuracy of the sensing system.

It is shown by various papers including [Hodgson and Bresnahan \[2004\]](#); [Su and Bork \[2006\]](#); [Kraus et al. \[2006\]](#); [Raber et al. \[2007\]](#); [Peng and Shih \[2006\]](#); [Chow and Hodgson \[2009\]](#); [Aguilar et al. \[2005, 2010\]](#); [Guo et al. \[2010\]](#) that there are local factors influencing *vertical* Lidar accuracy that are independent of the sensing equipment, and thus vary from survey to survey. In production datasets, whether they are considered at all or not, they are almost never *reported* locally, i.e. on the level of individual measurements. This is mainly because they are difficult to estimate without a complex analysis of the measured data and potentially, that of external data. Unless the global errors reported in the survey's specifications were derived empirically (e.g. by using ground control points), the effects of local factors specific to the survey may not be reflected in them at all, and they can be considered purely theoretical sensing-related values.

### What influences measurement accuracy locally?

First and foremost, local accuracy depends on the inclination of the surveyed terrain at the point where the Lidar reflection occurred, as shown in Figure 2.4. Any uncertainty in the lateral position of the point of reflection will be scaled by the tangent of the slope angle, denoted by  $\alpha$ . The vertical error thus increases linearly as a function of increasing slope (commonly derived from a 2D slope map). Therefore, if the accuracy of a Lidar survey was derived empirically, it will indicate higher errors than the sensing equipment's specifications would suggest, in survey areas with considerable relief.

Elevation accuracy also depends on the vegetation encountered. In all cases, the presence of vegetation decreases it, with the significance of the error depending strongly on the type of vegetation. Mature trees and evergreens tend to influence accuracy to a lesser extent, whereas bushes, shrubs and undergrowth in general tend to have a decidedly larger impact. [Peng and Shih \[2006\]](#) quantified this as a function of *vegetation angle*, a qualitative metric that describes how "open" certain types of vegetation are to Lidar. They found that there is a linear correlation between elevation errors and vegetation angle, as well as canopy volume. The one exception I found is [Raber et al. \[2007\]](#) which reported specifically that in very strongly vegetated areas, no correlation could be found between vegetation classes and accuracy (or even point density and accuracy). Still, the majority of relevant research indicates that Lidar accuracy reflects the extent and type of vegetation coverage in addition to its dependence on the relief of the surveyed terrain.

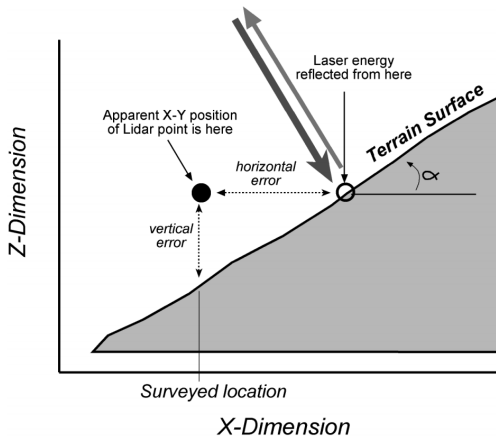


**Figure 2.4:** Illustration of the effects of terrain slope on vertical accuracy from [Hodgson and Bresnahan \[2004\]](#).

## 2 Related work

Both the official quantification of measurement accuracy and research tackling these topics often uses empirical methods. They generally consist of surveying ground control points accurately and either directly comparing these with nearby Lidar points, or first constructing a spatially continuous DTM and comparing the DTM-interpolated elevations with the surveyed reference elevations, with the latter approach being more relevant to the next section. The global value is usually specified as the measurement error (in metres or centimetres) at one or two standard deviations, with separate values given for horizontal and vertical errors. The two errors differ in terms of the equipment influencing them, and also because the local factors I outlined above affect elevation accuracy only (as a *function of* horizontal accuracy in the case of local terrain slope). They are generally reported as one or two standard deviations, corresponding to 68% or 95% confidence, in metres or centimetres.

### Sampling density as a survey property

Sampling density describes how many reflections the sensor records per unit area. This is the third descriptor that is commonly found in the documentation of Lidar datasets, and like vertical and horizontal accuracy, it is generally represented by a single global value. This, too, fluctuates locally, and in this case anything between zero and the maximum nominal value of the survey's sampling density is possible. The maximum possible value depends on the sensing equipment and the number of times any given area is scanned (the number of passes). Sampling density does not directly affect the accuracy of individual Lidar measurements, which is one of the reasons why it is reported separately - its effects are more relevant to the next section.

Sampling density is mostly reported as the mean number of points per square metres found in the dataset, occasionally as a range if one or two standard deviations are taken into account. It can be derived from the data directly, i.e. it needs no additional processing or surveying. Relevant studies report that sampling density varies mostly as a factor of terrain relief, vegetation cover, and vegetation angle, with increases in any of these factors resulting in decreases in local point density. For instance, sampling density falls off logarithmically with increasing terrain slope ([Peng and Shih \[2006\]](#), [Chow and Hodgson \[2009\]](#)).

### 2.2.2 Accuracy description of Lidar-derived DTMs

#### Spatial interpolation in the context of DTMs

In practice, the quality and accuracy of Lidar-derived DTMs is most commonly evaluated via sampling their surfaces to serve as the basis for comparisons. Sampling a DTM takes place via spatial interpolation. The DTM's relationship with the raw data can be established by interpolating at the horizontal locations of Lidar points, while that with the real-world terrain can be examined via surveying control points and interpolating at their 2D positions in the DTM. Intuitively, DTMs provide a link between ground control points and Lidar measurements, which in turn also provides a convenient interface for evaluating Lidar survey accuracy empirically (as I mentioned in the previous section), provided that interpolator's effects on accuracy are known.

Raster DTMs are themselves produced via spatial interpolation. One may convert a Lidar point cloud into a TIN-based DTM without interpolation (the TIN vertices will be Lidar points), but to create a raster DTM, one will need to use a suitable interpolator, such as inverse distance weighting (IDW). Alternatively, a TIN-based DTM can be constructed as an intermediate model and the raster can be derived from it via applying a TIN-based spatial interpolator, such as the Laplace interpolator. These observations entail that a comparison between the Lidar points and their TIN-interpolated counterparts would yield no residuals, i.e. TIN models do not lose information relative to the *ground reflections* found in the Lidar data.

### Evaluating interpolation accuracy

Spatial interpolators do not leave accuracy unchanged, which cannot be neglected when performing the above benchmarks. For us in this research, the effect interpolators have on accuracy is particularly interesting because the final [NWB](#) elevations are produced via spatial interpolation in a Lidar-derived [DTM](#). There exist various approaches to establishing the nature of the relationship between input and output accuracy, such as deriving exact error propagation formulae from the mathematical descriptions of interpolators, as well as the more popular empirical approaches based on *testing* accuracy post-interpolation via split-sample, cross-validation or jack-knife methods. Theoretically, input accuracy (survey accuracy) and any necessary metrics of local influences can then simply be plugged into the formula to obtain the local accuracy post-interpolation.

### Propagating local factors through interpolation

However, we know from the previous section that the survey accuracy is *itself* influenced by local factors. Since only global accuracy values generally exist for Lidar surveys, the theoretical or empirical error propagation formula may need to be extended with additional terms approximating the influence of these additional factors, depending on how accurately one wishes to approximate output accuracy. The exact nature of this part of the relationship depends on the fundamental principles I outlined in the previous section, and it too, can be modelled both theoretically and empirically. Theoretical approaches are more common for simple relationships (such as that with local slope, as shown in Figure 2.4), while empirical ones are almost always employed in more complex ones (such as the relationship with vegetation). In the context of digital terrain modelling, there is an additional factor we need to consider: ground filtering accuracy. While we wish to model the terrain surface only, the raw Lidar data includes non-terrain reflections that need to be removed before constructing the [DTM](#). This accuracy is also generally estimated, rather than derived theoretically. It is also possible to try to derive the combined effects of all these factors at once, e.g. via Monte Carlo simulations.

For instance, the research [Aguilar et al. \[2010\]](#) applies a hybrid empirical-theoretical method, in part propagating errors mathematically through the [IDW](#) interpolator to obtain part of the relationship, and for the other part relying on Monte Carlo simulations. They model accuracy to be a factor of the error-propagated value computed from global Lidar accuracy, as well as sampling density, terrain slope and ground filtering accuracy. The research [Kraus et al. \[2006\]](#) also applies mostly theoretical methods to analyse errors propagating through the moving [MLE](#). Post-application statistical evaluation was performed by for instance in [Peng and Shih \[2006\]](#) (jack-knife, using surveyed reference points), and [Guo et al. \[2010\]](#) (ten-fold cross-validation). Notably, [Smith et al. \[2005\]](#) used all three approaches (split-sample, cross-validation, and jack-knife) for a wide range of interpolators in an urban setting.

Like [Aguilar et al. \[2010\]](#), many of the other papers also examined the influence of gridded [DTM](#) resolution on accuracy, i.e. the effects of Lidar sampling density in conjunction with the raster cell size. [Chow and Hodgson \[2009\]](#) examined via regression techniques (on [IDW](#) interpolation) how it is correlated with point density and found that the effect of increasing the cell size has a more severe negative effect on accuracy than that of gradually decreasing sampling density, and that a certain degree of correlation between them is observable. [Guo et al. \[2010\]](#) argues that for most interpolators, the overall trend is mainly linear between accuracy and grid resolution, up to the scale of the Lidar point density, from where no further increase is observable. They also found that differences in accuracy between interpolators were most prominent at the finest resolutions they examined. [Bater and Coops \[2009\]](#) found that the local influence on accuracy of slope and point density are mostly invariant relative to [DTM](#) resolution, i.e. no correlation is observable. In the case of [TINs](#) constructed from Lidar points directly, cell size and point density are in a more direct relationship, i.e. only by ignoring Lidar points can one increase the cell (triangle) sizes.

## 2 Related work

### Which interpolator is the best in terms of accuracy?

In terms of the accuracy and quality ranking of interpolators, there is a clear consensus that no such ranking exists that is independent of the size and type of the study area, and the purpose of the interpolation. For instance, the accuracy of piecewise spline-based, quintic-type, kriging and ANUDEM methods were found lacking in the context of their insensitivity to small, sudden changes (such as natural faults in the terrain and anthropogenic modifications thereof) while they were proven to work well for large-scale terrain, as described by [Bater and Coops \[2009\]](#) and [Guo et al. \[2010\]](#) for instance. All reviewed papers agreed that the accuracy of all interpolators decreases the most in areas of *high topographical relief* (also called surface ruggedness and surface heterogeneity) and *reduced point density*, with spline-based, [IDW](#) methods generally producing the worst results in such areas - especially for large-scale terrain.

The relative importance of interpolation-introduced errors is reportedly *low* relative to instrument-related errors and surface-related local sources of error, according to research such as [Hodgson and Bresnahan \[2004\]](#) and [Aguilar et al. \[2010\]](#). The former, which used TIN-linear interpolation, goes as far as to state that the decrease in accuracy after the application of an interpolator is insignificant, or that interpolation may even increase the overall accuracy. This is supported by the error propagation formulae derived by [Fan et al. \[2014\]](#) for the same interpolator, which shows that in areas with negligible relief, the input error may decrease by as much as 50%. [TIN](#)-based interpolation methods were recommended specifically by [Bater and Coops \[2009\]](#) for complex geometries and found it in their research to be the most conservative in terms of [RMSE](#)-analysis. Furthermore, [Peng and Shih \[2006\]](#) also used [TIN](#)-based interpolation in their research, in which they found local influences on elevation accuracy highly predictable. Unlike most papers, [Aguilar et al. \[2010\]](#) considers the accuracy of ground filtering explicitly, and states that its success is a precondition of accurate terrain interpolation wherever the terrain is occluded or shaded partially.

### Oversampling the terrain

The point is made in several of these papers that because of the commonly seen logarithmic correlation between point spacing and accuracy, increasing the target point density of a survey is only justified up to a certain point. This depends strongly on the study area because point density itself is correlated with the vegetation cover and the terrain relief. It is argued by several authors, most prominently by [Guo et al. \[2010\]](#), that in vegetation-free areas of low relief, most [ALS](#) surveys oversample the terrain by as much as 30 to 50 percent, leading to increased processing times, reduced algorithmic stability, and no improvement in accuracy. [Bater and Coops \[2009\]](#) comes to the same conclusion, and the logarithmic trend generally observed between point density and elevation accuracy further supports this. Conversely, in rugged, vegetation-covered terrain additional cross-flight surveys can increase accuracy significantly by improving ground point density, as [Peng and Shih \[2006\]](#) noted.

The matter of oversampling the terrain is particularly important when using [TIN](#) models, because they use the Lidar points directly and may become too complex to process and visualise when they become too detailed. Considering the above correlations between point density and most other influences on accuracy, we may then assert that for flat, well-exposed surfaces the sampling density may not need to be high. This is particularly important in the context of this research, because roads represent such surfaces in most places.

## 2.3 Input assessment

In terms of comparing our results with the commercial ones, we were particularly interested in revealing how the effectiveness of the two sets of methods differ. To make it straightforward to isolate differences related strictly to how well the methods perform, we decided to use the same set of datasets as input, as [RHDHV](#). This means that in addition to using [NWB](#), we made use of the same two elevation sources as they did.



**Figure 2.5:** An example render of NWB, colour-coded to indicate the owner.

In addition to helping with isolating purely processing-related differences between the results, these datasets have the additional benefit of being open data. This fits well with the mentality represented by those concerned with this research, as well as the faculty in general. For the same reason, the implementation created as part of this project is also made available in the same manner, i.e. it is open-source. Alternatives, such as Kadaster's orthoimagery-based point cloud were considered, but eventually excluded from further consideration, due to not being open data, and offering inferior overall accuracy compared with [AHN3](#) and [DTB](#).

- NWB - National Road Database
  - AHN3 - Current Dutch Elevation
  - DTB - Digital Topographic Database

In the sections below, I will present the result of assessing the general properties and quality of each of the three datasets listed above. As this project does not specifically concern the formal quantification of the accuracy of these datasets, it will rely on the global, nominal values provided in the specifications of the datasets. Regardless of this, I still present qualitative results on this topic based examining the degree of agreement between them and attempting to explain the differences based, both below and in Chapter 4.

### 2.3.1 Nationaal Wegenbestand – NWB

[NWB](#) (or more specifically, NWB-Wegen, the [NWB](#) roads product) is a vector dataset comprised of a semantically enriched set of 2D LineString objects released in the *ESRI Shapefile* format. The LineStrings - dubbed *wegvakken* in the documentation - are interconnected in such a way that [NWB](#) can be regarded topologically as a graph representation of the Dutch road network. Although [NWB](#) contains all named and numbered roads in The Netherlands, we are only interested in roads that are semantically marked as state-owned or province-owned (Rijkswegen (motorways) ([R-roads](#)) and Provinciewegen (provincial roads) ([P-roads](#)) respectively), because the new noise regulation only concerns these types. The [NWB](#) product is managed by [NDW](#), but it is owned by [RWS](#) ([NDW](#) being a division of [RWS](#)).

NWB and the road types it contains are illustrated in Figure 2.5. Yellow is used for R-roads, red denotes P-roads and magenta means Gemeentewegen (municipal roads) (G-roads). RWS-managed roads (W-roads)

## 2 Related work

are not shown in this figure. Blue roads are roads which do not fall into the above 4 categories, in this case they are managed by the TU Delft. This render also contains examples of challenging 3D relationships. Where the provincial road Kruithuisweg crosses the municipal road Schoemakerstraat and the motorway A13, no intersection occurs in 2D because the roads cross over one another in 3D. These locations are indicated in the figure by red circles. Furthermore, where the bike path IJsmestertunnel (a municipal road in [NWB](#)) crosses the A13, a series of 3 short tunnels are located in reality. This is indicated in the figure by a blue oval. Although not all these road types are relevant to this project, the 3D relationships represented by these examples still are.

In addition to representing the topology of the road network, the [NWB](#) lines are georeferenced with mediocre accuracy to also represent its approximate spatial layout. The quality description includes only a single figure, which is 5 m accuracy at 95% confidence, i.e. two standard deviations from the mean. It is not described in any detail, how the accuracy is evaluated for each road, for instance whether it is based on the accuracy of the vertex locations of the road, an arbitrary sampling along their length, and how exactly these are aggregated into the error figure. Furthermore, we do not know whether the reference for the accuracy assessment was empirical (surveyed control points) or whether it is purely theoretical and is based on the sources and the methods involved in creating and updating the dataset.

Adding to the uncertainty is the fact that both the topological and the geographical information content of [NWB](#) is assembled from a wide range of providers ranging from large national providers such as [RWS](#) and Kadaster, to local providers such as specific road authorities and civil engineering agencies. No clear indication is given in the documentation about the sources used for the compilation of specific [NWB](#) road types or the estimation of their accuracies, but it is mentioned that they are not the same ([Rijkswaterstaat \[2020c\]](#)).

In interpreting the 5 m accuracy, it is important to note that the [NWB](#) lines represent road centrelines, but not of the whole paved surface. The centrelines in [NWB](#) approximate the centre of the traffic-occupied parts the roads, excluding hard shoulders and other paved surfaces connected to the road. It is also important, that [NWB](#) often does not contain vertices for more than 200 m based on my inspection (where roads are relatively straight), and even in sharp bends for up to 20-30 m at a time. Especially in bends, this circumstance, combined with the official error figure, means that [NWB](#) often leaves the traffic occupied road surfaces, and sometimes even the paved areas. I confirmed this problem by comparing [NWB](#) with [DTB](#), [AHN3](#).

One such comparison is shown in Figure 2.6. [AHN3](#)'s ground points are coloured blue in this figure, and [NWB](#) centrelines are shown in white. As they have no elevation, they appear below [AHN3](#) points and are consequently masked out partially by them. I shifted them to match [AHN3](#)'s mean elevation locally, to make them better comparable. Comparisons such as these reveal that [NWB](#) gets close to the edges of the paved surfaces quite often, and sometimes even leaves their surface. In sharp bends, this is made worse by the angularity introduced by the coarse lengthwise discretisation of [NWB](#), for instance in the location pointed out by the green arrow. In later stages of the project, I made further comparisons with [BGT](#) and with orthoimagery (Luchtfoto 2020 from Kadaster), discussed in Section 4.3.3 and with an example shown in 4.20. These comparisons further confirmed the issues.

Although the above nominal accuracy and its description are certainly not good enough for compliance with the new noise regulations, the 3D conversion of [NWB](#) is not concerned with improving it – in fact, it is a requirement of the project not to displace [NWB](#) horizontally. Hence, we may say that the intended outcome of the 3D conversion is to devise a method that can produce accurate elevations for [NWB](#) assuming that its accuracy complies with the requirements set by the new noise regulations - 20 centimetres at 95% confidence. To achieve this compliance in practice, lateral refinement is being carried out in a separate project by matching [NWB](#) roads with their counterparts in other, more accurate datasets. Specifically, [DTB](#) is being used for this purpose, as well as another open data dataset called [BGT](#). As these datasets are already theoretically compliant with the accuracy requirements, correcting [NWB](#) geometries based on them will foreseeably solve the lateral accuracy problems of [NWB](#). However, at the time of writing of this report, the [BGT](#)-based correction has only been released for municipality-owned roads (category G for Gemeente - not relevant to us), while the [DTB](#)-based corrections for motorways are still being finalised. Consequently both the commercial and the scientific 3D-NWB project still rely on [NWB](#) data that lacks this correction ([NDW \[2020\]](#)).

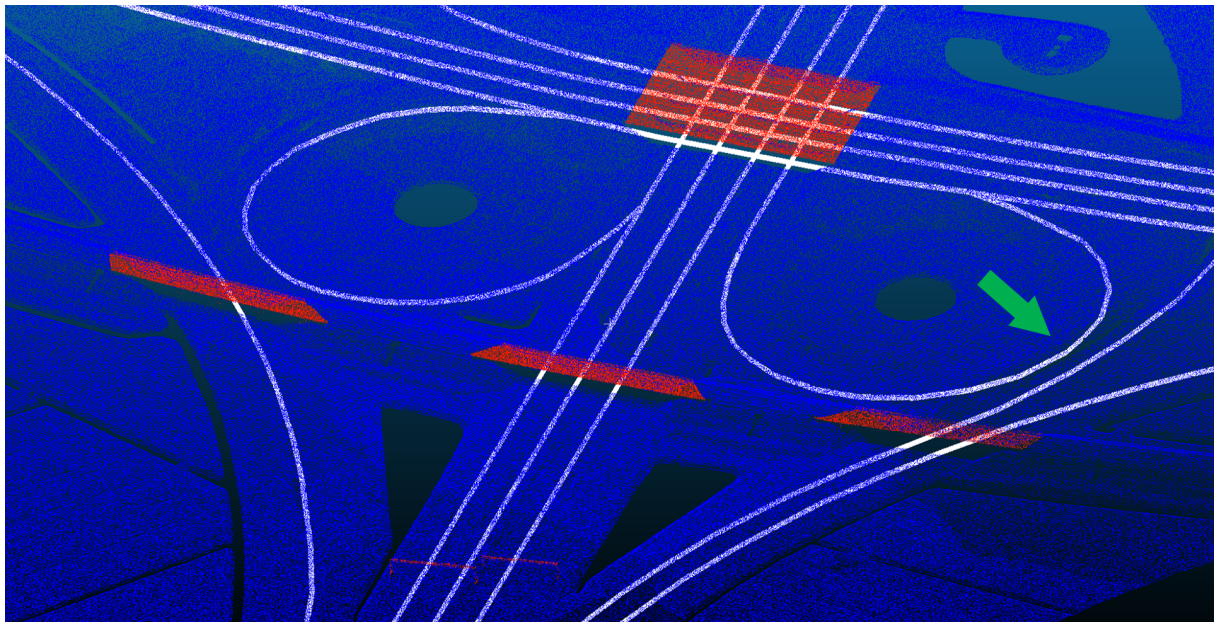


**Figure 2.6:** Render comparing [AHN3](#) with the relevant 2D [NWB](#) centrelines.

Regardless of improving [NWB](#)'s lateral accuracy not being within the scope of this project, it is important to be aware of it, because of its implications when overlaying [NWB](#) with [AHN3](#) and [DTB](#) in the processing part of this research. The problems caused by it and the necessary workarounds are discussed in-depth in the relevant sections of the next chapters.

The [NWB](#) product is updated every month with particular attention to always including new roads, removing outdated (demolished or permanently closed) roads and updating refurbished roads as necessary. This frequency means that [NWB](#) is always up-to-date with changes to the road network, at least to the extent where navigation (in e.g. Google Maps, which uses [NWB](#)) can take place without any disruptions. However, this does not mean that [NWB](#) has a temporal resolution of one month; for that to be true, all roads would need to be re-measured every month. The monthly releases merely mean that effort is concentrated into releasing known changes to the road network frequently. Since no physical phenomena exists that would move the roads laterally (without human intervention) by a significant distance, this does not cause issues in practice.

### 2.3.2 Actueel Hoogtebestand Nederland – AHN

AHN are [ALS](#) datasets available as open geospatial data in The Netherlands. The surveys are commissioned every few years with [AHN](#) (the first version) to [AHN3](#) already complete (1996 to 2019), and the first AHN4 tiles nearing release. At this stage of the project, we are interested only in [AHN3](#), as it is the most recent iteration of this product. The [AHN](#) product is owned and managed by [RWS](#).

The dataset has a combined systematic and stochastic elevation error of 15 centimetres at two standard deviations (i.e. 95 % confidence), and 6 to 10 points per square metre point density on average, corresponding to a 0.32 to 0.41 metre posting distance. The lateral error is 18 centimetres at two standard deviations ([Rijkswaterstaat \[2020a\]](#)). Comparing these to the descriptors of Lidar datasets used in the research examined as part of our literature review (see the Relevant work section), we may assert that [AHN3](#) can be considered accurate, and to have excellent point density. It is especially accurate and dense relative to the older Lidar datasets that are mentioned in these papers, including the first iteration of [AHN](#).

The [AHN3](#) point cloud has been classified semi-automatically with similarly excellent accuracy and is released with the classification included. This means that for most purposes, the point cloud needs not

## 2 Related work

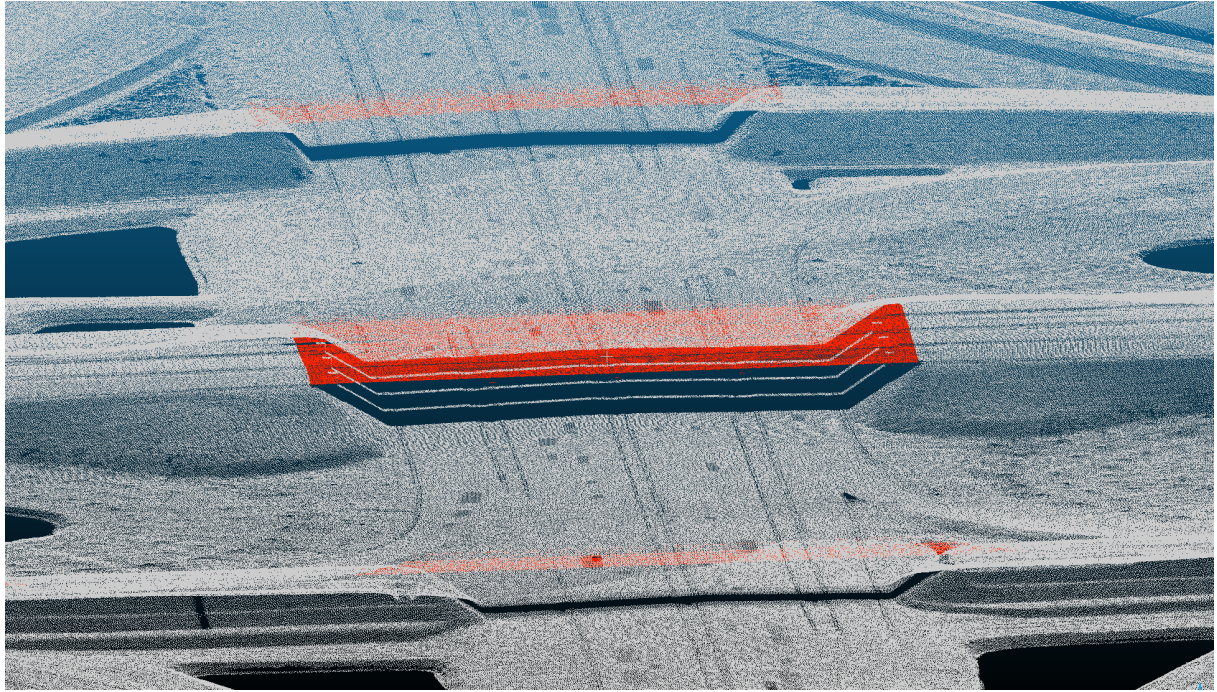


**Figure 2.7:** Example render of [AHN3](#) at Knooppunt Deil, SW of Geldermalsen, showing ground points and bridges.

be ground filtered by users, and that extracting certain features is made far easier. Of the various classes available, we are interested in class 2 the most, which corresponds to ground points, and class 26 which contains, among other things, bridge structures and the roads that are found on them.

Ground points are primarily interesting to us because they contain the points reflected from land-based roads. This includes roads that were constructed directly on the terrain, as well as roads constructed on altered terrain, such as elevated ground or open trenches. It also contains the points that represent the terrain in the vicinity of the roads. Elevated roads and bridges are not considered ground points and are generally represented by gaps in class 2, which can, in most cases, be filled by using data from class 26, as shown in Figure 2.7. The white colour corresponds to ground points (class 2), red corresponds to bridges (class 26). All other classes were removed. The shapes of motorway lanes and ramps, as well as bridges are clearly defined. Road constructed on elevated ground is reliably classified as ground, bridges are cleanly split off by the classification. Even under thin bridges, data becomes gradually sparser at the border and becomes extinct directly below the bridge. This render also makes it clear that wherever vehicles were encountered on ground-based roads, the sampling is worse locally. It does not *generally* go entirely extinct however, as most locations have been scanned multiple times. Data gaps are only observed where slow or stationary vehicles were encountered.

Class 26 also contains other types of objects, for instance large motorway signs arching over road surfaces, as well as the civil engineering structures of elevated roads and bridges (in addition to the road surfaces on them). Reflections from vehicles transgressing bridges are also present in this class. Figure 2.8 shows a render from the same location as 2.6 and 2.7. The full-width motorway signs are clearly visible above the motorway lanes, coloured red because they originate from class 26. It also shows that the presence of water results in holes (the dark, linear features running parallel with the motorway in this render) in the ground-only point cloud. In this render, it is also visible that in my testing datasets, all points falling outside a 150-metre buffer zone around the NWB centrelines were removed (see more information on this in Section 4.1.2)

[AHN3](#) is released in the form of a point cloud, as well as DSM and DTM rasters. Both were produced using basic radial IDW interpolation with a fixed parametrisation. The DTM was generated by including only points from class 2 in the interpolation step. They are available at 0.5-metre and 5-metre resolutions, with the 0.5-metre resolution being relevant to this project in terms of the target accuracy. For con-

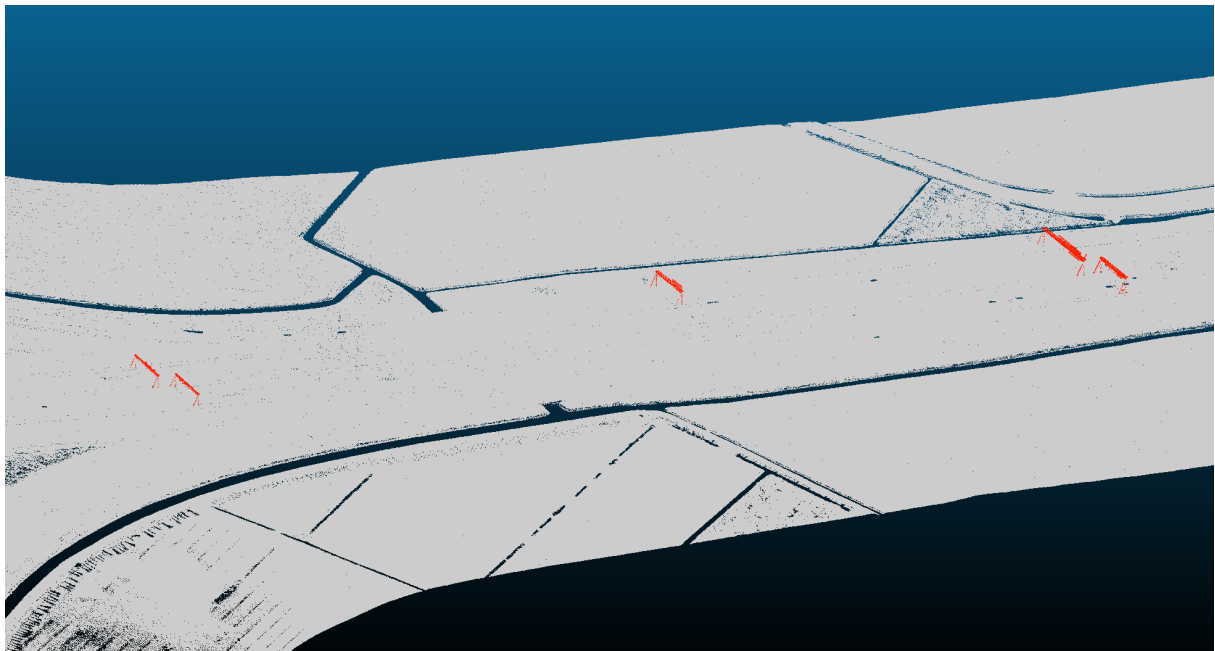


**Figure 2.8:** Example render of [AHN3](#) at Knooppunt Deil, SW of Geldermalsen, showing ground points and motorway signs.

text, this raster converts (on average) 1.5 to 2.5 points into a single raster cell based on [AHN3](#)'s nominal sampling density. The commercial implementation uses these rasters, as explained in Section [2.4.2](#).

The Lidar tiles are released in the binary LAZ format (compressed LAS, or LASzip), and are generally several gigabytes in size. As each tile only covers an approximate area of 32 square kilometres and the LAZ compression ratio for this dataset is 0.1 on average, scaling considerations are relevant to this project if the implementation is to be capable of fully converting [NWB](#) to 3D using the raw point clouds rather than the rasters.

### 2.3.3 Digitaal Topografisch Bestand – DTB

Like [NWB](#), [DTB](#) (or more specifically, [DTB-Droog](#), the [DTB](#) product relevant to roads) is a Dutch open data geospatial dataset in the *ESRI Shapefile* format. For the purposes of this project, we only need only those [DTB](#) line features, which correspond to street surface markings, hence we can also regard this as a dataset comprised exclusively of [LineString](#) objects, making it identical to [NWB](#) in its data structure apart from being a 3D dataset. [DTB](#) is also managed by [RWS](#) and it is concerned only with state-owned roads and roads on state-leased land, which translate almost exclusively to [NWB R-roads](#), that is, motorways. [DTB](#) is, hence, not a reliable source of information about provincial roads elevations ([NWB P-roads](#)), our other road type of interest.

There are various types of [DTB](#) road markings that are of interest to us, the main one being a category called *verflijnen*. These [DTB](#) lines represent the painted lines marking the outermost edges of the area open to traffic. This is a lucky correspondence with [NWB](#), as it too, contains the centrelines of the areas of roads that are open to traffic. The other two types I found to be reliably represent road surface elevations are the categories *verfstippellijn* and *blokmarkering*, which are lane separation lines and block marks respectively. The category *lijnverlichting* also appeared to be interesting at first, as it corresponds to road surface lighting features (not street lighting). However, I found it to not be reliably located on road surfaces in practice, hence I excluded it from further consideration.

Figure [2.9](#) shows a visual comparison with [NWB](#), illustrating various types of significant issues that primarily stem from [NWB](#)'s crude georeferencing. [NWB](#) symbology is identical to that which I used in [2.5](#), and blue dashed lines are the [DTB](#) lines. Only *verflijnen* are present in [DTB](#) in these locations. The

## 2 Related work

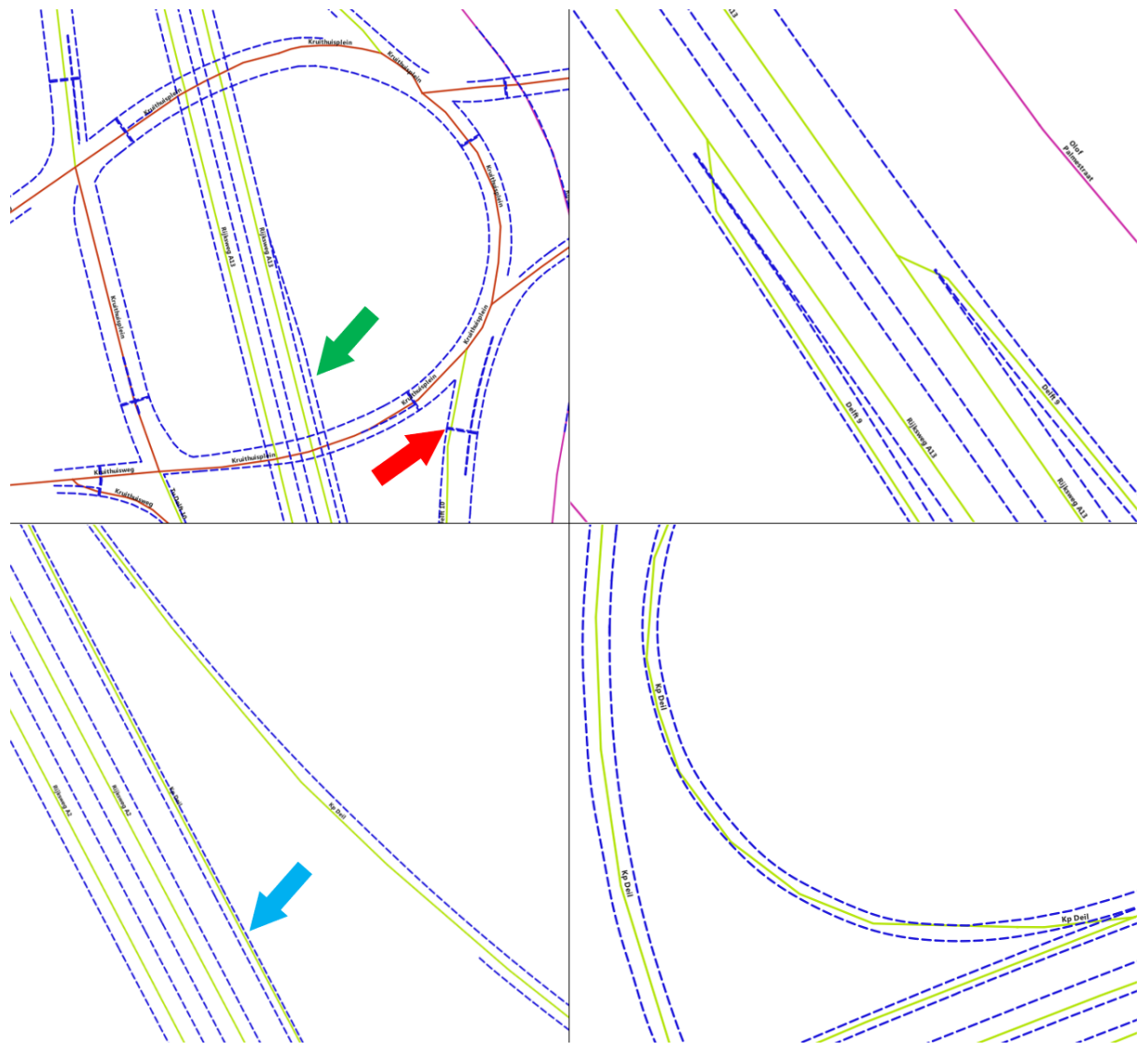


**Figure 2.9:** Renders of DTB *verflijnen* overlaid with NWB centrelines, illustrating "compatibility issues" and individual DTB issues.

image in the top left shows that in practice [DTB](#) contains many road markings, rather than just one on either side of [NWB](#). The illustration in the top right shows that [NWB](#) motorway ramps often merge with the motorway lanes at unrealistic angles, causing [NWB](#) to intersect the [DTB](#) edge markings at these locations. The image in the bottom left illustrates that while in some places there are many [DTB](#) road edges, in other places they are incomplete or missing entirely. Furthermore, [NWB](#) centrelines may also get very close to [DTB](#) edges outside of sharp bends and motorway ramps, as indicated by the blue arrow. In the bottom right, the figure shows that [NWB](#) discretisation and inaccuracy leads to angular lines in sharp bends. [NWB](#) often gets close to, or even intersects [DTB](#) in such places.

Like [NWB](#) (but unlike [AHN3](#)), [DTB](#)'s production pipeline also concerns several organisations performing various types of sensing, which are then semi-automatically assembled into the complete [DTB](#) product. While many [DTB](#) features are photogrammetry-derived, road surface markings are mainly from accurate land-based manual surveys or extracted from car-mounted [MLS](#) data ([Oude Elberink and Vosselman \[2012\]](#)). The documentation of [DTB](#) consists of its formal specifications ([Rijkswaterstaat \[2020d\]](#)) and a handbook ([Rijkswaterstaat \[2020b\]](#)). The former contains the accuracy-related details, reporting 10 cm vertical and 5 cm horizontal standard deviations, or 20 cm and 10 cm at 95% confidence to make it comparable with the reported accuracy of [NWB](#) and [AHN3](#).

Theoretically, [DTB](#) is not only accurate, it also has a good temporal resolution. It is updated multiple times a year, specifically to always be up-to-date in terms of newly constructed roads and refurbished roads - just like [NWB](#). This update frequency is comparable to that of [NWB](#), which is part of the reason why it forms part of the commercial solution. The other part of the reason is, that it theoretically always contains data for occluded roads, even in tunnels. This means that the combined information content of [DTB](#) and [AHN3](#) theoretically amount to having complete coverage of the Dutch road network. Because of the ease with which elevations can be extracted from [DTB](#) to be used in the 3D conversion of [NWB](#) (especially considering the crudeness of [NWB](#)'s georeferencing) prompted [NDW](#) to consider [DTB](#) as its *primary* dataset, wherever it is available.

In practice, I found evidence to support that the above decision is fundamentally flawed, already during the input assessment stage of my project. There are places where [DTB](#) lives up to the above *theoretical* standards, but this is not the case in most of the areas I examined. Even in terms of motorways, [DTB](#) is often incomplete to the extent that it lacks coverage over tens of kilometers. Even where it exists, its coverage may be patchy, especially in sharp bends. An example is shown in Figure 2.9. Commonly it only contains a single line rather than the theoretical minimum of three (two edge markings and one separation line). The separation line is the one I observed to be missing the most frequently.

Furthermore, already by considering the update methodology of the dataset, one may remark that some of the elevation measurements in it must be very outdated. Indeed, most of them are almost as old as the roads themselves, meaning that they were taken more than 20 years ago. This is where it comes into play that the update methodology of [NWB](#) and [DTB](#) does not really represent a high temporal resolution. In the absence of a physical phenomenon causing significant lateral ground motion, this does not cause problems with [NWB](#), but there *is* one that may move roads up or down: subsidence. Although the surface load due the weight of the road and passing vehicles may play a role, subsidence is primarily caused by natural, geological processes. In some parts of The Netherlands, groundwater and natural gas extraction may also play a role. Although this work does not specifically study the correlation between subsidence and problems with [DTB](#), there is little else with which the 0.5 to 1 m differences between [AHN3](#) and [DTB](#) could be explained. The [AHN3](#) measurements are at least 15 years more recent than the oldest ones in [DTB](#), which is where the biggest differences can be observed in elevation, as one would expect from subsidence.

Interestingly, the opposite can also be observed, although less commonly, and in a highly localised manner. In some places, [DTB](#) is above the road surface measurements of [AHN3](#) by a significant margin, often by more than 0.5 m. While subsidence cannot be used to explain these disagreements, there is evidence to support that the elevations in [AHN3](#) are indeed correct and the ground has shifted upwards noticeably. The latest subsidence survey of The Netherlands reported positive changes in addition to the decreasing elevations that are associated with subsidence. I primarily observed [DTB](#) to be below [AHN3](#) where this map indicates negative elevation changes, and above in regions where no changes or slightly positive changes were observed in the subsidence study, verifying my hypothesis.

## 2 Related work

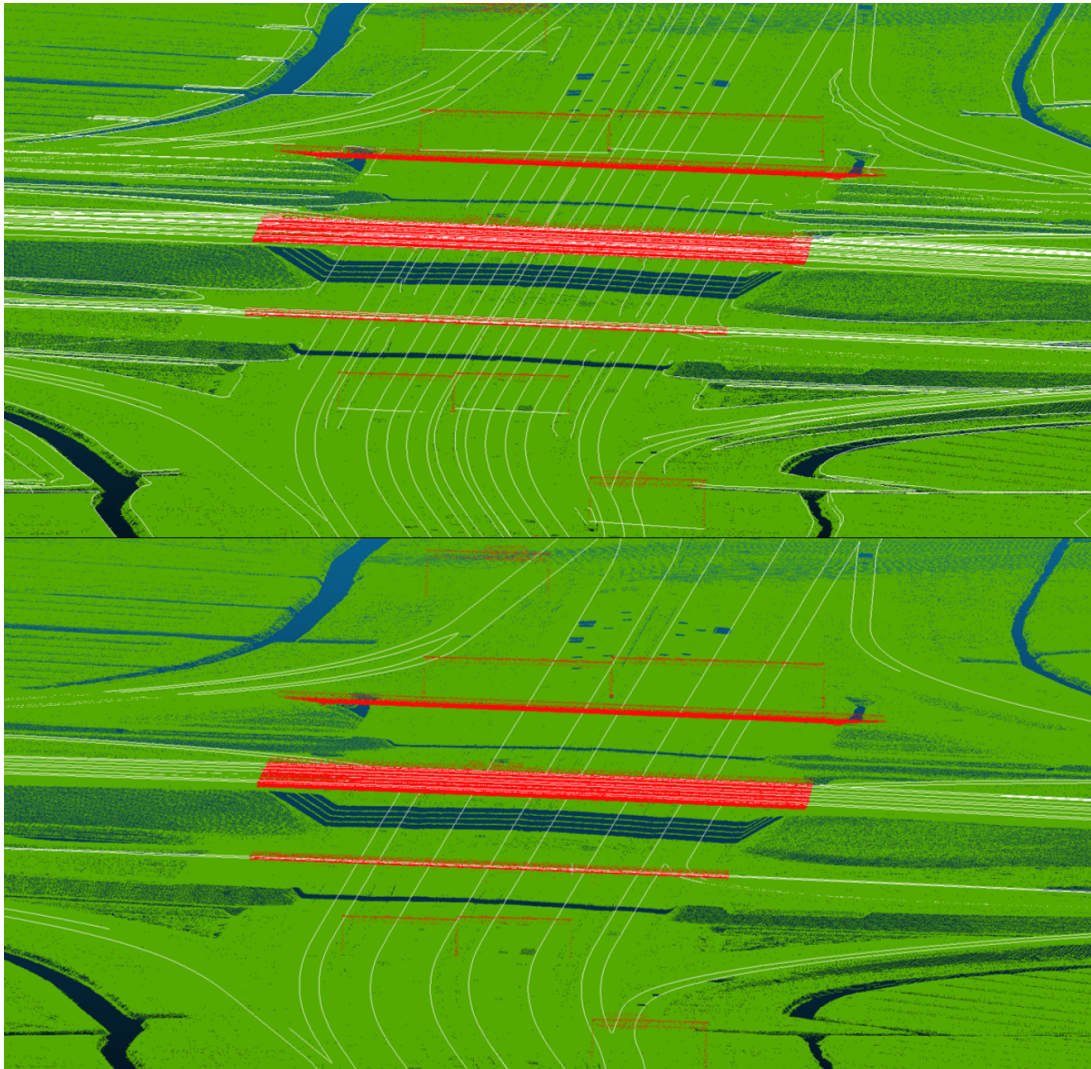


**Figure 2.10:** Renders of [DTB](#) all line features (above) and [verflijnen](#) only (below) overlain with [AHN3](#) in 3D.

Figure 2.10 shows renders of [DTB](#) overlain on [AHN3](#) with all [DTB](#) features shown (above), and with only [verflijnen](#) shown (below). Ground points are shown in green. The top render illustrates that other features, such as roadside slopes, canals, ditches, safety rails are represented in [DTB](#). Full-width motorway signs are also occasionally represented (either by lines on the road, or on the structure itself). The bottom render shows that locally, the edge markings are in good agreement with [AHN3](#) visually, and are only occasionally incomplete. This location has the best vertical correspondence with [AHN3](#), and also the best completeness, of all the areas I examined. For illustrations of the *disagreements* between [DTB](#) and [AHN3](#), please refer to Figure 4.7 and the associated discussion in Chapter 4.

## 2.4 Methods of existing implementations

### 2.4.1 NDW prototype

[NDW](#) themselves produced a prototype implementation, which can achieve a 3D enrichment of [NWB](#) with only a few gaps in the produced elevation profiles. Although their workflow does not have a formal documentation, I have been given a verbal description of it, as well as the output. Based on my understanding of these, their primary technique involved snapping close-by [AHN3](#) Lidar points to the

line geometries of [NWB](#). Notable problems with the implementation included non-road points being snapped to centrelines, causing road centrelines to be given overestimated elevations, in turn resulting in abrupt spikes in the elevation profiles.

Furthermore, no close-by points could be found for underground roads (i.e. tunnels), and strongly occluded parts of roads. For small gaps, this was resolved partially by writing an algorithm to interpolate linearly inside [NWB](#), using the closest vertices where snapping was successful. For larger gaps, an attempt was made to resolve issues by including information from external sources semi-automatically. Neither issue could be fully resolved via these approaches, hence the results of this project were only used by [NDW](#) to gain a better understanding of the problem and the expected challenges. For the development of a reliable digital toolbox they subsequently commissioned a commercial implementation from [RHDHV](#).

## 2.4.2 RHDHV's commercial implementation

[RHDHV](#) developed their implementation in parallel with the planning of the present scientific research. During this time, I attended [NDW-RHDHV](#) meetings, discussed the commercial system design and implementation details directly with [RHDHV](#) personnel, and was granted access to the codebase of the project. Understanding their implementation was crucial for the planning and realisation of my research, as it was among my goals to estimate the effectiveness of the commercial implementation's methods, as well as assess the quality estimate the accuracy of the their final results. In addition, creating my system design while learning about the known and suspected shortcomings of their methods allowed me specifically focus on areas where a different, less pragmatic approach could yield better results.

### Overview of system design

First, where [NWB](#) vertices are too sparse, vertex densification takes place; i.e. additional vertices are created inside [NWB](#) line segments until all vertices are found less than a certain threshold distance from their neighbours. From then onwards, *different* workflows are initiated for [R-roads](#) and [P-roads](#).

For [P-roads](#) (where [DTB](#) data does not generally exist), the workflow is conceptually similar to the one in the prototype, with the notable difference of using [AHN3 DTM](#) rasters rather than the point cloud. Because [AHN3 DTM](#) rasters are badly affected by both large holes and small groups of missing pixels (due to the fixed-parameter [IDW](#) interpolation that was used to generate them), [RHDHV](#) could only make use of them by filling in the gaps of the raster using linear interpolation in a 3D [TIN](#) created from extruded raster pixel centres. They then simply interpolated elevations for [NWB](#) from the raster using bilinear interpolation. Intermediate results of this procedure are shown on the right in [2.11](#). It shows a raster being overlain with [NWB](#) to yield elevation values. The raster still contains the holes that [AHN3](#) rasters contain by default; these are filled in before interpolating elevations for [NWB](#) but are shown here for demonstration purposes. Two types of holes generally occur: small-scale ones due to objects such as street furniture, vehicles and vegetation, and large ones that are typically due to large-scale occlusion due to buildings or bridges (as in this case). The test build shown here used [AHN2](#) rasters, but their production implementation uses [AHN3](#).

For [R-roads](#), [DTB](#) is available, and the assumption is made that it is more accurate than [AHN3](#) (or at least the stock [DTM](#) tiles generated from [AHN3](#)), to the extent where it should be the primary source of elevation data. Priority is thus always given to it in the procedure, with [AHN](#)-based interpolation used only as a fallback mechanism in case [DTB](#)-based height estimation fails for any reason (anomalous elevations computed, or missing [DTB](#) geometry).

The goal of the underlying algorithm is to find the closest, roughly parallel [DTB](#) line segments at any [NWB](#) vertex, and to deduce elevations from them. First, 2D cross-sections are constructed on [NWB](#) vertices, with each given the mean azimuth of the two [NWB](#) line segments that they are part of, and then rotated 90 degrees. For vertices created during densification, this simply means the rotated azimuth of their parent line segment. [DTB](#) lines are then intersected with the cross-sections and for each cross-section, the closest [DTB](#) line that satisfies a relative angle condition is picked on both sides of [NWB](#). Elevation is then first

## 2 Related work

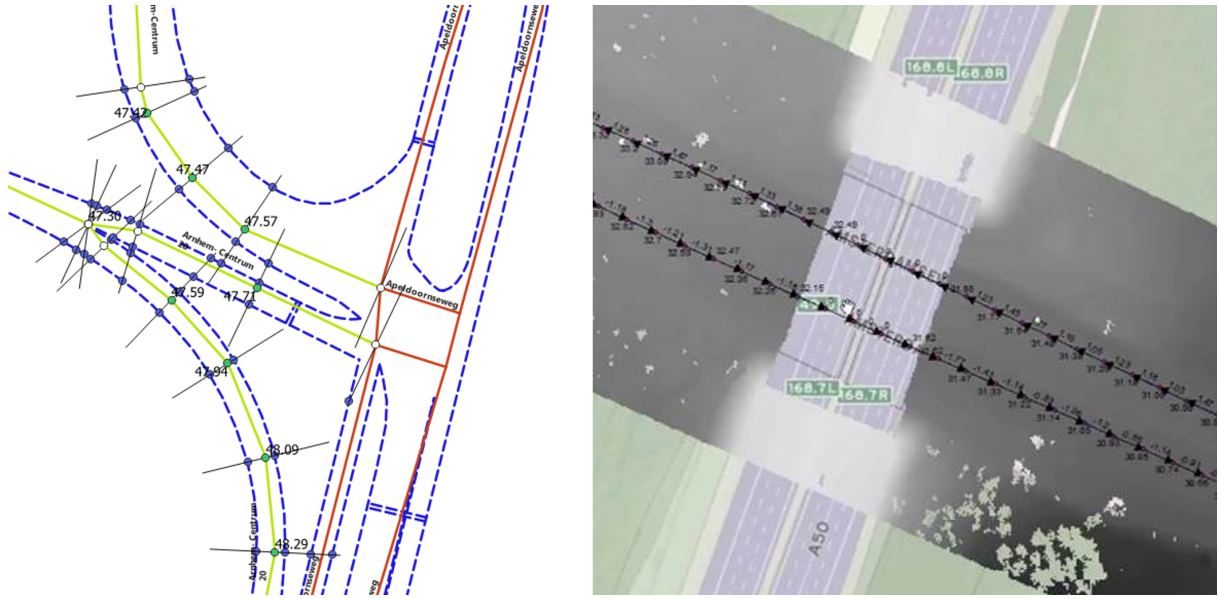


**Figure 2.11:** Illustrations of RHDHV’s procedures to convert NWB to a 3D dataset.

linearly interpolated inside the two chosen DTB segments to yield values exactly at their intersections with the cross-section. Lastly, elevation is interpolated linearly along the cross-section itself to yield the final elevation at the location of the NWB vertex.

The angle condition I mentioned above is a threshold-based evaluation concerning the angle between intersected DTB line segments and the cross-sections, and is used to ensure that the chosen DTB segment is indeed roughly parallel to NWB locally. This helps ensure that the algorithm does not accidentally choose a DTB line segment that belongs to a different (underlying or overlying) road surface. The assumption is thus made that the DTB line segments representing surface features of a given road are roughly parallel with the relevant NWB centreline, and lie close to them. Implicitly, this also assumes that even if no other DTB road markings are present, NWB centrelines will still lie between two DTB road edge markings, i.e. *verflijnen*.

In practice, backup mechanisms needed to be implemented because these assumptions do not always hold. Primarily, this is because in sharp bends NWB may not be parallel with the relevant DTB lines locally, and because it is frequently not complete enough to be used for the above operations. To bridge these issues, wherever the algorithm only finds a suitable DTB intersection on *one* side of NWB, it is only that side from which the elevation value is deduced. If no suitable intersection can be found whatsoever, the AHN3 raster-based interpolation is used instead (the same workflow that is always used for P-roads).

This procedure is illustrated on the left in 2.11. The cross-sections that are constructed on NWB vertices are shown as black lines. Green circles denote those vertices where the cross section could be properly intersected with DTB lines (blue circles) and thus be given an elevation value. White circles denote where the procedure failed, and AHN raster-based interpolation was necessary. This render illustrates that in sharp bends the assumption that NWB and corresponding DTB lines are parallel does not necessarily hold, because of how coarse and inaccurate NWB’s georeferencing is, especially relative to DTB which is very accurate horizontally. The render also illustrates that P-roads are not processed in this way, not even if they have DTB lines next to them (which frequently occurs in the vicinity of motorways).

### Potential limitations

At the time of finalising this report, the preliminary results of the commercial implementation have already been made public, as described in NDW [2021]. In this section I discuss the *suspected* limitations of their methods, not yet the properties of their results. These will only be discussed in the context of the

comparison of the two sets of results. During the project planning, system design and implementation stages, the commercial results were not yet available and as a result, the bulk of my work - almost everything apart from Section 4.4 - is based on verbal descriptions of their methods and the commercial source code.

First and foremost, I suspected that using AHN3 rasters in place of the point cloud would affect the quality of their conversion. Point cloud to raster conversion is, by definition, associated with inherent information loss (less raster cells than point cloud points), and further reduction in accuracy is introduced by the interpolation mechanism itself, that created the rasters. Radial IDW was used to generate AHN3 DTM tiles, which several of the reviewed papers found to be specifically unsuitable for interpolating large-scale areas in which zones of decreased point density or gaps exist – both of which characterise ground-filtered AHN data (e.g. Guo et al. [2010]). In addition, the procedure performs another layer of interpolation to infill gaps, which may further deteriorate accuracy. Furthermore, RHDHV uses bilinear interpolation inside the raster to produce NWB elevations, which is suggested by Shi et al. [2005], to be less accurate than other common methods such as bicubic.

Furthermore, there is no mechanism built into the software to deal with occlusion in the case of P-roads, and also R-roads where DTB is unavailable. This means that wherever NWB elevations are interpolated in occluded road segments from AHN3 rasters, they will be incorrect. Just like in the NDW prototype, these values will show up as spikes in the elevation profiles, as well as longer bumps where wide features (e.g. bridges) are encountered. Since there is no outlier filtering or smoothing algorithm built into the software either, the severity of this issue is not mitigated in any way.

Based on the input assessment, it is also evident that prioritising DTB wherever it is available may itself be a questionable decision, in view of the fact that the output's accuracy needs to measure up to the noise regulation's expectations, at least theoretically. DTB is accurate horizontally, in fact it is theoretically more accurate than AHN3. However, even if its vertical accuracy was also satisfactory at the time of its acquisition, it no longer is, due to various degrees of vertical ground motion taking place in the country. As elevations in DTB are not updated where no civil engineering changes have taken place in the road network, its road surface markings are often far too outdated to be used with any certainty, especially considering that there is no reason to do so given that AHN3 contains equally accurate, but significantly more recent data.

Lastly, the commercial implementation lacks a formal accuracy assessment. Although this is common with comparable commercial products, in this case the output dataset needs to comply with formal accuracy *requirements*. Without a quantitative or at least qualitative accuracy assessment of some form, there is not enough evidence to support the applicability of the commercial results to the noise modelling applications they are intended for.

Since the accuracy of AHN3 rasters is known and simple bilinear interpolation is used to obtain elevations from them, deriving output accuracy would not be difficult wherever their solution uses AHN3. This excludes interpolating in gap-filled pixels, which would need further considerations. In the case of DTB, the evaluation of accuracy may be equally simple, as the underlying computations all boil down to linear interpolation. However, wherever DTB data is old, any accuracy quantification would be meaningless because DTB itself does not comply with its own formal accuracy, due to vertical land motion.



# 3 Methodology and methods

This first section of this chapter presents a description of the methodology of the planned dissertation work. This description is limited to matters relating to planning the execution of the work, without going into specifics about the methods themselves. The second section of the chapter presents an overview of the methods themselves, including information about how these plans evolved since the P2. This section also includes detailed accounts of the thought processes leading to the most important design choices. The rest of the chapter is devoted to a detailed account of the methods that underlie each of the processing steps in the final "proof-of-concept" software implementation, with accompanying flowcharts to illustrate the system design represented by the methods. A short section at the end of the chapter describes the implementation's software architecture, with explanation about certain technical design choices regarding the implementation.

## 3.1 Methodological framework

This section contains a written account of the key stages into which the execution of this research can be divided. Each subsection describes one such stage, discussing the specific tasks performed during each stage as well as what has changed relative to my original plans. The methodology is also visually illustrated on a flowchart in Figure 3.1.

### 3.1.1 Preparation

This project concerns a client - [NDW](#) - with specific requirements and a pre-existing attempt at implementing a solution, in addition to aspects that are purely scientific. As a result, the first stage of the project involved *consultation with the client* and with their commercial developers - [RHDHV](#) - in addition to the task of *familiarising myself with the research topic and literature*. The results of these preparation tasks were *discussed internally* with my supervisors and used to *define the final list of formal research questions* on the basis of focusing primarily on academic topics while also fulfilling the requirements of the client. This combined knowledge was then used to *produce the P1 submission*. This stage roughly coincided with Q1 of the academic year, and with the P1 period of the dissertation research.

I executed this stage of the project according to my initial plans, little has changed during its realisation.

### 3.1.2 Preliminary analysis, proposal writing

The second stage of the project involved *further consultation with the client and their developers* to determine to what extent the commercial and scientific branches of the 3D-NDW project could be linked, and to allow me to understand the exact methods used in the prototype and the commercial implementation (which was being actively developed during this period of time). In parallel with these tasks, I *performed the necessary in-depth literature review* and preliminary analysis. The preliminary analysis was comprised of a *close examination of the input datasets and their documentations* (input assessment), and based on this and the research questions, the *final selection of relevant concepts and methods*. I also selected a range of illustrative geographical regions during the preliminary analysis, and cropped the datasets to their extents to *create testing input files* for later development and testing. Lastly, the results of this stage were

### 3 Methodology and methods

distilled to produce the P2 document. This stage roughly coincided with Q2 of the academic year, and with the P2 period of the dissertation research.

I executed this stage of the project according to my initial plans, but with a few small alterations. My initial plan was to put a slightly larger emphasis on performing preliminary analysis tasks, but the abundance of relevant literature and the complex task of creating a preliminary design for the methods (and the pipeline itself) limited the amount of time I could spend on it. I focused most of my effort at this stage in the research on the literature review and the preliminary system design instead. This meant that during the next stage, I had a solid starting point in terms of background knowledge, and specific plans regarding what to start implementing.

#### 3.1.3 Analysis

The third stage of the research spanned the period between my P2 and P4 presentations. This stage concerned carrying out most of the analysis. The period was characterised first and foremost by the intense development effort focused on the *implementation of individual algorithms and steps of the workflow*. My original plan was to isolate this set of tasks and perform it during the period between my P2 and P3 presentations, and to *assemble the pipeline* from the individual modules after the P3. However, it proved to be more effective to develop the modules and incrementally extend the pipeline with them at the same time - an approach to which I switched after implementing the first few modules. This allowed me to resolve pipeline-level issues as part of the incremental refinement of methods, in addition to problems related to specific pipeline steps only.

Carrying out the *accuracy-related analysis* was the last stage of the project that required active development on the program code. Testing the individual procedures and the pipeline was continuous during the implementation, with larger tests performed after reaching major milestones. Testing, and the assessment of performance and accuracy used the testing datasets I produced as part of the preliminary analysis. This was followed by a self-evaluation of the overall results of the research and a discussion of them with my supervisors, as well as a comparison of the commercial results and mine. The stage was concluded by *writing the present draft thesis* ahead of my P4 presentation.

#### 3.1.4 Finalisation

The last stage of the project will last a few weeks between the P4 presentation and the P5 presentation. Both *the implementations and the present report itself will be improved and finalised* during this time. The final version of the source code and its documentation will be published in the project repository on GitHub. Furthermore, the outcome of the research and its findings relevant to improving the commercial implementation will be discussed with our client.

## 3.2 Overview of methods

This section provides a structured overview of the steps of the processing pipeline. While the detailed descriptions in Section 3.3 focus on explaining how exactly each step works, the purpose of the present section is to provide the rationale justifying their necessity and the reasons underlying certain major design choices, as well as to describe their role in the context of the system as a whole.

While the exact aims of the project materialised during the first two stages listed in Section 3.1 above, a brief description of the project existed before it. The project was originally conceived as a an academic continuation to the pre-existing attempt of [NDW](#) to implement a solution to the 3D conversion of [NWB](#), re-using [NDW](#)'s prototype implementation as the basis for a completed, academically sound version. During the aforementioned two stages, it became clear that [NDW](#)'s pre-existing implementation is not robust and flexible enough to justify building the academic project on top of it. Hence, the entirety of the below pipeline was designed and implemented specifically for this academic project, no part of it represents code borrowed from the NWD prototype (or the RHDVH implementation).

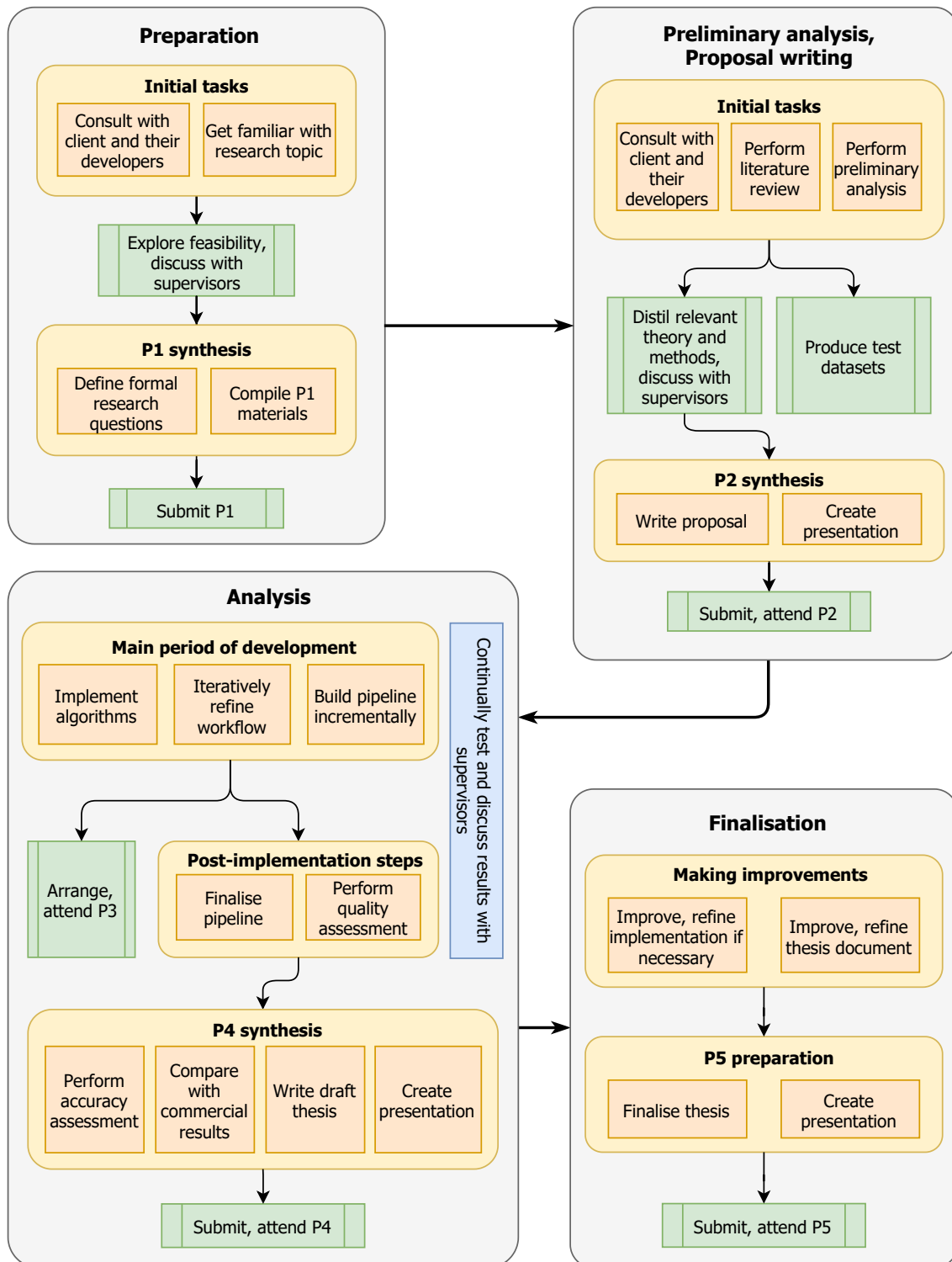


Figure 3.1: Flowchart-style illustration of the top-level methodology of my dissertation research.

### 3.2.1 Proposed processing pipeline

The design of the pipeline is the result of a combined understanding of concepts described in related work, my own knowledge and experience relating to the geomatics discipline, as well as inspiration from the methods of the commercial implementation. The proposed workflow was built with a strong focus on finding answers to the research questions. Furthermore, it is also the result of a process of iterative refinement. In most cases, this only concerns the technical details of the algorithms implementing the pipeline steps, but in some cases I also made major changes to certain aspects of the general approach. Hence, in the structured overview below, I added a list item per pipeline step specifically to describe what changes, if any, were made to the given step.

As a brief summary of the general idea, the pipeline takes [NWB](#), decomposes it into roads whose surface can be modelled by 2.5D methods, and applies a set of mostly geomatics operations to produce the 2.5D road surface models that the elevations are then derived from to produce 3D-NWB. Accuracy-related considerations are not yet described in this section, these are first discussed in Section 3.2.4 below. A visual illustration of the main pipeline steps is shown in Figure 3.2, showing only the titles of each workflow step in the order in which they are executed.

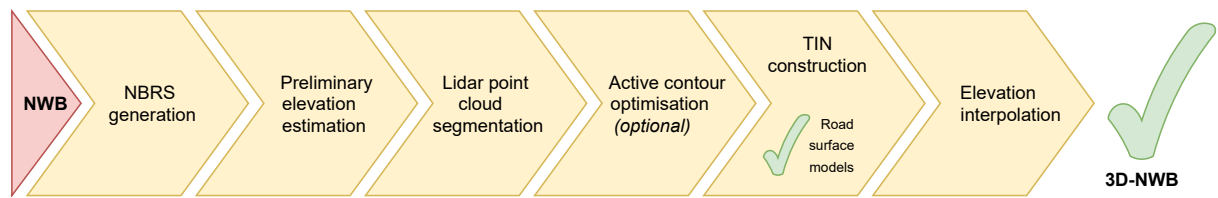


Figure 3.2: Illustration of the top-level steps and output of my processing pipeline.

#### 1. Generating NBRS

- a) **Goal:** assemble optimal 2D profiles from the building blocks of [NWB](#).
- b) **Approach:**
  - i. Assemble *non-branching road segments*, henceforth referred to as [NBRS](#) (in both plural and singular) from [NWB](#) geometry. To do so, look for series of [NWB wegvakken](#) (LineString objects) that represent the same road and join them into optimised 2D profiles - [NBRS](#).
  - ii. Perform the assembly of [NBRS](#) in a way that maximises their length (optimal for length-wise 2D operations such as polynomial fitting), minimising internal angles at the same time. Disallow self-intersection, so that each [NBRS](#) can be modelled in 2.5D.
- c) **Purpose:** this step is necessary, because in addition to working with small-scale (short wavelength) features in the road network, we wish to be able to inspect trends that take place over longer distances in the network. The building blocks of [NWB](#) (*wegvakken*) can sometimes be short, occasionally only a few metres long. Hence, assembling them into [NBRS](#) provides a better starting point for later steps.
- d) **Changes:** from the outset, I expected that simple methods based on progressing along 2D profiles, as well as modelling 2D profiles as a whole, would be useful for this project, and that a data structure serving this dual purpose would be necessary. Hence, [NBRS](#) have always been part of my plans and their exact specifications did not change much during development.

#### 2. Preliminary elevation estimation

- a) **Goal:** create a rough, preliminary 3D version of [NWB](#).
- b) **Approach:**
  - i. Based on the median elevation of nearby Lidar points, associate [NBRS](#) vertices with preliminary elevation approximates, thereby performing a crude 3D conversion of [NWB](#).

- ii. Perform polynomial fitting on the 2D profiles that [NBRS](#) represent. Identify vertices that are outliers with respect to the general shape of the [NBRS](#) and interpolate values for them linearly.
- c) **Purpose:** this step is necessitated by the next one, point cloud segmentation. While it is possible to perform it without first performing a rough 3D conversion, I found it to be much more effective when the approximate 3D locations of [NBRS](#) are already known by that point.
- d) **Changes:** this step represents and addition relative to the original plans. I started suspecting its benefits during the implementation stage, and subsequently added it to the pipeline design.

### 3. Point cloud segmentation

- a) **Goal:** create subclouds from the Lidar data containing points relevant to the roads represented by individual [NBRS](#).
- b) **Approach:**
  - i. Using their preliminary elevations, find “patches” of Lidar points in the 3D vicinity of [NBRS](#) vertices. Progressing along the vertices of each [NBRS](#) in a linear manner, fit planes on their Lidar patches. Where an unexpected change in the plane fits is detected, rely on [DTB](#) to provide a reference and to help navigate through the ambiguous region.
  - ii. Where [DTB](#) is also unavailable, accept the shifted (or missing) plane fits but perform a polynomial fit afterwards to identify planes that are unlikely to belong to the relevant road surface. Split the [NBRS](#) into parts in such places, excluding the undesired regions from further consideration until the last pipeline step.
  - iii. Based on the plane fits, decide which points in the patches are relevant to the road surface represented by a given [NBRS](#), and create subclouds by merging them (one for each [NBRS](#) part). Include [DTB](#) points that were used in places where [AHN3](#) data was missing.
- c) **Purpose:** like [NBRS](#) generation, this step also has a dual purpose. Firstly, it associates each [NBRS](#) with a set of candidate Lidar and [DTB](#) points that are likely to be relevant to them, thereby reducing the amount of Lidar points that will need to be processed later on. Secondly, it also excludes the majority of points which are close to a given road, but which were reflected from occluding geometry instead of its surface.
- d) **Changes:** originally, I only wished to detect where plane fits become inconsistent to exclude small-scale occlusion at this point. However, I eventually realised that by tracking changes in certain metrics, I could do so even in relatively long occluded regions. I then incorporated [DTB](#) as a backup dataset to increase the reliability of this method, which made the solution work even where significant changes in elevation take place inside the occluded regions (such as in tunnels). I added the splitting of [NBRS](#) into parts as a last tweak, after implementing the rest of the pipeline. This improved the results of later steps by removing areas without [AHN3](#) and [DTB](#) coverage from the [NBRS](#).

### 4. Preliminary edge approximation

- a) **Goal:** create line geometries on both sides of [NBRS](#) approximating the edges of the road surfaces.
- b) **Approach:**
  - i. construct cross-sections on [NBRS](#) vertices and convert them to 2D elevation profiles by sampling [AHN3](#) along their length. Perform linear regression on each, and select the outermost stable inlier points on both sides of the [NBRS](#). The two points are taken to represent the road edge locally.

### 3 Methodology and methods

- ii. Assemble approximate road edges from the discrete edge points generated by the previous step, enforcing constraints regarding the expected shape of the road edges. Relax the constraints after a certain number of successive failures, to allow the algorithm to adapt to real-life changes in the road geometry.
- c) **Purpose:** the sole purpose of this step was going to be to provide edge estimates for active contour optimisation. After I made the decision to make active contour optimisation optional in the pipeline (due to its ineffectiveness), preliminary edges also became optionally needed for later steps, in place of the optimised contours.
- d) **Changes:** Due to the optional use of preliminary edges in TIN construction (in case optimisation is skipped), I needed to improve their quality significantly. This entailed the implementation of significant refinements to the underlying algorithm, as well as the constraints enforcement steps that I mentioned above.

#### 5. Active contour optimisation (*optional*)

- a) **Goal:** refine the preliminary edges based on road surface smoothness as described by Lidar.
- b) **Approach:**
  - i. Construct an attractor map from the subcloud of each NBRS part, based on a scalar metric describing the local smoothness of the points.
  - ii. Use the preliminary edges and the attractor maps to perform active contour optimisation.
  - iii. Find a parametrisation for the active contour optimisation algorithm that works well with all testing datasets.
- c) **Purpose:** the original purpose of this step was to optimise the preliminary edges to the extent where they can be used to classify subcloud points either as surface or non-surface points. Since this was found not to work reliably, the current purpose of the step could be described as *simplifying and enhancing the shapes of the preliminary edges*.
- d) **Changes:** even after improving all prior steps of the pipeline and sufficiently refining the parametrisation, the algorithm still produces mediocre results. As a result, I eventually implemented a bypass so that it can be skipped. Furthermore, I originally planned to apply morphological operations to attractor maps composed from maps generated using multiple different metrics. I found this to be ineffective in practice, the final implementation simply uses the raw results of the sole best-performing metric.

#### 6. TIN construction

- a) **Goal:** model each NBRS part by a TIN based on the subclouds and preliminary or optimised edges.
- b) **Approach:**
  - i. Seed each TIN by inserting points around the centre of the road unconditionally. Define the "centre of the road" based on the *edges*, not the 2D location of the underlying NWB centreline of the NBRS part.
  - ii. Initialise each TIN by conditionally inserting points within the preliminary or optimised edges.
  - iii. Extend each TIN by conditionally inserting points further and further away from the centre of the road, beyond the edges if desired.
- c) **Purpose:** this step also serves a dual purpose. On one hand, it satisfies our academic interest in creating 2.5D surface models of the roads. On the other hand, these models can then be used to interpolate final elevations for NWB efficiently. Lastly, as the TIN consists of input elevation measurements, it allows output accuracy to be estimated in a straightforward manner.

- d) **Changes:** the original idea for this step was that the optimised road edges would be hard-coded in the [TIN](#) (a [CDT](#) was planned), and only points within these constraint geometries would be inserted. Due to the ineffectiveness of active contour optimisation, I instead needed to create a [TIN](#) construction workflow that can make the best of the edges and subclouds *without* making the assumption that the edges have near-perfect accuracy.

## 7. Elevation interpolation

- a) **Goal:** derive a final elevation for each [NWB](#) vertex while enforcing continuity across intersections, and augment the original dataset with the results.
- b) **Approach:**
  - i. Interpolate in the respective [TINs](#) to obtain a final elevation value for each vertex of each [NBRS](#) part.
  - ii. At intersections, use the first elevation that was interpolated at that approximate 3D location and connect (snap) all other [NBRS](#) to it that end or begin at that intersection.
  - iii. Use linear interpolation to fill in elevations in [NBRS](#) where [TIN](#)-based interpolation was not possible.
  - iv. Mark the origin of each output elevation either as [AHN3](#), [DTB](#) or linear interpolation.
- c) **Purpose:** obtain the final [NWB](#) elevations and output 3D-NWB, keeping a record of which elevation comes from where.
- d) **Changes:** originally, I thought that enforcing continuity across intersections was going to be a bigger challenge. However, I found the [TIN](#) representations of the same intersections across different [NBRS](#) to be consistent reliably, hence interpolating a single elevation (based on the first [NBRS](#) part encountered) and snapping all subsequent ones to it works without issues in almost all scenarios examined.

I was inspired by concepts and ideas from related work (see Chapter 2) while designing the original pipeline, and the final implementation retains many of these similarities. For instance, the point cloud segmentation step was inspired largely by [Oude Elberink and Vosselman \[2009\]](#) and [Boyko and Funkhouser \[2011\]](#). The cross-section based edge detection workflow was inspired by curb detection-related work, such as [Yang et al. \[2013\]](#) and the methods of the commercial implementation. The use of 2.5D-based modelling methods to represent surfaces extracted from the point cloud comes from [Oude Elberink and Vosselman \[2006\]](#). The active contour-based workflow was inspired by [Boyko and Funkhouser \[2011\]](#) and [Göpfert et al. \[2011\]](#). In a way, my work can also be interpreted as a study of the effectiveness of relevant methods commonly found in the literature.

### 3.2.2 Dependency of methods on specific datasets

In this report I commonly refer to [DTB](#) as a *support dataset*. This is in part due to it always having been secondary to [AHN3](#) because its spatial coverage is vastly inferior to [AHN3](#) and it could not, by itself, fulfil the role [AHN3](#) was given in this project, which may therefore be called the *primary dataset*. [AHN3](#) contains enough data to make it possible to run the pipeline in the complete absence of [DTB](#). [DTB](#) merely improves the results of the point segmentation step and extends the [TINs](#) into areas not covered by [AHN3](#) (preventing them from being split into parts in the process).

The reason why I often refer to the two elevation sources in such a way, is that it describes their *roles* rather than their exact *identity*. For the same reason, I also often refer to [NWB](#) simply as the "road network". This is in line with my goal to make my methods as independent from the exact identity and properties of [AHN3](#), [DTB](#) and [NWB](#) as possible. Most parts of my methods should work regardless of the exact datasets used, as long as a few assumptions are satisfied. For instance, the primary Lidar dataset needs to be accurately classified, in particular vegetation should be clearly isolated from ground reflections. [DTB](#) could also be replaced with any generic dataset that contains accurate 3D geometries representing the surfaces of the relevant roads - or better still, with [MLS](#) data providing coverage where

### 3 Methodology and methods

the primary [ALS](#) one does not. The main difference is in scale between the primary and the support dataset; the purpose of the latter is to introduce data where the primary dataset has data *gaps*.

The main concerns regarding generalisation (how well the methods and the implementation work independently from the properties of the datasets) are not related to the input datasets, but to the parametrisation of certain parts of the implementation. While many such parameters are exposed as arguments and can be customised by the user, there are also many that are hard-coded to avoid creating an API with an inconveniently long list of arguments. While the default parametrisation works in all the study areas of this project, there is no guarantee that they would always work equally well with other datasets - especially with ones containing road networks that possess different properties than that of The Netherlands (e.g. mountainous areas). However, being an open-source, proof-of-concept software, there is nothing to prevent potential reusers of my code from adapting it to their needs, including making changes to its fixed parametrisation.

#### 3.2.3 A note on [DTB](#)'s role

In my P2 document, no specific mention was made about the role intended for [DTB](#), but a section was dedicated to speculating about potential uses. The evolution of its role in the final implementation was entirely up to the iterative refinement of the methods. In the end, the deciding factor in determining how [DTB](#) could be used was that I found it to be useful for patching in gaps in [AHN3](#) coverage, which is how the roles of primary and secondary dataset for [AHN3](#) and [DTB](#) came about.

Among potential uses I speculated about before starting the development was the use of [DTB](#) as a means of contributing to edge estimation/optimisation, and to the lateral refinement of [NWB](#) positions. However, I found [DTB](#) road markings to be missing most commonly in the exact locations where they could have contributed to these aspects, for instance in sharp bends.

Using [DTB](#) as a secondary dataset with the sole intention of characterising occluded road surfaces also generalises better, as the previous section makes clear. Consultations with [NDW](#) also made it clear that they are in the position to commission the survey of additional georeferenced points or lines from Kragten (via a vehicle on which commercial [GNSS](#) systems are mounted) or to purchase [MLS](#) data from Cyclomedia. Unlike [DTB](#), such data would *not* correspond to specific road markings.

These circumstances are what prompted me to treat [DTB](#) in a more generic manner, and to then extend this mindset to the way the rest of the datasets are used in my methods.

#### 3.2.4 Accuracy assessment of processing steps

As I emphasised in various places in this report already, it was among the aims of this research to perform the 3D conversion of [NWB](#) in a way that output accuracy is as close to the input accuracy as possible, and that it can be evidenced and quantified either for the process as a whole, or for each output vertex individually.

As the literature review results in Chapter 2 already indicated, there are various ways to go about this problem. The first and foremost decision one needs to make is whether an empirical or a theoretical approach is better suited to the given procedure. For our procedure, both appeared equally suitable at first. I first attempted an empirical approach, but having produced uncharacteristic results using this approach, I eventually settled on a combination of simple decision-making logic and a theoretical, mathematical framework. I will provide the details about the procedures later in this chapter, in Section 3.4.

Below, I will outline the general approach, and the assumptions that are made when using it.

### Assumptions about influences

My system design interpolates the output elevations from a [TIN](#) whose vertices are the Lidar road surface measurements themselves. I opted for this approach specifically because my literature review indicated that interpolating in such a [DTM](#) appears to be the best option for large-scale terrain as well as in terms of accuracy, and because - assuming perfect ground filtering - it introduces no errors relative to the original Lidar data. However, as I explained in Section 2.2, the output accuracy in such a process is a factor of not only the generated [DTM](#) and the interpolation technique used, but also of local, "environmental" factors. I made a range of assumptions regarding these influences before proceeding to the accuracy estimation step, which I will explain below.

The first factor to consider is the local *accuracy of ground filtering*. In this project, most of the Lidar data was already ground filtered, as I made use of the excellent stock classifications that are present in [AHN3](#) (please refer to Section 2.3.2 for more information on this topic). There is one exception to this rule: roads found on bridges were manually classified as bridges, including all objects on the roads such as guardrails and vehicles. Using the bridge classification also added objects over other roads (such as motorway signs), which locally violate the assumption that the road surfaces are ground-filtered.

However, processing steps in this research remove most non-road reflections from above road surfaces, and any remaining ones are eliminated by the careful conditional insertions of the [TIN](#) construction step. This holds both in theory and practice, as 4 explains. The number of outliers *on road surfaces* is so small, that if we make the assumption that we only wish to interpolate elevations on road surfaces, we may regard the theoretical ground filtering effectiveness to be 100%. As a result, the influence of non-road reflections (outliers on road surfaces) needs not be considered in the accuracy assessment.

The second factor to consider is the local sampling density of the Lidar points (and [DTB](#), where it was used in place of [AHN3](#)). The assumption I made here is that as long as the [TIN](#) locally conforms with the theoretical minimum Lidar sampling density required to characterise a flat surface without oversampling it, the output accuracy will not suffer from any detrimental influence. I implemented simple logics to detect where interpolation has taken place in a location where the sampling density drops below this level. Vertices interpolated in such places do not receive an output accuracy value, and are thus flagged as having *undetermined* accuracy. The details regarding the identification of a suitable local density threshold is found in Section 3.4.1 later in this chapter.

This second assumption holds, because in flat areas that are *oversampled* by Lidar, literature indicates sampling density to have little to no correlation with empirically-derived error. In such areas, oversampling already occurs at point densities far lower than what is typical of [AHN3](#), apart from places where there are gaps in the data. Hence, a simple threshold-based evaluation can be deemed a sufficient measure to deal with the influence of this factor. This decision was made in view of the results of my empirical accuracy assessment results, which also indicated no correlation between sampling density and [TIN](#) model accuracy (see Section 4.3.1 for the details).

The last non-interpolation influence to consider is that, which is caused by terrain slope and ruggedness. Relevant literature discussed this topic also in the context of local sampling density, because it is especially in sparsely-sampled regions small, local variations that the ruggedness introduces may not be captured adequately. Road surfaces are, however, smooth. Furthermore, even inclined roads in our datasets are always characterised by smooth, gradual slope transitions - which makes sense, considering that both the motorways and municipal roads we are working with have high speed limits. The effects of local curvature on accuracy in this case may be neglected.

This combination of factors and assumptions lead me to implement an accuracy assessment workflow that either deems the accuracy to be undetermined (where sampling density is very low) or computes its accuracy solely based on the principles of error propagation through TIN-linear interpolation. This error propagation method predicts an *increase* in the standard error relative to that of the input for surfaces that are not very steeply inclined. The two categories also correspond with whether the output conforms with the requirements of the noise regulations or not. The details of this are found in 4.3.2.

### 3 Methodology and methods

#### Influence of prior steps

It may strike the reader as odd that it is almost only the last two pipeline steps that are discussed above in terms of what defines output accuracy. The reason behind this is that the [TINs](#) are constructed entirely of [AHN3](#) and [DTB](#) points, thus making the standard vertical and horizontal error of each [TIN](#) node known. If the [TINs](#) were constructed from points which were themselves "secondary information" (i.e. derived information) relative to the input, then the estimation of output accuracy would be more involved. However, this is not the case here - and therefore, wherever the above three assumptions hold, the quality of the [TIN](#) and the interpolation technique define the output accuracy alone.

The rest of the pipeline steps only affect whether the above assumptions are violated in a certain place or not. In particular, they may affect the local density of vertices in the [TINs](#) and whether a [TIN](#) exists at the 2D location of a particular [NWB](#) vertex or not. If we focus only on the influence of processing steps (i.e. we ignore the effects of physical factors and problems with the data), this may for instance be the result of a very poor polynomial fit in the preliminary elevation estimation step causing Lidar segmentation to fail locally, or the rare cases where preliminary edge estimation fails too many times in a row. Such blunders may cause issues in the [TIN](#), but these too, will be picked up by the threshold-based evaluation and classified as unreliable accordingly.

Furthermore, we must also consider the fact that [DTB](#) is densified prior to being converted to a pseudo-point-cloud. This is important because [DTB](#)'s accuracy is defined in terms of its vertices, it does not apply directly to the line segments connecting them. For simplicity, I did not specifically consider how [DTB](#)'s measurement error propagates to the densified vertices because if we considered such details regarding [DTB](#), then we would also need to consider its *temporal* inaccuracy, which affects older [DTB](#) geometry significantly. Since subsidence and potential other vertical land motions do not affect all areas uniformly, we cannot draw a simple relationship between the local age of the [DTB](#) data and its accuracy without relying on relevant external data - such an analysis was not within the scope of this research. Furthermore, such an assessment may not apply to other support datasets. Instead, the assumption is made about the support data in general, that it possesses identical properties to that of [AHN3](#).

In another words, in this proof-of-concept implementation, [DTB](#) merely *simulates* a reliable support dataset, as [DTB](#) itself does *not* represent one. It is treated like an [MLS](#) dataset, and its accuracy is also evaluated on the same basis. Users specifically interested in the accuracy of the output when using [DTB](#) should consider all output elevations marked as originating from [DTB](#) data to be unreliable, and to certainly not confirm with the requirements of the noise regulations - even if the threshold-based evaluation does not indicate a missing accuracy value.

#### Linear interpolation accuracy

In areas with a complete lack of measurements, [NWB](#) elevations are interpolated *linearly* inside the [NBRS](#), based on the [TIN](#)-interpolated elevations that already exist by that point. This generally occurs under large occluding features (such as bridges), but also, less commonly, in the case of short road segments that are very poorly georeferenced in [NWB](#), as well as occasionally in places where large vehicles or dense vegetation resulted in smaller gaps of data in both [AHN3](#) and [DTB](#). In more general terms, it occurs everywhere where it was not possible to interpolate a value in an underlying [TIN](#), because none existed locally.

A typical, practical example is as follows: the Lidar segmentation workflow encounters a bridge with no [AHN3](#) or [DTB](#) coverage underneath. It splits the [NBRS](#) into parts, one extending to the last [NWB](#) vertex before the bridge, and the other starting at the first [NWB](#) vertex after it. [TINs](#) are constructed for the two [NBRS](#) parts, but not in the space between them, i.e. underneath the bridge. The vertices in-between the two [NBRS](#) parts (most likely 5-10 of them depending on the width of the bridge) will receive elevations that are linearly interpolated based on the closest elevations interpolated in the [TINs](#) of the two [NBRS](#) parts.

The output accuracy of these points is also not estimated. The primary reason for this decision is that the local sampling density is effectively zero. Since we do not estimate the accuracy in places with low

sampling densities, it is well justified to also not do it where there sampling is even worse. In such places, formal accuracy can be safely assumed to be worse than that which is required by [NDW](#) and the noise regulations.

To summarise, elevations marked as having been linearly interpolated always have undefined accuracy. However, undefined accuracy may also correspond to elevations that were interpolated from a [TIN](#), but where the local [TIN](#) vertex density (Lidar sampling density) was too low to trust the value.

## 3.3 Detailed methods

Previous sections of this chapter described the methods underlying the pipeline steps in general terms. This section will go into more detail about the underlying processing algorithms. The level of detail will be greater than in previous sections, but not to the point where every step in the code is explained. Features of the implementation that are of a very technical nature are not included - the reader is referred to the open-source code and its documentation if they find themselves interested in learning about further details.

The focus of each subsection below is to explain, with the help of accurate flowcharts, how each pipeline step works, and to discuss major challenges encountered during development and how they affected the course of development. Most of these can be interpreted as further details about the top-level changes relative to the P2 plans that I already described in Section 3.2.1.

### 3.3.1 Splitting NWB into NBRS

The first step of the pipeline is to create 2D profiles from the input road network with the properties mentioned in Section 3.2.1, as this benefits various subsequent steps. The [NBRS](#) are in practice made from a connected series of LineString objects from the road network in [NWB](#) (i.e. they are *assembled from the wegvakken*). I implemented two algorithms based around the same general idea.

The first algorithm, which I call the "geometric algorithm", uses geometry only and thus generalises fairly easily; it could be used with any dataset comparable with [NWB](#). I call the second algorithm - which is an *alternative* to the first - the "semantic algorithm", because it uses data from [NWB](#)'s attribute table to try to assemble [NBRS](#) in a way that only roads with identical roles (ramp, motorway lane, etc.) get added to the same [NBRS](#). This algorithm generalises less easily, but it demonstrates that the semantic information can provide important insights into network properties that would be difficult (even impossible) to recognise based solely on the geometry. Both algorithms are illustrated in Figure 3.3, and further textual descriptions are provided below. The results of the two algorithms are compared in Figure 4.2 in the Results chapter.

#### Geometric algorithm

This algorithm first creates a topological data structure from the input *wegvakken*. Each *wegvak* is a valid LineString, i.e. a connected series of line segments, which can be a few metres long or even hundreds of metres long. From here on in this section, I will consistently refer to *wegvakken* as LineString objects to make the description more general. The topological data structure records which LineStrings of the road network start and end in which intersections. As this algorithm is not allowed to use the pre-made [NWB](#) intersections from the attribute table, intersections are defined by their coordinates, rounded to one decimal. The topological data structure is based on hashing, hence it has good performance despite its reliance on coordinate-based lookup. The procedure consists of examining both ends of each input LineString and either creating a new intersection with it (if one does not exist at that location yet), or adding a reference to it in the intersection that is already found in the topological data structure. This is shown on the left in Figure 3.3.

### 3 Methodology and methods

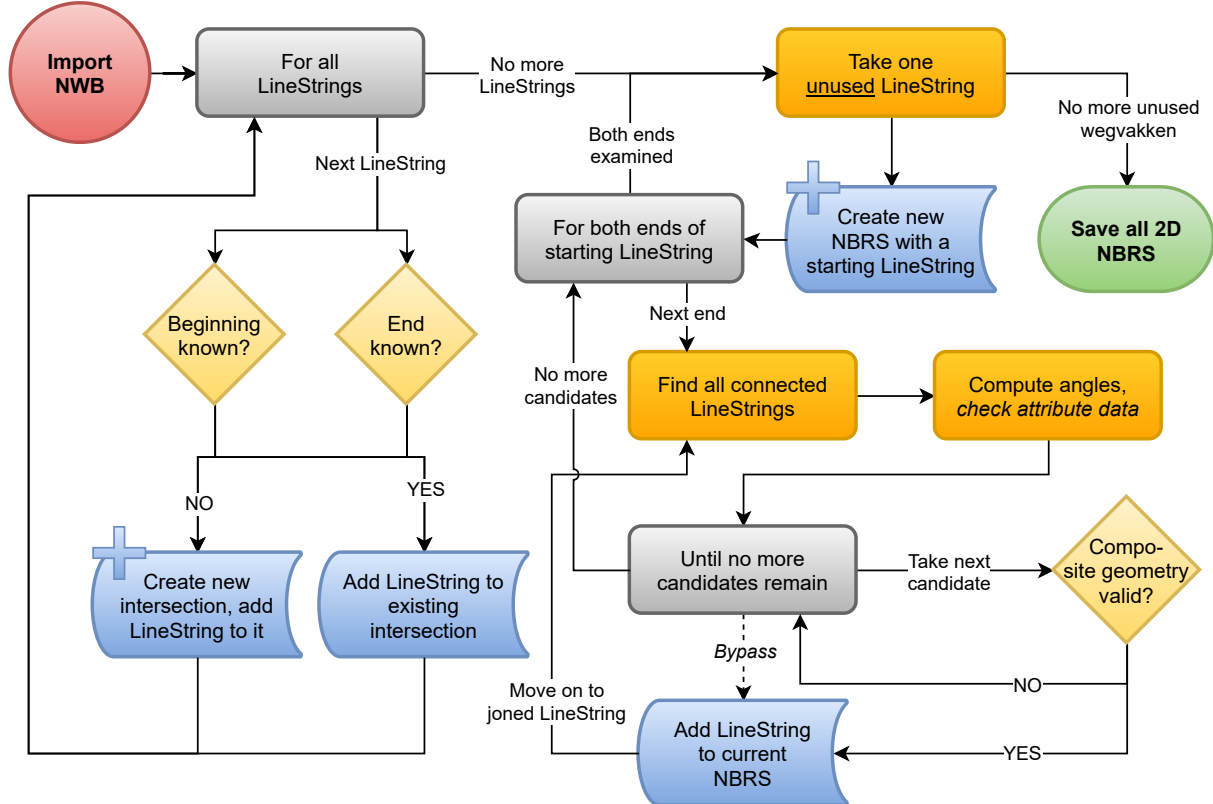


Figure 3.3: Flowchart-style illustration of the NBRS generation step of the pipeline.

The next step is to iteratively nucleate NBRS generation until no unclassified LineString objects remain. The algorithm takes one LineString, initialises an NBRS with it, and then attempts to extend it with further LineStrings on both ends. First, recursive extension is initiated on the last vertex of the LineString, and once that has completed, on its first vertex. The recursion examines the vertex, uses the topological data structure to find connected LineStrings and to connect one of them if certain conditions are met. Then, it progresses deeper into the recursion by doing the same with the LineString it just connected. The recursion ends, when no more suitable "extensions" can be found.

When the search for connected LineStrings succeeds in the above recursion, either a single one or multiple ones may be found. The latter corresponds to reaching a real-life intersection, in which case the algorithm needs to decide which one to connect based on a set of geometric conditions. First, the angles between the last line segment of the previous LineString and the first line segment of all the candidate LineStrings are examined, and the one with the angle corresponding to the straightest possible continuation of the road is selected. A composite geometry of the pre-existing NBRS and the new segment is then created and tested for self-intersections. If the composite geometry fails this test, the next best candidate is examined, and so on until a candidate succeeds, or the iteration runs out of candidates - in which case none of the candidates are accepted and the recursion terminates. When both recursions (starting from the first and last vertices of the LineString that nucleated the NBRS) have finished, the NBRS is deemed complete and the next NBRS is nucleated. The self-intersection test is also performed when only one connected LineString is found, i.e. not only when an intersection is encountered.

### Semantic algorithm

The semantic algorithm is built on the same framework as the geometric one, as it is intended as a comparable alternative to the geometric one. Most steps of the procedure are slightly modified equivalents of the ones in the geometric algorithm, hence here I will focus on describing the differences.

The topological data structure of the semantic algorithm is based on the *junctie* (intersection) ID number ([JTE ID](#)) records found in [NWB](#), which are unique identification codes belonging to each intersection of LineStrings in the dataset (including those of only *two* LineStrings, i.e. not real intersections). Each LineString possesses an "end JTE ID" and a "beginning JTE ID" which are used to assemble the navigation structure in place of the coordinates in the geometric algorithm. The [JTE IDs](#) can be used to represent the topology of the dataset entirely, without any consideration for the geometry - indeed, it often describes topology more accurately than the geometry itself.

The nucleation of [NBRS](#) takes place in a similar manner to the geometric approach, but here each [NBRS](#) is associated with a specific wegnummer (road number) and BST code (a code related to the role of each road). LineStrings are only joined to an [NBRS](#) if they have matching road numbers and BST codes, which is what the text *check attribute data* in the flowchart refers to. The candidates are still processed in the order of decreasing angle optimality, like in the geometric algorithm. However, the composite geometries need not be checked for self-intersections, as roads satisfying the semantic conditions do not self-intersect in real life. This improves performance, as the intersection and validity checks of the resulting geometry is costly in terms of computational complexity. This shortcut is indicated by the dashed *bypass* path in Figure 3.3.

### Challenges encountered

I encountered three distinct issues while I was developing this part of the software. The first problem was that while [NWB](#) has a near-perfect topological (graph) structure in its attribute table (represented by the [JTE IDs](#)), the same topology is not always represented by the geometry due to small-scale georeferencing issues. This means that the topology suggested by the geometry does not necessarily map to the [JTE IDs](#) exactly. In particular, LineStrings (*wegvakken*) that are connected according to the attribute table may occasionally have disjoint or even overlapping geometries, which originally caused my software not to be able to merge them into the same [NBRS](#). Fortunately, once I started using the coordinate-based topological structure, I discovered that reducing the coordinate precision to only one decimal solved the issue in most places by effectively "snapping" the LineStrings together. However, this is not a full solution - [NWB](#) georeferencing mistakes larger than 10 cm cannot be fixed this way.

A second issue was that the geometry of *wegvakken* often *reverses* in the middle of a connected series of LineStrings, requiring the implementation of a workaround in the code that computes the angles. The implementation now recognises where the geometry is stored in a reversed order relative to the [JTE IDs](#) and adjusts the angle computation accordingly. Lastly, for reasons related to external requirements that [NWB](#) needs to meet, motorway ramps are connected to motorway lanes at unrealistic angles, occasionally causing the algorithm to merge ramps with motorway lanes and vice-versa. A dedicated workaround was also necessary here, to recognise this specific situation and to treat it correctly.

### 3.3.2 Elevation estimation

The elevation estimation stage of the pipeline consists of two operations. The first operation is to associate each [NBRS](#) vertex with a preliminary elevation estimate based solely on nearby Lidar points, and the second a refinement step to eliminate occlusion-related artefacts. The procedure is illustrated by the flowchart in Figure 3.4.

#### Initial elevation estimation

The process starts by importing [AHN3](#), from where elevations will primarily be derived. It is assumed that the input file is sufficiently small to allow in-memory use, i.e. that it is a cropped or clipped version of the full point cloud tile. Thus, this is the point in the procedure, where a global scaling solution would be most important. All other parts of the program work on the basis of processing subdivisions of the road network independently ([NBRS](#) or the underlying LineStrings themselves), which is already a good starting point for scaling.

### 3 Methodology and methods

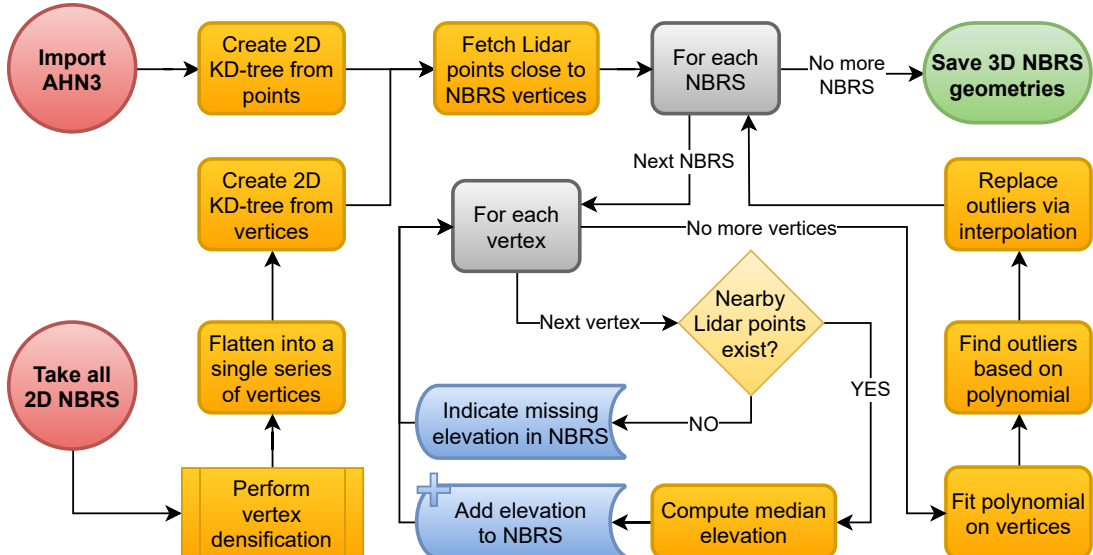


**Figure 3.4:** Flowchart-style illustration of the elevation estimation step of the pipeline.

The imported point cloud is first converted into a 2D KD-tree, so that area-based queries can be performed efficiently on it. Then, points closer than a certain distance are fetched for each **NBRS** vertex. The median elevation of the nearby Lidar points of each **NBRS** vertex is then computed as a representative elevation estimate. Where too few points were found, the elevation is instead marked to be missing.

#### Refining the preliminary elevations

Following this step, each of the 3D-enriched **NBRS** are fed into an outlier filtering algorithm. The algorithm generates a distance series based on the horizontal coordinates of the **NBRS**, and fits a polynomial to the corresponding elevation estimates. Since occlusion (due to overpasses or other objects) is almost always represented by short-wavelength data gaps or positive outliers in the Lidar data, these vertices are easy to isolate. The former is explicitly marked in the elevation series, while the latter show up as local clusters of large errors relative to the polynomial model. By interpolating values in such places, the quality of the preliminary elevations is improved considerably. The steps of this procedure are shown on the right in Figure 3.4. The resulting coordinates now represent 3D lines that preserve the input road network's 2D georeferencing, but which are enriched with elevations.

The replacement values are interpolated *linearly* based on the series of inlier vertices, i.e. they are not determined by the polynomial fit. The reason for this is, that it is not always possible to find good fits using a fixed-degree polynomial, and while the polynomial model is always good enough to *detect* outliers, its values are not conformant enough to *replace* the original or missing elevations with.

This polynomial-fitting approach is reused in various subsequent parts of the implementation. It is similar to the approach in Boyko and Funkhouser [2011], but it simplifies the global optimisation of splines into individual polynomial fits. Adapting the exact approach proposed in that research would certainly improve the effectiveness of my methods somewhat, but not drastically - I implemented subsequent steps in a way that they can deal with occasional mediocre-quality fits, and my results do not indicate that implementing a more sophisticated algorithm is justified.

#### Vertex densification

Although it is not strictly related to **NBRS** generation, vertex densification is not listed as a discrete pipeline step as it is a rather trivial operation. It is only presented in this report as a pre-processing

operation of preliminary elevation estimation. It is shown in 3.4 as the first processing step that acts on 2D NBRS.

Vertex densification of the NBRS vertices refers to the operation of taking the LineStrings that make up each NBRS, and adding vertices to their line segments until no distance between the vertices is bigger than a certain threshold. In my implementation, this takes place as a recursive iteration. Each LineString of each NBRS is considered, and the densification algorithm is called on each line segment. The recursion consists of breaking the line segment in two halves if it does not comply with the threshold (a vertex is added in the middle), and then proceeding deeper into the recursion by doing the same with the two resulting halves. The densified geometries are assembled when returning from the frames opened by the recursion.

Like NBRS generation, vertex densification is done for the benefit of subsequent operations. Many operations - such as the present step - act on each vertex separately, gathering information related to the vertex from its AHN3 and DTB neighbourhood. Since the posting distance of AHN3 is several magnitudes smaller than the line segments of NWB LineStrings, increasing the density of NWB's vertices has practical benefits. It not only increases the resolution at which elevation can be sampled, but it also means that large-scale trends in the data will be represented more dominantly, i.e. algorithms will be better able to tell which parts of the road represent the road surface, and which ones are outliers due to occlusion. The practical benefits of this step were observed during development, and vertex densification was made an intrinsic part of various other parts of the pipeline too.

### Challenges encountered

The main challenge encountered was related to the random reversals of LineStrings (*wegvakken*) that I already mentioned in Section 3.3.1. At this point, I needed to implement a workaround that flips reversed *wegvakken* into the correct orientation before moving on to the polynomial fitting step. In fact, it is the polynomial fitting step that had first drawn my attention to this problem, as it was impossible to get it to work before realising that parts of the 2D profiles contained vertices in the wrong order. The rectification of the orientation of the geometries takes place relative to the first LineString in the NBRS. These are then rotated back into their original orientations after the refinement step, to avoid introducing changes to the 2D geometry of NWB.

A second challenge was to find a good benchmark of what to consider outliers after fitting polynomials. I needed to choose a metric that works well with all the types of typical occlusion-related artefacts that show up in the data, such as overlying bridges of various heights, civil engineering structures of such bridges next to and above roads, motorway signs, tunnels, and so on. After experimenting with various approaches, I settled on one that involves setting the threshold dynamically, as a multiple of the standard deviation of the residuals between the initial elevation estimates and the polynomial-based elevations. Where the standard deviation is smaller than a certain threshold, I artificially raise it to a preset minimum to avoid performing linear interpolation where the conformance is very good.

### 3.3.3 Lidar segmentation

The Lidar segmentation step is more complex than the previous two, and some of the intricacies are omitted in the relevant flowchart (Figure 3.5) to keep its complexity manageable. I will attempt to fill in some of these details here in the text, referencing where approximately in the flowchart they occur. The goal of this step is to create subclouds from the Lidar data containing points relevant to the roads represented by individual NBRS.

#### Preparation and plane fitting

The program first creates KD-trees from the 3D point cloud, all 3D NBRS vertices, as well as all vertices found in the support dataset, DTB. The lines in DTB are also vertex-densified prior to being converted into a point cloud and then into a KD-tree. The densification drastically increases the effectiveness of

### *3 Methodology and methods*

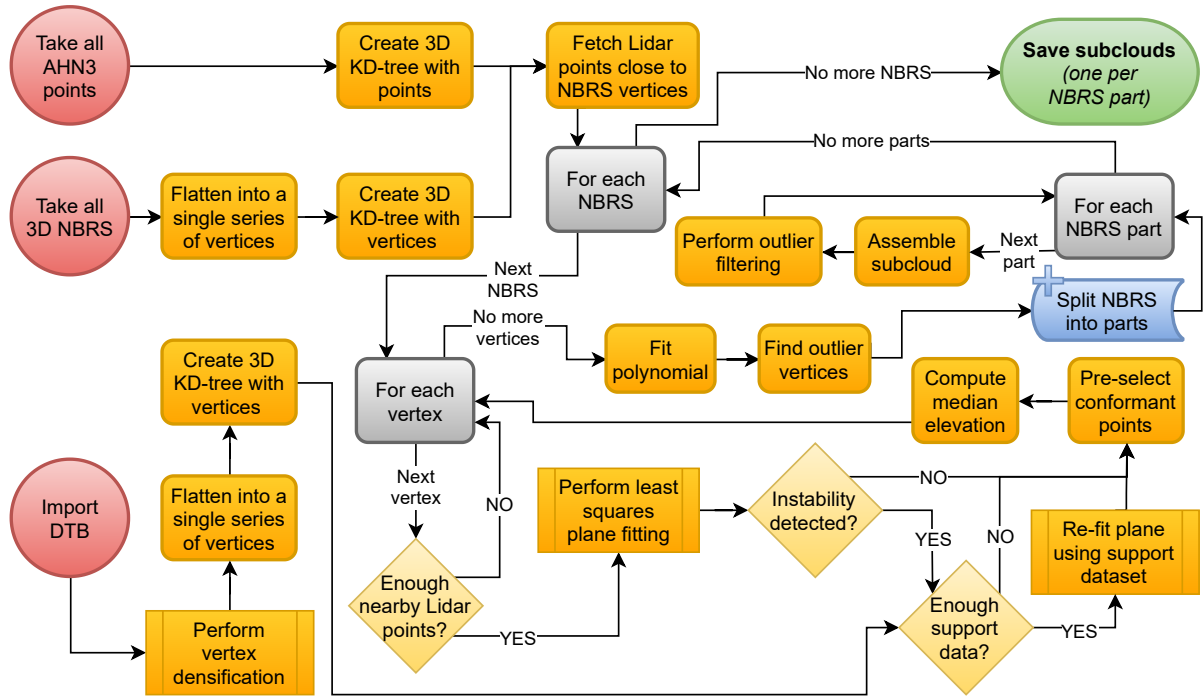


**Figure 3.5:** Flowchart-style illustration of the Lidar segmentation step of the pipeline.

using [DTB](#) as a point cloud. The reason why [DTB](#) is treated like a point cloud was discussed in Sections [3.2.2](#) and [3.2.3](#).

Much like in the preliminary elevation estimation workflow, a Lidar point cloud KD-tree query is performed as a bulk operation on each [NBRS](#) vertex (using the KD-tree made from the [NBRS](#) vertices). This results in a "patch" of Lidar points being selected for each [NBRS](#) vertex. Here, the underlying selection geometry is a sphere, rather than a 2D circle (as was the case in preliminary elevation estimation). This means that the relevance of the selected points will already be far more certain than before.

Each of these patches are further processed to enhance the results. The program fits a plane on each patch of Lidar points using the [MLE](#). Planes are only fitted if there are a set minimum number of points to support it, a threshold which is defined in terms of reaching a certain minimum point density inside the patch. If it is not reached, the points may still be passed on if a lower threshold is reached, in the hope that the support dataset ([DTB](#)) can re-position the plane to them in later stages of the algorithm and find some of them to be conformant with it. Below this second threshold, neither a fitted plane, nor the points are passed on. In the flowchart (Figure 3.5), this stage is shown in a simplified form which excludes the logical branch between the two thresholds.

## Refining plane fits and pre-selecting points

Next, the program considers the vertices of each **NBRS** one by one, in the order in which the vertices geometrically represent a valid road centreline. The program searches procedurally for places where the succession of fitted planes may indicate a break in shape of the surface. At the beginning of the iteration, the program initialises three variables describing the *previous* plane fit's relative position to the 3D **NBRS** centreline, the median elevation of the relevant patch's Lidar points, and the standard deviation of their distances to the fitted plane. By examining variations in these metrics, the algorithm can detect where the plane fits become unstable. It always compares the values of the current iteration to the ones from the previous iteration. Significant changes relative to the previous vertex and plane may indicate the presence objects occluding the sensor's view of the road's surface. I determined the exact metrics and parameters (thresholds) to detect "plane instability" based on experimentation and iterative

refinement. The current setup works well with all testing datasets examined. This step is represented in the flowchart by the conditional element labelled “*Instability detected?*”.

Originally, the algorithm was configured to automatically revert to the previous plane in case of plane instability and be allowed to use the reverted plane for a few iterations before asking help from the support dataset, in case the road emerged from underneath the occluding object after a few iterations at roughly the same elevation at which it disappeared. If the support dataset could also not help (due to e.g. a lack of coverage) after the expiration of the tolerance period, the algorithm would “give up” and move on to the next [NBRS](#). This meant that long occluding objects and no [DTB](#) coverage could prevent the algorithm from processing certain [NBRS](#), for instance ones containing tunnels.

### Handling breaks in the trend and missing data

I eventually revised this algorithm to be more robust and to produce useful results even in a complete absence of a support dataset such as [DTB](#), wherever there is [AHN3](#) coverage. In the current version of the implementation, the algorithm is only allowed to attempt to use the previous plane *once* before trying to use [DTB](#). The point cloud generated from [DTB](#) contains road surface measurements only, so it can be relied on to provide “assistance” where [AHN3](#) is ambiguous.

If a previous valid plane exists, then [DTB](#) is queried for points relatively close to it. If not, then the centre of the query becomes the current [NBRS](#) vertex itself. If a reasonable number of [DTB](#) points could thus be recovered, then the process is repeated by performing a second KD-tree query on the centroid of these [DTB](#) points, and the plane is then re-fitted onto the retuned points. This second query ensures that as many useful [DTB](#) points are included as possible. The program then assesses the distribution of [AHN3](#) Lidar points in the patch close to the re-fitted plane, and if the majority are found to be conformant with it, then the plane is re-fitted a third time to make sure that in the end it is based on the Lidar points and not the support data wherever possible. The necessity of this last step is related to the temporal problems with [DTB](#) already mentioned in Section 2.3.3.

In the new version of the algorithm, the program does not declare failure if it is no longer allowed to revert the current plane to the previous one, and also finds support data to be unreliable or missing. Instead, it simply relaxes its conditions and continues as though it were starting to process anew (i.e. as if it were initialising a *new* [NBRS](#)). This bypass allows the program to continue the procedure even if it is aware that there was a noticeable shift in the position of the fitted planes, or a gap in [AHN3](#) coverage. These areas are now handled separately, outside of this iteration.

Each successful iteration of this algorithm finishes by pre-selecting those [AHN3](#) and [DTB](#) points which conform well with the final plane fit, and saves them as individual patches. The median elevation of the pre-selected points is saved, as it will be used in the next step.

The above iteration is shown as the loop labelled “*For each NBRS vertex*” in Figure 3.5. In the implementation, the nesting of the iterations in different, but this description is easier to understand and is fully equivalent to the implemented version in terms of what it achieves. The same is true about the top-level iteration (“*For each NBRS*” in the flowchart), which in the implementation is broken into several parts for programming convenience.

### Breaking NBRS into parts

After the above iteration, a post-processing procedure is executed before moving on to the next [NBRS](#). Based on the median elevations of the patches saved during the iteration, the program once again has a new 2D profile which it can examine for outliers. Missing elevations in the series are indicative of a lack of coverage in both [AHN3](#) and [DTB](#). Outlier elevations indicate that the corresponding plane fit was corrupted by occluding features that caused occlusion or partial occlusion, and that it was also not possible to rectify the plane fit based on [DTB](#).

The program generates a boolean mask of where either of these issues are present in the elevation series. This is used to construct a list of intervals inside the [NBRS](#) that were found to be affected by neither of the

### 3 Methodology and methods

above two problems. Through this, a further subdivision of the road network is introduced: [NBRS parts](#). Each part corresponds to an interval in its parent [NBRS](#) with reliable combined [AHN3](#) and [DTB](#) coverage. Before splitting the [NBRS](#) in such a way, the boolean mask is post-processed to eliminate references to artefact affecting a few vertices only. Removing references to such small problems ensures that [NBRS](#) do not get split into too many parts. Unlike larger data gaps or zones of occlusion, such small ones do not affect the quality of the results of subsequent steps.

The patches of [AHN3](#) and [DTB](#) points are then combined into a subcloud, one for each [NBRS](#) part, making sure not to add duplicate points (the same point may be part of multiple patches). A quick outlier filtering step is applied to them, to eliminate points which are isolated (have no neighbours within a certain distance). This is easy and computationally efficient to execute by converting the data into KD-trees and performing nearest-neighbour queries on them.

A hashed structure is initialised at this point in the program that allows the program to remember which points in the subclouds originated from the support dataset. The use of this structure is described in Section [3.3.7](#).

#### Challenges encountered

The above description already contains mentions of how my methods relating to treating breaks in the trend and missing data evolved. Here, I will further elaborate on this topic.

The simple approach of starting on one end of the [NBRS](#) and examining its vertices one by one turned out to have significant limitations when I began to debug my implementation with the testing datasets. As it has no concept of global trends in the [NBRS](#), it can only rely on its previous iterations to detect breaks in the trend and to make decisions based on it. Because of this, in regions with occlusion-related or missing [AHN3](#) data and missing [DTB](#) coverage, significant problems could arise.

The original algorithm was able to detect where a data gap with or without occlusion-related data would occur, but it was not always capable of continuing on the other side of the problematic area. Projecting the last "trusted" plane to the other side would not work, because even a small erratic tilt in the plane would become a large enough problem by the time the algorithm reached the other side of the problematic region, that all the valid road surface points would be found non-conformant. Furthermore, even if a perfect plane fit existed before the problematic area, if the elevation of the road changed by the time it emerged on the other side of it (e.g. on the opposite side of a long tunnel), the method would still fail.

Eventually, I realised that moving part of the decision-making mechanism outside of the iteration would solve these issues. I transitioned to first saving Lidar patches per vertex separately (instead of adding them straight to a subcloud), constructing a polynomial based on their centroids to describe the overall trend, and detecting and excluding patches with unrelated points this way.

A second revision to the algorithm was necessary after the implementation of the next three pipeline steps. Keeping regions with no coverage inside [NBRS](#) meant that in subsequent steps, I was optimising contours and continuing road surface models across them as well - sometimes over hundreds of metres or more. This turned out to be problematic especially with active contour optimisation, which frequently ended up producing corrupted outputs as a result. This is the issue that splitting [NBRS](#) into parts solves. Regions that lack any elevation measurements do not become part of any of the [NBRS](#) parts, and as a result, later steps of the pipeline do not need to handle them. They are only considered again at the very last step of the pipeline, described in Section [3.3.7](#).

#### 3.3.4 Edge approximation

The generation of preliminary edges is based on approximating the location of the two road edges at road centreline vertices. For each [NBRS](#) part, the two road edge lines are assembled from these discrete edge point estimates. The process is illustrated in Figure [3.6](#).

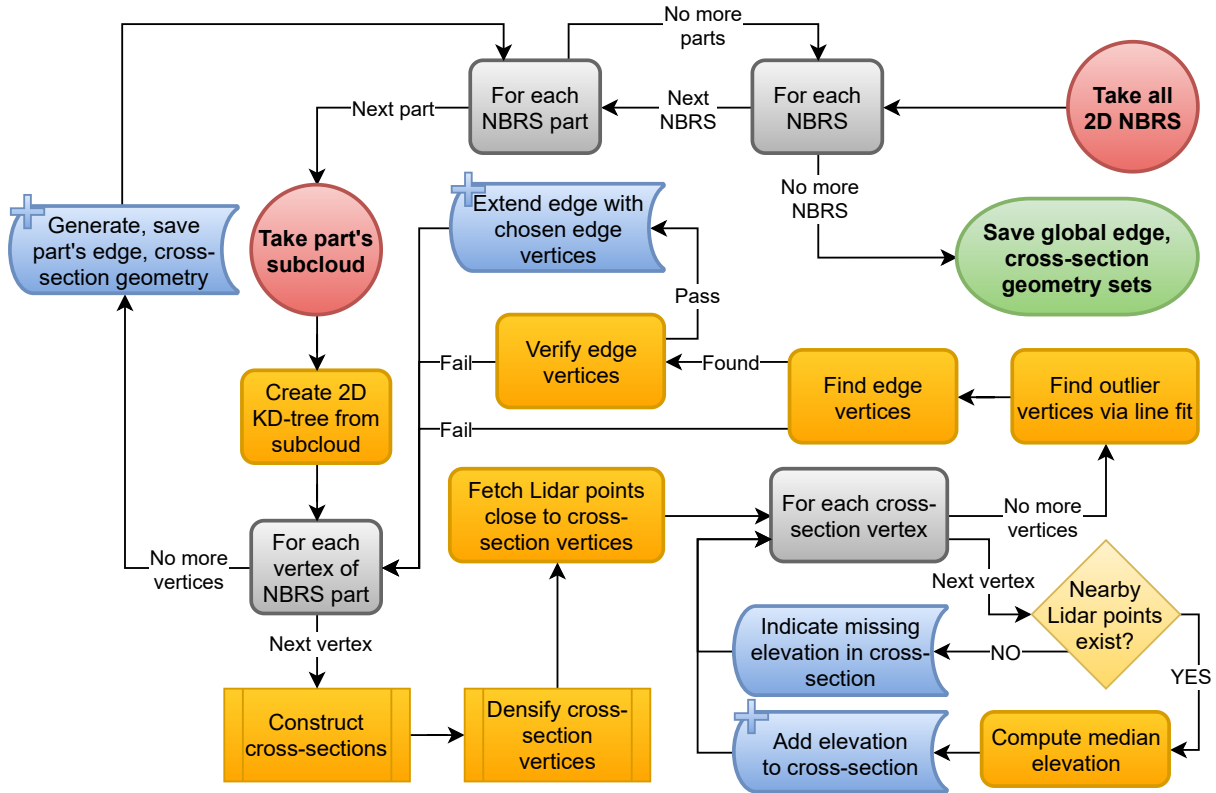


Figure 3.6: Flowchart-style illustration of the edge approximation step of the pipeline.

### Constructing edge point candidates

First, the subcloud of each **NBRS** part is used to create a 2D KD-tree. 2D suffices here, because it is a reasonable assumption to make at this point that the subclouds of **NBRS** parts no longer have a significant number of points that violate the 2.5D assumption (e.g. reflections from occluding objects). On each vertex of each **NBRS** part, a cross-section is then constructed. Cross-sections are line segments roughly orthogonal to the centreline locally. Their azimuths are based on the mean azimuths of the two line segments that contain the given vertex, except for the first and last vertices, which are simply based on their single parent segment's azimuth. The cross-sections are vertex-densified, and their densified vertices are used in a bulk KD-tree query. Lidar points close to cross-section vertex are thus identified, and the median elevation of each group is saved as the elevation of the given vertex. This step works on a small, sub-metre scale, meaning that using the native density of **AHN3** (no thinning applied) is particularly important from here on.

Each cross-section then represents a 2D elevation profile, with the corresponding centreline vertex in the middle. A line fit for the 2D profiles of each cross-section is computed and outlier vertices are identified based on them. The program then tries to find suitable edge points among the inlier cross-section vertices on both sides of the centreline, in each cross-section. Together, these points will form the preliminary edges. In each of the cross-sections, the program starts from the outermost cross-section vertex and progresses inwards. Once a certain consecutive number of inliers is encountered (with no outliers in-between them), the program assumes having reached the road surface and flags the current vertex as the edge vertex.

The total length of the cross-sections, which is a constant parameter, represents the maximum road width the program can work with. The optimal value of this parameter depends on the possible road dimensions in the given road network. If too small a value is used, the preliminary edges may lie too far inwards from the real-life edges, thereby excluding large parts of the real-life road surface as a result. If

### 3 Methodology and methods

it is too large however, false positive hits outside the real-life road surface will corrupt the preliminary edges, especially where roads are thin and other smooth surfaces are found in their surroundings.

#### Enforcing constraints

Flagged vertices are only accepted as edge vertices if they also pass a range of further conditions relating to a minimum road width, as well as sudden elevation changes and road width changes. The minimum road width is enforced for each pair of edge points individually. However, much like in the first part of the Lidar segmentation step, the latter two conditions are evaluated on the basis of comparing the metrics of the current edge point candidates to a mean value from a set number of previous iterations. Only if this verification procedure succeeds, does the program extend the [NBRS](#) part's preliminary edges with the new vertices.

In areas where the above procedure fails multiple times consecutively, "gaps" are created in the preliminary edges. These are not real gaps in the sense that the last pair of edge points before the gap, and the first pair after, are still connected in the output - it simply means that there are no edge vertices locally. Compared to the artefacts that would appear in the absence of the above threshold enforcement procedure, creating small gaps is an acceptable compromise, especially if the [NBRS](#) were sufficiently vertex-densified prior to this step.

However, long gaps may cause various problems in later pipeline steps. To avoid creating them, a relaxation of the conditions takes place after a set number of failures. After relaxing the conditions, the first inlier point on both sides is selected when fitting the next cross-section with a line, and the constraint regarding sudden changes in width is also ignored. Immediately after a success, the constraints are re-enabled. This temporary relaxation allows the algorithm to regain its references even if a sudden real-life change in the road's dimensions is encountered. It also helps in scenarios where the location of the edge is ambiguous.

Lastly, once per [NBRS](#) part the program generates the final 3D cross-section and edge geometries and saves them. After all [NBRS](#) parts have been processed, the global cross-section and preliminary edge object is also created.

#### Challenges encountered

Originally, this step was going to be a preparatory step for the sole purpose of providing initial edge shapes for the active contour optimisation algorithm. I first implemented it almost exactly to the specifications found in the P2 document. However, it soon became clear that better active contour optimisation results require better preliminary edge estimates, and thus I had to implement a range of tweaks and improvements in an iterative manner. It seemed that the best active contour optimisation results corresponded to where the preliminary edges were on the road surface, slightly inwards from the location of the real-life road edges. This is why the algorithm starts from the outer edges of the cross-sections, and progresses inwards until it can safely conclude that it has already been inside the road surface for at least a few vertices.

A further challenge corresponded to the point in development when I decided to make active contour optimisation optional. I needed to implement modifications to these methods to allow preliminary edges to be used for [TIN](#) construction directly, at the same time maintaining compatibility with active contour optimisation. This is what resulted in the addition of the system of constraint enforcement and constraint relaxation that takes place right before accepting a pair of edge point candidates. The main reason why this is beneficial for [TIN](#) construction is that it ensures that the edges cannot shrink too much, while also reducing the chances of road widths being overestimated due to small-scale issues.

The former ensures that road centrelines are found between the preliminary edges under normal circumstances, and with enough distance between them and the edges to ensure that Lidar points will be found there during the [TIN](#) initialisation step. Without this, it may be possible in certain exceptional cases, that the [TIN](#) would not exist at the 2D position of the [NWB](#) vertices and we would therefore not be able to interpolate an elevation for [NWB](#) there. The latter (maximum road width) decreases the chances

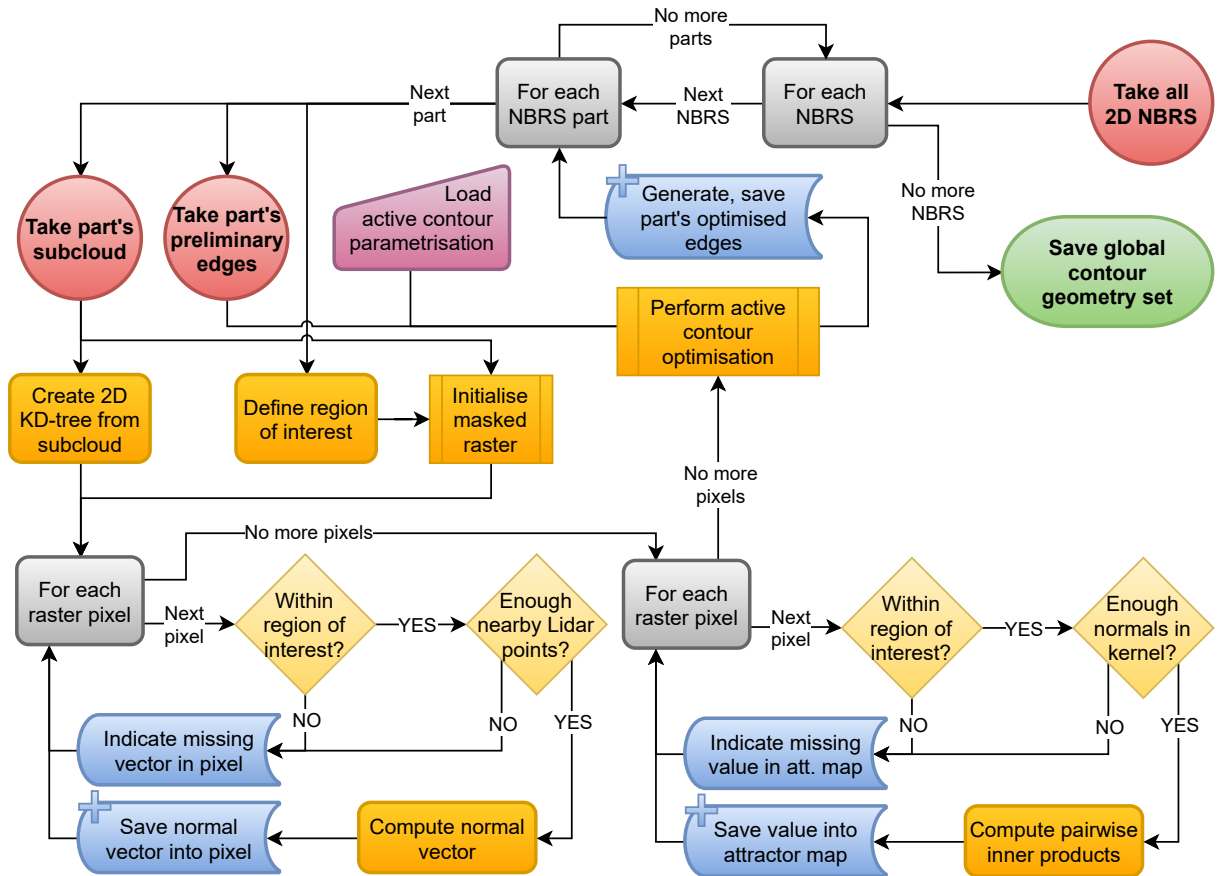


**Figure 3.7:** Flowchart-style illustration of the active contour optimisation step of the pipeline.

of including off-road points in the road surface models, both during TIN initialisation and extension. For more information about the TIN construction step, please refer to Section 3.3.6.

### 3.3.5 Active contour optimisation

The optimisation of preliminary edges is based on generating one attractor map for each NBRS part based on subcloud point normals, and running active contour optimisation to attract the preliminary edges to certain features in the attractor maps. The procedure is illustrated in Figure 3.7.

#### Attractor map generation

The procedure underlying this step is once again based on a 2D KD-tree of the subcloud of the NBRS part. 2D suffices because attractor maps are 2D rasters, and once again, because we are safe to assume at this point that the subclouds of NBRS parts mostly describe 2.5D surfaces. The rasters are first georeferenced in the same coordinate system as the rest of the data, after they are initialised. For each of them, a region of interest is derived by buffering the appropriate centreline by a certain amount. The rectangle-shaped raster is then masked out everywhere except for pixels whose centres lie within the geographical region delineated by the buffer polygon.

The centre of each unmasked pixel is then used in a bulk KD-tree query to find a small patch of nearby Lidar points for each. For pixel centres that have a sufficient number of neighbouring Lidar points, a normal vector is computed. These normal vectors are computed as the normal vectors of the local plane

### 3 Methodology and methods

fits of each such patch of Lidar points, and the [MLE](#)-based approach is re-used in my implementation (originally written for the Lidar segmentation step).

Normal vectors can be stored in the pixels in my framework, but they cannot be used directly in active contour optimisation because it requires scalar pixel values. To derive scalar values from the vectors, I designed a kernel-based approach. The pairwise inner products of the normal vectors of pixels falling into the moving window are computed, and the median of the value is saved. Since computing inner products is computationally expensive, not all pairwise combinations of the normal vectors in the kernel are dotted, only a representative random subset.

#### Running the optimisation algorithm

From here on, all operations take place in a temporary coordinate system which is defined simply in terms of the number of pixels in the X and Y dimensions from the top left corner. Before the preliminary edges can be overlain on the attractor map, they each need to be transformed into this coordinate system via an affine transformation. Together with the attractor maps and a suitable parametrisation, the preliminary edges are now ready to be optimised. The optimisation algorithm is run separately for the edges on the two sides of the centreline, and the output optimised edges are then assembled into a single polygon.

The scikit-image implementation of active contour optimisation is based on the original paper in which this procedure was first described scientifically: [Kass et al. \[1988\]](#). In addition to taking the attractor maps and the preliminary contours as input, it also takes a set of parameters that can be tweaked to manipulate aspects of the optimisation. The most important aspects for us in this project are contour smoothness, attraction to brightness or darkness, attraction to edges and the total number of allowed iterations. In Section 4.2.5 I describe the final configuration of values for these parameters.

#### Challenges encountered

In terms of the first version of my implementation, the main challenge here was the trial-and-error nature of getting active contour optimisation to perform acceptably for the wide variety of road geometries and attractor map features that are possible in our datasets. I needed to refine the parametrisation to work well with the input data, but since I was also producing the input data myself, I was also in the position to fine-tune that in turn. As a result, the task was a joint refinement procedure involving all prior steps in the pipeline leading up to this point, in addition to just adjusting the parameters.

Of all the aspects of the input data that I tried to optimise, I invested the greatest amount of effort in trying to pre-process the attractor maps to enhance their compatibility with contour optimisation. I tried various moving-window techniques such as many types of edge detection, edge enhancement, blurring, as well as morphological operations such as dilation, erosion, opening, closing, and many combinations thereof. I also tried compositing the resulting rasters. Sadly, I eventually concluded that none of these operations can achieve a noticeable improvement in the results, with the original kernel-based normal vector attractor maps and the native edge detection of active contour optimisation still producing the best results after several days spent on this.

Making matters worse, I found active contour optimisation to work only at high raster resolutions, with a pixel size around 0.5 metre typically producing the best results overall. Unfortunately, computational complexity grows non-linearly with decreasing pixel size, making debugging and fine-tuning very difficult, as well as putting the usefulness of such an algorithm into question considering the scale of the input data.

A further problem I found is that there are occasional small-scale features in the input data that tend to confuse active contour optimisation. Even for relatively short iteration lengths, such small artefacts may unpredictably corrupt entire [NBRS](#) part contours. For instance, small Lidar gaps due to stationary vehicles frequently overlap with the region where the road edges are suspected to be found. Active contour optimisation has no concept of no-data pixels, and reacts unpredictably to these holes regardless of what one uses as filling values. Another similar issue is that road edges are often characterised by

sudden slopes beyond their edges, but with further flat regions beyond them. This often creates a second contrast in brightness that active contour optimisation may confuse with the real road edge. Features such as these frequently draw the contours further from the road than what would be acceptable to accurately classify Lidar points within the contours as road reflections.

Lastly, the effectiveness of the method is also far too reliant on the accuracy of the preliminary edges. The algorithm is sensitive to even the smallest of blunders in preliminary edge detection, and is also prone to fail in no-data regions. After I implemented the code to split [NBRS](#) internally into parts where longer regions suffer from the absence of data, part of this issue was solved, but another remained: where [DTB](#) is available but not [AHN3](#), preliminary edges tend to shrink significantly, which often corrupts the optimised edges.

While the method works and produces usable results, the poor quality of the output and its unreliability in general prompted me to make it possible to bypass its use in the software. This required modifications to various previous steps of the pipeline, as well as all subsequent ones - a significant challenge. This bypass in turn puts into question the relevance of much of the pipeline structure, many parts of which were intended to lay the groundwork for active contour optimisation, and to make use of its output. I elaborate on this topic further in [Section 5.7.1](#).

### 3.3.6 TIN construction

As I emphasised in the previous section, various aspects of active contour optimisation were found to be lacking. The severity of the issues with this step prompted me to develop [TIN](#) construction in a way that enables it to function without active contour optimisation. Bypassing the active contour optimisation step altered the requirements that the [TIN](#) construction algorithm needs to satisfy.

In my planned pipeline, I made the assumption that points falling within the area of contours could be safely considered road points, and that conditional insertions would primarily be used to filter out any remaining *vertical* outliers. Working with preliminary edges (as well as *inaccurate* optimised edges) necessitates a less straightforward, but more robust implementation that is capable of telling apart road surface reflections and other reflections, in general. The result is an algorithm that borrows ideas mainly from region growing and ground filtering algorithms. An in-depth explanation of the algorithm is found below.

The outermost iteration loops over [NBRS](#), and [NBRS](#) parts are iterated one level below. In [Figure 3.8](#) this is explicitly indicated as an iteration over [NBRS](#) IDs and [NBRS](#) part IDs respectively. In contrast with previous steps of the pipeline, the centrelines themselves are no longer used, hence the change of notation.

#### Preparation for [TIN](#) initialisation

Based on the parametrisation, the outermost boundary within which points will be considered for insertion (including [TIN](#) extension) is constructed as a polygon, and points falling outside of its interior are excluded from further consideration. Then, either the preliminary edges or the optimised edges are fetched for the given [NBRS](#) part. Since they are almost identical structurally, they can be treated the same way for the most part.

They are used for two tasks: firstly, to construct a line halfway between the two edges to form the basis of seeding the [TIN](#), and secondly, to select points that fall within the edges as insertion candidates for the [TIN](#) initialisation step. This step is labelled “*Grow the initial [TIN](#) surface*” in [Figure 3.8](#), marked as a pre-defined procedure because the underlying procedure is fairly complex. To keep the complexity of the flowchart manageable, both the [TIN](#) initialisation and the [TIN](#) extension workflows of this step are illustrated in a separate diagram, shown in [Figure 3.9](#).

### 3 Methodology and methods

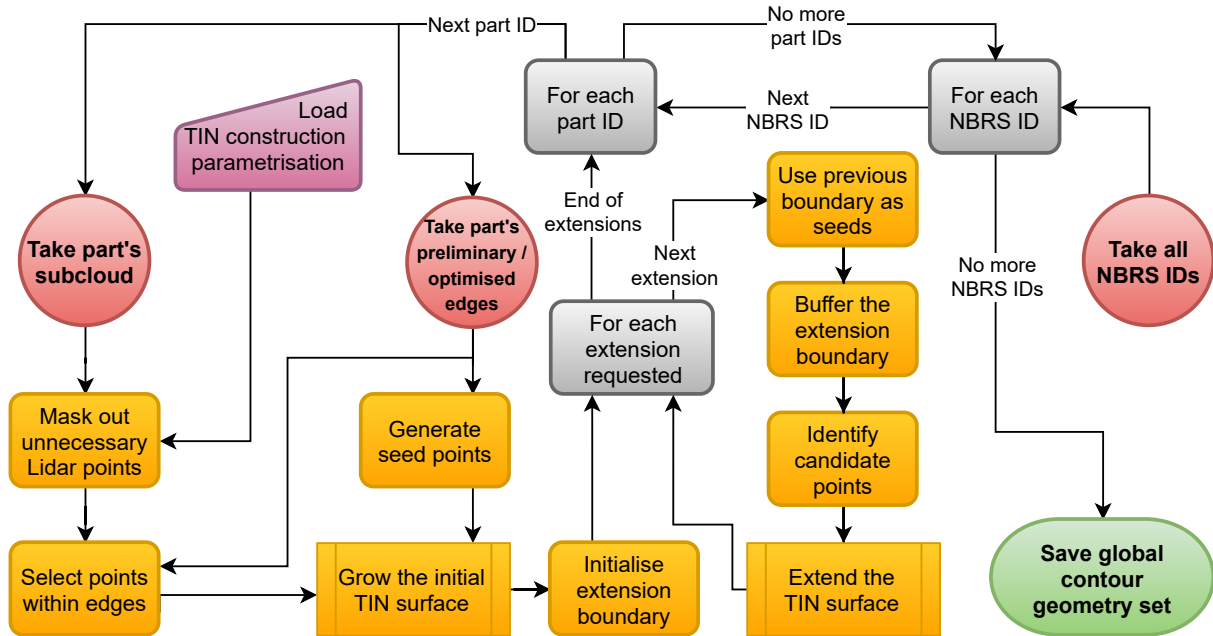


Figure 3.8: Flowchart-style overview of the TIN construction step of the pipeline.

#### TIN initialisation

TIN initialisation refers to the process of constructing an initial, conservative approximation of the road surface. As I noted above, it considers those Lidar points only, which fall between the preliminary or optimised edges. It first looks up those Lidar points, which are very close to the seed points. As these points are all but guaranteed to fall on the real-life road surface, they are unconditionally inserted into the TIN and are then pushed on a stack that in this case I will refer to as the "buffer". At this point in the algorithm, as Figure 3.9 shows, we leave the "*TIN initialisation*" group of operations and enter the "*TIN growing*" group (which is shared with "*TIN extension*"). The boundary vertices are also inserted into the TIN at this time (at an elevation of zero), which guarantees that the program can identify situations in which it is working with a triangle that is touching the boundary.

At this time, the TIN contains a high density of small triangles in the immediate vicinity of the original centreline of the NBRS part. Furthermore, it contains large triangles connecting this area with the boundary inside of which the road surface is allowed to grow. During the initialisation stage, this boundary is represented by the preliminary edges or optimised edges themselves. Inserting these in the TIN serves a dual purpose. Firstly, it avoids raising errors when a conditional insertion test is being performed outside of the convex hull of inserted AHN3 and DTB points. The boundary itself becomes the convex hull even before the insertions begin, so each time the program tries to locate the triangle into which a given point would be inserted, it will be guaranteed to succeed. Secondly, since the boundary is at an elevation of zero in the TIN, the program can easily identify when it is *growing* the Lidar-defined surface because one or more of the located triangle's vertices will be found at an elevation of zero. This also means that the program is aware of the position of the tested points relative to the detailed surface and the boundary.

The buffer at this point consists of all the seed points that were inserted unconditionally. It is used to query all the points between the edges in a bulk KD-tree query, and is then emptied. All points returned by the query are pushed on a stack, and this stack forms the basis for the conditional insertions. One by one, the candidate points are popped, and are conditionally inserted into the TIN. Figure 3.9 does not describe the conditions themselves, but I will go into detail about them here.

First, the triangle containing the popped point is located. If the triangle is defined only by subcloud points, then the elevation of the point according to the triangle is interpolated, and the difference in elevation is treated as an elevation discrepancy to which a threshold applies. If the threshold is not

violated, then the distances to the three vertices of the triangle are computed, and based on that, the angles between the triangle's plane and the line segments connecting the popped point to the three vertices. If any of the three angles violate the applicable threshold, the point is not inserted.

If the located triangle contains one or more boundary points, the elevation discrepancy is computed in a different way. Growing the TIN needs to be done with some caution, as introducing erratic points around the edges of the current convex hull would entail that future insertions would have an incorrect basis for the conditional insertions and as a result, the surface would occasionally be allowed to grow in undesired directions. To minimise the chances of this happening, growing the surface takes into account multiple pre-existing TIN triangles in the neighbourhood, not just the closest ones. Specifically, all triangles containing the non-boundary vertices of the located triangle are fetched. Then, this is repeated with all the vertices of the resulting set of triangles. The vertices of this collection of nearby triangles are then fitted with a plane (re-using, once again, the least-squares method), and the distance of the tested point to the plane is taken to be a good approximation of the elevation discrepancy. Points in the buffer are always close to the pre-existing Lidar points in the TIN (see below for the reason), hence this is a reasonable assumption. The angle-based test is then administered the same way as for regular insertions.

Each popped point that ends up being inserted into the TIN is also pushed onto the buffer, which was previously emptied after it had been used for the KD-tree query to fill the stack. Once the stack becomes empty, the procedure restarts by performing another KD-tree query using the buffer, and refilling the stack with new points to try to insert. Only those points from the spatial query results are considered, which are not part of the TIN yet. In other words, as long as points are being inserted, and these points have *uninserted* neighbours in the subcloud, the procedure will repeat. The buffer and the stack are kept separate so that KD-tree queries can be performed periodically as bulk operations, rather than individually - this is more efficient computationally.

As soon as no more insertions are taking place, the iteration ends and returns all points inserted into the TIN, in the order they were inserted. The TIN itself is not kept, instead it is reconstructed later on - this is due to the fact that point deletions in the triangulation package *startin* do not appear to work reliably in this workflow, but we do not wish to keep the boundary points in the TIN. The straightforward way to achieve this without point removal is by reconstructing the TIN with the subcloud points only.

While the final implementation of this step is not too complex, it is in fact the result of an experimental development process in which several previous versions of the design were implemented and discarded after I found them lacking in effectiveness. The final version of the TIN initialisation procedure is effective, and not too complex computationally owing to the buffering-based implementation of the spatial queries. Other than improving its performance via adding the buffer-based approach, I also needed to improve its reliability. Originally, I implemented TIN point removals to remove the insertion boundaries. In fact, in the first version of the implementation, I inserted points and then conditionally removed them depending on the geometry of the tree triangles created upon insertion. However, as I mentioned above, I found that using point removals in practice made *startin* unstable, causing it to crash at random points in the process. However, from previous experience with this package, I knew that it is extremely efficient in building TINs and interpolating in them, owing to its Rust-based implementation. Ultimately, I made to choice to keep using *startin*, but to implement the workflow in a way that the TINs are rebuilt once after initialisation (and then again after each extension iteration), "removing" the insertion boundaries implicitly.

A further important performance consideration was to efficiently find Lidar points falling within the insertion boundaries prior to starting the insertions. I found that testing the points one-by-one using *shapely* takes an unacceptable toll on performance, hence I modified this procedure to work as a bulk task via the path module of *matplotlib*, which is capable of finding points within a polygon formed of a single ring of coordinates with much lower computational complexity.

### 3 Methodology and methods

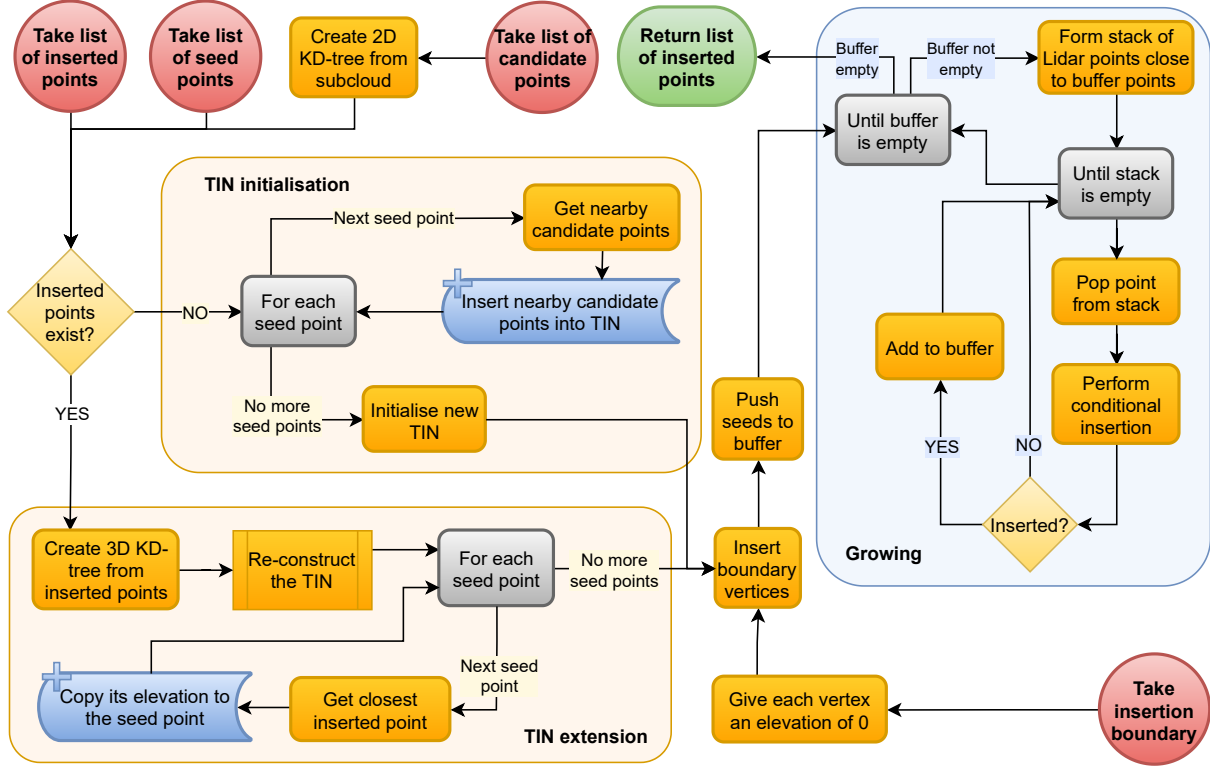


**Figure 3.9:** Flowchart-style illustration of the details of TIN initialisation and construction.

#### TIN extension

The extension of the TIN takes place in an iterative manner. The implementation accepts arguments that set the amount by which the boundary should be buffered in each iteration, as well as the number of extension iterations (steps). The starting boundary is *not* the same as the one used during the initialisation of the TIN. There, the preliminary or optimised edges were used, but here the first iteration's boundary is buffered from the seed line (the line halfway between the preliminary or optimised edges). This allows the algorithm to take another look at the points between the edges in case it missed any good candidates during initialisation, while also allowing it to consider points outside the edges in later iterations.

The seeding of extension iterations is different than that of the initialisation step. The seed points are always derived from the boundary used in the previous iteration. Furthermore, in TIN initialisation the candidate points included all points between the road edges, whereas in the extension steps only the points located in-between the previous and the current boundary (in 2D), are considered. Depending on the parametrisation, the boundary may be buffered to examine areas *beyond* the preliminary or optimised edges. This allows the program to try to grow the surface into areas which were not between the edges because of issues with the edges themselves. It is specifically intended to counteract the problem where road surfaces might get very thin where edge detection or optimisation significantly underestimated their width.

Each iteration first reconstructs the TIN yielded by the previous iteration, and inserts its new, buffered boundary into it. Since boundaries are always at an elevation of zero, when the previous iteration's boundary is reused to seed the current iteration, it first needs to be *transposed to 3D*, otherwise spatial queries based on it would not work. This is done by creating a KD-tree from all pre-existing TIN vertices and associating the closest one's elevation with each vertex of the 2D geometry. It is then ready to seed the new iteration, by itself being the basis for KD-tree queries on the new candidate points. However, the results of this seed-query are not inserted into the TIN unconditionally like they are in TIN initialisation, because the assumption that points close to the seed geometry are sure to be part of the real-life

road surface no longer holds. Instead, they are simply pushed to the buffer to start the main iteration involving the conditional insertions.

Once **TIN** extension has finished, the final **TIN** is reconstructed and is saved. Thus, one **TIN** object per **NBRS** part is saved, and these are not merged or joined together into a single **TIN** in any way.

### Challenges encountered

As implementing such a complex algorithm in this pipeline step was not originally intended, the biggest challenge here was to come up with a good solution within the timeframe reserved for the project. In terms of the methods themselves, I spent the most amount of time and effort on developing a solution that allows the road surface to grow into regions not covered by the preliminary or optimised edges. While in all cases, the surface generated by **TIN** initialisation is adequate to generate 3D-NWB, my desire was to not only model the central, traffic-occupied part of the road, but to grow it to the real-life edges of the paved surface as best as possible.

I initially wished to build the **TIN** as a single growing operation, but this proved to be prone to spreading into off-road regions. Depending on what order certain groups of points are examined in, even relatively sharp breaks in the underlying surface may appear smooth. A good way to deal with this problem would have been to decrease the query radius used in the buffer queries, but this in turn often prevented the **TIN** from growing at all. This is the reason why I eventually implemented the final version of the method as a combination of first initialising a conservative **TIN** in a large-scale growing operation, and then extending it carefully by examining thin "layers" of additional points progressing outwards from the centre of the road.

Performing conditional insertions outside of the convex hull of the pre-existing **TIN** points was also a challenge. Interpolating in the triangles is not a possibility here, but the importance of assessing the compliance of the tested points with the neighbourhood is ever so important - it depends on these surface growing insertions, whether a **TIN** might accidentally spread into an off-road area, or not.

### 3.3.7 TIN-based interpolation and vertex snapping

#### Interpolation and origin tracking

This is the last step in the pipeline, and its primary purpose is to use the **TINs** generated in the previous step to enrich the source road network with the final elevations. As Figure 3.10 shows, the first step in this procedure involves iterating through all **NBRS** parts, and performing the interpolation step itself on each of their vertices.

An additional step takes place during this iteration. To make it possible to keep track of which elevations come from where exactly, the algorithm recognises triangles that have vertices that originate from **DTB**. Before performing the interpolation, the triangle in which the interpolation will take place is fetched, and the origin of its vertices is examined. If any of them are from **DTB**, then the origin of the triangle is deemed to be **DTB** overall. For simplicity, the algorithm does not explicitly indicate what mixture of **AHN3** and **DTB** vertices were found in the triangle. These labels are used in the accuracy estimation step, primarily to advise the user which output elevations were affected by **DTB**, and should therefore be treated with some skepticism. Please refer to Sections 2.3.3 and 4.4 for more information about this topic.

The implementation uses linear interpolation in the **TINs** (also called TIN-linear interpolation). This is one of the simplest interpolation techniques available for **TINs**, and it is also the one most widely studied among them in the literature I studied (see Section 2.2). It is particularly suitable to this research, because its error propagation formulae are readily available in the literature, and because an implementation of it forms part of the *startin* package which I use to build the **TINs** and interpolate in them. This interpolator uses the barycentric position of the point where interpolation is desired. The closer it is to one of the vertices of located triangle, the bigger the vertex's influence becomes on the interpolated elevation. If

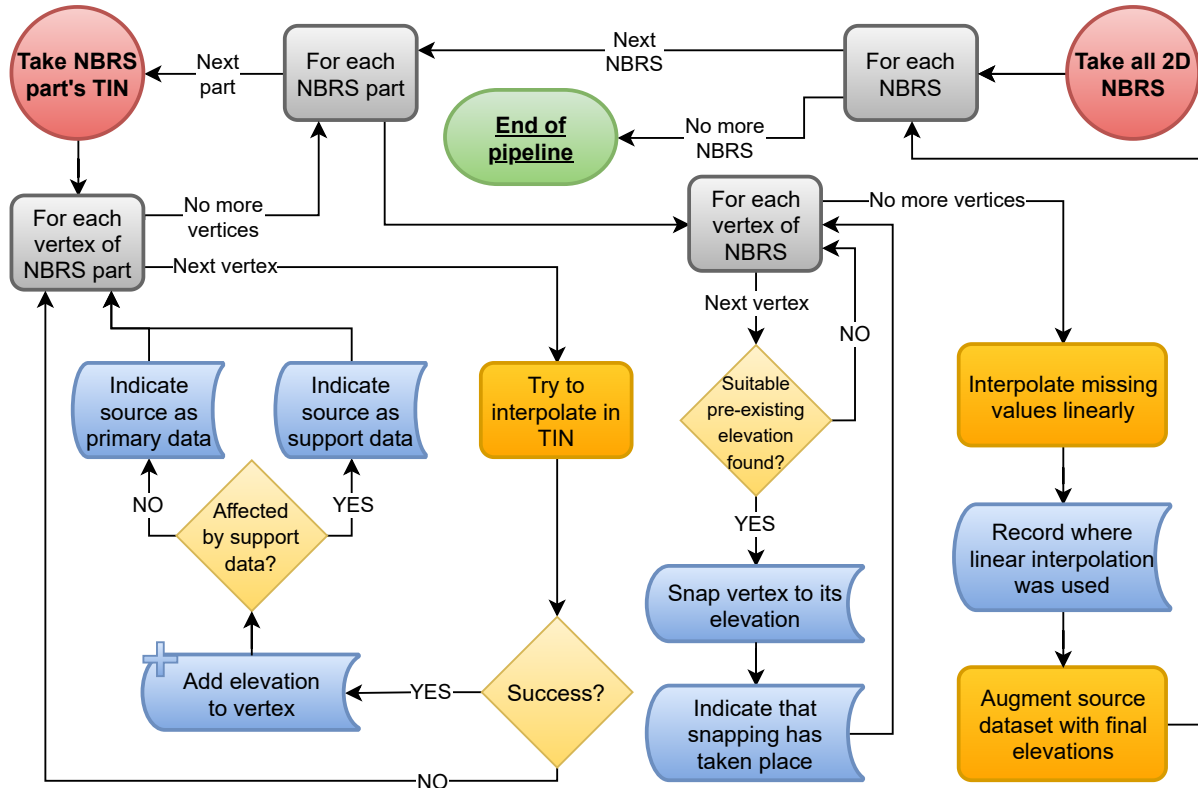


**Figure 3.10:** Flowchart-style illustration of the elevation interpolation step of the pipeline.

it is closer to the centre of the triangle, the influence of the vertices is more evenly distributed. The technique is governed by the formula

$$z_p = \begin{bmatrix} x_{pt} \\ y_{pt} \\ 1 \end{bmatrix} = \begin{bmatrix} a_0 & a_1 & a_2 \\ b_0 & b_1 & b_2 \\ c_0 & c_1 & c_2 \end{bmatrix} \begin{bmatrix} z_0 \\ z_1 \\ z_2 \end{bmatrix}$$

where  $x_{pt}$  and  $y_{pt}$  denote the X and Y coordinates of the location of interpolation (inside the triangle), the matrix in terms of  $a_0$  to  $c_2$  contains terms dependent on the 2D geometry of the triangle, and where the last vector corresponds to the three elevations of the three vertices of the triangle. Lastly,  $z_p$  is the interpolated elevation. Please refer to Fan et al. [2014] for the expressions for  $a_0$  to  $c_2$ .

## Vertex snapping and gap filling

The next step is to perform vertex snapping at intersections. TIN surfaces close to intersections are expected to be comprised of roughly the same vertices, hence the assumption is made that snapping intersection vertices together will not introduce abrupt elevation discontinuities. The procedure, performed for each **NBRS**, consists of taking each vertex one by one, and constructing a hashed data structure mapping their approximate 2D positions (coordinates to one decimal) to their exact elevations. In the underlying iteration, if the approximate 2D position of a point is already found to exist in the hashed storage, its elevation is replaced with the one already mapped to that 2D location (i.e. it is snapped to it). Since self-intersections of **NBRS** are not possible, such a match necessarily represents a location where one or more other **NBRS** end or begin - in other words, a real-life intersection.

Due to NWB's coarse georeferencing (often only one decimal or no decimals), checking 2D matches of coordinates is not enough. Each time a match is found, vertical distance is also examined prior to snapping, to avoid snapping together vertices that are at (nearly) perfectly matching 2D coordinates,

but which in fact belong to roads that are in a non-intersecting 3D relationship, i.e. one passes above the other.

The last step of the procedure is to infill gaps in the elevation profiles left by failed interpolation. Missing elevations are most commonly the result of there not being [AHN3](#) and [DTB](#) coverage in a certain place. Vertices in such locations are not part of an [NBRS](#) part, meaning that their elevations cannot be extracted from an underlying [TIN](#). Elevations may also occasionally be missing due to problems with the preliminary or optimised edges, in turn mostly due to the problems with [NWB](#)'s georeferencing.

These gaps are filled in using linear interpolation, and instead of indicating their origin as either [AHN3](#) or [DTB](#), it is recorded to be the result of such interpolation.

### Outputting 3D-NWB

The last step of the pipeline converts the internal road centreline data structure of the program ([NBRS](#) parts and [NBRS](#)) back into the data structure used by the input data, which are the LineStrings that are called *wegvakken* in [NWB](#). In effect, the 2D geometry of each input LineString is overwritten with the new 3D geometry created using the original 2D coordinates, and the newly generated final elevations. Unlike at the end of preliminary elevation estimation (see Section 3.3.2), the original orientations of the *wegvakken* is automatically respected irrespective of some of them having been internally flipped earlier in the pipeline. This is because the elevations are taken from the hashed data structures linking 2D positions to elevations, not from the flipped internal representations of these geometries.

### Challenges encountered

As the tasks carried out in this pipeline step are relatively trivial, all challenges encountered were equally simple to solve. The only part of the implementation that proved to be less straightforward was the tracking of the origin of vertices through the [TIN](#)-based interpolation - this required some minor modifications to previous steps. The implemented approach is based on hashing: all [DTB](#) points that make it into the subcloud of an [NBRS](#) part are stored in a hashed data structure at one decimal precision of their coordinates, making it quick to identify whether one of the triangle's vertices are among them that is being used for the interpolation of an [NWB](#) vertex.

## 3.4 Accuracy assessment

As I explained in Section 3.2.4 above, the estimation of output accuracy assumes no other influences than that which can be propagated through the interpolation technique relative to the input accuracy, in zones that are properly sampled. The task of identifying such regions and computing output accuracy represent the two main tasks in this step, the details of which are explained in this section.

### 3.4.1 Detecting regions with poor sampling

#### Details of sampling-related assumption

The circumstance that local sampling density *below a threshold value* does not affect interpolation accuracy is proven by previous work in this field, as mentioned in my literature review results. Of particular importance for us is [Guo et al. \[2010\]](#), which provides the most amount of detail on this topic. Neither this work, nor any other work to my knowledge derives an explicit mathematical formula that expresses a relationship between local sampling density and output accuracy below the threshold level, but this is not strictly necessary for my research, for a specific reason which I outline below.

[AHN3](#) has a nominal mean point posting distance of around 30 to 40 centimetres (6 to 10 points per m<sup>2</sup>). Considering that the dataset has a high vertical and horizontal accuracy (around 15 to 20 centimetres at

### 3 Methodology and methods

two standard deviations), we may start to suspect that [TINs](#) generated directly from [AHN3](#) will heavily oversample the road surfaces. Any unevenness seen in the models will be due to stochastic Lidar *noise*, rather than systematic errors due to local variations in sampling density or real-life road features.

In practice, the sampling density on road surfaces is often even higher than the nominal value I quoted above (see Section 4.3). At such exceptionally high baseline sampling rates, typical small-scale variations in local sampling density are of no consequence regarding the overall output accuracy. This is simply because these random, stochastic variations will never decrease the local point density to anywhere near the threshold below which output accuracy would become affected.

#### Picking an appropriate threshold

The thresholds I used are based on the results of [Guo et al. \[2010\]](#). They concluded that in the case of general terrain (not roads specifically) modelled by a raster [DTM](#) at a 0.5 m resolution, [RMSE](#) with respect to control points does not significantly decrease below 0.2 points per grid cell. Cross-validation-based [RMSE](#) values around this density were still consistently below 20 cm. In other words, 0.2 points per 0.25 m<sup>2</sup> appears to be sufficient, or equivalently, 0.8 points per 1 m<sup>2</sup>. This is much lower than [AHN3](#)'s mean density of 6 to 10 points per 1 m<sup>2</sup>, especially considering that this is even higher on locally on road surfaces owing to their flatness. Furthermore, the Lidar data used in [Guo et al. \[2010\]](#) has inferior accuracy relative to [AHN3](#).

The extra points may be useful for detecting small-scale features (such as e.g. small slumps in the roads surface), as well as better characterising the edges of roads. However, if we look at the problem strictly from the point of view of the 3D conversion of [NWB](#) and the modelling of the surface's overall shape, then we are only interested in monitoring where the point density goes below the threshold above which the [RMSE](#) with respect to surveyed control points remains relatively constant. If we assume that about 1 point per 1 m<sup>2</sup> is sufficient to characterise a rugged surface using Lidar, then we could consider drops of up to 95% in [AHN3](#)'s point density to be acceptable.

To make sure I use a conservative value, I opted to stay somewhat above this estimate. At each [NWB](#) vertex, I examine the number of [TIN](#) vertices that fall within 3 metres of it, and if it is less than 3 points, then flag the output accuracy at that point to be unreliable. This corresponds to a a threshold of 3 points per 1 m<sup>2</sup>.

#### Types of areas violating the assumption

In most places, the local sampling density must drop by more than 80% to reach the above minimum threshold, which means that it only happens in extreme events. As we lack a mathematical formulation describing the exact nature of the influence below the threshold sampling rate, the best we can do is mark the accuracy of vertices falling into such areas as *unknown* in the output.

Places where linear interpolation was used, the threshold-based evaluation is automatically assumed to be violated. They generally correspond to areas where there is no [AHN3](#) and [DTB](#) coverage, meaning that the local sampling density is zero, or nearly zero. Even in areas where linear interpolation had to be used due to the poor georeferencing of [NWB](#), the values were not based on the samples in the local [TINs](#), hence sampling density can considered to be zero there, too.

The threshold may also be violated due to an insufficient amount of detail in the [TIN](#), but this is atypical in practice. Sampling density can only reach such low values in the [TINs](#) due to *significant* amounts of occlusion due to objects opaque to Lidar (so not vegetation). Notably, the threshold of 3 points per m<sup>2</sup> deems it reasonable to regard most elevations reliable which were interpolated inside medium-sized gaps resulting from vehicles or other stationary objects on the roads, as well as some that are found in regions where only [DTB](#) coverage is available - although the latter should be treated with some skepticism, as I noted in Section 3.2.4 earlier in this chapter.

### 3.4.2 Effect of interpolation of accuracy

Theoretical proof suggests that the interpolation step generally *improves*, rather than deteriorates the output accuracy. This can intuitively be thought of as the result of basing each output elevation on the combined information stored in the three vertices of the triangle in which the elevation is being interpolated.

This is contrary to what one might assume based on thinking about the pipeline as a whole, but both in practice and in theory, it is the *other* influences on accuracy that generally have the opposite effect. For instance, problems with ground filtering and a sparse local sampling may have negative effects on accuracy locally. However, the interpolation itself has no such effect on the output under normal circumstances. We can thus assert that the formal accuracy of the output will *mostly* increase relative to the input in well-sampled regions. I present the relevant error propagation results from [Fan et al. \[2014\]](#) below.

Let  $\sigma_{z_{vx}}^2$  denote the elevation variance of the vertices of the triangle, and  $\sigma_{xy_{vx}}^2$  denote the horizontal variance. We may then express the relationship between the elevation accuracy at the point of interpolation  $\sigma_{z_{pt}}^2$  as

$$\sigma_{z_{pt}}^2 = M \left( \sigma_{z_{vx}}^2 + \sigma_{z_{node}}^2 \left( \tan(\alpha_x)^2 + \tan(\alpha_y)^2 \right) \right)$$

where  $\tan(\alpha_x)^2$  and  $\tan(\alpha_y)^2$  correspond to the angle between the triangle's plane and the X and Y axes of the CRS. The expression takes into account the steepness of the plane to be able to propagate the horizontal error, hence the necessity of computing these angles. The variable  $M$  is a parameter that needs to be pre-computed for each triangle, as it depends on their 3D geometry. The underlying formula will not be listed here as it is not relevant to this discussion, please refer to the original paper for it.

Since [AHN3](#) and [DTB](#) points and vertices have no individual accuracy measurements, the above formula takes a single accuracy value per triangle, rather than a separate value for each vertex. Like in the origin-labelling step I described in Section 3.3.7, I make the assumption that [DTB](#)'s accuracy should only be used in this formula, if all three triangle vertices are based on [DTB](#) data.

The expression is, in essence, a sum of the input variances scaled by geometric variables. Most importantly  $M$  has a range between about 1/3 and 1, taking its lowest value around the centroid of the triangle, and increasing to 1 at the triangle's vertices. Intuitively, the closer we are interpolating to one of the vertices, the smaller the other two vertices' influence is going to be due to the nature of TIN-linear interpolation. We are thereby gradually taking into account less and less information, decreasing to the minimum at the vertices, where only one input elevation measurement is considered. Assuming that the [NWB](#) vertices are randomly distributed relative to triangle vertices, the expected value of  $M$  is 0.5.

Substituting values into the above formula with  $M = 0.5$  reveals that applying TIN-linear interpolation to surfaces with sufficiently low inclinations decreases the elevation error relative to the input. For instance, a triangle with a 2-degree inclination and vertices with 10 cm vertical and horizontal standard deviations (similar to [AHN3](#)) yields an output elevation standard deviation of 7 cm, a 30% decrease. Increasing the inclination to 45 degrees decreases the vertical accuracy of the output to 12 cm, which is now worse than that of the input.

Such steep roads are practically absent in The Netherlands. For Dutch roads, the accuracy is thus expected to increase. However, oversampling the surfaces too heavily with a non-zero stochastic scatter in the elevations can yield small artefact triangles that are inclined anomalously. These inclinations are meaningless, as they do not represent the geometry of the underlying road surfaces, and care should thus be exercised when interpreting the accuracy assessment values of results that were generated using most of the original Lidar points. More information on this topic is found in Section 4.3.

### 3.4.3 Evaluating TIN surface completeness

To evaluate how complete the generated [TIN](#) road surfaces are relative to the true road surfaces, I relied on a visual comparison of the [TINs](#) with the subclouds, as well as on a comparison with [BGT](#) ([Kadaster \[2021\]](#)). Like [AHN3](#) and [DTB](#), it is a Dutch open data geospatial dataset. It is maintained by Kadaster, the national cadastral agency. It is a topographical map of the country which contains a wide range of classified areal features - such as city, building, and *road* extents.

Like [NWB](#), [BGT](#) is also primarily intended to offer good topological accuracy, thus its 2D georeferencing is also relatively crude. However, upon a comparison with the Luchtfoto 2020 orthoimagery (also from Kadaster, see [PDOC \[2021\]](#)), I deemed its road polygons reliable and accurate enough to serve as a reference with which my results can be compared. To make the comparison, I plotted some of the output [TINs](#) against the relevant [BGT](#) road outlines in 2D and assessed the agreement between them visually. An example of the results of this step, as well as a comparison of [BGT](#) and [NWB](#) with satellite imagery, are shown in Figure 4.20.

## 3.5 Comparison with commercial results

A simple method to evaluate the relative quality and accuracy of the commercial results is to examine variations in the agreement between the elevations predicted by the academic and commercial results visually, and quantitatively by computing residuals and [RMSE](#) values.

However, we know from the previous section that the academic results have an output accuracy that is either on par with or better than that of the input, with the exception of areas with poor sampling density. Where the sampling density is high, we can use the academic results as reference to advise us about the *absolute* accuracy of the commercial results, not just relative to the academic ones.

In places where the academic results have unknown accuracy, the commercial elevations are also necessarily uncertain because the same datasets were used in their production. However, their overall quality may still be different than ours, because their methods use the input data differently. In such places, the comparison relies on human interpretation. To aid the interpretation, I computed and plotted the residuals between the two sets of results in a number of LineStrings (*wegvakken*) that I picked for comparison. Correlating these with comparison plots of the elevation series, as well as 3D plots of the data and underlying [AHN3](#) and [DTB](#) points provided further input to this process. I also employed the generation of [RMSE](#) values on the level of *wegvakken*, as well as for entire testing datasets. The [RMSE](#) is given by

$$RMSE = \sqrt{\frac{\sum_{t=1}^T (z_{a,t} - z_{c,t})^2}{T}}$$

where the elevation samples in a profile are numbered from  $t = 1$  to  $T$ , and where  $z_{c,t}$  denotes the elevation estimated by my method and  $z_{a,t}$  denotes the commercial result at the same location.

When performing the above comparison on a LineString, the distances from its first vertex along the profile from  $t = 1$  to  $T$  are computed, this is what the elevation series and residuals are plotted against. The residuals are the values taken by  $z_{a,t_{nwb}} - z_{c,t_{nwb}}$  where  $t_{nwb}$  corresponds to *original NWB vertices*. Both the academic and the commercial pipelines use vertex densification, but the resulting vertices are not located in the same place. Thus, the residuals and the [RMSE](#) values describe only how well the two methods agree at the location of the *original NWB* vertices.

## 3.6 Programming framework

The implementation part of this project is intended to investigate how well each step of the pipeline works in practice, how well they work together as a pipeline, and how accurate their output is. In turn, these serve the purpose of answering the research questions detailed in Section 1.4. In addition,

implementation-related tasks were also important in iteratively revising the methods based on the practical experience gained in the process, making them better adapted to real-life scenarios (and as result, more relevant to reusers).

### Notes on performance

As the implementation is primarily intended for demonstration and reference purposes, it is by no means ready for all types of academic and commercial use out of the box. One limiting factor in this sense is the lack of a scaling mechanism in the implementation, as such considerations were not part of this research. Furthermore, I developed all parts of the pipeline in Python 3.8, which means that the code is more concise than a binary implementation would be, but its runtimes are higher. To improve performance, I relied on binary-based libraries such as *numpy*, and parts of *scipy*. In addition, I used hashing-based data structures (in Python these are called dictionaries and sets) extensively, which are also known to benefit performance greatly. Many of these uses of hashing are mentioned previous sections explicitly, and wherever I mention using KD-trees, I refer to building code on top of the binary implementation in *scipy*. Uses of *numpy* are so pervasive in the code, that I opted not to mention them explicitly in the text.

While geometries (and geometric operations) are often handled in *shapely*, I avoided its use in all cases where geometries are bulk-processed via long iterations. I found that implementing the geometric operations from first principles in *numpy* in such cases resulted in a noticeable gain in performance.

Unfortunately, the implementation of active contour optimisation in *scikit-image* is mostly based on native Python iterations, not on binary packages. This circumstance, in conjunction with the large number of vector inner products that the attractor map generation requires, means that the computational complexity of the active contour-related part of my software is a magnitude slower than all other parts.

### GitHub release and code structure

I released the source code of the implementation in the following GitHub repository: <https://github.com/kriskenesei/geo2020-modules>. Most functionality resides in the class `nbrs_manager` inside the file `nbrs_generation.py`. I factored out some functionality into `lib_shared.py` to somewhat simplify the code in `nbrs_generation.py`. Both files contain an extensive set of docstrings and inline guidance on what each part of the code does. The intended audience of this information includes those simply interested in knowing more about the practical aspects of processing that underlies this research, as well as potential reusers.

The class `nbrs_manager` is intended to be instantiated with the cropped road network, followed by the invocation of class methods corresponding to each pipeline step. In addition, vertex densification is also implemented as its own class method, and a range of methods are provided for basic operations such as setting individual *wegvak* geometry, as well as writing the intermediate results of each pipeline step to disk separately. Furthermore, the class holds certain intermediate results in its class variables which cannot be written to disk natively, but which may be interesting to reusers.

The structure of relevant part of the next chapter (Section 4.2) is modelled on the steps one would take to run my software, to create a stronger link between the explanations and the implementation. The method invocations that I used to generate the results shown in the chapter are explicitly listed at the end of the sections describing the relevant pipeline steps. A condensed explanation of how the implementation is meant to be used can also be found in the docstring of `nbrs_manager`, and a set of example calls are also provided at the end of the file `nbrs_generation.py`.



# 4 Results

In the previous chapter, I described the theoretical structure of my processing pipeline, giving a detailed account of the algorithms and procedures relevant to each pipeline step. Being the result of a process of iterative refinement and revision, these were partly based, in fact, on my practical experience at implementing them and testing how effective they are at fulfilling their roles. As a result, the final methods and results of this research are interlinked and were thus difficult to separate into two chapters.

In this section, I will not dedicate much attention to the changes introduced during development, as I already addressed this topic in the previous chapter. Instead, I will restrict the discussion to focus only on the relationship between the final version of the code and the outputs it produces. In this chapter, I will only mention the challenges that lead to changes in the system design, where figures are shown that illustrate them well.

In the following sections (4.1, 4.2), I will show the intermediate results of each step of the pipeline visually in figures, as well as describe them in the text. This showcase and description of the results will focus primarily on the effectiveness of the final implementation and system design, and the quality of the results it produces.

The last sections of the chapter (4.3, 4.4) contains a section in which the results of quantifying the quality and accuracy of the output are shown and discussed, followed by a section in which the commercial results and the present academic results are compared, especially in terms of the overall quality of the results they produce.

## 4.1 Manual pre-processing

### 4.1.1 Producing the testing datasets

Implementing a scaling solution was not part of this project, although all parts of the implementation were designed in a way that a scaling framework could be added to it with a relatively small amount of effort. Among other things, scaling in this project concerns the need to subdivide the input data in a way that the software never runs out of memory while processing it. These subdivisions could be generated, in the simplest case, based on tiling, i.e. overlaying a 2D raster on the extents of the data and examining which cell certain features fall into.

As scaling was not part of this project, the task of creating manageable subsets of the input data was carried out manually. The procedure consisted of cropping the input vector datasets ([NWB](#), [DTB](#)) into tiles showing interesting and representative road layouts, and for each of them, creating an [AHN3](#) file with those points, which are a set maximum distance from any relevant roads ([R-roads](#) and [P-roads](#)) in their respective [NWB](#) tiles. For vector data processing, I used [QGIS](#), and for Lidar processing I used [LASTools](#).

I derived the area of interest in which to keep Lidar points by buffering the centrelines in the [NWB](#) tiles by 150 metres, and passing these geometries on to LASTools to use to *clip* the relevant [AHN3](#) tiles. [AHN3](#) itself comes tiled in the official release (on a much larger scale), and I derived each testing dataset from a single [AHN3](#) tile to keep the manual procedure simple. I also discarded [AHN3](#) points not classed as ground or bridge points at this stage (2 and 26 respectively), as they are not relevant to our methods.

Visualisations are shown in Figure 4.1 in which an [NWB](#) tile and the Lidar clipping polygon (on the left) is shown alongside the clipped point cloud tile (on the right). The clipping polygon was manually edited to have sharp, linear boundaries and [NWB](#) *wegvakken* (yellow lines) intersecting its interior (red

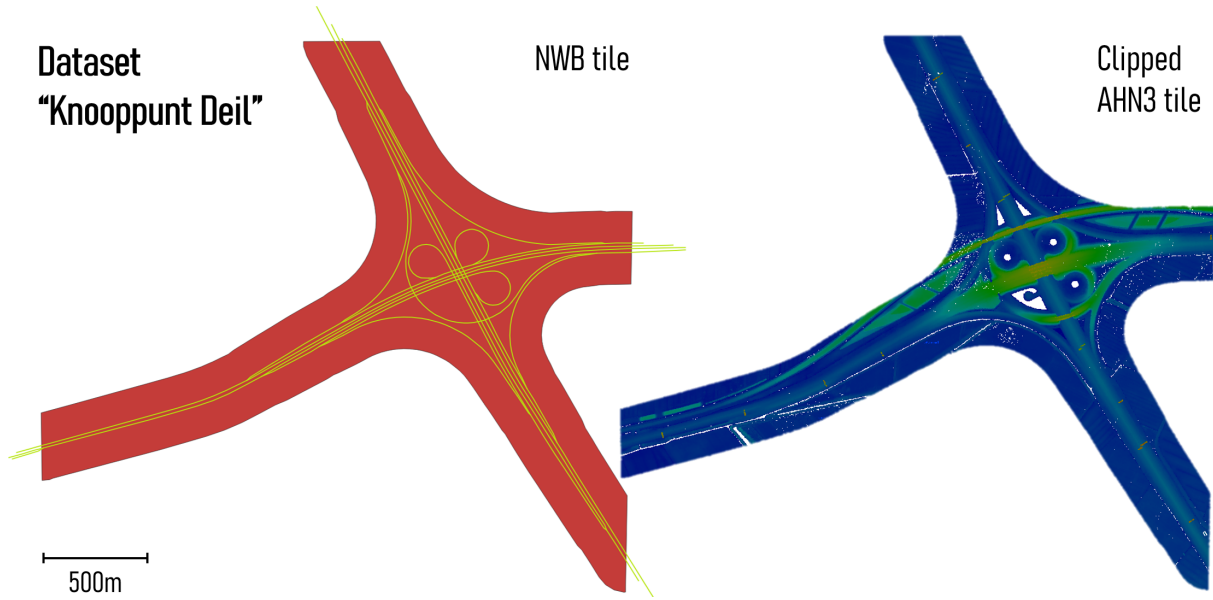


**Figure 4.1:** Visualisations illustrating the results of manual pre-processing.

areas) were included in the testing dataset. The resulting occasional overshoots of NWB centrelines (relative to AHN3) allowed me to test how well the procedure performs in areas where AHN3 is completely unavailable for a short distance, but where DTB coverage is present - hence, I kept them. They also caused unforeseen issues in the accuracy assessment, which I will discuss in Section 4.3.5. On the right, the point cloud is shown in its original density, not a derived DTM. Darker areas represent lower elevations, the total elevation range shown in the image is about ten metres.

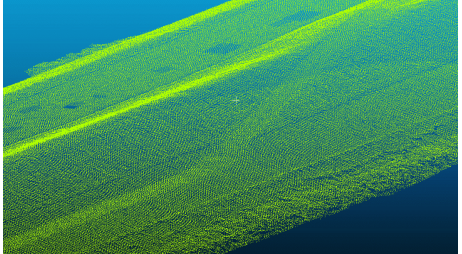
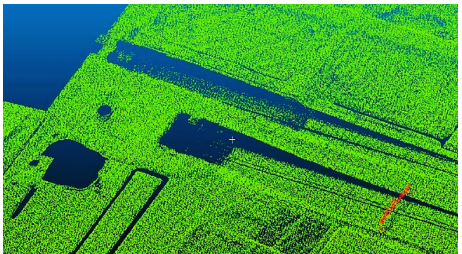
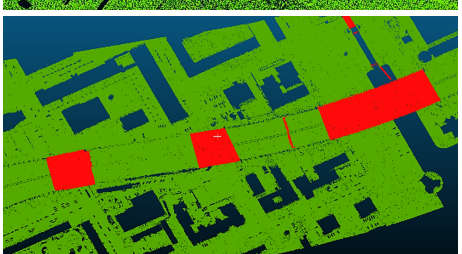
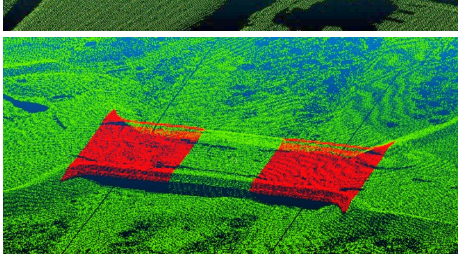
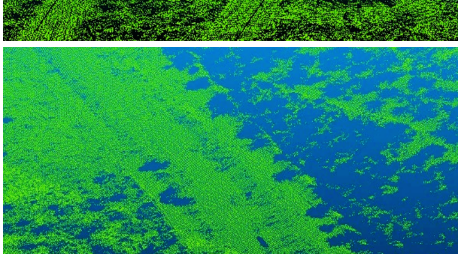
I created 11 testing datasets in total, each with its own cropped NWB, DTB and AHN3 files, which are described in the next section. The dataset shown in this figure is *Knooppunt Deil* (from AHN3 tile 39CZ1).

I picked 150 metres as a buffer distance for point cloud clipping not because I expected road surfaces to be so wide, but because I found that it reduced the volume of points to manageable levels in my testing tiles, while retaining plenty of neighbourhood information which I found to be useful for debugging purposes, and for the assessment of how well my algorithms perform in various environments next to roads - in other words, they provided context for the interpretation of intermediate results. Using a smaller buffer distance would lead to slightly reduced runtimes, but only by a small margin.

#### 4.1.2 Description of testing datasets

The set of chosen areas needed to be representative of the whole country to provide an insight into the effectiveness and performance of the algorithm in as many scenarios as possible. Furthermore, I also deliberately included areas which I thought would prove especially challenging, such as roads with many stationary vehicles, roads in multi-level 3D relationships (in motorway junctions), as well as tunnels.

Table 4.1 provides an inventory of these datasets. The tile identifier in the first column refers to those used in PDOK [2020]; each dataset is found within a single AHN3 tile as I mentioned in the last section. The resulting datasets fit into memory easily even on a mediocre computer, and are also small enough to allow intermediate results to be visualised and interpreted quickly.

Title, tile	Features	Render
Markerwarddijk, 20BN1	provincial road on a dike in the Markermeer. Very limited amount of terrain around the road. Road consistently built on ground, there are no bridge structures.	
Amsterdam Hemhavens, 25BZ2	Ringweg-West motorway as it crosses the IJ through the Coentunnel in a densely built-up environment. It is built on artificially elevated ground and on bridges in this area. Part of Westrandweg also included, built entirely on a long bridge.	
Amsterdam Zuid, 25DN2	R-roads with many closely spaced bridges, small tunnels, dense grouping of holes around roads due to presence of water and buildings	
Bunschoten, 32BN1	P-roads with three big roundabouts, and one road that ends in a small roundabout. Amersfoortseweg has its two lanes on separate road surfaces (like motorways), but with frequent connecting segments.	
Veluwe, 32FZ2	Straight R-roads surrounded by dense forest and crossed by wide wildlife overpasses.	
Apeldoornseweg, 32HZ2	P-roads in dense forest with canopy frequently occluding the road surface, decreasing point density and occasionally creating gaps. The road has small parallel branches running very close to it, which may make it difficult for the algorithm to distinguish between them. It also has roundabouts.	

## 4 Results

Hoenderloo,  
33CN2

P-roads in extremely dense, continuous forest with canopy frequently occluding the road surface, decreasing point density and occasionally creating gaps. Both lanes are on the same road surface



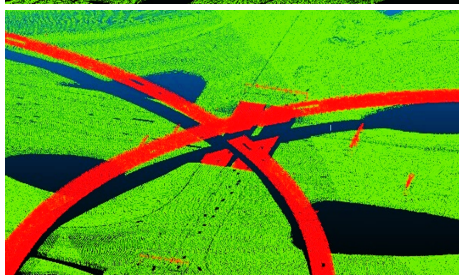
Rotterdam  
Ketheltunnel,  
37EZ1

This segment of the A4 heading North from Rotterdam has been recently reconstructed in an underground tunnel. In addition, a significant portion of this motorway now runs in a trench towards Delft. AHN3 was imaged during the reconstruction, and hence contains anomalous data about the road surface.



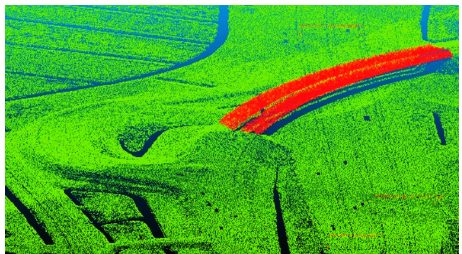
Knooppunt Ridderkerk, 37HN2

The Ridderkerk junction is one of the largest of its kind in The Netherlands, in one place containing 4 overlapping R-roads. Furthermore, it contains a high density of R-roads in a small area, many of them very tightly packed. Many of them have very sharp bends.



Gorinchem,  
38GZ1

Complex junction between P-roads and R-roads with small ramps, roundabouts and overlapping geometries.



Knooppunt Deil,  
39CZ1

Less complex, but analogous junction to the Knooppunt Ridderkerk.

*Please refer to Figures 2.7, 2.8, 2.6 and 2.10.*

**Table 4.1:** Inventory of testing datasets

One instance of my software can process a single testing dataset at a time. However, running multiple Python instances in parallel allows one to easily parallel-process multiple tiles depending on the CPU installed in the computer. Each dataset consists of a cropped NWB and DTB file, and the clipped AHN3 point cloud.

All datasets mentioned in Table 4.1 are part of the GitHub release of the results. A compressed archive with the input testing files (and all intermediate results and final results) can be downloaded via a link found in the repository's readme file.

## 4.2 Results of processing steps

The results below are presented in the same section structure as the detailed methods were in Section 3.3 of the previous chapter. This is intended to make it easy for readers to correlate the results with the theory underlying the relevant processing mechanisms. In each section, I describe - with the help of 3D visualisations - how well each processing step performs, and how effective and useful they are in the

context of the entire pipeline as a whole. I also devote attention to describing typical scenarios in which algorithms are useful and perform well, as well as ones where the opposite is true and they may produce sub-optimal results. Lastly, in each of the pipeline steps I make mention of how exactly the underlying software implementation is meant to be used, with notes on the recommended arguments.

### 4.2.1 Splitting NWB into NBRS

Each line colour in Figure 4.2 corresponds to a specific **NBRS** ID, meaning that LineStrings (*wegvakken*) belonging to the same **NBRS** are also coloured the same. The figure demonstrates that as a result of the **NBRS** generation step, the cropped road network becomes semantically enriched with identifiers linking certain LineStrings together, based on semantic or geometric conditions depending on which algorithm was used.

The colours are generally inconsistent between the results of the two algorithms (top and bottom parts of the figure). Although the same colour scheme was used to prepare them, the two algorithms distribute the **NBRS** IDs differently.

#### Issues with geometric algorithm

The figure also serves to illustrate the fundamental differences that exist between the results of the two algorithms. The geometric algorithm makes the assumption that the 2D georeferencing of **NWB** is fully representative of the real-life geometry of road centrelines. However, I found this to be violated in various places as already mentioned in Section 2.3.1. In short, where **R-roads** intersect (this includes ramps, motorways and all combinations thereof), they often do so at abrupt angles, which can be observed in various places in Figure 4.2, and especially in the insets. These angles are not representative of the real-life road geometry, they were drawn manually by data handlers to ensure that **NWB** complies with certain external requirements. Consequently, they may prevent correct decisions from being made based on the intersection angles.

In places where the above intersection angle related problem exists, choosing the straightest continuation across an intersection when building an **NBRS** does not necessarily represent the optimal choice, because the angles are artificial. This can be observed in the inset of the top chart in Figure 4.2, where I numbered some of the **NBRS** on the geometric results. While the geometric algorithm obviously made the right choice *based on the pairwise angles* between the individual road segments concerned, attribute table data told the semantic algorithm that the role and road number of certain parts of **NBRS** 0 and 2 are the same as that of **NBRS** 1, which resulted in these parts of **NBRS** 0 and 2 connecting via **NBRS** 1. The "discarded" ends of **NBRS** 0 and 2 then became two unique **NBRS** by themselves. In the overall large-scale context of the local road network, the semantic algorithm evidently made the correct choice, even though this introduced some small, abrupt internal angles into the **NBRS**.

#### Issues with semantic algorithm

The green dotted circle in the semantic **NBRS** generation results points out a place where the role and road number of a ramp changes suddenly, outside of a real-life intersection, which results in the algorithm abruptly starting a new **NBRS** there. This is indicated by a change of colour from dark to light purple. The break happens in an unfortunate location, in the middle of a multi-level junction where the continuation of **NBRS** is crucial so that large-scale trends across the complicated zone may be recognised effectively in later steps. This demonstrates that while the geometric algorithm is sensitive to problems with the georeferencing of the data, the semantic algorithm is sensitive to issues with the attribute table data. Within the testing tiles I examined, the two algorithms offered a comparable amount of benefits and drawbacks.

## 4 Results

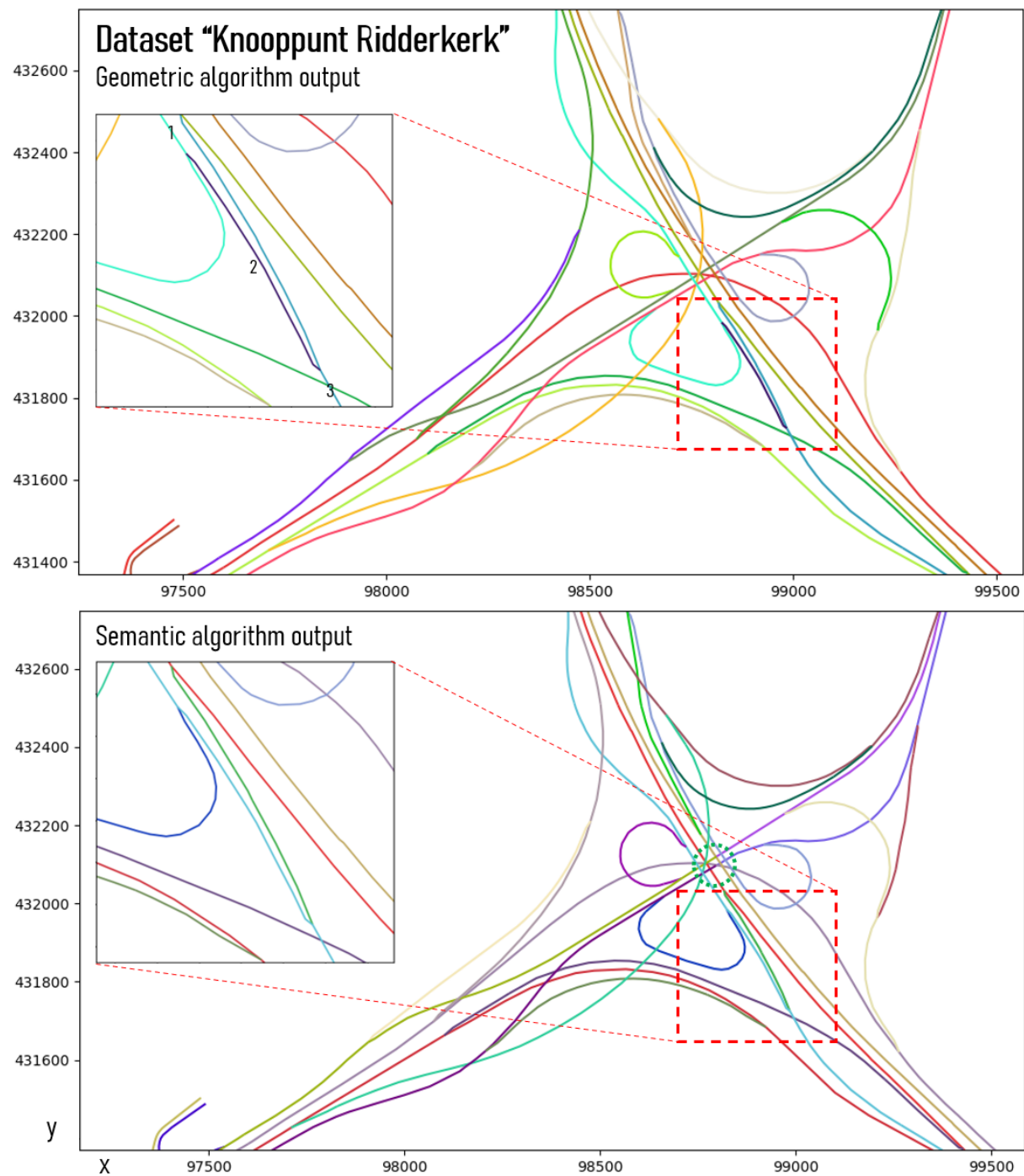


Figure 4.2: Visualisations illustrating the results of NBRS generation.

### Evaluation and choice of algorithm

Both algorithms produce usable results overall. In general, the resulting chains of *wegvakken* (LineStrings) satisfy all the original requirements I set for the outputs of this step (minimise internal angles, maximise length, disallow self-intersections and branching). Based on some further testing after implementing the rest of the pipeline, I also verified that the choice of algorithm does not significantly influence the output of subsequent steps.

Since the geometric algorithm generalises to arbitrary road networks better than the semantic algorithm (i.e. does not rely on specific properties of [NWB](#)), I used it to generate the rest of the results shown and discussed in this report.

### Using the implementation

In the software, before [NBRS](#) generation can be executed, the `nbrs_manager` class needs to be initialised with the file path to the cropped [NWB](#) file of the desired dataset. Example calls to perform geometric [NBRS](#) generation are provided below.

```
roads = nbrs_manager(fpath = nwb_fpath)
roads.generate_nbrs(algorithm = 'geometric')
```

In the code snippet above, `nwb_fpath` refers to a variable containing the file path in the operating system to the cropped [NWB](#) file of the desired testing dataset. For instance, the file path could end in `.../C_39CZ1_nwb.shp`, using the naming convention of the released testing files, the dataset called *Knooppunt Deil* is desired. Switching to `algorithm = 'geometric'` triggers the use of the semantic algorithm.

The invocation `roads.plot_all()` may be executed to plot the results on a 2D diagram using random colours to distinguish between [NBRS](#). At this point, [NBRS](#) generation results are saved in class variables only (see `roads.nbrs_wvkn`), hence running `roads.write_all()` at this point is **not** going to write the [NBRS](#) IDs into the attribute table. The imported road network is stored in `roads.nwb` in a GeoDataFrame which also contains the generated [NBRS](#) IDs.

### 4.2.2 Elevation estimation

Figure 4.3 shows the results of this step in two 3D visualisations. The [NWB](#) centrelines are shown once again in random colours based on which [NBRS](#) they belong to, but now they are shown at their estimated elevations. The vertical dimension in this visualisation and all other 3D visualisations in this chapter are exaggerated 5-fold, so that changes in elevation are made better visible. The figure contains two visualisations that allow the reader to examine the same results from multiple viewing angles.

### Vertex densification

The vertices were densified before running preliminary elevation estimation; I used a threshold of 5 metres for the final outputs shown here. This means that no individual line segment in the 3D road network is longer than 5 metres. I found this threshold value to offer a compromise between longer processing times (in later steps) and more refined results.

We may say that while the horizontal dimensions were merely oversampled, the vertical sampling benefited from the vertex densification in the sense that it is far more detailed than it would be without them (as also mentioned in Section 3.3.2). An example visualisation of what happens to a specific [NBRS](#) during vertex densification is shown in Figure 4.4.

## 4 Results

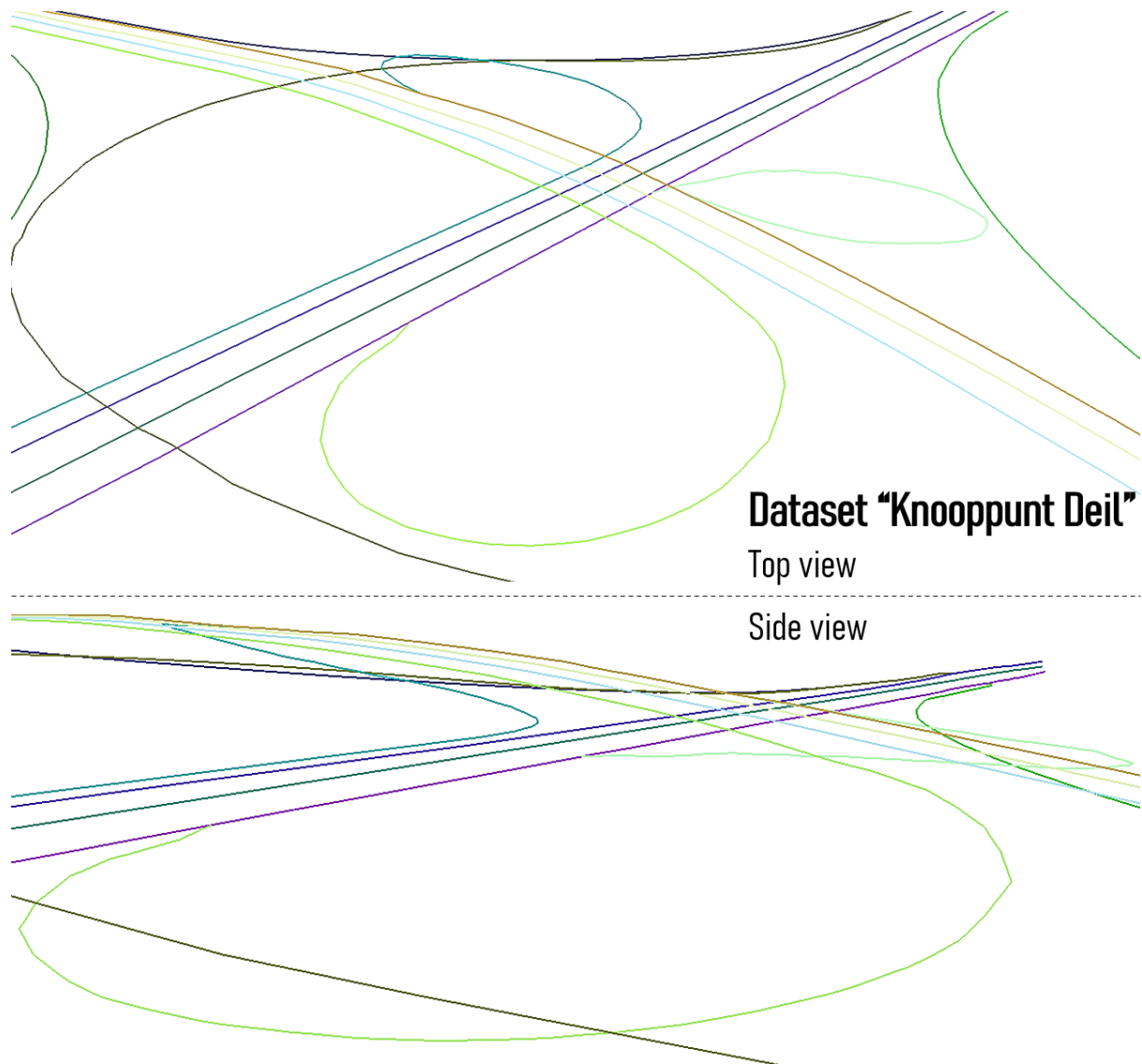


**Figure 4.3:** Visualisations illustrating the preliminary elevation estimation results.

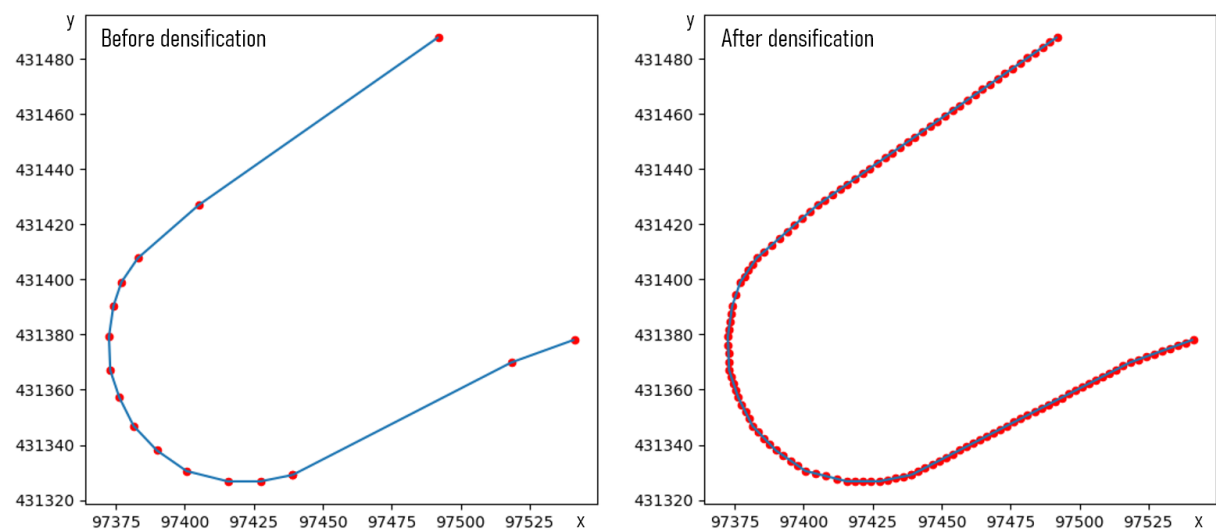


**Figure 4.4:** Visualisations illustrating the vertex densification feature.

### Types of challenging scenarios

Instead of focusing on details, I will only comment on the general quality of the results, since accuracy is not yet important at this step - this 3D conversion is merely a stepping stone towards the goal of performing Lidar segmentation. It only needs to fulfil its purpose in the processing workflow (to yield candidates for the subclouds), rather than to be a perfect representation of the surface. In fact, in practice it just needs to be closer to it than to any overlying points present due to occlusion.

There are two main aspects of the output that require our attention: how well the 3D centrelines conform with the real-life road surface (effectiveness of the 3D conversion), and how successfully outliers are being eliminated (effectiveness of the refinement step). The former can be assessed via a visual comparison with the underlying [AHN3](#) point clouds, while the latter can be examined by looking for artefacts at locations where occlusion happens. Figure 4.5 shows two further 3D visualisations that contain examples of the features that are relevant for this assessment.

### Effectiveness of 3D conversion

The top visualisation in Figure 4.5 illustrates that in the case of flat lengths of roads, centrelines are generally positioned very close to the Lidar-defined road surface (within a few centimetres in general). Outliers are atypical in well-exposed areas, corresponding to the lack of outliers in [AHN3](#) itself (and its ground classification). The procedure is fast, runtimes for the testing datasets are generally in the range of 1 to 5 seconds on a mediocre computer.

Thinning the input point cloud aggressively can marginally improve the performance of this step, but it also drastically reduces its effectiveness in areas that are poorly sampled. This in turn may result in artefacts on a scale that also confuse the refinement step. I found that working with no thinning applied, or a maximum thinning factor of 3 (33% of points kept) at most, works best. My final configuration uses a thinning factor of 2 when it imports the [AHN3](#) data, which is carried over to all subsequent steps that work with it.

There is a range of factors that may result in the computation of anomalous preliminary elevations due to occlusion. Firstly, if an [NWB](#) centreline is positioned far from the actual road centreline (or next to the road), then the 3D elevations will be derived from a patch of Lidar points that may include a significant number of off-road points. This may result in both positive and negative outlier elevations being computed relative to where [NWB](#)'s georeferencing is correct. Furthermore, bridges in [AHN3](#) include reflections from civil engineering structures, which are often attached to roads close to their edges. If the centreline of an [NBRS](#) falls too close to the edge of the road where such objects are present, its elevations may be corrupted by Lidar points reflected from them, rather than from the road surface.

Furthermore, slow or stationary vehicles and motorway signs (due to their presence in classification 26), and larger occluding objects (e.g. bridges built *over* a given road) tend to generate a sequence of outlier vertices, depending on the size of the object. Gaps in [AHN3](#) coverage (e.g. where a road passes underneath water in a tunnel) can also give rise to missing elevations in the output of this step. Both the outlier elevations and the missing elevations resulting from these artefacts are mostly eliminated by the refinement step.

The query radius used in the KD-tree queries in my final configuration is 1 m. At the typical local posting distances found in [AHN3](#), this represents a compromise between fetch enough samples to minimise the effects of small-scale outliers and minimising the chances of including off road points where [NWB](#) deviates from its optimal position. This query radius corresponds to a query area of  $1 \pi$ , which typically corresponds to selecting about 30 to 120 [AHN3](#) points in practice, depending on the local sampling density (assuming a thinning factor of 2 was used).

#### 4 Results

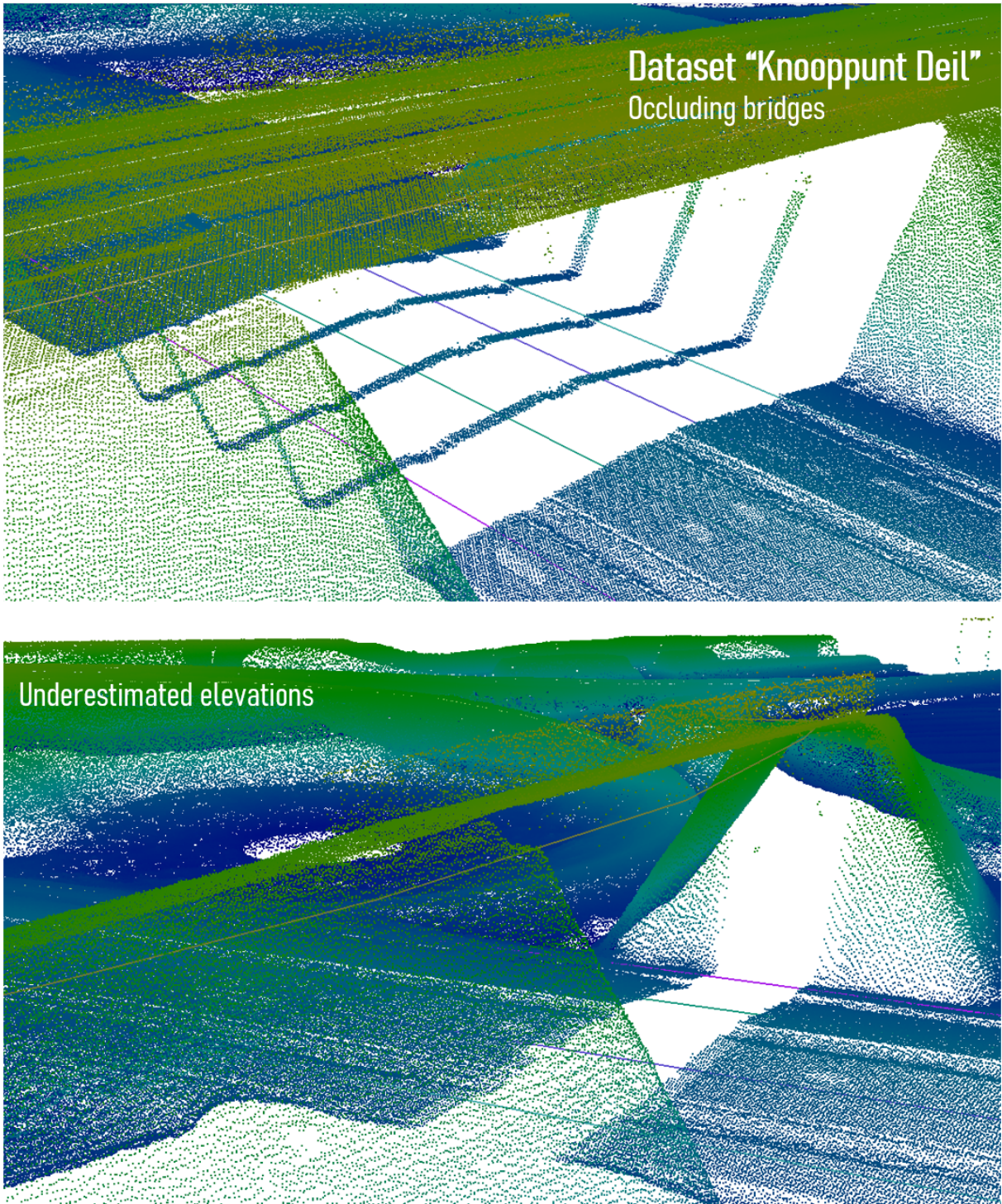


**Figure 4.5:** Visualisations comparing preliminary 3D conversion results with the [AHN3](#) point cloud.

### Effectiveness of refinement step

The effects of the refinement step can be observed in the shape of the *lower* set of 3D centrelines shown in the top visualisation in Figure 4.5. The series of bridges causes occlusion, meaning that Lidar coverage is intermittent for the lower set of roads, for a distance of about 70 metres. Initially (before the refinement step), the centrelines of the lower set of motorway lanes thus became snapped to the elevation of overlying roads. The resulting outliers were easily identified and eliminated by the refinement step, and new values were interpolated based on the polynomial model that was fitted on the NBRS.

For my final outputs, I used a degree of 8 for the polynomials, and set the outlier filtering threshold to 0.2 times the standard deviation of the data-model errors in the given polynomial fit. I found that in general these parameters work best with the testing datasets. Standard deviations below 0.4 metres are artificially increased to 0.4 metres to avoid modifying elevations in roads whose conformance with the model was already found to be near-perfect. More information about the detailed processing (and thus, the exact way in which these parameters are used) in Section 3.3.2.

This approach proved to be an effective solution in terms of eliminating occlusion-related artefacts, it is ineffective only in places where the occluding geometry is very close to the road surface. For instance, stationary vehicles occasionally introduce outliers that are not far enough from the model to be detected in the refinement step, thereby giving rise to small spikes in the output. This does not happen frequently, and does not represent a problem in the context of the pipeline as a whole. This step also fixes any outliers caused by motorway signs, which are high enough above the road surface to be detected.

A lower limit for the outlier filtering threshold is set, in practice, by the accuracy of the polynomial fits themselves. If the value is set too low, elevations that were in fact already correct may be replaced with values from poor polynomial fits. This issue arises where the vertical curvature of the modelled roads is unusually high, such as in the overpass shown in the bottom visualisation in Figure 4.5. Such curvature is difficult to approximate using polynomials, especially if the corresponding NBRS is long and also contains other types of curvature.

Even when using a sufficiently high outlier filtering threshold, the algorithm may occasionally identify lengths of such roads as outliers and reposition them to the incorrect elevation level set by the polynomial model. I successfully bridged this relatively uncommon issue by taking it into account while implementing the Lidar segmentation workflow, which will be mentioned in the next section. Therefore, these inaccurate elevations do not represent a problem on the scale of the pipeline as a whole, because the next pipeline step is not sensitive to them. Shorter NBRS lengths could help deal with this problem in a more explicit manner, but this would also mean that certain longer trends would become impossible to model later on.

### Using the implementation

The below code snippet shows the code that I used to generate my final results.

```
roads.densify(thres = 5)
roads.estimate_elevations(fpath = ahn_fpath, r = 1, thin = 2)
roads.write_all(fpath = simpleZ_fpath)
```

The first line performs vertex densification with a threshold of 5 metres. The second line performs the preliminary elevation estimation (and refinement) step, the variable ahn\_fpath is assumed to contain a file path to the clipped AHN3 file belonging to the desired testing dataset. For instance, it could be .../C\_39CZ1\_2\_26\_clipped.las using the naming convention of the input files I released on GitHub. The tags \_2\_26\_clipped in these file names refer to having kept only points in classes 2 and 26 (ground and bridge points respectively), and having clipped it to the extents of buffered centrelines. The variables r and thin control the query radius and thinning factor respectively, their default values are shown.

## 4 Results

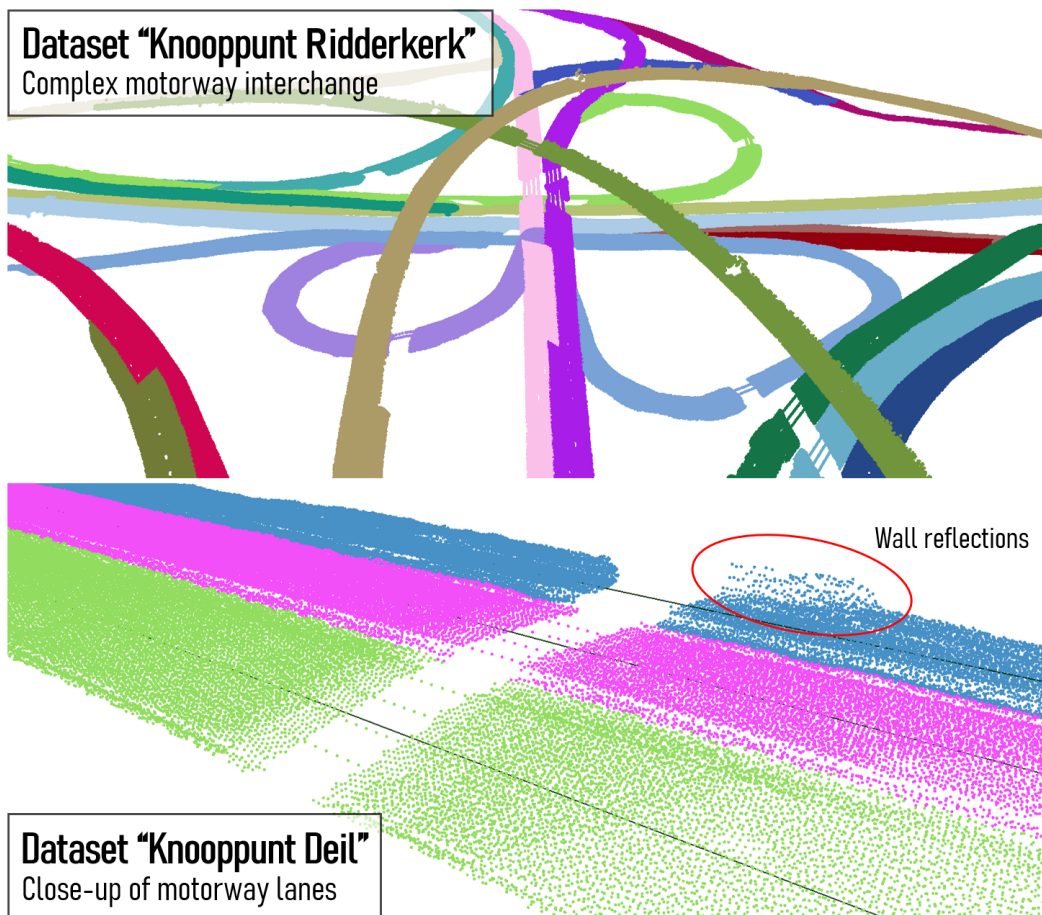


**Figure 4.6:** Visualisations illustrating the results of Lidar segmentation.

The last line of code writes the resulting 3D geometry to disk, “mimicking” the structure of the input file. The variable is named in such a way to distinguish it from the variable containing the file path where the final 3D-NWB results will be written, called `accurateZ_fpath`. This step is optional, it is intended for debugging and demonstration purposes only.

In the class itself, the results of this step are not stored in a separate variable, but are added to the GeoDataFrame representation of the input NWB Shapefile, found in the `.nwb` variable of the `nbrs_manager` class.

### 4.2.3 Lidar segmentation

Figure 4.6 shows some visualisations of the results of Lidar segmentation. Like in figures depicting NBRS alone (such as e.g. Figure 4.3), I used colours to distinguish between the subclouds of each NBRS. On the right in the figure, the centrelines are also shown (in black, to help distinguish them from their subclouds). For subclouds which are positioned far from each other, a clear separation is observable. However, ones that are close to one another often overlap, such as in various places in the centre of the visualisation on the left in Figure 4.6. This is the result of there not being much space between the roads themselves. The overlapping parts of such subclouds may contain duplicate points (in other words, points may be part of multiple subclouds). Out of these “duplicate” points, the visualisation only shows the ones that were loaded last, hence some subclouds may appear thinner than they are.

### General description of results

The properties which we are looking for in the resulting subclouds is that they contain as many of the road surface points, and as few of the surrounding unrelated points, as possible - especially with regards to points reflected from occluding objects. Figure 4.6 illustrates quite vividly that indeed, each [NBRs](#)'s subcloud is clearly related to the underlying real-life road surface and that very few unrelated points are included.

Since this is not yet the stage where conservative thresholds are enforced, it is possible that a small amount of undesired points will be retained. This mostly happens just before and after regions of occlusion, where the underlying plane fits have already been affected by the occlusion but not enough to be excluded. An example of such a group of points (the bottom part of a wall) is found in the blue subcloud on the right in Figure 4.6. Reflections from tall vehicles, as well as from roadside guardrails and small signs may also be retained in this step sometimes, which explains the fuzzy appearance of the bridges on the left in the same figure.

This problem arises because the Lidar patches inevitably include off-road points, causing the fitted planes not to lie perfectly on the road surfaces. This in turn means that using very strict point-to-plane thresholds is not advisable, opening the possibility for unrelated points to make it into the subclouds. While iteratively refining the plane fits could reduce the impact of this issue, it would also introduce unnecessary computational complexity. This step of the pipeline does not *need* to produce perfect results, the small number of artefacts can be handled by later pipeline steps.

The visualisation on the left in Figure 4.6 shows the *Knooppunt Ridderkerk* motorway junction in which many motorway lanes and ramps are present in complex 3D relationships, in one place including an area with 4 overlapping roads. The correctness of the resulting subclouds demonstrates that although some of my approach is procedural and relies on a fixed parametrisation, it is still robust enough to work in the simplest, as well as the most challenging environments.

### DTB's usefulness

As discussed in-depth in Section 3.3.3, the final version of my code works regardless of the presence of long occluded regions, even without [DTB](#) coverage. However, [DTB](#) is still used wherever available and useful. One clear benefit is that [DTB](#) can help rectify plane fits, thereby segmenting [AHN3](#) more accurately in the vicinity of the gaps. Often, this automatically fixes the outlier-related issue I mentioned above in the context of slightly corrupted plane fits just before and after data gaps.

Furthermore, even in the knowledge that [DTB](#) is severely outdated in many places (see Section 2.3.3), it is still the only information source we have about roads where [AHN3](#) coverage is missing. Where the break in [AHN3](#) coverage is short and [DTB](#) is outdated (or missing), linear interpolation prevails. However, where longer gaps are present and the road's elevation may change inside of them, [DTB](#) prevails even if its data is outdated.

Unlike in most locations, [DTB](#) has good coverage in the particular motorway junctions shown in Figures 4.6 and 4.7, especially in the *Knooppunt Ridderkerk* junction. Each of the visualisations in these figures contain examples of how [DTB](#)-based "assistance" manifests itself in the output. Where subclouds contain Lidar-gaps filled with points in a linear arrangement, one can be certain that [DTB](#) was used to re-fit planes and to supply points to the subcloud. On the left in Figure 4.6, these linear sets of points appear in the lowest motorway lanes and ramps wherever the 3 overlying roads cast "shadows" on it, creating occluded zones of various shapes. Each level of the stack of roads has such a feature, except for the one on the top, which is not occluded by any objects.

While this demonstrates that [DTB](#) - or any support dataset with road surface elevation measurements - can be helpful in complementing this procedure (which is otherwise based entirely on [AHN3](#)), it also highlights one of [DTB](#)'s weaknesses. While the areas shown in these figures have good [DTB](#) coverage, the [DTB](#) lines in the *Knooppunt Ridderkerk* dataset are in some cases approximately two decades older than [AHN3](#) (they are up-to-date in *Knooppunt Deil*). Figure 4.7 demonstrates that there are noticeable systematic differences between the road elevations as depicted by [AHN3](#) and [DTB](#).

## 4 Results

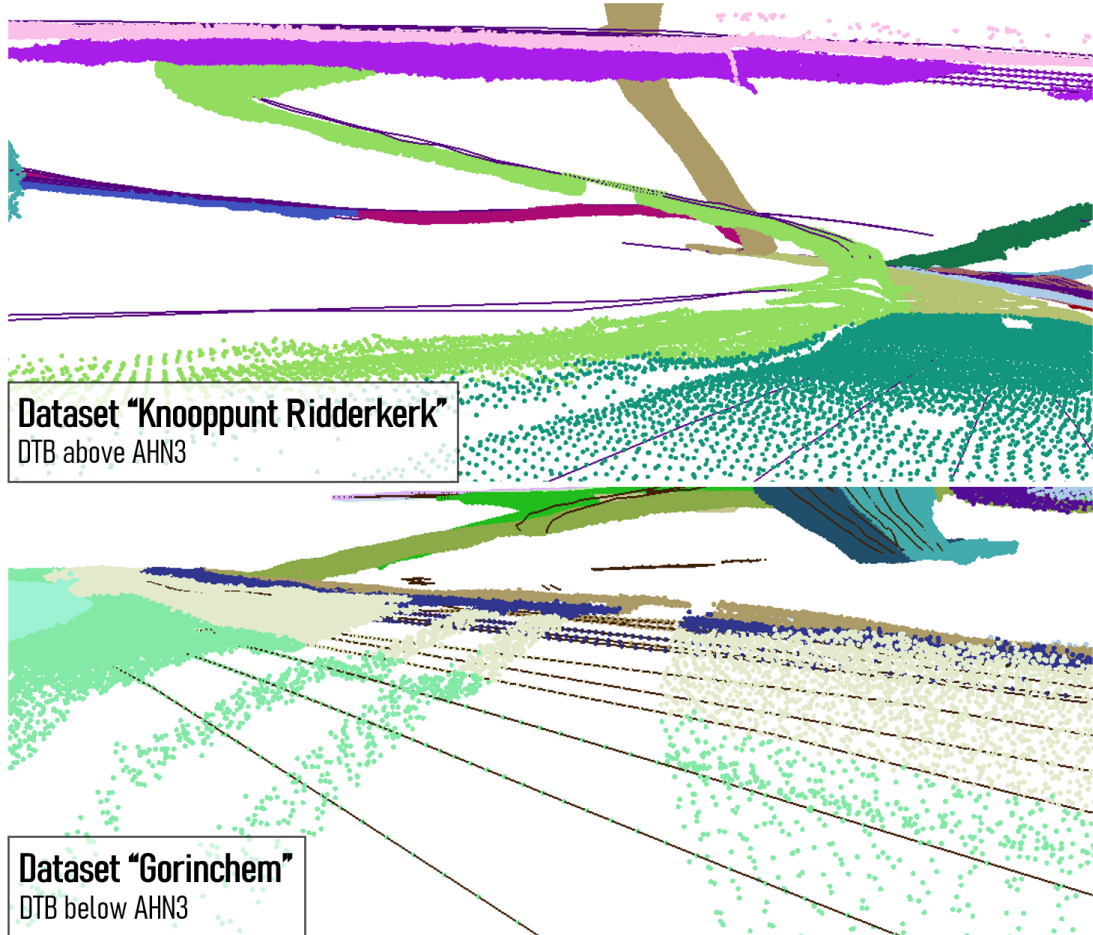


**Figure 4.7:** Visualisations illustrating the disagreement between [AHN3](#) and [DTB](#).

In *Knooppunt Ridderkerk*, [DTB](#) is above [AHN3](#) consistently, but the *Gorinchem* dataset and several others show [DTB](#) below [AHN3](#). Moreover, as the top visualisation in Figure 4.7 shows, perfectly and poorly matching [DTB](#) and [AHN3](#) data and can often be found side-by-side, with only a few years of difference between the [DTB](#) acquisition times. While in Section 2.3.3 I primarily attributed these problems to the effects of subsidence, a further investigation of the problem is justified based on these results. The reasons for these differences may be more complex than simply just being the result of subsidence.

This issue draws our attention to the general issue of temporal discrepancies between all our datasets - [NWB](#), [AHN3](#), and [DTB](#). This is further discussed in Sections 4.2.6 and 4.2.7 in the context of how it affects our results. Overall, the results suggest that even if we solely attribute the vertical land motion to subsidence, a 20 cm vertical accuracy can only be guaranteed by periodically re-measuring the input elevations in both the primary and the support datasets.

### Splitting NBRS into parts

On the left in Figure 4.8, a region with neither [AHN3](#), nor [DTB](#) coverage is shown. In this location, the [NBRS](#) was split into two parts and in the figure, this is illustrated by the fact that I could highlight the subcloud on one side of the gap separately. The matching colour of the points shows that they still belong to the same [NBRS](#), but the program stores a separate subcloud for each [NBRS](#) part, meaning that they are loaded as a separate MultiPoint object in the 3D viewer I used to generate these figures. [NBRS](#) splitting also works well in general, it performs as expected.

## Parametrisation

The parametrisation of this pipeline step is extensive, because many parts of the algorithm are of a procedural nature. Hence, I will dedicate some attention here to describing the final parametrisation I used to produce my outputs. Here I will not go into details about the exact way in which these parameters are used, as I have already described this in Section 3.3.3 without specifying numerical values.

All parameters were derived from a process of experimentation and fine-tuning, although a good understanding of the problem, the procedures, and the properties of the input data were also essential in being able to define the parameters as well as to find suitable values for them.

Firstly, a query radius for the generation of the Lidar patches needs to be specified. I used a query radius of 10 metres, which is sufficiently long to allow most of road surface reflections to be included between centreline vertices. Using a smaller radius could, in some cases, improve the plane fitting results, but it would also cause the exclusion of useful Lidar points from the patches simply due to the spherical geometry of the query regions. While the radial queries are not perfectly suitable for this step, I did not implement a custom query mechanism because the performance of the radial KD-tree queries is needed for this step. The performance of this querying step is also heavily affected by the vertex densification threshold and Lidar thinning factor used previously; denser NBRS vertices and a denser input point cloud means that the processing time will increase considerably.

When the program examines the Lidar patches corresponding to each NBRS vertex, it either fits a plane and passes on the patch, only passes on the Lidar patch, or does neither. The program stops fitting planes below 2 points per square metre, and stops passing on points below 1. In this context, "points per square metre" is interpreted rather loosely, since the patches are actually based on points falling into spheres of a given radius rather than circles. However, since Lidar points are assumed to have been reflected from a *nearly* 2.5D surface locally, this assumption is not unreasonable.

The next set of parameters controls the detection of "instability" while examining the succession of plane fits and underlying Lidar patches. DTB-based assistance is attempted if any of the following conditions are met: the standard deviation of the Lidar patch's elevations exceeds 0.1 metres, the distance between the plane and the corresponding NBRS vertex grew by more than 50% since the previous iteration, or the median of the Lidar patch's elevations grew by more than 50% since the last iteration. The latter two conditions are only considered if the absolute value of the underlying metrics (distance from NBRS, median elevation) exceeds 0.2 metres.

The way the metric related to the centreline-subcloud elevation differences is enforced ensures that the occasional poor polynomial fits of the previous step do not cause problems here. Such fits cause the centreline to underestimate or overestimate the elevation of roads in a consistent manner. Making the metric detect abrupt *changes* in these distances rather than simply setting a distance threshold adds enough flexibility to bridge the issue.

When DTB-based assistance (re-fitting of plane) is attempted, the initial query radius when looking for DTB points is 0.4 metres. If enough points were found to re-fit the plane (more than 2), then the second repositioning query is performed with the same radius as the one used in the generation of the Lidar patches (10 metres in my final parametrisation), because at this point it is assumed that the query position has been moved relatively close to the true elevation of the road surface. When deciding whether to do a final re-fit on the nearby part of the Lidar patch, the program once again uses the condition that the density of these points should at least be 2 points per square metre. Lidar points are deemed to be close if they are less than 1 metre away from the plane.

When pre-selecting the final set of conformant points from the patches, the program uses a threshold of 5% of the query radius used in the Lidar patch queries, corresponding to 0.5 metres (from the final plane fit) in my final parametrisation. Outliers that are further away than 0.5 m from the subclouds do not violate this condition, they simply indicate that the underlying plane fit was somewhat tilted relative to the road surface.

While the post-processing operations of this pipeline step (breaking into NBRS parts and filtering outliers) also have a few parameters, these are insignificant and are thus omitted from this discussion.

## 4 Results

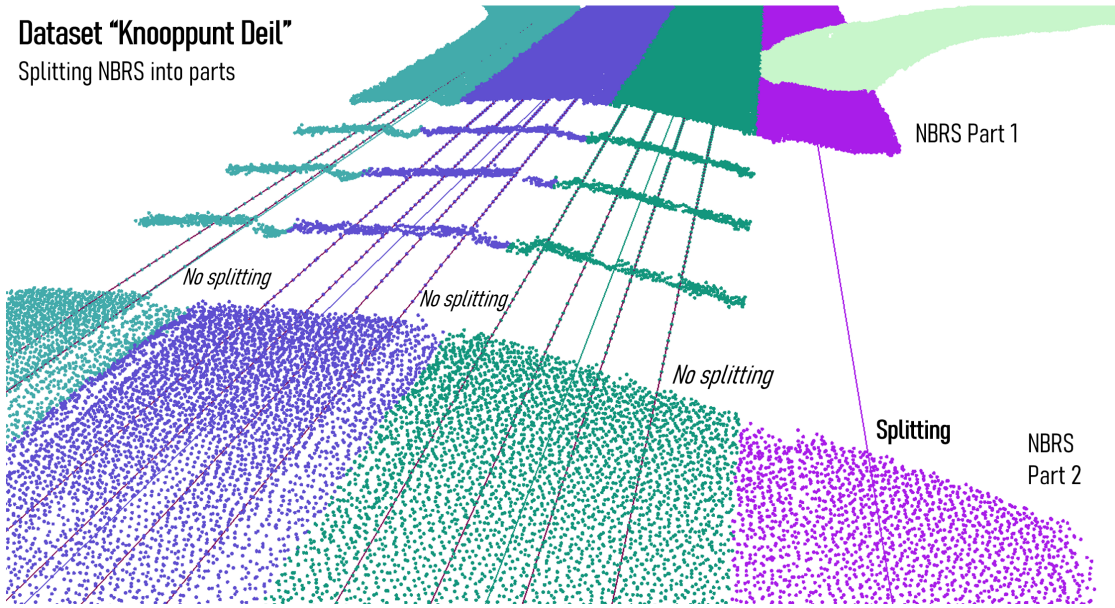


**Figure 4.8:** Visualisation illustrating the handling of gaps in [AHN3](#) coverage during Lidar segmentation.

### Using the implementation

The below code snippet shows the code I used to generate my final results.

```
roads.segment_lidar(fpath = dtb_fpath, r = 10)
roads.write_subclouds(fpath = subclouds_fpath)
```

The first line performs the point cloud segmentation itself, with a radius of 10 metres for the KD-tree queries that generate the Lidar patches. The variable `dtb_fpath` is assumed to contain the file path to the cropped `DTB` file belonging to the desired testing dataset. The second line writes the resulting subclouds to disk, the argument variable is assumed to contain the file path to the desired output file.

The intermediate results that the second line writes to disk "mimics" the structure of the input LAS file. However, each point is given three new properties. The property `ORIGIN` determines whether the given point originates from `AHN3` (denoted by the value 0) or `DTB` (denoted by the value 1). The properties `NBRS_ID` and `PART_ID` determine which `NBRS`, and which part of that `NBRS` a given points belongs to. `NBRS` that were not split into parts are still represented by the same data structure, but all their points are found in a single part with `PART_ID = 0`.

In the class itself, the resulting subclouds can be accessed via `.ntrs_subclouds[ntrs_id][part_id]`, where `ntrs_id` and `part_id` are variables which should contain the ID of a specific `NBRS`, and the ID of one of its parts respectively. Furthermore, one can find the indices corresponding to intervals with `AHN3` or `DTB` coverage in `.ntrs_parts[ntrs_id]`, which effectively defines the `NBRS` parts in the software.

#### 4.2.4 Edge approximation

Visualisations showing the results of the edge approximation step are shown in Figure 4.9. The black lines correspond to `NWB` centrelines, while the closely spaced, orthogonal lines are the cross-sections that are attempted to be created on each centreline vertex. The lines connecting the ends of the cross-sections on each side of each centreline are the preliminary edges that are the main product of this processing step. As in all 3D visualisations in this chapter, the vertical dimension is once again exaggerated five times to make vertical changes better visible.

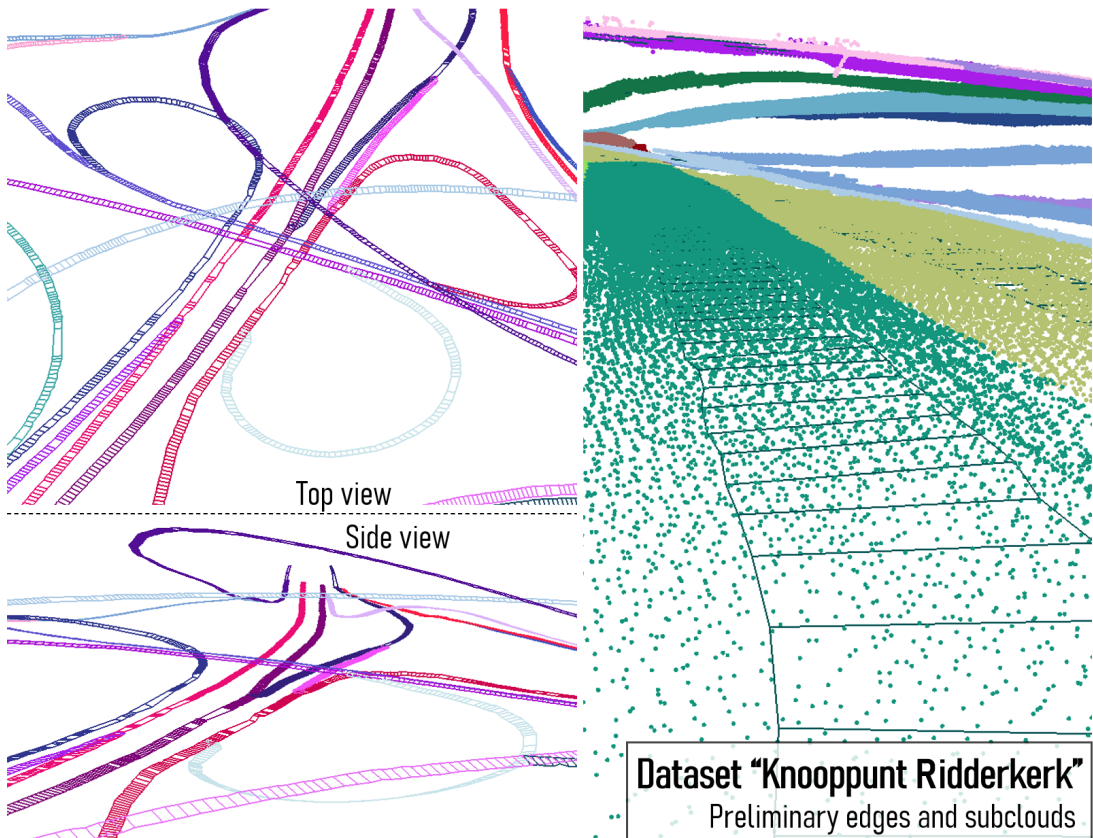


**Figure 4.9:** Visualisations illustrating the results of preliminary edge approximation.

### General description of results

The output of this step is mostly satisfactory, no road layouts apart from tunnels are known to me which would cause the algorithm to fail, or produce unusable results with the final parametrisation. Furthermore, owing to the verification step that takes place before accepting a cross-section (and extending the preliminary edge with its end vertices), the general shape of the edges is also quite well-behaved, and their elevation reflects what one would expect based on the underlying subclouds. In my final configuration, cross-sections have vertices every 10 centimetres (created via densification), and their elevation is derived from points no further than 25 centimetres away. This dense quantisation allows the algorithm to reconstruct road edges on a fine scale.

In the two visualisations on left in Figure 4.9, I visualised the preliminary edges only. The top image looks down on *Knooppunt Ridderkerk* from above, while the one below shows the same roads from the side. On the right in the figure, I show a visualisation in which a pair of preliminary edges and the underlying cross-sections can be compared with the subcloud that was used to generate them. In most cases, cross-sections and preliminary edges lie flat on road surfaces, and even where noticeable blunders are observed, they correspond to underestimating or overestimating the road surface extents by about 2 metres maximum.

While the overall quality is good and the results are certainly usable in terms of the requirements of the next two pipeline steps, there are a few properties and limitations of these results that are worth discussing.

## 4 Results

### On road width bounds

As I already mentioned in Section 3.3.4, the algorithm works with a fixed minimum and maximum road width. The maximum is enforced by using it as the length of the constructed cross-sections, while the minimum is enforced as part of the verification step.

The enforcement of the minimum width is less of a limitation; it merely prevents the cross-sections from shrinking too short. However, the way in which the maximum width is enforced can be considered a limitation because road surfaces that are unusually wide will not be covered by the edges in their entirety. Using very long cross-sections (increasing the maximum width) increases the chances of returning false hits due to short successions of off-road points that conform well with the line fits of the cross-sections. With shorter cross-sections, the chances of this happening are reduced drastically.

My final parametrisation uses minimum and maximum road widths of 3.5 and 7 metres respectively.

While the maximum limit may exclude meaningful road surface areas in the case of unusually wide roads, there are special roads in which road and off-road reflections are not clearly distinguishable in the cross-sections. Motorway lanes are represented by discrete centrelines in [NWB](#), which means they will be treated as separate [NBRS](#) in my system. However, such lanes are often constructed on a single paved surface, meaning that my method cannot be used to derive edges at least for one side of them. This is another reason why the maximum width is important; one such scenario is shown on the left in Figure 4.10.

It is primarily [NWB](#)'s crude georeferencing that necessitates the use of a lower-than-optimal value for the maximum road width. If [NWB](#) itself is shifted towards the edge of a road locally, generated cross-sections will be corrupted there by off-road elevations. Using larger values for the maximum width will only make this problem worse. In the absence of this problem, the value could be increased by a few metres based on my experience with accurate parts of [NWB](#).

I implemented a workaround that mitigates the effects of this issue. The line fits that are generated for every cross-section are actually only fitted on the central 40% of the densified cross-section vertices, and it is extrapolated to the outer vertices. This helps minimise the effects of the off-road elevation measurements that may affect the outer cross-section vertices.

### Failed edge detection

While in well-exposed, straight roads this does not generally happen, there are lengths of roads where finding edge points will fail repeatedly. In such places, the algorithm does not save the cross-sections, and also does not add edge points to the preliminary edge LineStrings. One the left in Figure 4.9, this can be clearly observed, as it occurs frequently in occluded areas.

The most common reason for skipping cross-sections is the lack of data. If not enough Lidar points are found close to the cross-section vertices, then it will be skipped. This happens in data gaps where both [AHN3](#) and [DTB](#) are missing, but also in most gaps where [DTB](#) is available. The latter is due to the fact that [DTB](#) samples linear features *along* the length of each road, and has a poor sampling rate in the direction that the cross-sections are attempting to sample.

Such data gaps may exist under bridges for instance, but also in places where vehicles occluded a significant portion of the road. In the latter case, artefacts may be generated if the cross-sections are accepted because there is enough data not to trigger a skip. Most commonly, it causes noticeable width changes, which may be accepted by the algorithm if the relevant cross-section is processed while the conditions are relaxed due to repeated previous failures. This is shown on the right in Figure 4.10.

The second most common reason is the generation of poor line fits. If the elevation estimates of the cross-section vertices are scattered, the errors in the fit will be large. Elevations further than one standard deviation of the data-model error are not considered any further. If too many points are filtered out in such a way, the cross-section will be skipped. This happens most commonly due to [NWB](#)'s poor georeferencing, i.e. in the rare cases when not even only using the central 40% of the cross-section vertices could avoid including a large number of off-road elevation measurements.

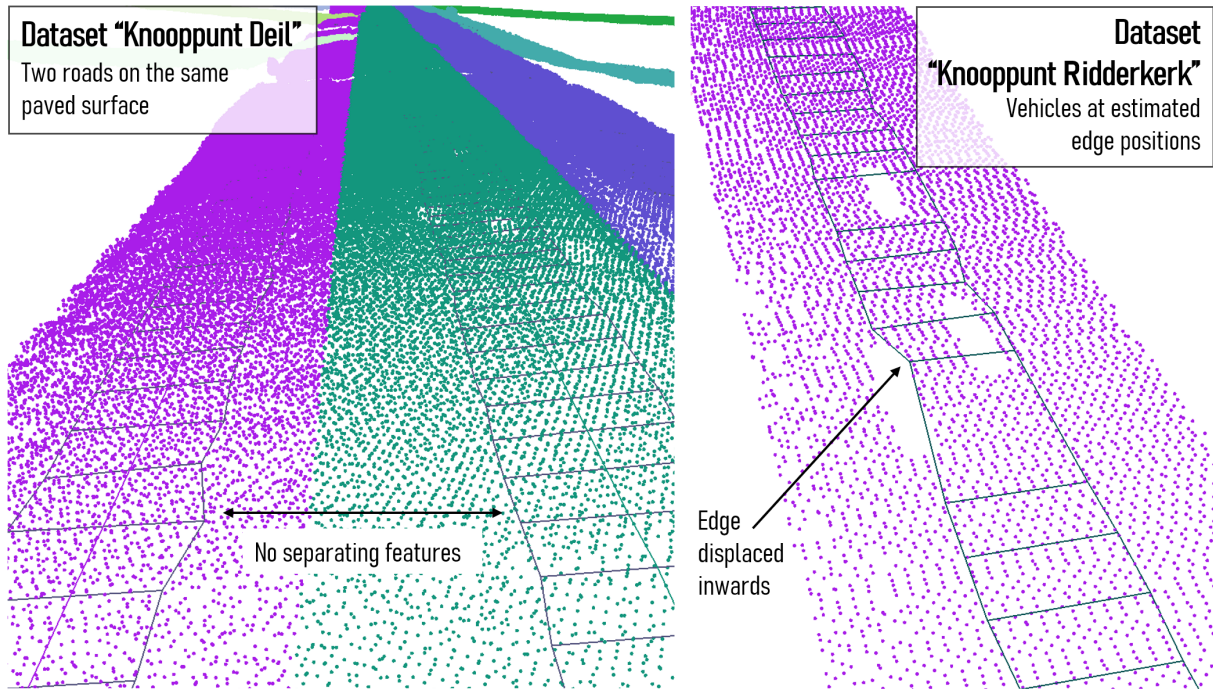


**Figure 4.10:** Visualisations illustrating challenging edge approximation scenarios.

Lastly, failures may also be the result of violating the conditions of the verification step. Namely, if a unrealistically sudden width or elevation change is detected, the cross-section is skipped. If this is the sole reason for the failures, then generally only a limited number of cross-sections and corresponding edge vertices will be missing, as the conditions are relaxed after 3 successive failures.

### Edge generation in data gaps

In the absence of [AHN3](#) data, vertices will be skipped frequently, as I already mentioned above. However, quite frequently, one or two cross-sections will be accepted in such regions too, if [AHN3](#) coverage reappears temporarily, for instance due to a small gap between two bridges. Due to the repeated skipping of vertices, the conditions will almost certainly be relaxed most of the time, and hence sudden width or elevation changes will be allowed. This combination of factors may result in the generation of strange edge geometries in occluded zones.

Where roads are straight and the gaps in coverage are short, this does not represent a major issue. Even if their shape will be sub-optimal in these zones, it will still respect the minimum road width condition, meaning that most [DTB](#) and [AHN3](#) points that may appear in the gap will still fall between the edges, which is ideal for [TIN](#) construction.

Serious problems only arise when the gap appears at the end or the beginning of an [NBRS](#) part. In such cases, especially if there is no intermittent [AHN3](#) coverage in the gap, no cross-sections will be accepted at all, and therefore the program will be unable to extend the edges to the end of the [NBRS](#) part. The beginning or the end of the centreline will simply not be covered. Later in the [TIN](#) construction step, this means that the local [DTB](#) points will not be inserted into the [TIN](#) (because they are not between the generated edges), and the [TIN](#) surface will, as a result, also not extend all the way to the end of the [NBRS](#) part. This directly introduces incorrect (linearly interpolated) elevations to the final 3D-NWB output.

A similar problem arises when a road is occluded in a bend. Depending on the sharpness of the bend and the extent of the occlusion, the preliminary edges may end up directly connecting the last cross-section before the occlusion and the first one after. Taking such a "shortcut" means that [DTB](#) points in the data gap will mostly be ignored during [TIN](#) generation because they will not fall between the preliminary edges.

## 4 Results

I have not observed the above limitations to cause issues with roads that are built on the surface in practice. However, they do mean that my system design is not compatible with tunnels out-of-the-box. Unless the tunnel is completely straight and the relevant [NBRS](#) part continues across its full length, the [DTB](#) points in the tunnel will be ignored during [TIN](#) construction, and therefore the [TIN](#) models and the 3D conversion of [NWB](#) will be incorrect locally. I tested and verified this issue with the *Amsterdam Hemhavens* and *Amsterdam Zuid* testing datasets, which both contain tunnels.

As I noted in Section 2.3.3, I treat [DTB](#) as a “placeholder” for a better supporting dataset (optimally, an [MLS](#) dataset). As a result, its vector properties are not used - it is assumed to consist of generic point data. However, treating it properly as a 3D line dataset in [AHN3](#) data gaps would fix the above issues, i.e. it would become possible to generate edge estimates from [DTB](#) much like in the commercial implementation. Such an extra feature did not fit into the schedule of my project, hence it is only further discussed in the Future work section in the Conclusions chapter (see Section 5.7).

### Using the implementation

In my example code on GitHub, I use the following two lines to generate and export the preliminary edges:

```
roads.estimate_edges(min_width = 3.5, max_width = 7, thres = 1, perc_to_fit = 0.4)
roads.write_edges(fpatheres = edges_fpath, fpatheres = crosses_fpath)
```

The first line generates the preliminary edges. The arguments (all compulsory) set the minimum and maximum road width, the outlier filtering threshold, and the ratio of how much of the cross-sections should be fitted with lines. The first two arguments should be specified in metres. The second argument specifies the number of standard deviations of data-model errors, within which points should be considered inliers, so the current value means one standard deviation. The last argument accepts values between 0 and 1, the current value means that the central 40% of cross-sections will be used as the basis for the line fits.

The second line writes the results to disk. Both the edges and the cross-sections are written, `edges_fpath` and `crosses_fpath` are assumed to contain file paths where these should be written (as Shapefiles). In the class itself, the results are found in `.nbres_edges` and `.nbres_crosses` as GeoDataFrame objects.

#### 4.2.5 Active contour optimisation

As Figures 4.11 and 4.12 show, all planned parts of this pipeline step output the expected results, albeit with occasional artefacts and a mediocre overall quality. The contours are smooth, they generally reflect the shape of the roads accurately, and only occasionally suffer from major blunders. However, even small deviations beyond the road edges would cause off-road Lidar reflections to be classified as road points, and thus be inserted in the [TIN](#) model in the next step. Unfortunately, such deviations of various sizes occur frequently, as the close-up images in Figure 4.12 demonstrate. With the help of the results, this section will focus on explaining why exactly it is difficult to guarantee that this workflow functions reliably, as this was the reason for a major revision of the design of the preliminary edge detection and [TIN](#) construction steps, which I already mentioned in Section 3.3.4.

### Attractor maps

Some attractor maps can be seen in Figure 4.12. Each [NBRS](#) part has its own attractor map, and since subclouds may overlap, so can the attractor maps. In the figure, attractor maps that are separated from others by a fair amount of distance can be examined in their full width, while only the one the was drawn last by the visualisation software can be examined completely where overlapping occurs.

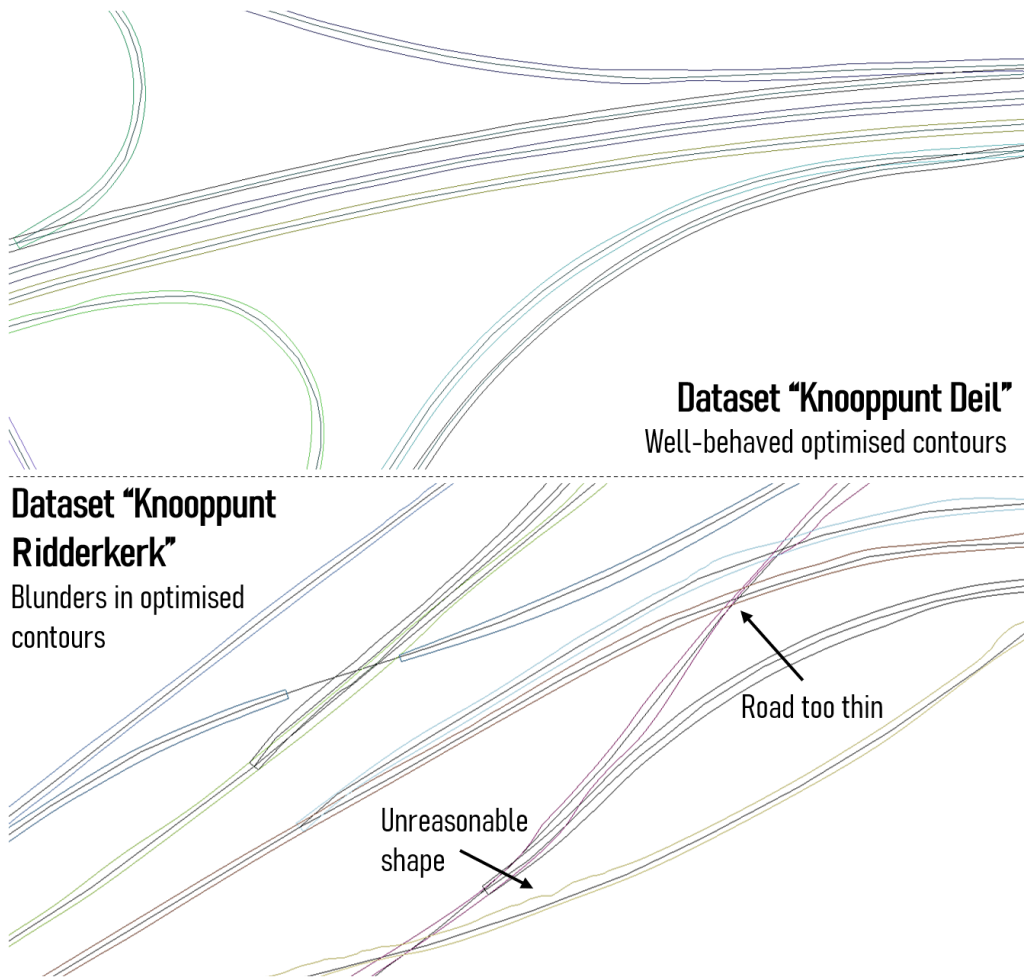


**Figure 4.11:** Visualisations illustrating various degrees of active contour optimisation success.

The bright parts of the attractor maps correspond to regions where the normal vectors of the Lidar points are oriented uniformly, while the darker regions indicate divergent normal vectors. The linear boundary between such regions thus marks the edge of the smooth road surface in most places, as it corresponds to an abrupt increase in normal vector divergence. I used a pixel size of 0.5 metres (in both dimensions) to generate these attractor maps, and the attractor map values are based on using a 5-by-5 kernel, sampling the neighbourhood via approximately 30 inner products for each pixel.

The optimised contours are shown overlain on the attractor maps on the right in Figure 4.12. While the *general* appearance of the contours is acceptable, comparing *details* in the contours with the attractor maps reveals that they are not reliably positioned on the break in smoothness. So that the reader can better interpret the optimisation as a process, the left part of Figure 4.12 shows the preliminary edges overlain on the attractor maps. Comparing the preliminary edges to the contours in the context of the attractor maps allows one to better understand the effects of the optimisation procedure. In particular, patterns in the behaviour of the optimisation procedure may be recognised.

### Patterns of failure

One important pattern is that the contours are sensitive to small-scale features in the preliminary edges. A few outlier edge points (an short, abrupt expansion of the preliminary edges, for instance) can introduce large bulges into the optimised edges. Similarly, where the preliminary edges shrink (for instance due to the influence of stationary vehicles), the optimised contours will tend to do so too, but on a much

## 4 Results

larger scale. The severity of the generated artefacts also depends on the local properties of the attractor maps.

Another pattern, which I already mentioned in 3.3.5, is that where preliminary edges fall outside the bright part of attractor maps, the optimisation procedure will often fail to move them back to the primary break in smoothness. The off-road areas may contain other high-contrast features due to the unevenness of the underlying real-life surfaces, and the edges will often be drawn to these instead of the edge of the road. This is in part due to the large weight the optimisation algorithm gives to the *proximity* of the edges.

For the same reason, deliberately underestimating the road width (which was done in [Boyko and Funkhouser \[2011\]](#)) does not represent a solution here. If the preliminary edges are too far inwards from the break in smoothness, they will simply stay unchanged during optimisation. This behaviour cannot be changed simply via the parametrisation - I already give nearly full weight to edge detection in my final configuration. I also experimented with underestimating the preliminary road widths and giving more weight to attraction to darkness. Unfortunately, the results of this approach are even more unpredictable because the algorithm will frequently move the contours into the dark areas rather than stop at the edges.

Lastly, the contours may also become corrupted due to the break in smoothness itself missing from the attractor maps. The two most common factors that tend to cause this are unusually wide paved surfaces (wider than the maximum width of the underlying subcloud), and occluded zones where only [DTB](#) is available. The former is manifested in the attractor maps by the bright zone extending all the way to the edge of the map. In such regions, active contour optimisation will leave the preliminary edges mostly unchanged (there are no edges to attract it). The latter (missing [AHN3](#) coverage) may cause unpredictable artefacts because the edge needs to step into the no-data region and then back into the road surface on the other side, transgressing two "edges" that are orthogonal to its general direction. Using a no-data value that is almost the same as typical road surface pixel values helped, but it could not solve the issue completely. Only by splitting [NBRS](#) into parts here too, could this issue be eliminated.

Finding a suitable value for no-data pixels required some experimentation. I found it most effective to set all no-data pixels to a value close to the values seen in bright road surface areas. So, in addition to the occluded areas, all other parts of the rectangular rasters are set to this value (specifically, a value of 1). While this creates artificial high-contrast edges in the attractor maps at the boundaries of the underlying subclouds, the preliminary edges do not get drawn to them because they are almost always much closer to the edge introduced by the edge of the road.

### Active contour optimisation parameters

The  $\alpha$  parameter controls lengthwise shrinking. I set it to a value of zero to indicate that this behaviour is undesired. In theory, the optimisation procedure introduces length changes into the contours naturally, by adjusting their shape. In theory,  $\alpha$  should therefore be set to a small, but nonzero value to allow this behaviour. In practice, I found that this affects the results negatively.

The parameter  $\beta$  controls the smoothness of the resulting contours, which can also be intuitively thought of as controlling the tension of the underlying splines that active contour optimisation repeatedly fits. I set this value to 0.01, which in my experience corresponds to medium tension. Based on the testing I have done, smoothing the preliminary edges is one task in which active contour optimisation excels; it can eliminate small-scale protrusions that are generally meaningless, and can thus be considered noise. This in turn helps minimise the impact of the types of small-scale issues I already described above by keeping the contour relatively tense across them.

The parameter  $w_{line}$  controls attraction to dark or bright pixel values. The attractor maps that I described above have a sharp contrast between the brightness of off-road pixels (which are dark), and road pixels (which are bright). However, this contrast is localised to the edges of the roads, and any amount of attraction to either dark or bright areas would draw the contour deeper into that region rather than keep it on their boundary, both in theory and in practice. In my final implementation, it is set to 0.05 to

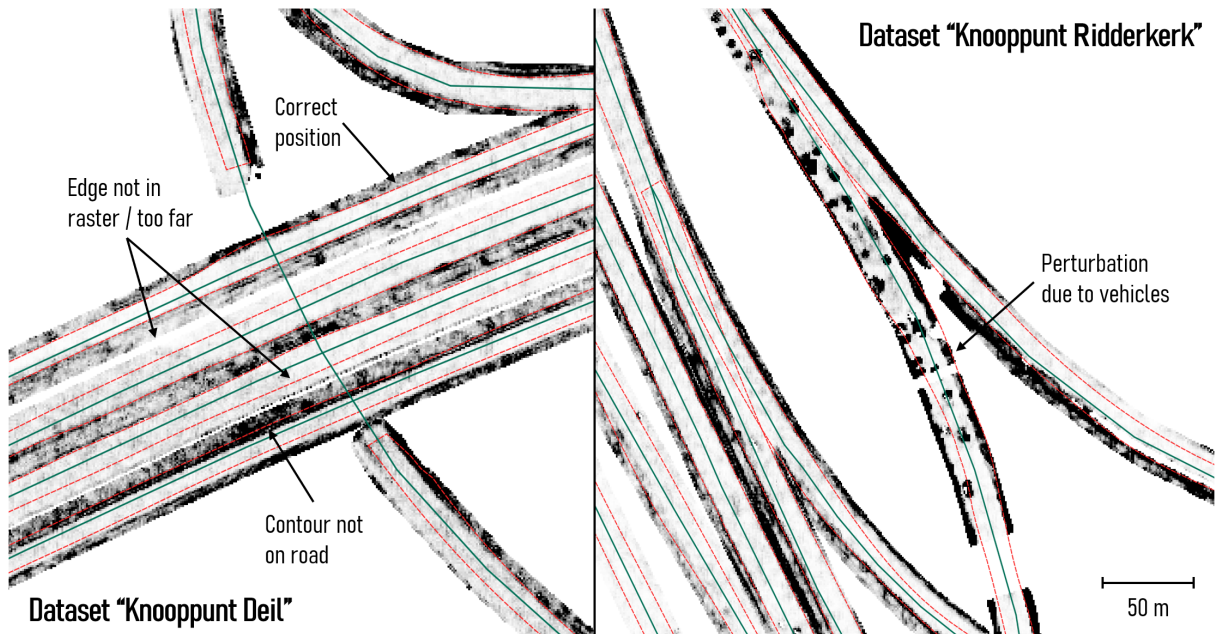


Figure 4.12: Visualisations comparing optimised edges to the underlying attractor maps.

introduce a very small amount of attraction to bright areas, so that the contours are more likely to stay on the inner side of the road edges rather than go past them.

Thus, attraction in my recommended parametrisation is controlled almost entirely by edge detection (parameter `w_edge`). I set it to 1, meaning that the iterative refinement of the contours will be governed primarily by attraction to edges, for reasons I already discussed above.

In terms of iterations, I decided to work solely with a maximum number of iterations (parameter `max_iterations`) rather than to use condition-based termination. Setting a condition would terminate the optimisation process when the contours no longer move significantly, i.e. it checks when a minimum displacement threshold first becomes violated. Where the attractor maps are perfectly suitable for active contour optimisation, this approach works well. However, letting the contours evolve in such a way where the attractor maps are sub-optimal results in the drastic enlargement of the generated artefacts, as well as an unacceptable increase in computational complexity. This happens, for instance, where edges are not defined well enough, and where Lidar gaps are present. I found iteration limits between 1000 and 5000 to be the most effective.

The time step parameter  $\gamma$  and the number of pixels the contours are allowed to shift in a single iteration (parameter `max_px_move`) can be used to further fine-tune how quickly the optimisation lets the contours evolve. I set these two values to 0.005 and 1 respectively, which corresponds to a relatively slow iteration, appropriate to the small-scale changes we desire (generally, we wish to move the edges only up to a few metres).

The above configuration of values is the result of a process of iterative combined revision of the values themselves, and the attractor map generation technique, as I mentioned in Section 3.3.5. While I experimented with a wide range of parametrisations, the possibility remains that a better one exists. The parameters themselves offer many permutations to try, and the fact that the preliminary edge and attractor map generation also affects the results only increases the range of possibilities.

However, despite having tried most types of parameter configurations and many different adjustments to the preliminary edges and attractor maps, I was unable to find a configuration that produces satisfactory results within the development time reserved for this step. The quality of the optimised edges is simply not good enough to be used to classify Lidar points reliably based on them. The situation was made worse by the fact that the combined computational complexity of generating high-resolution attractor maps and of using the optimisation algorithm made the refinement procedure a rather difficult

## 4 Results

and time-consuming task. This is what lead to my decision to instead focus on improving the quality of the preliminary edges and use them directly in the [TIN](#) construction step.

### Choice of algorithm

Contributing to the above uncertainty regarding the effectiveness of active contour optimisation is the fact that in relevant literature (e.g. [Boyko and Funkhouser \[2011\]](#)), mentions of its ineffectiveness relative to more sophisticated algorithms is made. My hypothesis was that with a sufficiently good pre-selection of Lidar points and pre-processing of attractor maps, conventional active contour optimisation could still work well, but this appears not to be the case in practice.

Lesser known, but more sophisticated offshoots of active contour optimisation exist, but have no open-source Python implementations. One such example is the "ribbon snakes" method. Considering the volume of further tasks in this project, I opted not to attempt to implement it based on first principles, especially considering that their superiority is not clearly demonstrated in relevant literature. They, too, are prone to producing artefacts of various types, even if they perform slightly better than conventional active contour optimisation.

### Using the implementation

The following lines of code may be used to run active contour optimisation and export the attractor maps and resulting optimised edges:

```
roads.optimise_edges(size = 0.5,
                      a = 0, b = 0.01, g = 0.005,
                      w_l = 0.05, w_e = 1,
                      max_iter = 1000)
roads.write_maps(fpath = maps_fpath)
roads.write_contours(fpath = conts_fpath)
```

The first argument `size` in the active contour optimisation method corresponds to the desired pixel size. The rest of the parameters expose some of the active contour optimisation parameters that I found to be useful for making smaller changes to the algorithm's behaviour. The arguments `a`, `b` and `g` correspond to  $\alpha$ ,  $\beta$  and  $\gamma$  respectively, while `w_l` and `w_e` correspond to the two parameters controlling attraction to brightness and edges (`w_line` `w_edge` respectively). The last parameter sets the maximum number of iterations.

The `.write_maps(maps_fpath)` method writes all attractor maps generated (one per [NBRS](#) part) as GeoTIFF rasters, tagging the file name with the relevant [NBRS](#) ID and part ID. Hence, the argument file name is expected to correspond to the first part of the file name only, e.g. `.../C_39CZ1_map` would work. Reserving a separate folder for these is recommended. The contours are written as a single Shapefile.

In the class, the maps can be found in the variable `.nbrs_maps[nbrs_id][part_id]`, while `.nbrs_contours` contains the contours in the form of a GeoDataFrame.

#### 4.2.6 TIN construction

By adjusting my methods to the circumstance of not being able to produce accurate enough optimised edges, I created a different implementation than originally planned, but one which is still robust and accurate. Figures 4.13 and 4.14 show examples of the resulting models compared with the preliminary edges and preliminary elevations. The images in Figure 4.13 show an initial [TIN](#) surface, and the same [TIN](#) after the extension stage. In these figures, the preliminary edges are shown because the initial [TIN](#) surface is seeded halfway between them, and because the [TIN](#) is only allowed to grow between them in the initialisation stage. The upper, large-scale image in Figure 4.14 shows an overview of all [TIN](#)

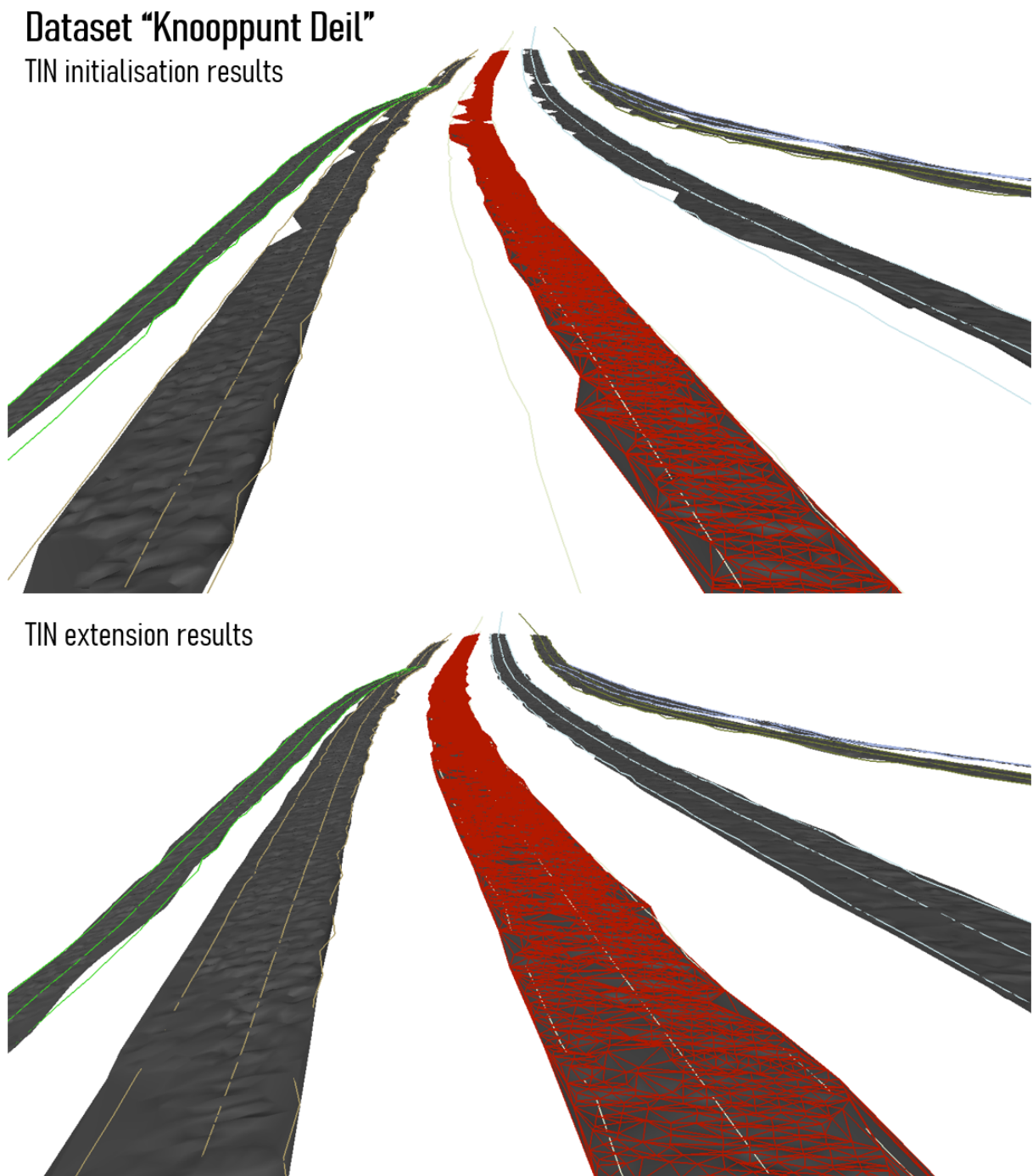


**Figure 4.13:** Visualisations illustrating the results of TIN initialisation and extension.

## 4 Results

surfaces in the *Knooppunt Deil* dataset, and the bottom two images show small-scale examples of typical extension artefacts. The [TIN](#) structure is highlighted in one of the [TINS](#) in Figure 4.13.

### TIN initialisation

A comparison of the initialisation step's insertion boundary is shown in Figure 4.13 both with initial [TINS](#) and extended ones. The pre-selection step takes place in 2D, but for viewing convenience I used preliminary edges in this example visualisation, which are originally 3D geometries (in contrast with the optimised edges, which are 2D geometries).

While in most cases this does not represent a practical issue, my results suggest that there is a theoretical limitation to my methods. Since they were inspired by ground filtering algorithms, they are not particularly sensitive to gradual changes in the road surface, and especially insensitive to smooth transitions. The approach appears to excel at eliminating outlier points that were left undetected during previous steps, and detecting the edges of the roads where they are clearly defined by a significant vertical shift in the Lidar points, for instance a high curb or a wall. However, the conditional insertion tests often have difficulty in reliably recognising points close to, but not quite on the road surface where the edges are not well defined. Avoiding the insertion of such transitional points is key, because they may then act as a bridge between road points and off-road points in subsequent iterations, thereby allowing the surface to grow in undesired directions.

The image on the bottom left in Figure 4.14 shows an area that exhibits the above type of challenging scenario and causes a small region of sloping terrain points to be added to the initial [TIN](#). The bottom right image in the same figure shows a similar type of artefact which occurs due to [NWB](#) getting as close as within 5-20 centimetres from the outer edges of the bending road, resulting in the insertion of many off-road points. In the latter case, it is possible that the "bridge" points were already inserted in the seeding step, because the outer preliminary edge was constructed far beyond the road's real edge.

Had my original intention of producing more accurate (optimised) road edges succeeded, this would not have been a problem because the pre-selected Lidar points would have nearly all part of the road surface. Although I adapted my approach to the less optimal quality of the input edges, I was unable to completely overcome this limitation without a complete redesign, which was not possible within the available timeframe. Fortunately, in practice the initial [TIN](#) models are almost always well-behaved around the centrelines, and suffer from very few artefacts of this kind where [NWB](#) is correctly positioned. The careful conditional insertions when growing the [TINS](#) (where not only one, but multiple surrounding triangles are used to model the planar trend in the surroundings) helped mitigate this issue significantly.

For the [TIN](#) initialisation step, I used an elevation discrepancy threshold of 10 centimetres, and an angle threshold of 0.12 radians (about 7 degrees) in my final configuration. For the radial point queries that occur at the locations of successful insertions (to fill the buffer for the next iteration), I used a radius of 1 metre.

In all study areas, and especially where [NWB](#) lies correctly on the road surface in 2D, my approach produces smooth 3D surfaces in which, as Figure 4.13 shows, most of the variation is solely due to noise in the Lidar data. Off-road points are only inserted in significant numbers, where the above conditions are satisfied; i.e. a smooth transition characterises the edge of the road or the underlying preliminary or optimised road edges were also significantly shifted outside of the road surface due to problems with [NWB](#).

### TIN extension

Figure 4.13 shows the visual appearance of one particular [NBRS](#) part before and after applying [TIN](#) extension, in a location where it works nearly perfectly. The effectiveness of this step relative to its planned purpose is not uniform across all areas. Most road geometries allow it to perform well, but in certain places it may only serve to further exaggerate pre-existing artefacts.

TIN extension considers additional "rings" of points progressing away from the road's centre and moving towards the edges - even beyond them, if desired. For the final results I used 5 steps, each extending the boundary by half a metre via buffering, and subtracting it from the polygon formed by the previous boundary to obtain the ring-shaped region of interest. Only those points are considered for insertion, which fall into the given region of interest in each iteration. The first iteration starts at a boundary half a metre from the seed geometry, hence 5 steps of 0.5-metres each expand the maximum distance from the centre to 3 metres, meaning that the largest boundary will be 6 metres from the centre of the road. One may notice that this is still smaller than the maximum road width I allowed in the preliminary edge approximation step (7 metres). There are two reasons for this; firstly, in my final results I primarily used TIN extension to extend initial TIN surfaces *within* the width of the preliminary edges. Secondly, wherever the width of the preliminary edges goes below the maximum (which happens quite often), this still represents an extension beyond those boundaries.

For instance, consider the example shown in Figure 4.13. In the highlighted initial TIN, the width of the model is only about 3 to 5 metres on average, even though the preliminary edges are 6 to 7 metres apart on average (close to the allowed maximum), not all points between them were inserted into the TIN in the "first pass" provided by TIN initialisation. TIN extension can solve this issue, effectively by executing additional passes over the candidate points.

In the same visualisations, the road on the left of the highlighted one has a slightly thinner representation in the preliminary edges, which are already mostly filled by the TIN during the initialisation stage. For this particular road, extending beyond the preliminary edges is more important than reconsidering data within the preliminary edges. In this specific case, it is the hard shoulder that gets added to the TIN during extension.

Since the extension procedure considers points beyond the preliminary or optimised edges, it needs to exercise caution against including off-road points. In places where the edges underestimated the road width, further surface points may be discovered and added to the model - which is the main purpose of this step. However, where the edges are correct, it is important that the algorithm does not add further points. The same goes for areas affected by the artefacts described in connection with the bottom two visualisations in Figure 4.14; i.e. TIN extension should try not to worsen them.

Therefore, the algorithm uses stricter thresholds for the conditional insertions than the TIN initialisation step. In my final configuration, the values are 3 centimetres for the elevation discrepancy threshold (elevation above underlying triangle), and 0.04 radians (about 2 degrees) for the angle threshold. The radius of the buffer-filling queries was also reduced to 0.8 metres.

While such a conservative parametrisation certainly avoids the addition of clearly defined outliers, I found it to offer only a partial solution to the above issues. After some careful inspection, I concluded that in almost all cases, pre-existing "bridge points" from the TIN initialisation step appear to be the culprits. They eliminate the gradients that would otherwise stop the extension from growing in a particular direction. Furthermore, it appears that the transition from road to off-road surfaces may occasionally take place on such a fine scale that not even these thresholds can prevent the surface growing towards them, even where TIN initialisation did not introduce such bridges.

### On using small thresholds

An obvious solution would then be to use preliminary edges that are close to the roads' centrelines, and to make the parametrisation of both TIN initialisation and TIN extension even stricter. However, there is a specific reason why this approach is guaranteed to fail: both parametrisations are already lower than AHN3's vertical accuracy. As 2.3.2 mentions, AHN3 has an elevation uncertainty of 15 centimetres at 95% uncertainty. This means that many insertions will actually fail due to the noise, not because of real-life features.

The parametrisation of TIN initialisation (10 centimetres for elevation/distance tests, 7 degrees for the angles) is already on a scale that falls within the territory of random noise. However, since the radial buffer-filling queries fetch many points rather than just a single neighbour, this generally does not affect the effectiveness of the method; the algorithm will inspect enough neighbours to still find at least

## 4 Results

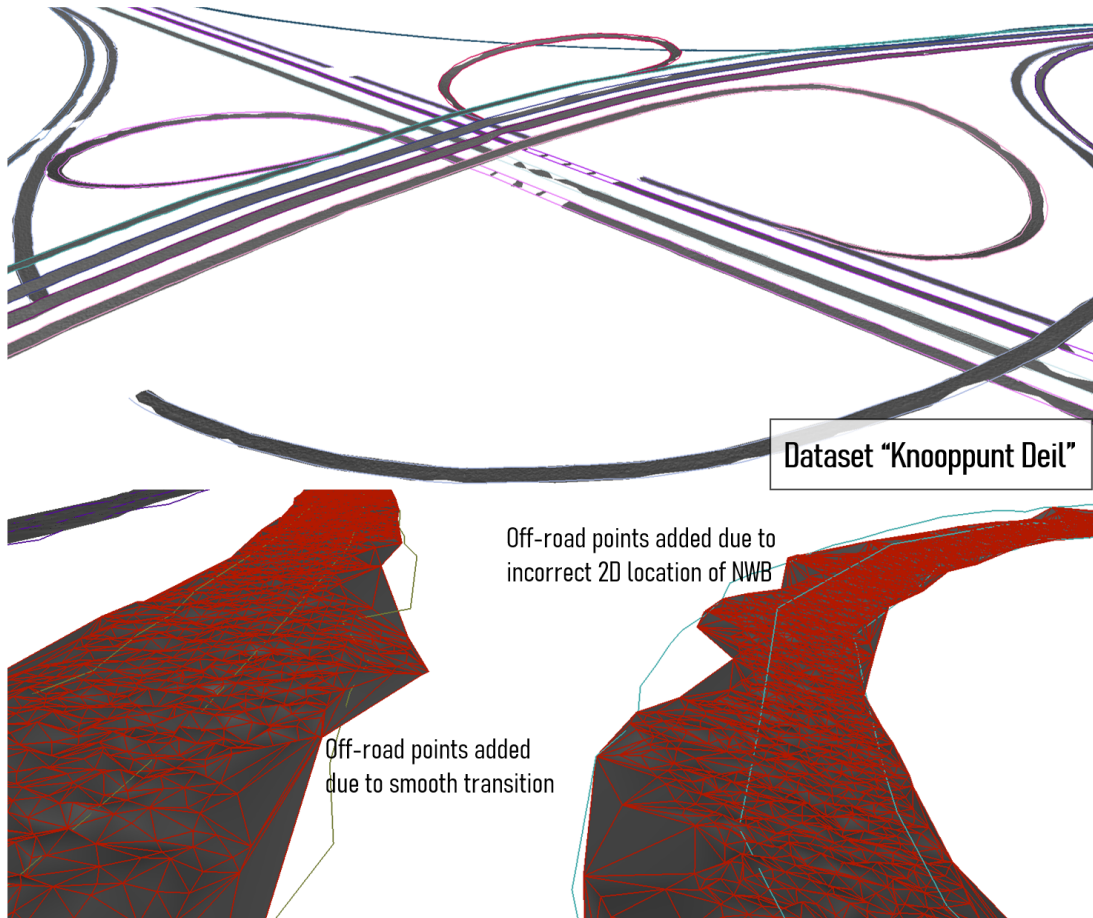


**Figure 4.14:** Visualisations providing an overview of constructed TINs and illustrating TIN artefacts.

a few that are conformant, despite the noise. Even where this fails to an extent, the TIN extension algorithm will provide the additional passes that are necessary to overcome the issue; this is precisely what happened with the highlighted road in Figure 4.13.

As a result of this phenomenon, reducing the thresholds any further without increasing the query radius will inevitably block the surface from spreading into certain areas. Increasing the query radius is, in turn, not desired because it will create too large buffers (increasing computational complexity drastically), and cause large triangles to be constructed in the TIN, which can in turn act as blocking factors in their own right, if they do not represent the trend of the points in their interior accurately. Using large query radii also increases the chances of spreading the TIN off the road surfaces, as it will result in more off-road points getting added to the buffers.

In TIN extension, I could use smaller thresholds than during initialisation because of the differences in the underlying workflow. Since extension considers “layers” of points progressing away from the centres of the road, it considers candidate points in a more “orderly” fashion. In TIN initialisation, the TIN only grows towards a certain area if insertions lead the algorithm there, whereas the repeated seeding mechanism in the extension stage represents a more *targeted* growing approach. In practice, this means that the candidates are simply examined in a better order, leading to more efficient decision-making. This counteracts the increased impact the Lidar noise has on the scale of the thresholds that are being used.

A side-effect of this is that growing may be restarted during extension after a relatively large hiatus, leading to large triangles appearing in the TINs. The hiatuses - or more precisely, the failed insertions in them - are mostly caused by the larger, slightly inaccurate triangles which I already mentioned in the previous paragraph. This can be seen in the TIN structure in the top image in Figure 4.13 - while the

right half of the suspected area of the road has points spaced uniformly, the left side has large, slightly inaccurate triangles that prevented Lidar points from being inserted within their areas and growing the [TIN](#) further in that direction. As the bottom image in the same figure shows, the "second pass" over the data via the [TIN](#) extension solved this issue for the most part, although some of the large triangles remained.

Inspecting a larger area around the point that is being considered for insertion (instead of just the one triangle containing it) could reduce the impact of this issue, but it is costly in terms of computational complexity. This is part of the reason why I only use that approach when inserting points in triangles touching the insertion boundary.

### Note on figures

Both figures in this section ([4.13](#) and [4.14](#)) show [TIN](#) road surfaces that appear to be constrained by "invisible" external line geometries, as one would expect large triangles to fill the rest of the convex hull of the vertices in the Delaunay triangulation. Originally, I planned to use a [CDT](#) to achieve this appearance, but in my final implementation I merely improved the appearance of the models before visualising them by removing meaningless triangles based on area and circumference thresholds. This proved to be effective in eliminating the large triangles and sliver triangles that appear in the Delaunay triangulation ([DT](#)) to fill the convex hull of the inserted points.

While these redundant triangles represent no issue in terms of interpolating elevations for [NWB](#), they make the visual interpretation of the results difficult. Exporting the [TINs](#) after generating them automatically applies this filtering step in the final release of my code.

In this context, it is also important to point out that while [AHN3](#) data gaps that are patched in with [DTB](#) data are always completely covered by triangles in the [TINs](#) if the preliminary edges extend through the gap. The reason why in the top image in Figure [4.14](#) this appears not to be the case, is that some of these triangles were large enough to be filtered out to improve visual appearance. The thresholds can be adjusted in my code to alter this behaviour.

### TIN point density

While using 50% of the [AHN3](#) point density (via a thinning factor of 2) offered practical benefits for all pipeline steps up to this point (especially the Lidar segmentation and edge approximation steps), the *quality* of the generated [TINs](#) does not significantly increase as a factor of point density.

Before running the [TIN](#) construction procedure, the program is equipped with subclouds, each with Lidar points relevant to a specific [NBRS](#) part. Since all prior steps are configured to keep as many of the surface points as possible, it is generally the case that their point density on the road surface is comparable to the thinned point density of the imported [AHN3](#) data. Inserting such a large volume of points into the [TIN](#) may not always be practical. For instance, visualising the generated surfaces becomes slow even with modern software, and the stochastic Lidar noise becomes clearly visible (the ripples can be seen very clearly in Figures [4.13](#) [4.14](#) due to the 5-fold vertical exaggeration). This much detail may also be impractical for applications that deal with modelling processes on the surface itself, and has implications for the accuracy assessment (see Section [4.3](#)).

The performance of this step thus depends on the input Lidar thinning. In practice, a thinning factor of 2 means that we are still working with around 10-30 Lidar points per m<sup>2</sup>, which results in mediocre performance. While my implementation did take performance considerations into account initially (for instance the buffer-filling approach is the result of this), later modifications, such as working with multiple triangles and plane fitting when growing the road surface, resulted in the performance of the final implementation decreasing gradually. In particular, not running [TIN](#) extension can improve runtimes drastically, which may be useful for users who are only interested in interpolating [NWB](#) elevations.

As I will further explain in Section [4.3](#)), the system design guarantees that [NWB](#) will generally lie on the [TIN](#) models in 2D, making it possible to interpolate elevations in it for its vertices. Exceptions to this rule

## 4 Results

occur in places where preliminary edge estimates or optimised edges disagree with [NWB](#) badly. Where this occurs, [TIN](#) initialisation will not be able to insert points in the [TINS](#) at the 2D location of [NWB](#). With preliminary edges, this may only occur where cross-sections were skipped too many times in a row where the road is not straight, which may happen in various circumstances I have already described in Section 4.2.4. With active contour optimisation, this may occur more frequently, depending on the local density of generated artefacts.

### Two different kinds of quality

While the above discussion focuses on describing issues with the quality of the generated [TINS](#), many of these issues are constrained to the academic goals of the project only. The academic goal related to the [TINS](#) is to make them complete and accurate representations of the real-life road surfaces. This is the quality on which I primarily focused in this section, while the next section will see more mentions of quality in terms of their suitability for interpolating elevations for [NWB](#).

These two qualities need to be distinguished not only because of the conceptual differences, but because there are much less issues with the less academic goal of converting [NWB](#) to 3D than with producing ideal road surface models. The reason is, that for the 3D conversion to be accurate, one only needs complete and accurate [TIN](#) surfaces close to where the centrelines are found in 2D. Fortunately, these locations generally correspond to areas which are less difficult to reconstruct accurately in 3D, than for instance the immediate vicinity of road edges.

### Using the implementation

The following two commands may be used to run [TIN](#) construction and export the resulting 3D surface models:

```
roads.build_tin(max_dh_int = 0.1, max_angle_int = 0.12, r_int = 1,
                 max_dh_ext = 0.03, max_angle_ext = 0.04, r_ext = 0.8,
                 ext_steps = 5, ext_dist = 0.5,
                 type_edges = 'preliminary')
roads.write_tins(fpath = tin_fpath)
```

The first method invocation performs the [TIN](#) construction itself. The first line of arguments corresponds to the elevation and angle thresholds, and the buffer-filling query radius used in [TIN](#) initialisation, respectively. The role of the second line of arguments is identical, with the exception that they are used for [TIN](#) extension. The next two arguments (`ext_steps` and `ext_dist`) specify the number of extension steps to be performed, and the distance by which the query region should be expanded in each step. The first insertion boundary for extension is always a polygon created by buffering the seed LineString by 0.5 metres; the extension starts from this base boundary. If no extension is desired, `ext_steps` should be set to 0. The last parameter, `type_edges` can be set either to `preliminary` or `optimised`; it controls which type of road edges the user desires to use.

The second method invocation writes the [TINS](#) to disk, one OBJ file for each [NBRS](#) part. As mentioned above, it also filters out large triangles and sliver triangles in the process. The supplied file path should only include the first part of the file name, as the [NBRS](#) ID, part ID and file extension will be added automatically (for instance `.../C_39CZ1_tin` would work). Using a dedicated folder is recommended.

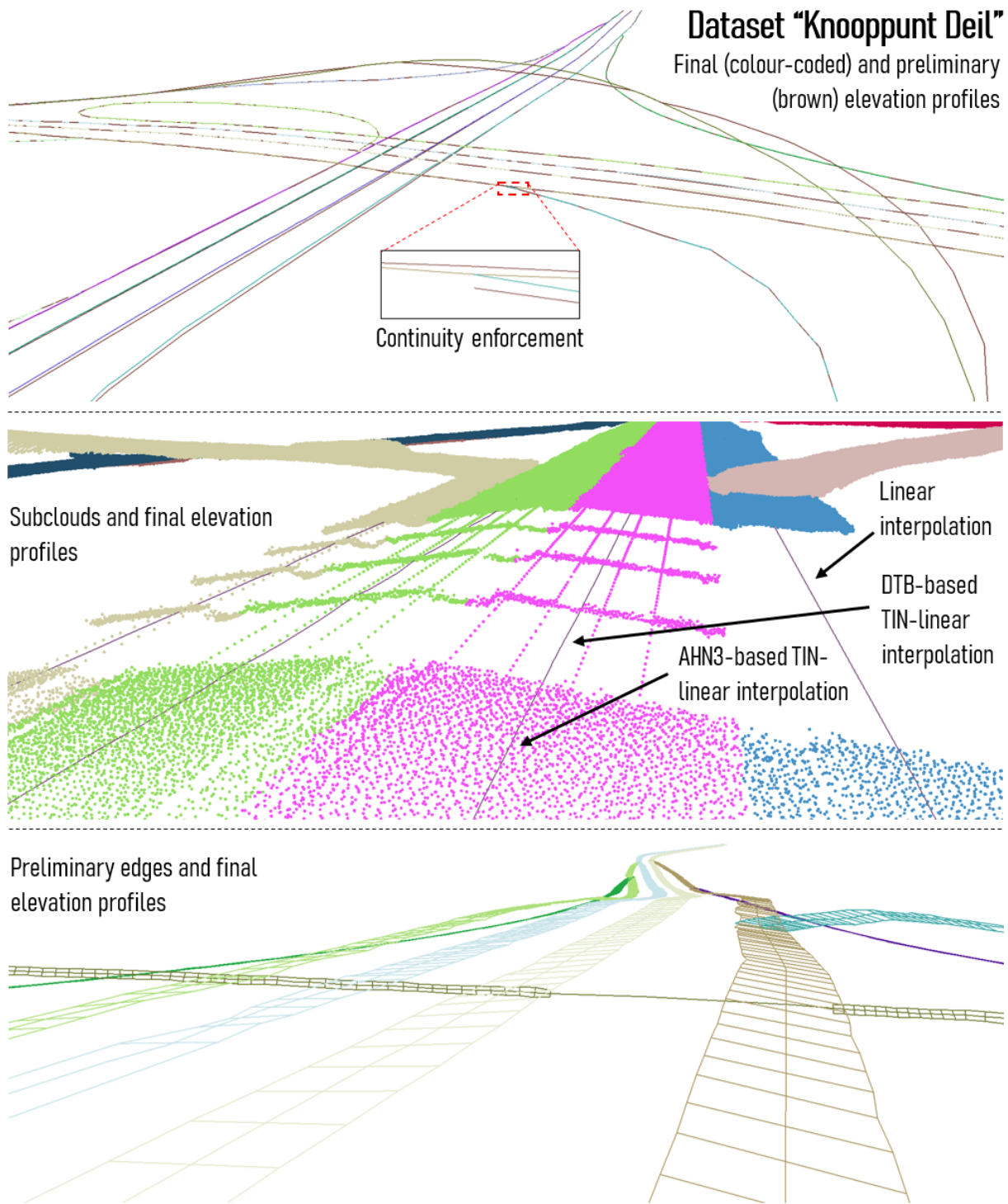


**Figure 4.15:** Visualisations comparing final 3D conversion results to preliminary conversion, subclouds, and preliminary edges.

### 4.2.7 Interpolation in TIN and snapping

Figures 4.15 and 4.16 show examples of the results of interpolating elevations for NWB in the TINs generated in the previous step (including the use of the snapping feature that enforces continuity)). Visual inspection of the results reveals that the methods used to generate them are robust and effective under almost all circumstances, including where complex 3D relationships and the extensive presence of other types of occlusion are encountered. The example visualisations shown here contain comparisons between the final elevation profiles and various intermediate results, namely the preliminary elevations, subclouds and preliminary edges in Figure 4.15, and the TIN models in Figure 4.16).

Generally, the results are in line with my expectations both in terms of overall completeness and quality. I do not attempt to characterise the accuracy of the results in this section, for a quantitative (rather than qualitative) analysis, please refer to 4.3.

#### Comparison with preliminary elevations

Comparing the final 3D-NWB results with the preliminary elevations sheds some light on the nature of the improvements that are the result of the complex processing steps that occur in the later stages of the pipeline. The preliminary elevations (shown in a brown colour in the top visualisation Figure 4.15) represent the 3D conversion that can be achieved using only a few simple steps of processing: NBRS generation, elevation estimation, and the polynomial-based refinement step. The final results are coloured randomly based on their NBRS IDs.

The first difference that stands out is that those NBRS that I described as having complex vertical curvature and being difficult to model by polynomials in Section 4.2.2 are modelled much more realistically in the final output. One only needs to take a look at the comparison in the top image in Figure 4.15) to tell that it must be the final results that are correct, not the preliminary ones. The change represents a fundamental difference between these two stages in the pipeline. Preliminary elevation estimation has to rely on a workflow to detect elevation estimates corrupted by occluding geometry and to supply replacement values for them, while the final elevations come from TIN models that are guaranteed to only contain vertices that represent measurements of the relevant road's elevation.

While the biggest differences can be observed where the polynomial fits were poor in the preliminary elevation estimation stage, there are many other scenarios where smaller improvements can be seen. For instance, the preliminary elevations may contain outliers that were not detected as outliers in the refinement step. For instance on bridges, AHN3 may contain reflections from vehicles. These are often not far enough from the road surface to be replaced by polynomial values, introducing small spikes into the elevation series. In the final results, such outlier points are guaranteed not to be inserted into the TIN models, and cannot affect the 3D conversion as a result. The inset in the figure also illustrates that while while preliminary 3D conversion is not continuous across intersections, the snapping workflow ensures that the final 3D conversion is.

Another scenario in which clear benefits can be observed (not shown on these figures) is the presence of many occluded regions concentrated into a small area, or equivalently, one long occluded zone. In preliminary elevation estimation, such occluding features may attract the polynomial towards themselves, thus corrupting the fit and potentially introducing incorrect elevations into the profiles. This may happen, for instance, where many bridges are constructed across a motorway in a row, and the NBRS is not long enough to include enough non-occluded elevation measurements. Later pipeline steps almost always recognise these mistakes for what they are (data gaps), and either use DTB if available, or break the NBRS into parts locally.

There are features in the final output that may be interpreted as a deterioration in quality with respect to the preliminary elevations, at least visually. Firstly, small jumps in elevation may be observed where AHN3 gives way to DTB points the underlying TINs. The new baseline elevation continues across the region where DTB was used, and reverts to the AHN3-based baseline elevation once the road emerges from the zone not covered by AHN3. This is simply due to the temporal discrepancy between DTB and AHN3; using better support data would eliminate these shifts from the output. This is only visible in the

middle image in Figure 4.15, and the reader is referred to Figure 4.7 and Sections 4.3 and 4.4 for further details.

Lastly, one may observe that the amount of small-scale noise in the final 3D-NWB output is noticeably larger than that in the preliminary profiles. This also has a simple explanation: the preliminary elevations are based on taking the median of the elevations of a small patch of Lidar points, whereas the final elevations are all based on 3 samples each, due to having used TIN-linear interpolation. The amount of noise is thus no greater than the stochastic scatter in AHN3; it is only visible in the visualisation due to the vertical exaggeration.

### Comparison with subclouds

This comparison is demonstrated in the middle image in Figure 4.15. The most important aspect here is that the final 3D road centrelines all lie flat on those parts of the Lidar subclouds, which one intuitively recognises as road surfaces. This is always the case as long as NWB is correctly positioned, such as in this location.

The figure shows that this also holds for regions affected by occlusion. In places where DTB was added to the subcloud in the Lidar segmentation step, the centrelines are shifted vertically to conform with the surfaces defined by DTB. Where AHN3 coverage reappears, they immediately shift back to its elevation, creating a geometry akin to suspension bridges in this example visualisation. Regardless of which dataset is used, the main point here is that the 3D conversion continues across the gaps without snapping to the bridges above that are causing the periodic occlusion.

The visualisation also illustrates that linear interpolation through regions with no measurements represents a good solution for small gaps of coverage where roads are straight. The road with the blue-coloured subcloud (on the right) has no DTB coverage, hence the small patches of AHN3 points between the bridges could also not be detected. In spite of this, the elevations are actually more optimal here than elsewhere, because they are not affected by the small shifts introduced by DTB.

### Comparison with preliminary edges

This comparison reveals the interestingly, the final 3D conversion of the centrelines and the preliminary edges are in near-perfect agreement with each other where coverage is good. As the bottom image in Figure 4.15 shows, even a five-fold vertical exaggeration cannot reveal significant differences between them. This is interesting, as there are various pipeline steps in-between the generation of these results; most importantly, TIN generation. Small differences are only found between the elevations of the preliminary edges and 3D-NWB, where the preliminary edges were generated off the road surface, in which case the final results represent the correct elevation.

While the two outputs are not directly comparable, the exceptionally good match between them indicates that a 3D conversion with similar quality could potentially be achieved via a procedure that involves the subclouds and 2D centrelines only, perhaps using a workflow based to some extent on that which currently I used to generate the preliminary edges.

It is also important to note here that while the preliminary edges may be missing vertices in some places (indicated by the cross-sections also being absent), this is not the case in any of my final 3D-NWB results. As long as the centreline is found between the edges, a TIN will be constructed locally and TIN-based elevations will be computed. As I already described previously, this is only violated in places where many cross-sections are skipped in a row, which is rare in my results.

## 4 Results

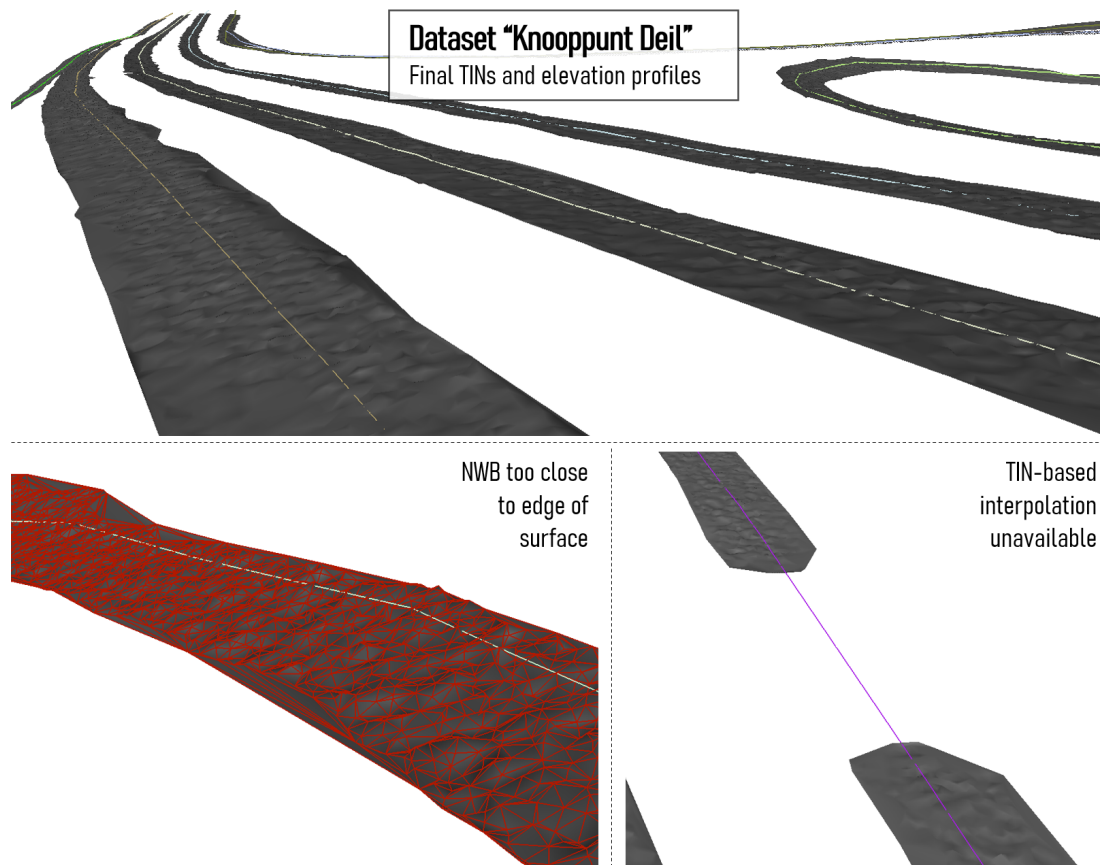


**Figure 4.16:** Visualisations comparing final 3D conversion results to the underlying [TIN](#) models.

### Comparison with TIN models

Example comparisons between the final output and the [TINs](#) are shown in Figure 4.16. An interesting aspect of this comparison is that the final 3D-converted centrelines are often found slightly above or below the model (less than a centimetre, typically). This is best evidenced in the output by the intermittent disappearance of the 3D centrelines beneath the [TIN](#) triangles. This is the result of the georeferencing of [NWB](#) being coarse *relative to the TINs* even after applying vertex densification. [NBRS](#) parts only have vertices approximately every 5 metres, whereas [AHN3](#) has up to 10 to 30 points per  $m^2$  after after thinning using a factor of 2. This disparity simply indicates that if we wanted to, we could sample the [TIN](#) at smaller intervals to increase the output's vertical resolution. However, [NDW](#) officially requires elevations only to be estimated at the original [NWB](#) vertices, which can be several times further apart even than my densified vertices. In other words, these [TINs](#) offer far more detail than that which would be minimally required for the conversion, as expected from such a high-resolution surface model.

An example where [NWB](#) gets close to the edge of the [TIN](#) is shown in the bottom left image. This is representative of the typical severity of the [NWB](#) georeferencing issue in sharp bends. While it was difficult to overcome numerous processing difficulties related to this problem with [NWB](#), it bears almost no influence on the effectiveness of the [TIN](#) interpolation process as long as the [TIN](#) exists locally. Where [NWB](#) lines are close to road edges, the underlying [TIN](#) models will still always describe the surface of the road according to our expectations. They will potentially include off-road points, but from the point of view of the 3D conversion of [NWB](#), this does not matter. Even if [NWB](#) is not on the road surface, the [TIN](#) will likely be constructed locally and off-road elevations will be interpolated for it.

The interpolated elevations will always correspond to [NWB](#)'s exact horizontal position, meaning that as long as its georeferencing is not corrected, the interpolated elevations will also not correspond to the road's real centreline. This could mean a significant deviation if [NWB](#) is not on the road surface, or even

if it is on the road but the road's surface is somewhat tilted sideways. Rectifying [NWB](#)'s georeferencing would automatically solve this, no modifications to the algorithms would be needed.

Where no [AHN3](#) or [DTB](#) coverage is available, the [TIN](#) will not exist and values are interpolated linearly inside the elevation profiles. A location with this property is shown on the bottom right in Figure 4.16. Such gaps correspond to zones *between* [NBRS](#) parts, hence the two [TINs](#) shown in this image belong to two different [NBRS](#) parts.

### Using the implementation

The following two commands may be used to run the final elevation interpolation code, and export the resulting 3D-converted version of [NWB](#) as a Shapefile:

```
roads.interpolate_elevations()
roads.write_all(fp校准 = accurateZ_fp,
               to_drop = ['geometry_simpleZ'])
```

The algorithm does not have a parametrisation, hence the method invocation does not require any arguments. The `.write_all()` invocation requires a list of GeoDataFrame columns to drop, as the Shapefile can only have one set of geometries in it. The column name in `['geometry_simpleZ']` corresponds to the preliminary elevation estimates. The original 2D [NWB](#) geometries are always dropped automatically, so that column does not need to be manually specified.

In the `nbrs_manager` class, the final results are added to the class's `.nwb` variable, as the `geometry_simpleZ` geometry column of the GeoDataFrame. Since Shapefiles also cannot accept arrays into their attribute tables, the vertex origin indicators (AHN3/DTB/linear interpolation) are also not written into the output file. These can be found in `.wvk_z_origins[wvk_id]`, a dictionary that needs to be indexed with the `wegvak`'s ID whose vertex origins are desired.

## 4.3 Accuracy assessment

In this section, I will present the accuracy assessment results focusing on a particular dataset: *Knooppunt Del*. This dataset exhibits most of the unique features that are relevant for this part of the analysis, and it is my hope that such a "case study" approach makes understanding the assessment's results more straightforward. Following the case study, I will present and discuss an overview of the relevant accuracy metrics for all testing datasets, in a tabulated format.

I will first focus on the results of computing local sampling densities and formal output accuracy values (error propagation results). Then, I will discuss how often the accuracy needs to be deemed unknown and for what reasons. Lastly, the completeness of the output [TINs](#) relative to the [BGT](#) reference polygons will be examined. Please refer to the relevant sections in Chapter 3 ([3.2.4](#) and [3.4](#)) for the background theory and the detailed description regarding the assumptions I made.

### 4.3.1 Empirical accuracy assessment

As I briefly mentioned in Section [3.2.4](#), I first attempted to assess accuracy based on an empirical approach. Before performing the necessary steps, I was yet unaware of how the combination of factors that define output accuracy interact in our particular case. Most importantly, I was yet to discover that a range of assumptions regarding ground filtering accuracy, influence of surface ruggedness and sampling density can be made. In fact, it was this failed attempt that directed my attention to the fact that in our particular case, there are very few external factors that influence accuracy.

My initial hypothesis was that the primary influence on accuracy has to be sampling density and interpolation error, because ground filtering errors and surface ruggedness already appeared to me as

## 4 Results

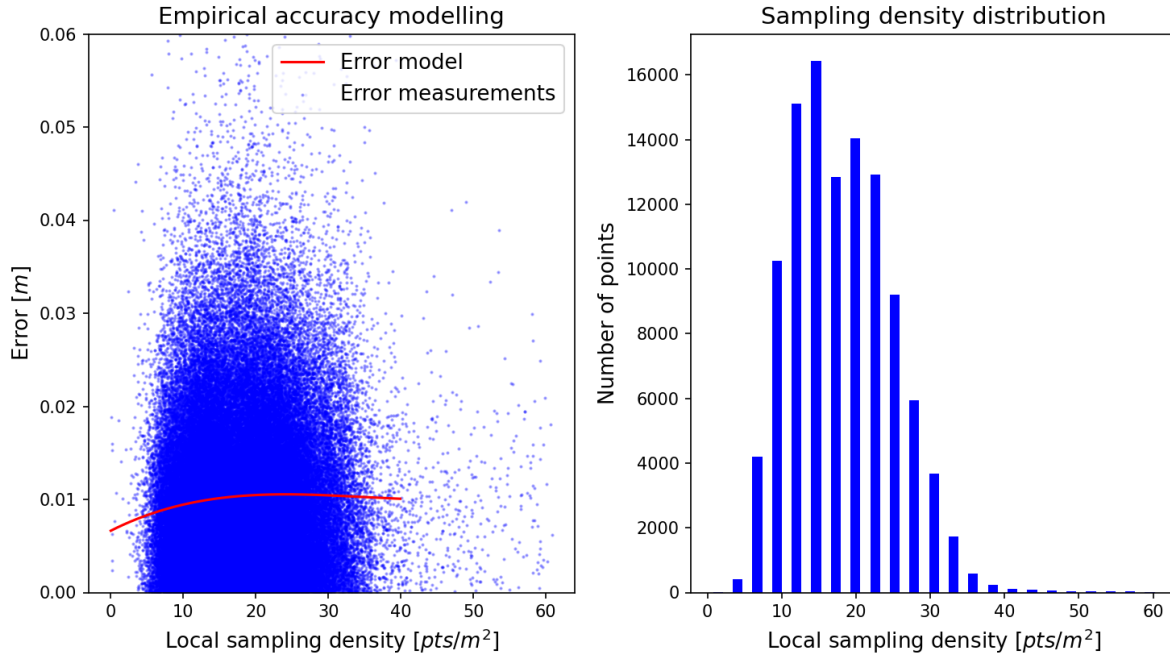


**Figure 4.17:** Charts demonstrating the outcome of the empirical accuracy assessment process.

irrelevant based on my experience with the data and the results. To be able to verify the hypothesis and compute empirical errors based on it, I constructed an error model and derived errors for each output vertex from it. I constructed the model by removing samples (vertices) from the output TINs, interpolating their values via the TIN-linear method, and computing the differences between the removed Lidar samples, and the interpolated elevations (in essence, a jackknife approach). I fit a cubic polynomial on the part of the scatter where we have enough data, and derived NWB accuracy values from it.

While I was doing this, I noticed that all my output errors were extremely small, and all roughly the same. This made me start suspecting the irrelevance of sampling density in our particular scenario, so I plotted the data and the model to verify this new hypothesis. Figure 4.17 shows an example visualisation created from the empirical accuracy assessment of testing dataset *Knooppunt Deil*. The chart on the left shows local sampling density plotted against the jackknife errors, computed for about  $10^5$  TIN vertices (10% of the total number of TIN vertices of all TIN models generated from this testing dataset).

While at a first glance one might think that the inverse parabola shape in the scatter plot represents a meaningful trend, it does not, in fact, possess the correct shape for the relationship. We know from literature that when a correlation exists between errors and sampling densities, it tends to be logarithmic, and the trend in my chart does not appear to have that property. The fitted model does appear to have a weak logarithmic component, but it shows errors to increase in the wrong direction (towards larger sampling density), and the predicted error magnitudes are far too small to be meaningful too. The histogram on the right reveals that the shape of the scatter plot does not correspond to a statistical trend that concerns a relationship between sampling density and jackknife error - it can be fully explained by the distribution of the sampling densities in the dataset.

What is also interesting in these plots, is that jackknife errors remain negligible even at the lowest values encountered. Overall, about 96% of the jackknife samples showed an error less than 3 cm, which is well below the nominal vertical and horizontal accuracies of AHN3 and DTB. In other words, we may safely conclude that the variation in jackknife accuracy, on the scale observed in this experiment can be explained simply by the noise in the input datasets. The random distribution of the variations, evidenced by the bell-shaped trend, further confirms this theory.

Although this analysis suggests that any errors in the output will be small and that they will be mostly independent of external factors, the qualitative and quantitative estimation of output accuracy is among

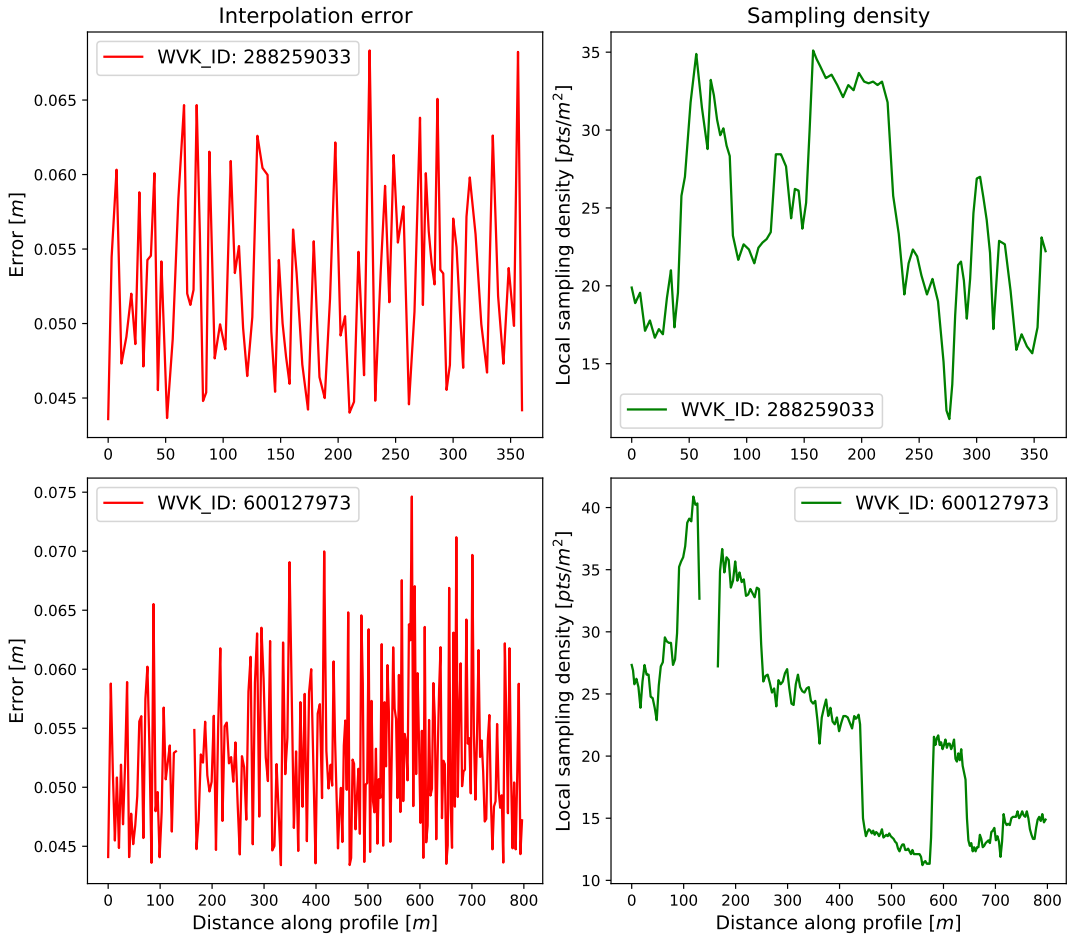


**Figure 4.18:** Charts illustrating the formal accuracy assessment results on two *wegvakken*.

the main goals of this project, hence I decided to find further evidence. This is why, even after performing the above analysis, I proceeded to propagate errors through the interpolation technique, and to also examine this in comparison with sampling density data.

### 4.3.2 Formal accuracy assessment

The charts in Figure 4.18 show interpolation error profiles from 2 *wegvakken* from our chosen testing dataset. From the lack of a trend in the errors, and their small magnitudes overall, we may deduce that the output accuracy is sufficiently high with respect to the 20-centimetre requirement of the noise regulations. Any differences due to the TIN-linear interpolation represent an *increase* in accuracy relative to the 15 cm elevation accuracy of AHN3. The two *wegvakken* shown in the figure exhibit theoretical interpolation elevation errors in a range of about 4 centimetres to 7 centimetres, with mean errors of 5 centimetres for both. The variation is always randomly distributed, because the positions of NWB vertices relative to the containing triangles' vertices also lack correlation (which is what controls the value  $M$  that determines how much the accuracy is improved). In theory, the only factor that could introduce correlation into these profiles would be roads with very steeply sloping surfaces, but no roads in this dataset (or any of my datasets) reach a slope steep enough to affect the errors significantly, and introduce correlation.

The top part of Figure 4.19 shows the 3D geometry of the subclouds and centrelines of the same two *wegvakken*. Wegvak #288259033 has a shape which is representative of the steepest slopes and sharpest

## 4 Results

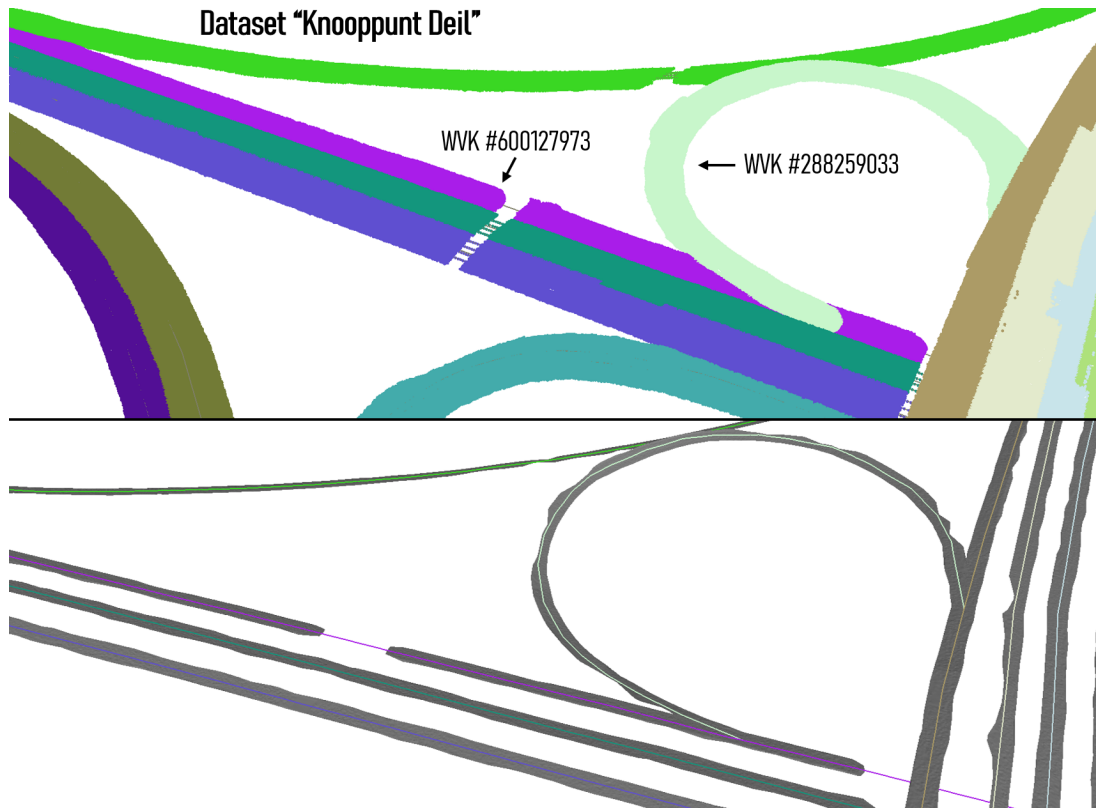


**Figure 4.19:** Visualisations showing the subclouds, TINs and 3D-NWB centrelines in the area concerned by Figure 4.18.

bends one can expect from the Dutch road network; it connects a ground-level motorway lane with another one running orthogonal to it directly above, on a bridge. *Wegvak* #600127973 is the ground-based motorway lane that it connects. It lies entirely flat on the ground, with little to no variation in its elevation. I picked it because its shape is the opposite of that of #288259033, and because it had been split into two parts due to a 15-20 m long data gap which is visible in the figure. The gap also lacks [DTB](#) coverage. The bottom image in Figure 4.19 shows the corresponding [TINs](#), and it is visible in this figure that [NWB](#) veers to the outer edge of the steep, curved *wegvak*, almost reaching it. The relatively thin width of the [TIN](#) and its rugged outer edge is a result of this; the preliminary edges were constructed partially off-road due to [NWB](#)'s poor georeferencing.

I added sampling density plots on the right in Figure 4.18. The first important observation to make about these charts is that the data gap in sampling density between 100 and 200 m along the profile in #600127973 is due to the data gap I mentioned above; here the density is 3 points per  $\text{m}^2$  or less - which is the threshold below which the cut-out happens, i.e. accuracy is not computed - visible in the chart on the left in the same figure. The sharp drops in density around the gap illustrate that the neighbourhood queries already indicate the presence of the gap right before and after reaching the centreline vertices that fall into it. The two *wegvakken* #288259033 and #600127973 have mean sampling densities of 24 and 21 points per  $\text{m}^2$  respectively - well above the nominal accuracy of the dataset, primarily owing to the flatness of the road surfaces.

The second important observation is that while local sampling density fluctuates by as much as 80-90%, it never reaches the minimum threshold in places other than no-data zones and where only [DTB](#) data is available (the latter is not separately illustrated here). The fluctuation is due to the inhomogeneous sampling rate of [AHN3](#). It is already present in the raw point cloud, and is simply a factor of how many times a given area was scanned by the aircraft's laser sensors. The figure was generated from my final results, which all use a thinning factor of 2 - meaning that the values seen in the charts are half of the maximum available. Increasing the thinning factor further may result in the sampling rate dropping

below the threshold in certain exposed regions, hence it is not recommended. The results shown in these two charts are representative of all testing tiles; significant deviations from what I described above and what is shown in the figure were not observed elsewhere either.

The third, and last important observation is that neither the recorded sampling rates, nor the theoretical accuracy values are indicative of locations where [NWB](#)'s 2D georeferencing is poor. While [NWB](#)'s location is far from the road's real centre in #288259033, it is not off the road, and as a result the interpolated elevations will still be correct, or at least they will definitely correspond to some part of the road surface. As far as theory is concerned, the elevation is the *correct elevation* at the *incorrect NWB location*. This also holds for places where [NWB](#) is not on the road surface, but in such places both the sampling density and the accuracy may drop, the former because the [TIN](#) construction algorithm is not meant to be used in uneven areas, and the latter because of (and only in the case of) introducing sloping triangles into the [TIN](#).

The mean error and sampling density of the entire testing dataset are 5 cm and 19 points per m<sup>2</sup> respectively.

### 4.3.3 Ratio of accurate vertices

The frequency at which the algorithm has to deem output accuracy unknown fluctuates significantly both inside and between testing datasets. How often this happens depends on the number of linearly interpolated values, and how often the sampling density drops below the 3 points per m<sup>2</sup> threshold. The percentage ratio of accurate vertices varies, under normal circumstances, between 85 and 95%. Special circumstances (such as tunnels) may further decrease this, which will be discussed in Section 4.3.5.

Where no special circumstances are encountered, variations can be traced back to two main controlling factors: how much of the road network is occluded, how accurate the preliminary elevations are, and how complete [DTB](#) is in the given testing dataset. The relevance of the amount of occlusion is straightforward to understand: the more the occlusion, the bigger the chances are of encountering an [AHN3](#) data gap where linear interpolation may need to be used.

The completeness of [DTB](#) is a factor here because it prevents linear interpolation from being used. However, for the program to consider interpolation accurate locally, [DTB](#) also needs to have good enough coverage. Therefore, only a subset of the [DTB](#)-covered data gaps will be deemed accurate. [DTB](#) rarely exists for provincial roads ([P-roads](#)), hence Lidar data gaps in such roads will *almost always* result in linear interpolation. In turn, this means that data sets comprised primarily of [P-roads](#) will have lower accurate vertex ratios. Preliminary elevation accuracy is important, because it controls [DTB](#) coverage. If the preliminary elevations are inaccurate (due to a poor polynomial fit, in most cases), then even if [DTB](#) exists locally, it may not be found.

As I mentioned in Section 3.2.4, [DTB](#) is effectively a placeholder for a more accurate dataset in terms of this accuracy assessment workflow. Records of which vertices were affected by [DTB](#) data are generated by my implementation, and reusers are advised to consider all of these vertices inaccurate due to the temporal issues. For the purposes of this accuracy assessment demonstration, [DTB](#)-based interpolation with high enough local sampling density was considered accurate and included in the percentage values. However, because [DTB](#)-based sampling density also reflects the line densification threshold used when converting it to a point cloud (in addition to the number of [DTB](#) lines available locally), I must emphasise here that [DTB](#)-based sampling density values are partly artificial.

Linear interpolation is rare outside of [AHN3](#) data gaps (including those due to occlusion), and especially rare where [NWB](#)'s georeferencing is correct - in my datasets, 98-100% of non-occluded vertices are interpolated in the underlying [TINs](#). The majority of these are due to the rare cases where too many cross-sections are skipped during preliminary edge estimation, preventing proper [TINs](#) from being constructed locally.

## 4 Results

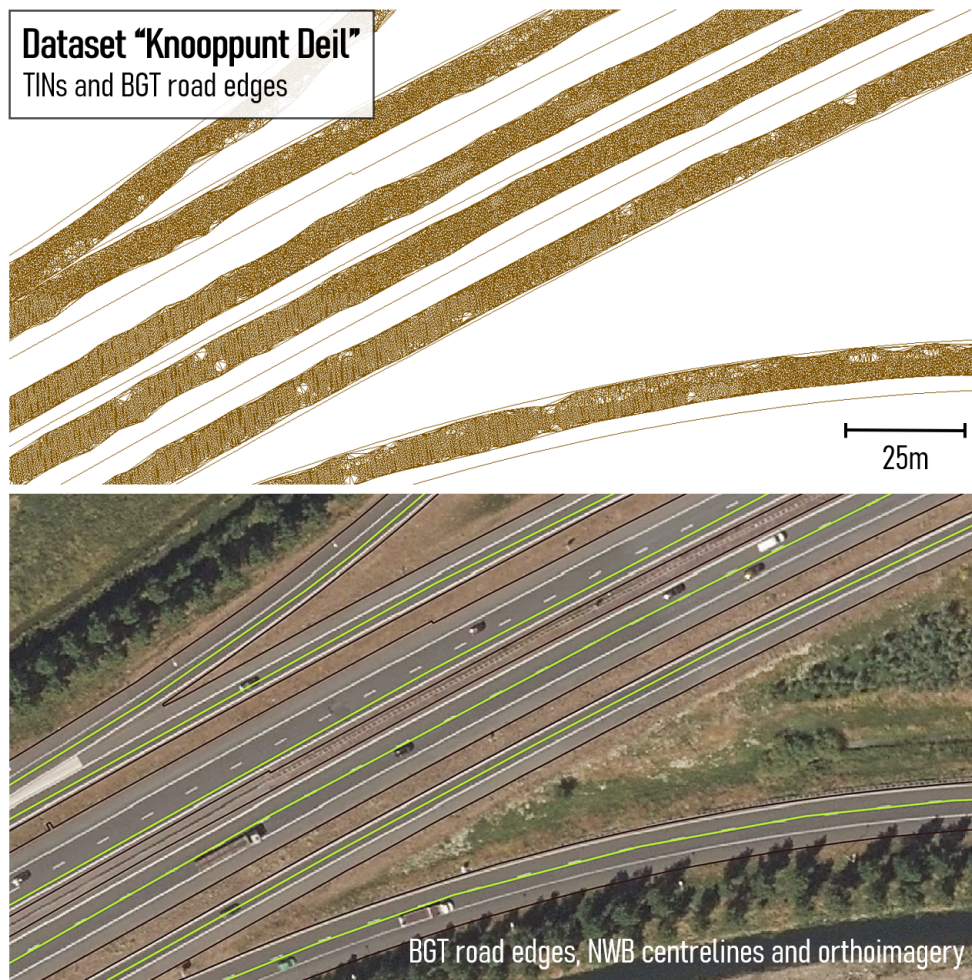


**Figure 4.20:** 2D Visualisations comparing [BGT](#) road edges with the [TINs](#), with [NWB](#) centrelines and with [Luchtfoto](#) 2020 satellite imagery.

### 4.3.4 TIN completeness

As I mentioned in the methods section, I evaluated the completeness of the [TIN](#) road surface models via a comparison with [BGT](#) polygons. Figure 4.20 below shows the results of one such comparison, which I deemed representative of the relationship overall. The top part of the figure shows some of the [TINs](#) overlain on the outlines of [BGT](#) geometries, which allows one to see how well the [TINs](#) agree with these reference geometries. The bottom half of the figure, in turn, compares the [BGT](#) geometries to satellite imagery - to verify how well [BGT](#) itself agrees with what we can consider an accurate representation of the visual appearance of these roads. The orthoimagery is from the 2020 edition of Kadaster’s [Luchtfoto](#) dataset, available as open data like all other datasets used in this research.

The [NWB](#) centrelines are also shown here to demonstrate the extent of the georeferencing issues relative to [BGT](#) and to the orthoimagery. The poor agreement is the result of two factors combined: [NWB](#) approximates the centre of the traffic-occupied road surfaces rather than the paved surfaces, and its georeferencing is inaccurate in general. The definition of traffic-occupied road surfaces excludes hard shoulders. If the traffic-occupied surface is on one edge of the full paved surface, [NWB](#)’s poor georeferencing is more likely to cause it to be close to, or beyond the real edge of the paved surface.

[BGT](#), on the other hand, appears to be an accurate 2D representation of the paved road surfaces. Its extents do not, however, correspond to that which I can *typically* model reliably using the pipeline I developed. Ideally, the surface model should cover the entire paved area, but as I described in Section 3.3.4, I found using a maximum road width to be the only viable means to ensure that my approach

works in most cases. The [TIN](#) extensions that are part of the [TIN](#) construction step (Section 3.3.6) mitigate this issue to a certain extent, but they do not eliminate it entirely. Allowing the [TIN](#) extension to go too far beyond the preliminary/optimised edges increases the chances of extending the roads into unwanted areas, and increases runtimes significantly.

Motorways with hard shoulders, which are shown in the centre of Figure 4.20, are particularly difficult to handle because the hard shoulders and potential extra lanes extend their width far beyond that, which could be reasonably expected from municipal roads and dual carriageways - which is what my parametrisation prioritises. A solution to this issue could be to automatically select pre-set configurations of the parametrisation appropriate to each road type, but this is not an area that my research explored.

The [TIN](#) models in the top part of the figure show that the [TINS](#) are in good agreement with the [BGT](#) geometries. The same issues which I described in Section 4.2.6 are also manifested here, for instance the on-ramp model in the top of the image contains some off-road points where both [NWB](#) and [BGT](#) appear to veer too far from their ideal positions. In general, based on examining all my results, I estimated that the [TIN](#) surfaces cover approximately 95% of the traffic-occupied surfaces found in my testing datasets, and about 75% of the total paved surfaces as shown by [BGT](#). The only major issue appears to be the one I mentioned above, that the full extent of the paved surfaces cannot be modelled without dynamically adjusting the parametrisation of the pipeline's algorithms.

Figure 4.20 is also illustrative in terms of showing just how detailed these [TIN](#) models are, even with an input thinning factor of 2 for [AHN3](#). On the scale shown in this image, and in comparison with the orthoimagery, it becomes visually perceptible that the road surfaces are being oversampled by inserting so many points into the [TINS](#).

### 4.3.5 Tabulated values

In the sections above, I focused on assessing the accuracy and completeness of specific LineStrings (*wegvakken*) in one testing dataset. In Table 4.2, I present mean error, sampling density and accurate output vertex ratio values for *all* my testing datasets.

Almost no variation is observed in the mean **formal output vertical error** across the datasets. As explained in the sections above, this is due to the fact that propagating errors through the interpolation technique only exhibits large (positive) fluctuations in the output error when steep triangles are encountered. The first row of tabulated values thereby represent evidence that triangles steep enough to affect accuracy are decidedly rare in our [TINS](#), and the output accuracy is, in effect, roughly constant and almost entirely determined by the input accuracy.

The **sampling density** values show that the density of points is reliably high, consistently staying well above the threshold, below which accuracy is deemed undetermined. However, large variations are still observable between the testing datasets, with values ranging from about 14 to 27 points per m<sup>2</sup>. The variation has several reasons based on my analysis, each with non-negligible influence. The first reason is that the stock sampling density of [AHN3](#) appears to vary on a large scale, in various parts of the country, and also locally, which I have already shown in Figure 4.18. The second reason is that accuracy is computed based on radial queries around [NWB](#) vertices, and will therefore show lower values for very thin roads where [NWB](#) is close to the edge of the road.

Lastly - but most importantly for us - it gives an indication of the pervasiveness of occlusion. Partial occlusion (due to vegetation) and complete occlusion (due to bridges and other opaque structures) decrease the [TIN](#) vertex density significantly. For instance, the low value seen in 33CN2 (*Hoenderloo*) is primarily due to the road being situated in a dense, old-growth forest, and the one in 37HN2 (*Knooppunt Ridderkerk*) is mainly due to occlusion resulting from the roads passing above and below one another in the motorway junction.

However, the medium value seen in 25BZ2 (Amsterdam Hemhavens) does *not* reflect the fact that there is a sizeable tunnel in the dataset. Since the tunnel has no [DTB](#) line coverage, the relevant [NBRS](#) part's [TINS](#) do not extend into the tunnel. As I explained in the sections above, these densities are computed

## 4 Results

	20BN1	25BZ2	25DN2	32BN1	32FZ2	32HZ2	33CN2	37EZ1	37HN2	38GZ1	39CZ1
A	5.26	5.26	5.30	5.27	5.28	5.30	5.28	5.36	5.30	5.30	5.30
B	26.82	19.81	20.05	14.89	16.58	14.96	16.20	13.54	13.78	15.49	19.29
C	93.03	76.15	95.09	91.74	95.51	94.21	90.52	56.26	85.25	89.09	91.73

A = Mean error [cm], B = Mean sampling density [pts/m<sup>2</sup>], C = Accurate ratio as % of all vertices

**Table 4.2:** Tabulated 3D-NWB accuracy and completeness results per testing dataset.

from the [TINs](#), and therefore road sections without [AHN3](#) and [DTB](#) coverage are not allowed to affect these sampling density measurements. I made this design choice because in these areas, my implementation simply interpolates output elevations via linear interpolation. Therefore, these areas do not, strictly speaking, constitute areas in which we can predict elevation with any certainty, especially not where they are long, such as the tunnel in this particular testing tile. Although I am providing linearly interpolated output values in these regions, I essentially consider them to be excluded from my analysis, and thus I also exclude them from the density computations.

The presence of the tunnel can still be recognised in the **accurate vertex ratio** row in Table 4.3.5. The lower value seen for 25BZ2 is simply due to the tunnel - almost all other parts of the roads in this dataset have detailed [TINs](#) associated with them. In this row, there is another value that stands out. The rest of the ratios show that between about 85% and 95% of the output vertices have reliable, estimated accuracy, whereas this ratio is only 56% in the case of dataset 37EZ1 (*Rotterdam Ketheltunnel*). This is the combined result of two factors: as the name implies, this dataset also contains a tunnel. But, as Table 4.1 mentions, the [AHN3](#) data pre-dates the completion of the tunnel and the surrounding parts of the motorway, and as a result, part of the output is corrupted. Already during preliminary elevation estimation, the standard deviations are a magnitude larger than those encountered in other locations, because the construction works do not represent a smooth surface. In the Lidar segmentation step, the roads are split into many small [NBRS](#) parts, with much of the road thereby becoming flagged for linear interpolation. As a result, many of the [NWB](#) vertices' accuracy will be deemed unknown. This issue could be resolved in this case, if the large standard deviation in the preliminary elevation estimation triggered an alternative workflow in which only the support dataset is used in the region in which the primary data is unreliable. Developing and implementing such a workflow was not part of this research, hence it is further discussed in Section 5.7 in the context of recommended future work.

The values in the bottom row of the table are sometimes slightly lower than I would have expected. For instance 85% for the 37HN2 (*Knooppunt Ridderkerk*) dataset seemed to me to be too low, because almost all gaps have good [DTB](#) coverage, and [NWB](#) almost never misses the [TINs](#). The reason why this value is lower than expected is because there are many [AHN3](#) data gaps, and the point density in the [DTB](#)-defined parts of the [TINs](#) appears to consistently miss the minimum above which the vertices would be deemed accurate. The process also appears to sometimes filter out vertices that were interpolated in locations where although [DTB](#) was "sparse", it still managed to characterise the road surface quite well. This further suggests that it would be better if the decisions regarding where to trust [DTB](#) were not based on the same type of evaluation as [AHN3](#), and were instead based on the geometric layout of the [DTB](#) lines. While this would indeed improve the accuracy assessment results, it would also mean that the procedure would become specialised to [DTB](#), and would not work with other types of support datasets. This is elaborated in more detail in Section 5.7.

Some of the [NWB](#) centrelines overshoot the Lidar testing tile extents by up to 20-50 metres. These were left in some of the testing tiles deliberately, to test certain aspects of the behaviour of the algorithms (as also mentioned in Section 4.1). These can further decrease the accurate vertex ratios by about 2-4% artificially. The overshoots are visible in Figure 4.1.

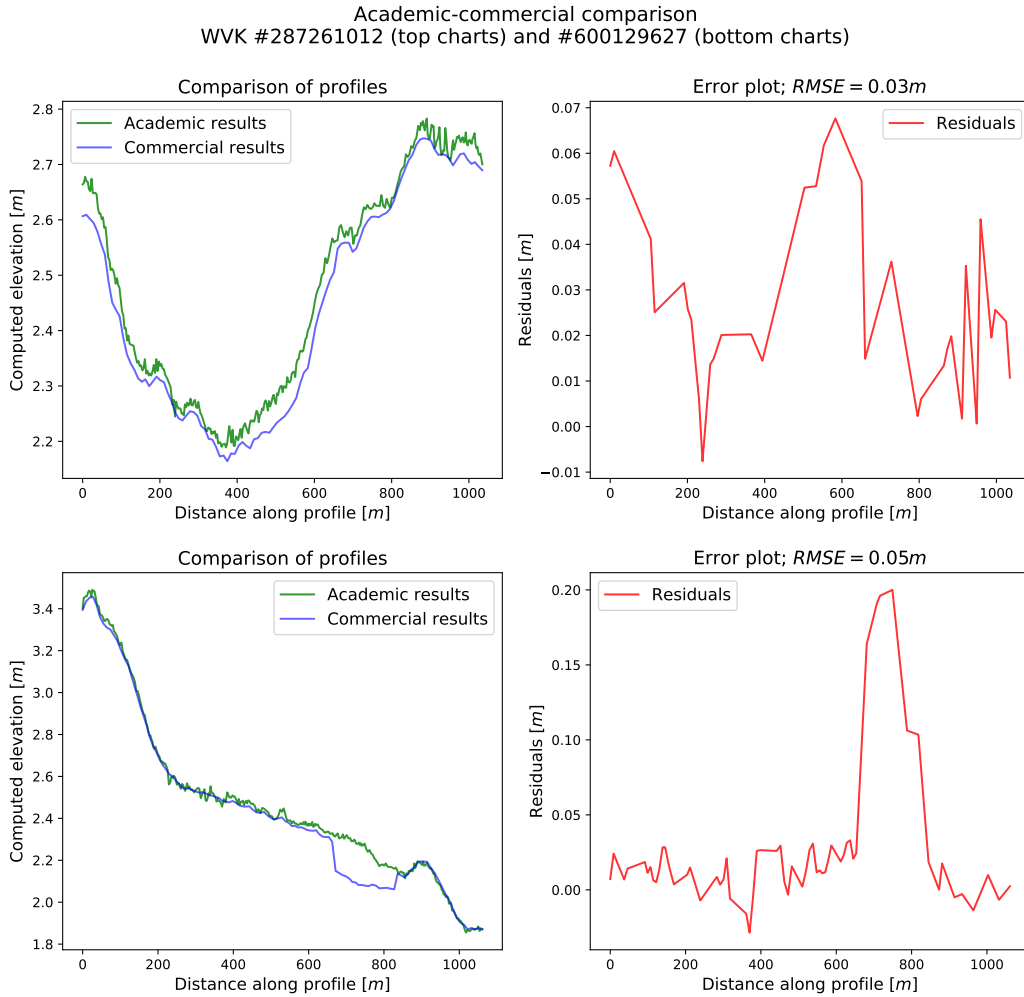


**Figure 4.21:** Charts comparing the academic and commercial results using two *wegvakken* from *Knooppunt Deil*.

## 4.4 Comparison with commercial implementation

Like in the accuracy assessment above, I picked some specific *wegvakken* that are particularly representative of the overall results of this comparison. However, here I did not restrict the selection to be from the *Knooppunt Deil* dataset, because the results are very different across my set of testing datasets. Where the agreement is good, the two sets of results can be similar to a degree where it is difficult to tell them apart in a 3D visualisation, unless the Z axis is grossly exaggerated. Examining the correspondence on 2D charts (see Figures 4.21, 4.22 and 4.23) works far better in terms of characterising the nature of both the small-scale and large-scale differences that are typically observed when comparing the two datasets. For this reason, I opted to show only 2D visualisations in this section. I also present tabulated mean RMSE values for all testing datasets in Section 4.4.2.

### 4.4.1 Representative example comparisons

#### Knooppunt Deil

The top chart in Figure 4.21 shows a LineString (*wegvak*) in which the RMSE between the two datasets is only 3 cm. The *Knooppunt Deil* dataset, from where these LineStrings in this figure were taken, shows

## 4 Results

exceptionally good agreement between the results and a 3 to 5 cm RMSE can be regarded as typical everywhere in it. Such a small disagreement could be deemed unimportant, unless systematic - however, in this case there appears to be a small systematic component to it. Notably my results seem to consistently estimate higher elevations for the roads than the commercial ones here. The reason for the systematic nature of these differences is that this LineString represents a motorway, and the commercial implementation always takes motorway elevations from DTB where it has coverage. My implementation does the opposite; it prioritises AHN3. As a result, the systematic differences between DTB and AHN3 are manifested in these 2D profiles. This is further illustrated by the residuals dropping to almost zero in one place at around 220 metres along the profile, and then for about 50 metres starting at 800 metres along the profile. Here, the chosen *wegvak* passes underneath bridges, hence my implementation also used DTB here - thereby triggering near-perfect agreement with the commercial results. Since the absolute value of these systematic differences is minuscule in this location, it can be regarded as unimportant.

In this particular dataset, the agreement between the two datasets is almost always this good - the one exception I found is shown in the bottom charts in Figure 4.21. The difference represents a roughly 20-centimetre erratic drop in elevation in the commercial results. I could not explain this blunder by looking at the input data, hence it must have been introduced by the commercial processing pipeline. The error is large enough to break compliance with the 20-centimetre accuracy requirement of NDW, but it is an isolated issue - I have not found other examples of it.

### Gorinchem

Both *wegvakken* in Figure 4.22 were taken from *provincial* roads in the *Gorinchem* dataset. The top two charts were generated from a LineString that is situated in a well-exposed area, free of occlusions. While the RMSE is extremely low - as in the previous figure - we may notice that here a systematic deviation can also *not* be observed at all. This is because the commercial implementation uses AHN3 *rasters* to interpolate elevations. Although this does not affect the RMSE, it is evident from this chart that the commercial results are less detailed than the academic ones. This is simply the result of the academic results using 10-metre vertex densification, whereas my final results were generated using 5-metre vertex densification. Both result in much denser elevation profiles than the original NWB vertices would allow, which is the sampling density that the residual plots reflect.

While it might first appear to the reader that the agreement for provincial roads is even better than that for motorways, this is in fact not the case. The commercial solution has no feature implemented to intelligently switch between AHN3 and DTB, and also lacks a set of features that could enable it to handle occlusion correctly in the absence of DTB. I illustrate both of these limitations in the bottom two charts in Figure 4.22. Between about 330 and 420 metres along the profile, the commercial results show a sudden elevation increase, while the academic ones show a (much smaller) abrupt change in the opposite direction. Everywhere else in the *wegvak*, the agreement is at least as good as in the top chart.

This artefact is created by the combination of the above missing features in the commercial software. At this location, the provincial road from which the *wegvak* is taken, passes underneath a series of bridges. At this location, the AHN3 rasters simply record the elevation of the surfaces *on* these bridges, hence this is what appears in the commercial outputs. This represents an approximately 5 m systematic overestimation of elevations over just under a 100 metres of distance along this road. My results, on the other hand, underestimate the elevations in this zone by about 30 to 40 centimetres. This is not an issue with the academic methods or implementation, it is due to DTB being outdated locally. For this particular set of provincial roads, DTB exists because of their proximity to motorways - in general, provincial roads do not have DTB coverage. My implementation recognised the presence of DTB lines, and made use of them.

The DTB data was close enough to the predicted elevation of the road for my implementation to deem it reliable. However, inspecting them on this 2D elevation profile reveals that DTB is, locally, itself underestimating the elevation of the road. This can be explained by the temporal difference between AHN3 and DTB locally. Had there been accurate support data available, my implementation would have produced correct results - and even in the absence of support data, it would have interpolated linearly across the

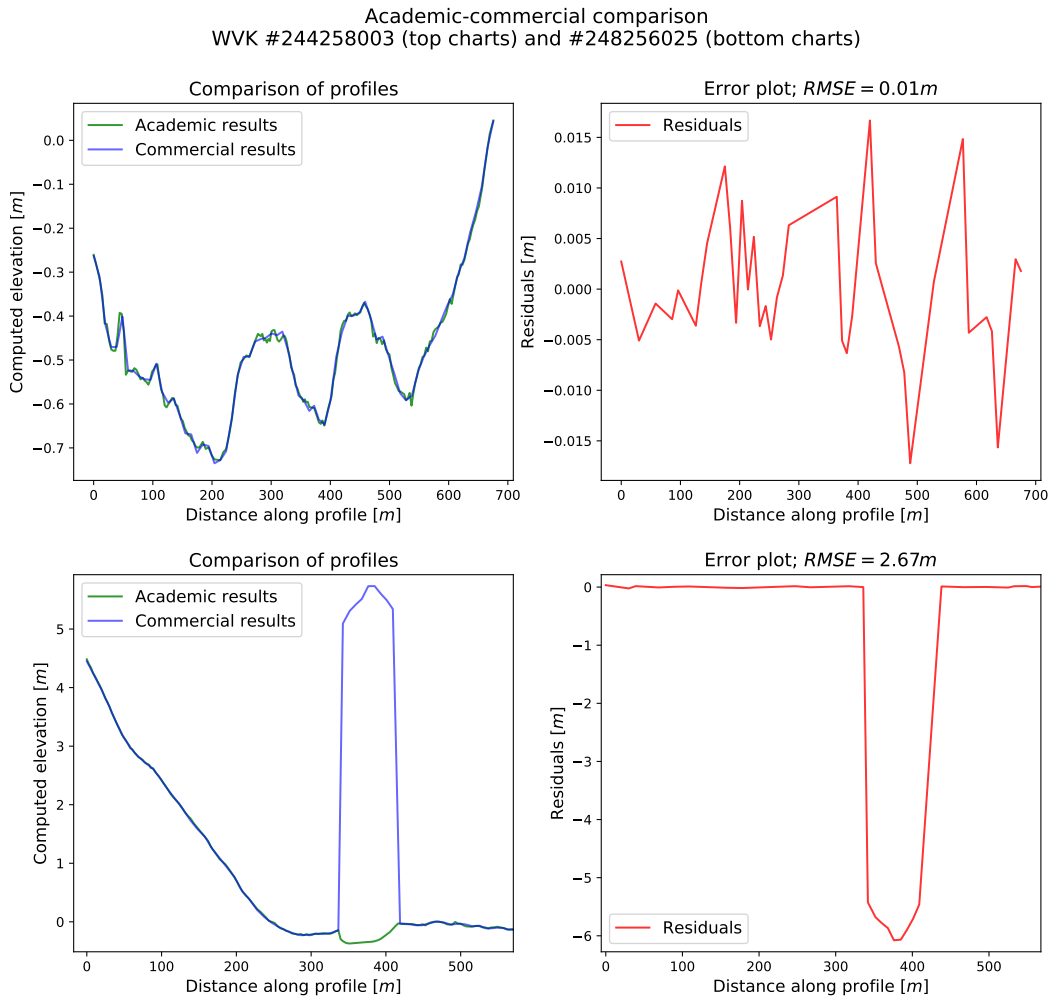


**Figure 4.22:** Charts comparing the academic and commercial results using two *wegvakken* from dataset *Gorinchem*.

region, which still represents a better solution than including the outliers the way the commercial results do.

### Knooppunt Ridderkerk

Figure 4.23 shows motorway *wegvakken* taken from the *Knooppunt Ridderkerk* dataset. The reader might recall that I used this dataset as an example of where the temporal differences between [DTB](#) and [AHN3](#) give rise to significant disagreements between the road elevations they contain. This last comparison figure serves to illustrate that this gives rise to significant differences between the commercial and academic results.

The outdated elevations in [DTB](#) are the only ones considered by the commercial implementation, which results in elevations being consistently overestimated by up to half a metre relative to [AHN3](#), and therefore also my results. Good agreement between the two sets of results only emerges where my implementation also resorted to using [DTB](#), because [AHN3](#) was missing locally. This is the same phenomenon that caused the small, systematic deviations in Figure 4.21, the only difference is that [DTB](#) is more affected by the temporal issues here, than there.

## 4 Results

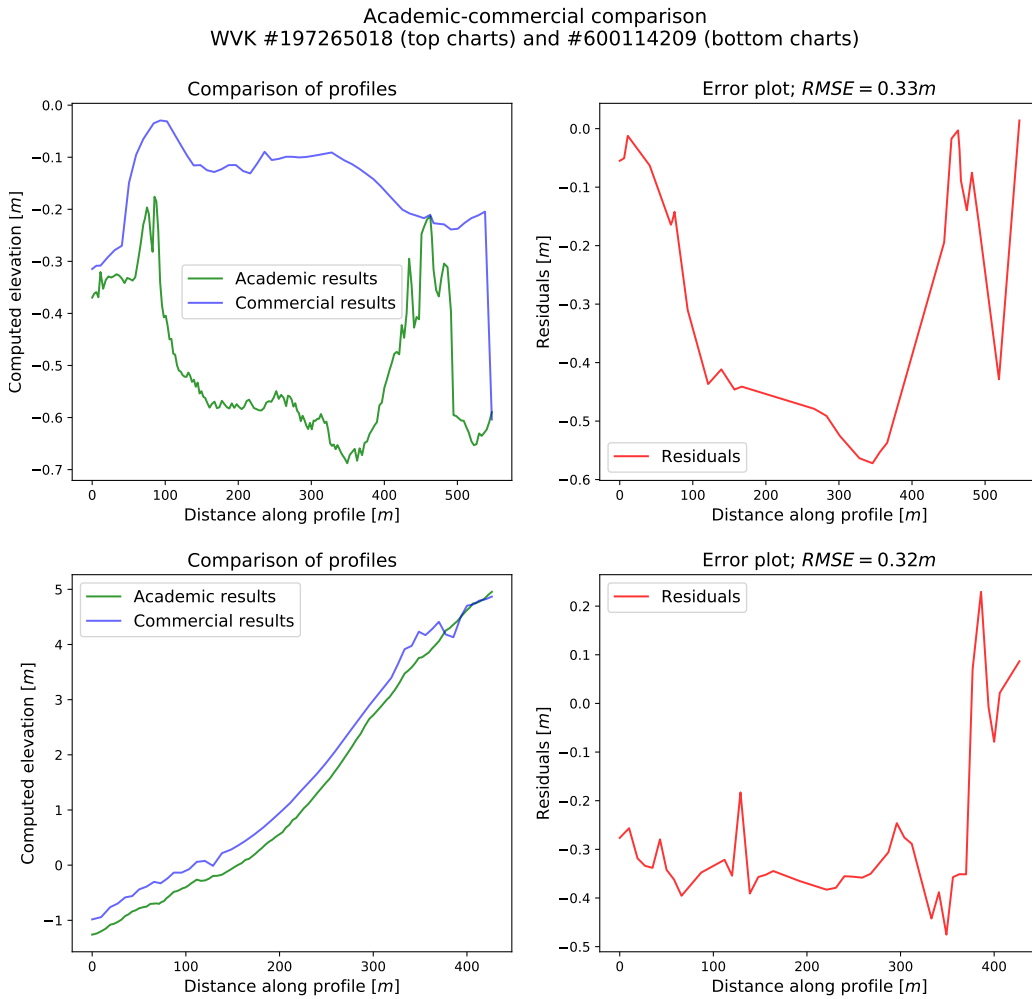


**Figure 4.23:** Charts comparing the academic and commercial results using two *wegvakken* from dataset *Knooppunt Ridderkerk*.

This demonstrates the flaws in [NDW](#)'s unconditional assumption that [DTB](#) is more accurate spatially and temporally than [AHN3](#), especially from a temporal updates perspective. They specifically opted to prioritise its use as it is updated far more frequently than [AHN3](#). However, this assumption likely did not consider the fact that the updates only concern roads that underwent refurbishment, upgrades or other modifications, and roads that were newly built. Otherwise, the position of [DTB](#)'s line features is *not* re-measured regularly, as I also mentioned in Section 2.3.3. These outdated elevations represent a further disparity between the noise regulations' requirements and the commercial implementation, and they affect the results in the *Knooppunt Ridderkerk* area significantly.

### Summary of detailed comparison

It appears that relative to the commercial implementation, there is a clear set of areas where the academic solution performs better. Notably, these are the smarter use of the available input data, and the better handling of occlusion. We may also add to this a better evaluation and quantification of output accuracy, as proof of such an analysis (or at least the assumptions made that justified omitting such an analysis) is missing from their results.

There is an area, however, in which the relationship is reversed: the commercial implementation can

	20BN1	25BZ2	25DN2	32BN1	32FZ2	32HZ2	33CN2	37EZ1	37HN2	38GZ1	39CZ1
AHN3	0.0081	1.5511	0.0385	0.0153	0.0787	0.0175	0.0087	1.7223	0.3426	0.7589	0.0693
DTB	-	-	0.0480	-	0.0383	-	-	1.9509	0.6170	4.3681	0.0150
L.I.	0.0108	7.0921	3.3205	0.0692	0.2635	1.1244	0.3528	2.7504	0.7173	0.3036	0.1634

L.I. stands for linear interpolation.

**Table 4.3:** Tabulated academic and commercial 3D-NWB similarity quantification results. .

be run on the whole country, using a user-friendly graphical user interface ([GUI](#)), and with a far lower computational complexity than that of the academic implementation. In fact, I needed to extract the LineStrings for this comparison from the official, country-wide 3D-NWB release that was generated using the commercial implementation.

This is a manifestation of the main difference between the two solutions' paradigms of an ideal implementation: the commercial project focused on developing a straightforward solution that works reliably out-of-the-box, even if corners need to be cut to achieve this and the results sometimes do not comply with the official requirements. On the other hand the academic project focused on exploring how various scientific approaches can be put to use in such a practical problem, and on scientific correctness and accuracy.

#### 4.4.2 Tabulated RMSE values

In the section above, I discussed detailed comparisons between my results and the commercial results, on the level of specific LineStrings. In addition to this, in the present section I present and discuss tabulated, aggregated comparison values to provide an overview of the similarity between the two sets of results on the level of testing datasets.

Table 4.3 shows the results of quantifying the similarity between the academic and commercial [NWB](#) 3D-conversions. It contains [RMSE](#) values for each testing dataset, computed based on the residuals between the elevations estimated by the two methods for the same original [NWB](#) vertices.

I looked up the commercial counterpart of each elevation I computed for original (non-densified) [NWB](#) vertices, and subtracted it from my results to obtain the residuals. Before computing the [RMSE](#) values, I separated the residuals into three groups based on which of the three possible origins is associated with the given vertex in the academic results: [AHN3](#), [DTB](#) and linear interpolation. The relevant classification rules are elaborated in 3.3.7. I expected the comparison to yield vastly different results for the three groups, because of the known conceptual differences between the two implementations, and also because the detailed comparison above (in Section 4.4.1) already indicated this.

Unlike in Table 4.2, clear trends cannot be observed in the data. There appears to be some scatter in all rows and columns. This is connected to the observation mentioned in the detailed comparison, that similarity is a factor of both the particular location in question, and the source of the data ([AHN3](#), [DTB](#) or simple linear interpolation). I will present examples based on the table above, to illustrate this.

Dataset 39CZ1 (*Knooppunt Deil*) generally shows good agreement between the two sets of outputs, with the [RMSE](#) metric not exceeding 20 cm in either of the three "classes". As I mentioned above, this is because at this particular location, [NWB](#) is comprised of [R-roads](#) only, the completeness of [DTB](#) is good, and [DTB](#) and [AHN3](#) are in good agreement. The extremely low [RMSE](#) in the case of the [DTB](#)-sourced academic elevations (only 1,5 cm) can be explained by both implementations relying on the exact same road surface elevation measurements locally.

In the case of 38GZ1 (*Gorinchem*), the middle value ([DTB](#)-based similarity) is equally simple to explain - the commercial methods were not aware of the presence of [DTB](#) data for provincial roads, and thus grossly overestimated road elevations in regions of occlusion. The [AHN3](#)-based [RMSE](#) of 0.75 m is because the dataset also contains [R-roads](#) where the [DTB](#) data is outdated (most of it is from 2004), and is consistently at lower elevations than [AHN3](#). In both cases, it is the academic results that show elevations that are closer to reality, considering that they are much more recent.

## 4 Results

The dataset 25BZ2 (*Amsterdam Hemhavens*) contains the largest tunnel among my datasets, and one which has no **DTB** coverage. As a result, the academic implementation interpolates linearly across the gap, resulting in the output containing an elevation profile close to the ground and water level above the tunnel. This is what gives rise to the 7 m **RMSE** in the table. The commercial results contain the correct, V-shaped elevation profile of the subterranean road - the explanation of this difference is simple: the commercial implementation considers a certain type of **DTB** line feature (*lijnverlichting* - road surface illumination) as reliable road surface measurements. My implementation filters these out, as I found examples of this line feature not lying flat on the road surfaces in other locations. In any case, including them in my results is a matter of adding this keyword to a variable in my code. The large **AHN3 RMSE** in this dataset is also due to the tunnel; my implementation erratically identifies Lidar points describing the tunnel service structure as a continuation of the road, and uses it in the elevation interpolation step.

In 25DN2 (*Amsterdam Zuid*), The agreement between the datasets is generally very good (as the **AHN3** and **DTB** values indicate), but the linear interpolation agreement is anomalously poor. This is the result of a single *wegvak*, which contains a medium-length tunnel. This tunnel contains good **DTB** coverage which my implementation correctly identifies and uses during the Lidar segmentation step, but which it then fails to make use of when constructing the preliminary edges, breaking off the edge geometry at the tunnel entrance. As I mentioned in Section 3.3.4, this is because preliminary edge detection will mostly fail to construct cross-sections where only **DTB** is available, which will result in no **TINs** being constructed locally, if there is a bend in the road in the occluded area, or if the given LineString ends there. The particular LineString in question falls into both categories, as it contains a bending road in a tunnel that ends roughly in the same place as the LineString itself does. Fixing this issue falls into the category of future work, as it did not fit into the timeframe reserved for this research.

The results in 32HZ2 (*Apeldoornseweg*) are interesting because the dataset contains tightly packed, thin, parallel provincial roads (no **DTB** coverage) in an old-growth forest that often completely covers the sky above the roads. This decreases the mean **TIN** vertex density to 14 points per m<sup>2</sup>, often dropping below 10 in the most densely vegetated areas. In this case, my attention was piqued not by a disagreement between the datasets, but near-perfect agreement. Of course, both sets of results rely on **AHN3** here, but the commercial ones used **AHN3** rasters, rather than Lidar points. The similarity is likely to indicate that the raster-based **AHN3** terrain model is very accurate in this area, despite the forest. The only (minor) artefacts - affecting both the academic and commercial results - are due to **NWB** sometimes missing the real centrelines by a significant margin, veering off into ditches and other sharp terrain features. The 1 m **RMSE** seen for linear interpolation in this dataset are due to the **NWB** centrelines often extending beyond the corresponding clipped point clouds, which I had already discussed in terms of the accurate vertex ratios, i.e. it is artificial and meaningless in the context of this comparison.

Lastly, all three **RMSE** values computed for 37EZ1 (*Rotterdam Ketheltunnel*) are anomalously high due to the tunnel construction works. The large **RMSE** values for **AHN3**-based and linear interpolation are easy to explain: both the small **TINs** that are constructed inside the construction areas, as well as the linear interpolation between them (where no **TINs** exist) are expected to be very inaccurate, and certainly different from the commercial results which rely on **DTB** here. **DTB** has already been updated with line geometries that correspond to the new "version" of the motorway. Hence the commercial implementation's single-minded goal to reflect **DTB** in its output prevails in this case. However, it is unexpected that even where my implementation also uses **DTB**, noticeable disagreement is still observed: an **RMSE** of 2 m. The reason for this is, based on a visual inspection of the results, that the confusing elevations shown by **AHN3** often result in the preliminary elevations matching the elevation of *unrelated* **DTB** lines, causing them to thus be added to subclouds in the Lidar segmentation step. The occasional use of such vastly incorrect **DTB** elevations corrupts the overall **RMSE**, which is what we see in the table.

In the context of the above paragraph, it is important to note that while **DTB** certainly is superior to **AHN3** in this particular location, its quality and completeness are still far from perfect. For instance, the *lijnverlichting* features (and various others) are still from the *old* version of the road, the one that used to run on the surface rather than in a tunnel. Furthermore, **DTB** is incomplete in this location, which prompted the commercial implementation to use **AHN3** rasters in certain places, especially on the ramps. Due to this, it still produced some artefacts much like the ones generated by the academic implementation.

# 5 Conclusions

In this chapter, I present an evaluation of my results in the context of the original aims of this research, and specifically, the research questions. Rather than to follow the report structure that I used in the previous two chapters (3, 4), here I will present overviews independent of the pipeline steps. The following sections are based on an integrated understanding of the problem and relevant literature, of the results of my solution, and the accuracy and quality assessment thereof.

Our original summary research question was "*How can we achieve a 3D conversion of the NWB dataset using Dutch open geospatial data and a primarily 2.5D-based surface modelling methodology, while guaranteeing optimal and quantifiable accuracy and completeness?*". I explored one possible way of performing such a conversion, which intuitively followed from the methods of relevant work, knowledge acquired during my geomatics education, and the main type of elevation measurements we used - [ALS](#). The exploration of these topics necessitated designing a processing pipeline and implementing it. The pipeline produces accurate 2.5D road surface models, and uses these to perform the 3D conversion of [NWB](#). The evolution of the data through this pipeline is comprehensively documented in the previous chapters of the present report, as well as the results of accuracy and quality assessment procedures.

Based on these, we may conclude that the process and the results of this research represent a fulfillment of its original aims as recorded by the research questions. Most planned topics were examined in detail, the system design and implementation were completed and the accuracy and quality assessment verified our results.

At the same time, it is important to note that this is only one possible avenue of producing a 3D version of [NWB](#), as illustrated by, for instance, the commercial results which use a different set of methods to generate comparable output data. While I managed to develop a working solution to the problem, it is by no means the *only* possible solution. It is merely the solution I found to be most fitting to our research questions (primarily academic, "pragmatic" only secondarily), the available tools and datasets, as well as the designated project timeframe.

In the sections below, I will present conclusive remarks regarding various aspects of the research. Some of these are based on specific research questions, which I indicated in their first paragraphs. These sections tackle the conclusive evaluation of both the processing pipeline and the results produced by it. At the end of the chapter, two final sections are found, providing summary conclusions (Section 5.6) and recommendations in terms of potential future work (Section 5.7).

## 5.1 Usefulness and generality of datasets

This section provides conclusions regarding the research questions "*How can the academic methods best make use of the combined information content of the datasets that the commercial implementation uses?*", "*What is the accuracy of our input elevation data sources? Can we structure the pipeline in a way that their input accuracy can be propagated to the output in a straightforward manner?*" and "*While solving NDW's specific problem, can we also ensure that our solution generalises well to other problems of a similar type?*". In addition, it contains further conclusive remarks related directly to the input data used in this research but not specifically related to these questions.

### 5.1.1 General remarks about AHN3 and DTB

We set out to use Dutch geospatial open data in this project, and succeeded in doing so. I made use of no data that is not available to the general public, facilitating the easy reproducibility and reusability of my results - which was part of the reason why I restricted my attention to such datasets in the first place. This also ensured that we build on exactly the same input data that the commercial implementation does, apart from the one difference of using point cloud data directly rather than via derived DTM rasters - although this appeared to make little difference in practice, judging by the comparison of our results with theirs.

Using AHN3 and DTB is also favourable in the sense that we may generalise their identities into a "primary dataset" and a "support dataset" respectively, the former with a nearly complete ALS coverage of the road surfaces, and the latter with accurate surface elevation measurements with coverage in the few places where there are gaps in the primary data. We may conclude that in terms of the necessary input data, my solution is quite versatile and general. Any large-scale datasets with a point cloud structure (be it Lidar data or orthoimagery-derived data for instance) could serve as the primary dataset, and any type of surface measurement data with areal coverage of road surfaces could serve as the support data (for instance, multiple GNSS-vehicle tracks for each road).

### 5.1.2 On the impact of input quality

In terms of the second research question above, my conclusion is that the accuracy of both input datasets is documented in their user manuals, which I successfully propagated through the interpolator to compute the formal output accuracy. However, it is worth noting that both datasets contain very basic accuracy information, i.e. a single vertical and horizontal accuracy value. While this is sufficiently detailed for most purposes typically concerned with using these datasets, in our case point-level information could be beneficial. The accuracy assessment steps could easily take vertex-level accuracy information into account.

This brings us to the wider topic of local accuracy quantification. While some such descriptors can be measured (such as the local sampling density), others, such as local ground filtering effectiveness or general classification accuracy cannot be determined with any certainty by users of the data. The concept of temporal accuracy is also relevant to these datasets and not explored by their providers; for instance the specifications of DTB suggest that the underlying linear road features have a vertical standard deviations of 5 cm, while I observed up to 1 m deviations from the present-day elevation of these roads.

Where the datasets indeed comply with their specifications, they make for a very good basis for my analysis, but not elsewhere. I found that on road surfaces, AHN3 almost always complies perfectly (even exceeds) the accuracy and sampling density suggested by its specifications, whereas DTB does not generally appear reliable in this sense. A large amount of the elevations contained by it are questionable due to their age, and its coverage is also far from optimal. This leads me to conclude that for my procedures to work with a better efficiency, a better support dataset is needed, preferably MLS data of the roads specifically where AHN3 is suspected to have little or no coverage. Both my results and the commercial results suffer from these third-party quality issues.

With this being said, both datasets were found to be useful for the pipeline, and especially for the analysis itself. Without DTB, I could not have created the dual primary-support input model and the associated pipeline workflows. Furthermore, even at the relatively poor quality that DTB represents now, it helps the procedure greatly where it *has* coverage. For instance, the processing of complex motorway junctions (such as *Knooppunt Ridderkerk*) would not have been possible with such effectiveness without relying on DTB to navigate across the gaps of coverage resulting from bridge-related occlusion, even if the elevations it contains are not entirely correct locally.

## 5.2 Effectiveness of processing steps

This section is based in part on the research questions "How should the road network be subdivided into parts that each represent a 2.5D problem?", "As we are using Lidar data, can we produce an accurate and complete TIN surface model for each 2.5D "unit"? Can we interpolate elevations for NWB through this model?", "Can the implementation be made robust enough to handle all (or most) challenging road layouts correctly, such as complex motorway junctions?" and "How can we make the implementation perform well in areas where input elevation data is scarce or missing over longer distances, such as in tunnels?". It also presents conclusions that are more general, regarding the overall effectiveness of my processing pipeline.

### 5.2.1 Decomposing the 3D problem into 2.5D sub-problems

My implementation followed, for the most part, the original plans I set out in the P2 document. Significant modifications were required only due to the unsatisfactory results of active contour optimisation, which I will describe in a separate section below in more depth.

The pipeline and its implementation adhered to our primary aim of decomposing the Dutch road network into segments which can be modelled via 2.5D methods. The NBRS (and NBRS parts on a lower level) represent the results of this "segmentation" - they are guaranteed never to violate the 2.5D assumption to a significant degree. As a result, all intermediate results of the pipeline - be it preliminary elevations or edges - will be concerned with modelling 2D elevation series and 2.5D surfaces of road surfaces that we can reasonably assume to be *mathematical surfaces*. This underpins the success of the TIN generation step, as without succeeding in this regard, it would have been impossible to generate TINs that behave correctly where occlusion occurs. This in turns also defines the effectiveness of the 3D conversion of NWB, as it relies on these TINs.

We may thus conclude that the divide-and-conquer approach to reduce the 3D problem into 2.5D sub-problems succeeded, and based on the quality and accuracy assessment, any remaining small-scale issues could be resolved by adjusting the parametrisation and making small revisions to the methods and the implementation. I encountered no problems that would have put into question the plausibility of employing this approach, in fact I found it intuitive to work with. Furthermore, based on the experience I gained during the development, this approach allows the computational complexity of the software to be reduced, and the generation of *independent* problems in the process also means that theoretically, it would be straightforward to convert the implementation to use parallel processing. From the creation of each NBRS up to the point where snapping takes place in the last interpolation step, they are processed independently. This can be regarded as the foundations on which a low-level scaling implementation could be built on (rather than a top-level one, e.g. one simply tiling the input data). Hence, we may conclude that we have also found at least a partial answer to the research question "Can [the NBRS] be processed individually to facilitate easy parallel processing?".

Owing to the general success of the approach, merging these independent results into a single 3D-NWB output was also far less challenging than originally suspected. Wherever the program managed to identify the correct approximate shape of roads early on and to carry this all the way into the TIN construction step, the TINs themselves became almost identical in intersections, meaning that snapping typically concerned moving end-vertices only by a few centimetres. This is in sharp contrast with my original suspicion that this would be a complex task. Hence a conclusive answer and practical solution was also found for the research question "How do we "stitch" the results of the individual 2.5D procedures back together into a 3D road network with the correct topology?".

### 5.2.2 Surface modelling effectiveness

The effectiveness with which surface models are being generated was comprehensively discussed in the Results chapter, hence here I will only present brief conclusive remarks. My work demonstrated that the TIN initialisation-extension procedure is capable of constructing accurate surfaces under most circumstances. We may conclusively remark that almost all the resulting TIN models lack outliers on

## 5 Conclusions

road surfaces, save for the relatively rare occasion of [NWB](#) getting very close to road edges or leaving the road surfaces altogether. This issue is not related to our methods or implementation, and [NDW](#) is already working on fixing it.

The fitted road surfaces are therefore smooth on the large scale. They are also almost as detailed as the underlying Lidar subclouds, meaning that most input information is piped directly into the models. In the accuracy assessment step, I discovered that the small-scale noise in the models is indicative of a significant degree of oversampling. The road surfaces are simple geometrically in the context of terrain in general, hence the high point densities (between 10 and 30 points per m<sup>2</sup> even after thinning by a factor of 2) seen in the [TINs](#) are not truly necessary.

The completeness of the generated surfaces is generally good, but not perfect. Due to the combined limitations of my preliminary edge detection and [TIN](#) construction methods, the [TINs](#) may not fully cover the paved surfaces, and in rare cases (motorways with 2+ lanes) also not the entire *traffic-occupied* road surface. For the ultimate aim of using these models to convert [NWB](#) into a 3D dataset, this is irrelevant because under normal circumstances, it will still be possible to interpolate at [NWB](#) vertices in the [TINs](#). Our original, academic aim of exploring the possibility of producing 3D road models in addition to 3D-[NWB](#) output was conclusively satisfied regardless, and it is my suspicion that by refining my methods, the average completeness of my road models could be improved from the current 75% relative to [BGT](#) road polygons.

This part of my research proved that it is possible to not only produce 2D elevation profiles for the underlying roads, but to increase the dimensionality to a surface-modelling level without having to rely on additional data relative to the commercial implementation. The most important question I found is that one either constructs edges that can be definitively assumed to contain most of the road surface reflections, or one needs to algorithmically grow the surface beyond the initial estimates of the edge locations. Having been unable to attain an edge quality where such growing is unnecessary, my implementation relies on the latter approach.

The downside of this method is that the generated [TINs](#) will often have rugged edges, depending mainly on the physical characteristics of the road's edges and their surroundings. In other words, the models may occasionally overestimate or underestimate the road extents. An ability to produce better edge estimates (with or without active contour optimisation) would have allowed the [TIN](#) construction step to have a better indication of where it should expect to find the road edges (or to omit a growing-type algorithm altogether), whereas in my current implementation needs to look *beyond* the edge estimates.

In terms of complex road layouts, we can assert that the [TINs](#) are as accurate as possible. In places where only [DTB](#) is available, the [TINs](#) shrink in width and become sparsely sampled, but this is expected given the nature of [DTB](#). The continuation of the [TINs](#) across these regions ensures that 3D-[NWB](#) elevations can be interpolated there the same way as elsewhere. Where [DTB](#) is also missing, the [TINs](#) become split into parts, each belonging to a segment of the [NBRS](#) with continuous [AHN3](#) coverage, and with properties identical to that which I described above. In tunnels, the existence of the [TINs](#) depends on the existence of [DTB](#) and the shape of the road. Depending on these factors, the program may or may not succeed in extending the preliminary edges into the tunnels, which in turn decides whether the [TINs](#) will exist there or not. More information on this topic is found in the next section.

We may conclude that this research proved that even in the lack of accurate edge estimates, [TINs](#) with reasonably good quality can be constructed. Proposed further improvements to the relevant pipeline steps may be found in the Future work section below.

### 5.2.3 NWB 3D-conversion effectiveness

There are many parts of my processing pipeline that are specifically aimed at characterising the shapes of the road surfaces and their boundaries well in the 2.5D models, and this is primarily where some issues were encountered. The 3D conversion of [NWB](#) was not affected by them.

The output elevation series lie flat on the [TIN](#) surfaces, and their overall visual quality is exceptionally good. In particular, spikes and other types of sudden outliers are absent from just about everywhere in

the output. The outputs offer 100% completion in the sense that linear interpolation is used to fill in all gaps. The snapping procedure almost never fails either, [NBRS](#) are all properly connected geometrically. The output therefore generally preserves (and even improves) the input's geometric connectedness.

The conversion effectiveness remains unchanged in the presence of both partial and complete occlusion where they occur over short distances. Weak occlusion (e.g. due to vegetation) does not decrease [AHN3](#)'s sampling density below the level from where noticeable problems in any part of the implementation would arise, up to an input thinning factor of about 4. In the case of occlusion due to opaque objects (such as where roads pass above and below one another in large junctions), the results are also not significantly affected as long as [DTB](#) exists locally. The exception to this rule is where [DTB](#) exists and is outdated, because this introduces noticeable jumps or drops in elevation. Even in the absence of [DTB](#), small data gaps generally do not represent a problem because linear interpolation is suitable to approximate elevations across them (affecting only the output accuracy), and because the [NBRS](#) splitting workflow ensures that they do not cause problems with any of the modelling steps.

The effectiveness of the conversion mechanism is only low where [AHN3](#) coverage is missing for longer distances, such as in long tunnels. If no [DTB](#) coverage is encountered, then the [NBRS](#) will be split into parts, and the distance in-between will be interpolated linearly. Such elevation series will be far from reality, but this behaviour is expected - the program cannot "predict" elevations where it has no data available. Due to certain limitations of treating [DTB](#) as a point cloud, even in tunnels where it has coverage, the preliminary edge detection algorithm will not always succeed in drawing edges all along the tunnel-based parts of roads, resulting in the same issue.

We may conclude that the overall effectiveness of the 3D conversion of [NWB](#) is exceptionally good, apart from the tunnel-related issue. To solve it, the preliminary edge estimation step of the pipeline would either need to be modified to work better with the specific vector geometry of [DTB](#), or [DTB](#) would need to be replaced with better support data (preferably, [MLS](#) data) with which the current methods would work also in tunnels, automatically.

## 5.3 Accuracy-related conclusions

### 5.4 Accuracy assessment conclusions

I set out to develop a means of performing the practical aims of this project in a way that allows output accuracy to be quantified in a straightforward manner. This is reflected by the main research question, as well as sub-questions such as *What is the effect of uncertainty in the lateral positions of [NWB](#) centrelines on the effectiveness of our methods, and on the output accuracy?* and [...] can we derive our output directly from input data points, despite the large number of processing steps that are potentially necessary? and *How good is the agreement between the commercial and the academic results? What physical features or sensing issues do disagreement between the results correspond to?*, as well as all the rest of the questions in the second half of the list in Section 1.4.

As the work I presented in the literature review (Section 2.2) and accuracy assessment methods and results sections (3.4 and 4.3, respectively) demonstrates, I examined this topic in-depth throughout the research. Below, I will present concluding remarks distilled from Section 4.3 in the previous chapter.

In terms of a preliminary evaluation of confidence in my results (prior to the accuracy assessment step), I classified the origin of all output elevations based on which input dataset was used in their generation. This classification is based on the [TIN](#) triangle in which they were interpolated. When the triangle was comprised of vertices sourced from a mixture of [AHN3](#) and [DTB](#) data, treated it as originating from [DTB](#) for simplicity, and because [DTB](#) is less reliable than [AHN3](#). Elevations not acquired via TIN-linear interpolation but through simple linear interpolation represent the third category, in addition to [AHN3](#) and [DTB](#). It is only the vertices marked as originating from [AHN3](#) that can be fully trusted. I recommend treating elevations derived from [DTB](#) and via linear interpolation as unreliable, due to the problems with the underlying data and the method's uncertainty, respectively. Only if visual inspection confirms their correctness locally, can they be trusted.

## 5 Conclusions

Through an attempt at estimating output accuracy empirically, I found that with the particular datasets, and surface types and geographical locations concerned by this research, ground filtering imperfection, surface ruggedness and sampling density can be assumed to have zero influence on output accuracy. This also assumes that local sampling density is higher than the minimum density below which it would start to have an impact on output accuracy, which does not hold everywhere and which is therefore measured and detected by my accuracy assessment workflow. This part of the assessment also yielded typical sampling density values in the final TINs as typically falling between 10 to 30 points in places that are not occluded by objects that are entirely opaque to Lidar.

Thus, my analysis considered the formal output accuracy to be a function of only error propagation through the interpolation technique above the sampling threshold mentioned above, and found that in such places vertical output error was almost always about 5.3 cm, so 10.6 cm at 95% certainty. The smallness of this value is explained by the fact that accuracy is expected to increase due to using 3 samples for each interpolation rather than just one, in triangles which are not significantly inclined - which is always the case with our TIN triangles.

In places where sampling density dropped below the threshold and where linear interpolation was used (zero sampling density assumed), I classified the output accuracy as "undetermined" to indicate that these values have little to no evidence to support their correctness. In testing datasets without large-scale problems (due to tunnels or construction works), this affected about 15 to 5% of the output elevations. These values are likely to be slightly exaggerated by DTB's sampling "density" often not being high enough to be included in the accuracy assessment, which is not a meaningful metric because it depends on the vertex densification used to convert its lines to a pseudo-point-cloud. Elsewhere, my results can safely be considered conformant with the vertical accuracy-related requirements of the new noise regulation.

## 5.5 Conclusions of comparison with commercial results

The comparisons with the commercial results often indicated a surprising degree of similarity, considering that I prioritised the use of the AHN3 point cloud, whereas RHDHV prioritised DTB and only relying on AHN3 rasters in its absence and while processing P-roads. In places where the agreement between DTB and AHN3 was good, the RMSE between the two sets of results was less than 10 cm, and often as low as 2-3 cm. Generally, this corresponds to regions where DTB contains up-to-date data with good coverage. In such locations, the academic results still tend to be more accurate, because the DTB results are generally still older even where the agreement is relatively good between the two datasets. In places where agreement was poor between AHN3 and DTB the RMSE was defined primarily by the mean magnitude of the difference between DTB and AHN3 themselves. RMSE values up to 0.75 m were observed in such places, with individual residuals sometimes exceeding 1 m in places where DTB data is more than 15 years old.

In *well-exposed* regions where both my results and the commercial ones relied on AHN3, the RMSE was typically less than 5 cm, with some datasets showing less than 1 cm. In these zones, both sets of results are equally accurate and reliable; using a raster DTM does not appear to have significant drawbacks. In places where the commercial results are based on the AHN3 rasters and *any amount of occlusion* is encountered, RMSE values up to several metres were encountered inside the zones of occlusion. This includes regions where the academic program interpolated linearly through small gaps and also ones where DTB was used by the academic software, but was missed by the commercial one. Wherever the occlusion does not represent a long tunnel, it is always the academic results that are closer to reality, regardless of whether their formal output accuracy exists locally, or not.

Where the commercial implementation certainly fares much better than the academic one is where only DTB data is available for long distances, especially in tunnels and on bending roads (or a combination thereof). The commercial method simply intersects nearby DTB lines with cross-sections extending from the NWB centrelines, and will produce elevations reliably wherever at least one DTB line exists. In contrast, the preliminary edge estimation in my pipeline may fail in such places. In the rare places where

[AHN3](#) is outdated relative to [DTB](#), the same is true because this is likely to indicate that the given road does not yet exist in [AHN3](#) in its present form (e.g. it is under construction in it).

To conclude, I have established that outside of the above two examples to the contrary, the academic results generally appear to be superior to the commercial results, but that the reason for this is not strictly related to the fact that the commercial implementation takes its output elevations from [AHN3](#) rasters rather than the point cloud. Instead, we can conclusively say that the reason is the combination of their unconditional prioritising of [DTB](#), and simplistic methods that do not attempt to deal with occlusion-related issues explicitly. The commercial results also lack an accuracy assessment analysis comparable with the one found in my work.

## 5.6 Summary conclusions

The above sections show that all planned stages of this research were conducted successfully, including a functioning proof-of-concept implementation and an associated accuracy analysis. The solution proposed in this research is capable of performing the 3D conversion of [NWB](#) with accuracy estimated on the level of individual elevation estimates. Error propagation yields output errors around 10.6 cm at 95% certainty, lower than that of our main dataset, [AHN3](#). This applies to more than 90% of the output elevations on average, not including locations with large scale issues such as tunnels and large-scale construction works captured by [AHN3](#). The implementation records where the minimum sampling density was not reached to advise users of locations where the output has undetermined accuracy. Similarly, the program also records which input dataset was used to interpolate the elevation of each 3D-NWB vertex and where linear interpolation was used, explicitly.

My output shows good agreement with the commercial results, with the best agreement seen in well-exposed provincial roads where both solutions rely on [AHN3](#) data, with some datasets exhibiting an [RMSE](#) as low as 1 cm or less. The worst disagreements are seen in places where the commercial implementation uses outdated [DTB](#) data, and where it neglects to handle occlusion correctly and snaps the road centreline to overlying features, the prior corresponding to up to 0.75 m [RMSE](#) values, the latter to residuals of several metres locally.

My work proves that the approach of decomposing the conversion problem to be solved as 2.5D sub-problems works well in this scenario, and offers not only a more straightforward implementation and more effective means with which the elevations can be estimated, but also an interface for adapting the solution in a potential scaling-enabled implementation. While the proof-of-concept implementation proves that my system design can perform the conversion of [NWB](#) to a 3D dataset, it also successfully explored the academic aims of this project - mainly, whether the 2.5D approach is also a suitable framework for the production of accurate surface models of the roads, from which the output elevations can be derived.

While issues were encountered with the active contour optimisation part of the planned system, a small set of revisions to the system design allowed me to still generate the 2.5D models - albeit at the price of increasing the complexity of design of certain pipeline steps and resulting in somewhat worse overall [TIN](#) quality than originally hoped. The [TIN](#) models cover about 75% of the cumulative paved road surface areas in the areas examined, which means that they may not be directly usable in some potential applications, such as the interpolation of elevation series reliably in places other than the road centrelines. They generally do, however, cover most of the traffic-occupied parts of the roads.

Fortunately, the system design guarantees that under normal circumstances, the [TINs](#) will be still be complete where they need to be to enable the interpolation of elevations for [NWB](#), even in places where otherwise their quality may be sub-optimal. Hence, the quality issues with [TIN](#) generation did not affect the models' suitability for use in the 3D conversion of [NWB](#), and the exploration of an alternative approach was not necessary. Recommended improvements to the [TIN](#)-related part of the pipeline are mentioned below, in the Future work section.

## 5.7 Future work

During my time working on this research, I identified several directions in which work could continue. I have ideas for both small-scale extensions and improvements, as well as large-scale design changes. In the sections below, I will present some of these ideas with particular focus on the most likely reusers of my methods, namely [NDW](#) and academics.

### 5.7.1 Eliminating active contour optimisation

As I discussed in the previous chapters, I found active contour optimisation to be ineffective in this application, regardless of its parametrisation. While attempting to improve its performance in a wide variety of manners, I discovered that the primary control on its effectiveness is preliminary edge and attractor map quality. Not only are these the most important controls on its performance - it is particularly sensitive to small imperfections in them. A few small bumps in the preliminary edges or a series of small vehicle-related [AHN3](#) holes in the attractor maps can, for instance, corrupt the output to the point where it will almost certainly not provide accurate road/non-road point classifications. In fact, the current [TIN](#) construction algorithm produces better results using the preliminary edges rather than the optimised ones.

As I outlined in previous sections, bypassing active contour optimisation and using the growing-type [TIN](#) construction approach does not affect the 3D-NWB conversion efficiency. However, it does make the output [TINs](#) less appealing visually and in terms of completeness and quality around the road surface edges. Depending on the application, reusers may wish to improve this. While other image-processing-type algorithms exist that can achieve similar, perhaps somewhat better results (ribbon snakes, Chan-Vese algorithm, etc.), my recommendation is not to invest time and effort in trying to replace the active contour optimisation algorithm with one of these.

The original system design was based on pre-processing the data in preparation for active contour optimisation, and relying on its output to determine which Lidar points are found on road surface, and which are not. While I managed to bypass active contour optimisation in the end by adapting the preliminary edge generation and [TIN](#) construction algorithms, the final (implemented) system design is still relatively conformant with this planned structure - to the point that active contour optimisation can be run, optionally, and produces usable results.

A larger-scale redesign of my system should eliminate active contour optimisation altogether. Doing this makes another pipeline step redundant at least partially: preliminary edge estimation. The original purpose of this step was to provide initial edge estimates for the active contour optimisation algorithm. In the final implementation this has changed; they are only used to provide better centreline locations than [NWB](#) for the seeding of the initial [TINs](#), and delineating the approximate location of the road surface for the [TIN](#) initialisation step.

However, neither of these uses may be absolutely essential, nor is their effectiveness satisfactory in their current state. [NDW](#) is already hard at work improving [NWB](#)'s 2D georeferencing quality, and I can think of no reasons why the [TIN](#) initialisation algorithm could not be slightly modified to work without the preliminary edges. It is even possible that simply buffering *accurate* road centrelines to yield theoretical edges corresponding to the minimum expected road width would work in place of these.

In short, eliminating active contour optimisation from the software would make preliminary edge estimation partially redundant. A few modifications to the [TIN](#) construction workflow (in addition to the assumption that [NWB](#) is accurate enough) could theoretically make it redundant entirely, in which case preliminary edge estimation could also be eliminated. This would reduce runtimes somewhat, and would make future work on the system simpler, by taking out two relatively complex steps from the pipeline.

### 5.7.2 Improving TIN construction effectiveness

In addition to the smaller modifications I recommended above, the TIN construction step could also use a few modifications. Based on my experience in working with the implemented system design, the approach works well, but there is one further component that could improve the results of the procedure.

Conditional point insertions into pre-existing TIN triangles are based on distance and angle thresholds that examine the conformance of the candidate point with a single TIN triangle only. Insertions *outside* of these triangles (ones that expand the surface towards the insertion boundary) are based on examining the candidate's conformance with a plane fitted on some nearby TIN vertices. Although the latter represents a better sampling of the overall local trend where the point is being considered for insertion, it still ignores the global trend that exists on, at least, the scale of the local width of the road at the time of the test. In other words, as long as the transition from road to off-road points is sufficiently smooth, it is not impossible that the surface will be allowed to grow beyond the true road edge.

This serves to highlight that most roads are flat on a scale larger than that which concerns the insertions. Making the conditional insertions perform tests on this scale could potentially improve the effectiveness of filtering out points that do not fit the overall shape of the road. This property already represents the foundation of the Lidar segmentation pipeline step, which fits planes on a the scale that could also potentially be appropriate here. Performing such larger-scale checks could eliminate insertions that cannot be detected as erratic on the local scale.

Another approach that could achieve a similar result would be to use point normals to detect breaks in smoothness that could indicate the approximate edges of the surface. The advantage of this approach over the simple plane-fitting one is that based on my experience, this method can detect much smaller changes reliably. One only needs to look at the generated attractor maps in active contour optimisation to see that a scalar field derived by the interaction between the point normals can characterise road surfaces very accurately. It is even possible that the attractor maps could be directly employed in the TIN surface growing algorithm.

Neither of the above recommendations addresses the matter of maximum road widths. While a refined implementation using the above ideas could offer a much better success rate in terms of accidentally over-growing the road surface, it would still not be able to identify places where no physical evidence exists that the road's surface should end, i.e. no sudden or even gradual change in elevation can be observed. In such places, I recommend exploring two possible approaches. Either one can implement a workflow that monitors the evolution on the width of the road along its length on-the-fly as the TIN is being grown, like the enforcement of the conditions in my preliminary edge estimation workflow. Alternative, one can simply enforce a maximum road width appropriate for the the specific road *type* in question. The advantage of the former is that it has good generality, i.e. one does not need additional road attributes to make it work. By keeping track of the evolution of the road width, one can effectively monitor, and perhaps model these edges and ensure that the growing algorithm does not introduce any sudden bulges into them. For this to work, growing would need to take place with a roughly identical "speed" along the length of each NBRS part, for which my TIN extension workflow is better suited than the TIN initialisatio algorithm.

### 5.7.3 Performance and scaling

While the comparison with the commercial implementation primarily discovered areas in which the academic implementation performed better than the commercial one, it is important to point out that the commercial software has a crucial property which the academic one does not: not only does it work for the whole country (with a total runtime of a few days on a computer optimised for ArcGIS processing), it works *without* having to rely on a scaling implementation even though it is also partially based in Python. This is not to say that its runtime could not be reduced by introducing a scaling solution into it - I merely wish to point out that their solution is far more lightweight than mine. Without performance improvements (and potentially, a binary implementation of my system design), the academic solution would not be able to process the whole country's dataset in a few days, it would possibly take

## 5 Conclusions

significantly longer. Based on my benchmarks, a week would be a rough estimate, assuming that active contour optimisation is not used, only [TIN](#) initialisation is enabled and not [TIN](#) extension, and also that a rudimentary scaling solution exists to at least automate the production of the input "tiles" of data and the stitching of the output back into a national road network.

In part, this inferior performance is to be expected - the academic implementation carries out computationally complex operations, such as plane fitting and vector inner products *in bulk*. Furthermore, it does so in a programming language not particularly good at processing long iterations containing such operations. The solution is therefore not practical for processing the whole of [NWB](#) (and the necessary [AHN3](#) and [DTB](#) data) all at once, it is more of a technology demonstrator than a production software package.

However, the system design and its open source nature leaves the door open to anyone to develop production software based on it, with an associated scaling solution potentially on the level of parallel-processing individual [NBRS](#). Reusers considering such a project must bear in mind however, that small-scale optimisations may be necessary. For instance, the analysis, and in particular the accuracy assessment, indicated that the constructed [TINS](#) oversample the road surfaces to a significant degree - in fact, to the point where the small-scale noise introduced is likely to have a negative effect, for instance it can give rise to small triangles at surprisingly high angles in places where samples are tightly packed into small clusters with a few centimetres of noise. Optimising the quantity of the inserted points would yield not only a significant improvement in terms of computational complexity, but it would also solve potential processing issues and make the models better suited to practical applications.

I suspect that introducing the enforcement of such a maximum sampling density earlier on, perhaps during the Lidar segmentation step, could increase the performance even more, because it would affect more processing steps - one simply needs to find the minimum sampling density, at which all parts of the pipeline still work reliably.

### 5.7.4 Conditionally accepting preliminary elevations as final

Part of the high computational complexity of my implementation may not be justified for all roads, assuming that one only wishes to convert [NWB](#) to a 3D dataset. As I mentioned in various places in this report, [TIN](#) extension is not necessary if one is only interested in the 3D conversion of [NWB](#); it can be safely disabled. However, there is an addition way in which bypasses could be implemented to make the overall process more efficient.

Assuming that the 2.5D surface models are not needed by the reusers for any purpose other than to interpolate elevations for [NWB](#), then it may be a good idea to modify the preliminary elevation estimation algorithm in a way that it can intelligently recognise where its output is already accurate enough and in such cases, skips all subsequent pipeline steps.

This is an idea came up while I was comparing the preliminary and final elevation profiles - for well-exposed roads, the [RMSE](#) between them can be as low as 0.5 to 2 centimetres and even where there are small gaps in coverage, the polynomial-based refinement step usually approximates elevations in the gaps very accurately. The deciding factor in terms of telling whether these results can be deemed "final" appears to be related to how much of the full length of a given [NBRS](#) is occluded, and how much vertical curvature it possesses. If either or both are high, then the polynomial fit will only be accurate enough to provide support for subsequent steps of the pipeline.

For roads where this is not the case, one may regard the preliminary elevation estimates to be almost on par in terms of quality with the final output. In fact, it may even be theoretically more accurate in certain cases, because each elevation that does not come from the polynomial model is sourced from more Lidar points than the constant 3 samples used by TIN-linear interpolation in the last pipeline step. Therefore, it may be an interesting area to explore in future work to identify such roads based on certain metrics (for instance, the standard deviation with respect to the polynomial model and the total number of outliers detected) and to skip all subsequent steps for such [NBRS](#).

Furthermore, an alternative avenue of research may be to attempt to base all output elevations on the type of simple computations performed during preliminary elevation estimation in my pipeline. For this to be possible, the polynomial fitting workflow would need to be changed to work on the scale of the entire dataset as a whole. Specifically, this would presumably require fitting polynomials piecewise, which is not something I had time to explore in my particular research. Successfully implementing such an alternative workflow would allow one to bypass all other steps in my pipeline apart from vertex snapping. This can be interpreted as adapting the spline-fitting pre-processing steps from Boyko and Funkhouser [2011] more accurately.

Both of these approaches would reduce computational complexity drastically, since NBRS generation and preliminary elevation estimation are very efficient operations in my implementation. However, this would come at the price of dropping TIN construction capability, and having to re-do the accuracy assessment of the output as my methods and results would no longer hold.

### 5.7.5 Using the support dataset more intelligently

Our support dataset, DTB, is currently used in a way that effectively ignores its topology. By converting it into a point cloud as soon as it is imported, my implementation treats it as an extension of AHN3, partly because I wished to make this step to have good generality (i.e. to make no assumptions about the topology of the support dataset), and because my solution would perform best if the support dataset were itself an MLS dataset. DTB is useful, but it offers too little coverage of the road surfaces to be used to construct good TINS, especially considering that even where DTB is available, it may only have a single line feature available for a given road. Assuming that at least two lines are available, this does not limit the effectiveness with which they can be used to convert NWB into a 3D dataset using our methods. However, it does mean that the TINS have poor quality where only DTB data was available. The targeted acquisition and use of MLS data in these regions could drastically improve my results. At the very least, elevation data should be used that delineates the entire road surface, for instance surveying accurate elevations for BGT polygon outlines would presumably do the trick.

However, if this is not an option, then users may wish to examine the alternative: to treat DTB properly as a line dataset, and to thereby use its topology to somewhat improve the quality of the output. Specifically, the cross-section workflow I use to construct preliminary edges could be adapted to create reliable elevation series on both sides of the road centrelines where at least a single DTB line exists via extrapolation and interpolation - this would improve the overall quality of TINS locally. However, it would not make them cover the full extent of the paved areas, and would also not be able to provide NWB elevation estimates with the desired accuracy. In fact, the relevance of such a procedure (which is not unlike the way the commercial implementation uses DTB) is drawn into question by my findings regarding the temporal and completeness issues that DTB has.



# 6 Reproducibility self-assessment

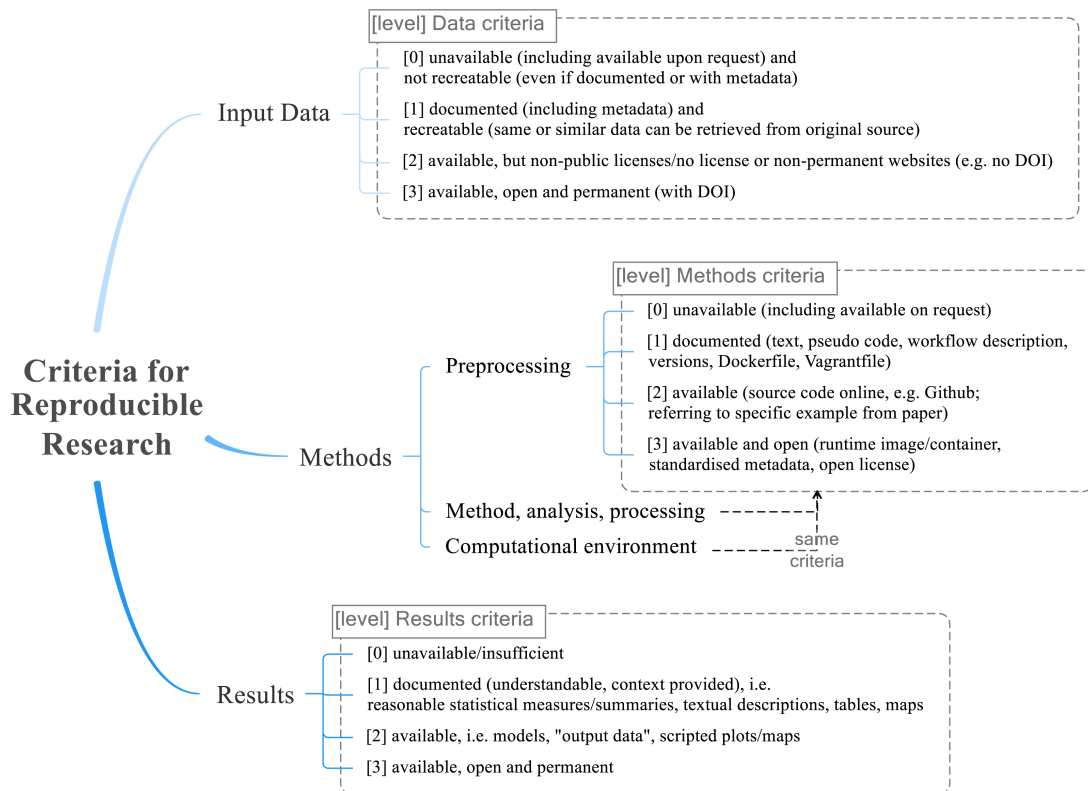


Figure 6.1: Reproducibility criteria to be assessed.

Preliminary reproducibility self-assessment grades on a scale of 1 to 3:

1. input data - **Grade = 3**
2. preprocessing - **Grade = 2**
3. methods - **Grade = 3**
4. computational environment - **Grade = 3**
5. results - **Grade = 2**

*[To be finalised for the final (P5) version of this report.]*

## 6.1 Self-reflection

*[To be produced for the final (P5) version of this report.]*



## References

- Aguilar, F., Agüera, F., M.A., A., and Carvajal, F. (2005). Effects of terrain morphology, sampling density, and interpolation methods on grid dem accuracy. *Photogrammetric Engineering and Remote Sensing*, 71:805–816.
- Aguilar, F., Mills, J., Delgado, J., M.A., A., Negreiros, J., and Pérez, J. (2010). Modelling vertical error in lidar-derived digital elevation models. *ISPRS Journal of Photogrammetry and Remote Sensing*, 65:103–110.
- Bater, C. and Coops, N. (2009). Evaluating error associated with lidar-derived dem interpolation. *Computers and Geosciences*, 35:289–300.
- Bell, M. and Lida, Y. (1997). *Transportation network analysis*.
- Bennett, J. (1997). The application of geographic spatial analysis in modeling traffic noise propagation away from a freeway. *Journal of The Acoustical Society of America*, 102.
- Boyko, A. and Funkhouser, T. (2011). Extracting roads from dense point clouds in large scale urban environment. *ISPRS Journal of Photogrammetry and Remote Sensing*, 66.
- Cai, H. and Rasdorf, W. (2008). Modeling road centerlines and predicting lengths in 3-d using lidar point cloud and planimetric road centerline data. *Computer-Aided Civil and Infrastructure Engineering*, 23:157–173.
- Caltagirone, L., Scheidegger, S., Svensson, L., and Wahde, M. (2017). Fast lidar-based road detection using fully convolutional neural networks. pages 1019–1024.
- Chen, C.-F. and Hsu, C.-J. (2020). Using a gis road network to improve gps positions.
- Chow, E. and Hodgson, M. (2009). Effects of lidar post-spacing and dem resolution to mean slope estimation. *International Journal of Geographical Information Science*, 23:1277–1295.
- Clode, S., Kootsookos, P., and Rottensteiner, F. (2004). The automatic extraction of roads from lidar data. *International Archives of Photogrammetry, Remote Sensing and Spatial Information Sciences*, 35.
- Clode, S., Rottensteiner, F., Kootsookos, P., and Zelniker, E. (2007). Detection and vectorization of roads from lidar data. *Photogrammetric Engineering and Remote Sensing*, 73:517–535.
- Durán Fernández, R. and Santos, G. (2014). A gis model of the national road network in mexico. *Research in Transportation Economics*, 46.
- Ekpenyong, F., Brimicombe, A., Palmer-Brown, D., Li, Y., and Lee, S. (2007). Automated updating of road network databases: road segment grouping using snap-drift neural network. *Proceedings of Advances in Computing and Technology*, pages 160–167.
- Fan, L., Smethurst, J., P.M., A., and Powrie, W. (2014). Propagation of vertical and horizontal source data errors into a tin with linear interpolation. *International Journal of Geographical Information Science*, 28:1378–1400.
- Fouque, C. and Bonnifait, P. (2008). Tightly coupled gis data in gnss fix computation with integrity test. *Journal of Intelligent Information and Database Systems*, 2:167–186.
- Gross, H. and Thoennesen, U. (2006). Extraction of lines from laser point clouds. *Fraunhofer FOM*, 36.
- Guarnaccia, C. and Quartieri, J. (2012). Analysis of road traffic noise propagation. *International Journal of Mathematical Models and Methods in Applied Sciences*, 6:926–933.
- Guo, Q., Li, W., Yu, H., and Alvarez, O. (2010). Effects of topographic variability and lidar sampling density on several dem interpolation methods. *Photogrammetric Engineering and Remote Sensing*, 76.
- Göpfert, J., Rottensteiner, F., and Heipke, C. (2011). Using snakes for the registration of topographic road database objects to als features. *ISPRS Journal of Photogrammetry and Remote Sensing*, 66:858–871.
- Hatger, C. and Brenner, C. (2003). Extraction of road geometry parameters from laser scanning and existing databases. *International Archives of Photogrammetry, Remote Sensing and Spatial Information Sciences*, 34:225–230.
- Hodgson, M. and Bresnahan, P. (2004). Accuracy of airborne lidar-derived elevation: Empirical assessment and error budget. *Photogrammetric Engineering and Remote Sensing*, 70:331–339.
- Hu, X., Tao, C., and Hu, Y. (2004). Automatic road extraction from dense urban area by integrated processing of high resolution imagery and lidar data. volume 35.

## REFERENCES

- Hu, Y. (2003). *Automated extraction of digital terrain models, roads and buildings using airborne lidar data*. PhD thesis, University of Calgary.
- Ishiyama, T., Tateishi, K., and Arai, T. (1991). An analysis of traffic noise propagation around main roads in tokyo. *Noise Control Engineering Journal*, 36.
- Kadaster (Accessed 07/05/2021). *BGT Home-page*. <https://www.kadaster.nl/zakelijk/registraties/basisregistraties/bgt>.
- Kass, M., Witkin, A., and Terzopoulos, D. (1988). Snakes: active contour models. *International Journal of Computer Vision*, 1:321–331.
- Kraus, K., Karel, W., Briese, C., and Mandlburger, G. (2006). Local accuracy measures for digital terrain models. *The Photogrammetric Record*, 21:342 – 354.
- Lin, Y., Wang, C., Cheng, J., Chen, B., Jia, F., Chen, Z., and Li, J. (2015). Line segment extraction for large scale unorganized point clouds. *ISPRS Journal of Photogrammetry and Remote Sensing*, 102.
- NDW (Accessed 07/05/2021). *Hoogte in NWB*. <https://nationaalwegenbestand.nl/nieuws/hoogte-nwb>.
- NDW (Accessed 09/12/2020). *NWB is Geometrisch Gecorigeerd*. <https://nationaalwegenbestand.nl/nieuws/nwb-geometrisch-gecorrigeerd>.
- Oude Elberink, S. (2010). *Acquisition of 3D topography: automated 3D road and building reconstruction using airborne laser scanner data and topographic maps*. PhD thesis, University of Twente.
- Oude Elberink, S. and Vosselman, G. (2006). Adding the third dimension to a topographic database using airborne laser scanner data. *International Archives of Photogrammetry, Remote Sensing and Spatial Information Sciences*, 36.
- Oude Elberink, S. and Vosselman, G. (2009). 3d information extraction from laser point clouds covering complex road junctions. *Photogrammetric Record*, 24:23–36.
- Oude Elberink, S. and Vosselman, G. (2012). Quality analysis of 3d road reconstruction. *International Archives of Photogrammetry, Remote Sensing and Spatial Information Sciences*, 36.
- PDOK (Accessed 07/05/2021). *Luchtfoto Home-page*. <https://www.pdok.nl/introductie/-/article/luchtfoto-pdok>.
- PDOK (Accessed 09/12/2020). *AHN3 Downloads*. <https://downloads.pdok.nl/ahn3-downloadpage/>.
- Peng, J., Parnell, J., and Kessissoglou, N. (2020). Spatially differentiated profiles for road traffic noise pollution across a state road network. *Applied Acoustics*, 172.
- Peng, M.-H. and Shih, P. T.-Y. (2006). Error assessment in two lidar-derived tin datasets. *Photogrammetric Engineering and Remote Sensing*, 72:933–947.
- Raber, G., Jensen, J., Hodgson, M., Tullis, J., Davis, B., and Berglund, J. (2007). Impact of lidar nominal post-spacing on dem accuracy and flood zone delineation. *Photogrammetric Engineering and Remote Sensing*, 73:793–804.
- Rijkswaterstaat (2020b). *Handboek DTB*.
- Rijkswaterstaat (2020c). *Handleiding Nationaal Wegenbestand (NWB-Wegen)*.
- Rijkswaterstaat (2020d). *Productspecificaties Digitaal Topografisch Bestand*.
- Rijkswaterstaat (Accessed 09/12/2020a). *AHN Kwaliteitbeschrijving*. <https://www.ahn.nl/kwaliteitsbeschrijving/>.
- Shi, W., Li, Q., and Zhu, C. (2005). Estimating the propagation error of dem from higher order interpolation algorithms. *International Journal of Remote Sensing*, 26:3069–3084.
- Smith, S., Holland, D., and Longley, P. (2005). Quantifying interpolation errors in urban airborne laser scanning models. *Geographical Analysis*, 37:200 – 224.
- Su, J. and Bork, E. (2006). Influence of vegetation, slope, and lidar sampling angle on dem accuracy. *Photogrammetric Engineering and Remote Sensing*, 72:1265–1274.
- Taylor, G., Blewitt, G., Steup, D., Corbett, S., and Car, A. (2001). Road reduction filtering for gis navigation. *Transactions in GIS*, 5:193–207.
- Thomson, R. and Richardson, D. (1995). A graph theory approach to road network generalisation. *Int. Cartographic Conference*, pages 1871–1880.
- Vosselman, G. and Liang, Z. (2009). Detection of curbstones in airborne laser scanning data. *Remote Sensing and Spatial Information Sciences*, 38.
- Wang, J., Lawson, G., and Shen, Y. (2014). Automatic high-fidelity 3d road network modeling based on 2d gis data. *Advances in Engineering Software*, 76:86–98.

- Yang, B., Fang, L., and Li, J. (2013). Semi-automated extraction and delineation of 3d roads of street scene from mobile laser scanning point clouds. *ISPRS Journal of Photogrammetry and Remote Sensing*, 79:80–93.
- Yue, Y., Yeh, A., and Li, Q. (2008). Road network model for vehicle navigation using traffic direction approach. pages 613–629.
- Zhang, H. (2011). *Uncovering road network structure through complex network analysis*. PhD thesis, Hong Kong Polytechnic University.
- Zhang, W. (2010). Lidar-based road and road-edge detection. pages 845 – 848.
- Zhu, L. and Hyppä, J. (2014). Fully-automated power line extraction from airborne laser scanning point clouds in forest areas. *Remote Sensing*, 6(11):11267–11282.
- Zhu, Q. and Li, Y. (2007). Review of road network models. pages 471–476.
- Zhu, Q. and Li, Y. (2008). Hierarchical lane-oriented 3d road-network model. *International Journal of Geographical Information Science*, 22:479–505.
- Zhu, Q. and Mordohai, P. (2009). A minimum cover approach for extracting the road network from airborne lidar data.

## **Colophon**

This document was typeset using L<sup>A</sup>T<sub>E</sub>X, using the KOMA-Script class `scrbook`. The main font is Palatino.

